Tribological Properties of B_4C Based Ceramics

ZHANG Wei

Tribological Properties of B_4C Based Ceramics

炭化ホウ素基セラミックスのトライボロジー特性

ZHANG Wei

张巍

Department of Chemical Systems Engineering,

Graduate School of Engineering

Nagoya University

2021

Contents

General introduction

Importance of ceramics in the field of tribology

Advanced structural ceramics are expected to be suitable for triboelements because of their excellent characteristics, such as high hardness and strength at room temperature and high temperatures, good wear resistance, favorable oxidation, etc [1]. Triboelements composed of ceramics are of important applications in both unlubricated and lubricated conditions.

In the past, metal/oil combination was always used as triboelements. With the development of society, energy saving and emission reduction have become an important trend in machine design, thus, it is expected that water lubrication system can be used to replace the oil lubrication system [2]. However, for metallic materials, water lubrication system presents some technical problems like corrosion, lubricity and reliability. In automotive industry, the new energy and eco-friendly targets are needed to decrease both the harmful emissions to the atmosphere and the fuel consumption. Gasoline direct injection engines can achieve these requirements, however, because of poor lubricity of gasoline and high pressure levels up to 80 MPa [3], it is expected to replace metal triboelements with more wear resistant ceramic materials.

Accordingly, the friction property of ceramics in water is gradually attracting keen attention for development of the water lubricated ceramic components. Ceramic materials, especially SiC and Si_3N_4, because of their superior mechanical and chemical performance, are increasingly applied in sliding components like journal bearings and mechanical face seals for water pumps. Compared with self-mated Si_3N_4 ceramics in water, self-mated SiC ceramics can maintain low friction in a much wider sliding velocity range and can show higher wear resistance against abrasive wear [4]. In particular, SiC/SiC and SiC/graphite tribopairs have been widely and successfully used in rotating seals. As mechanical seal materials, high friction and unwanted wear should be avoided to maintain good sealing surfaces. Compared with other materials sliding in water like soft alloys, polytetrafluoroethylene and rubber, SiC ceramics can not only show low friction, but also low wear even if the water contains ferrodebris or sand. Meanwhile, SiC ceramics have superior corrosion resistance to water, thus SiC ceramics are ideal candidate materials for triboelements in water environment. Therefore, instead of metal/oil combination, SiC/water is expected to be a potential combination that can be used for triboelements.

Tribology of SiC ceramics under dry sliding

SiC ceramics, as wear-resistant components used in sliding contact applications, are sometimes used in environments where lubricants can't be available and often suffer from high frictional losses. Moreover, both the friction and wear of SiC ceramics at high temperatures are high, and lubrication is difficult to work at that condition. Therefore, it is important to study self-lubrication property of SiC ceramics. Annealing heat treatment in air is an effective method to achieve self-lubrication for SiC ceramics [5].

It is widely reported that friction characteristic of SiC ceramics can be improved by the formation of thin layer composed of SiO_2 owing to tribochemical reaction. Based on this theory, the method of annealing heat treatment in air can be used to treat SiC ceramics to form oxide layer on the surface of SiC ceramics to achieve self-lubrication. Yamamoto and Ura [6] studied the frictional behavior of SiC ceramics after annealing heat treated at 1000 ℃ for 1 h in air. It was found that the oxide film composed mainly of SiO_2 was formed, whose thickness was approximately 80 nm. The friction coefficient of SiC ceramics with annealing treatment is lower than that of SiC ceramics without annealing treatment during initial 20 min at a load of 6.6 N, which is caused by the formation of the thin, soft SiO_2 layer. The oxide film which is softer than SiC itself can not only reduce the friction

coefficient and wear rate, but also increase the load capacity of SiC ceramics. However, this effectiveness of the oxide film disappeared when the sliding time was larger than 20 min. This phenomenon can be explained that oxidation of the friction surface is further promoted during the sliding, leading to an increased thickness of the oxidized layer. Therefore, the wear is increased, and the friction surface is roughened, resulting in an increased coefficient of friction.

Tribology of SiC ceramics under water-lubricated condition

To study lubrication mechanism of SiC ceramics sliding under lubricant condition, Stribeck curve is an obvious way, as shown in Fig. 1. The horizontal axis is the Stribeck factor (S_f), which is determined by velocity (v), viscosity (η), and load (W). Stribeck factor can be expressed as follow:

$$S_f = \frac{\eta \times v}{W}$$

The vertical axis is the coefficient of friction. There are three lubrication regimes, viz., boundary lubrication, mixed lubrication, and hydrodynamic lubrication. The Stribeck curve can be interpreted as a composite curve of the shearing force due to the contact between solids and the shearing force of the fluid that is the lubricant. Now, assuming that the coefficient of friction due to the shearing force between solids is μ_S and the coefficient of friction derived from the shearing force of liquid is μ_L, θ indicates the ratio of the area that is in contact via the fluid to the total contact area. If so, (1-θ) is the ratio of the area in contact between solids. The total coefficient of friction μ is the value obtained by multiplying each of μ_s and μ_L by the contact area ratio and adding them together. In reality, the shearing force of a fluid changes depending on the velocity gradient, so it depends on the type of liquid, but as the velocity increases, the shearing force increases.

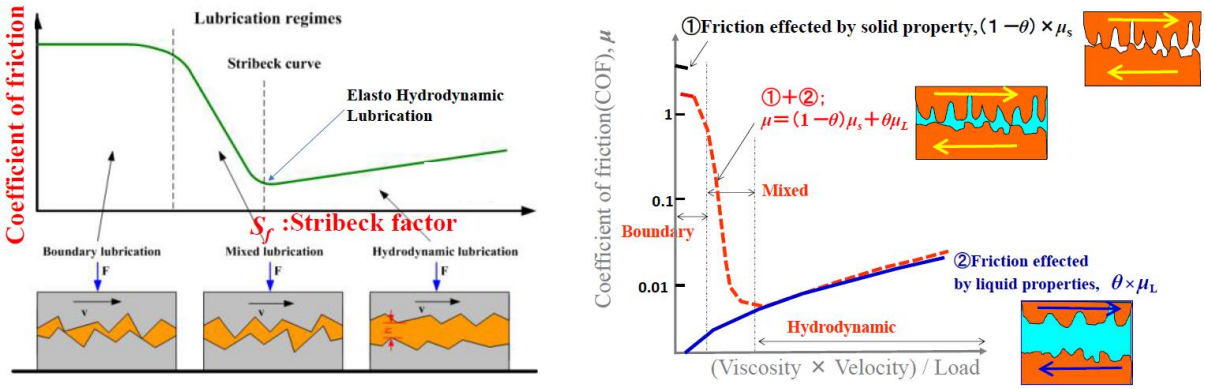

Fig. 1. Stribeck curve

Wang et al. [7] drew the Stribeck curves of self-mated SiC ceramics sliding in water at different sliding velocities (Fig. 2a). They used duty parameter $G=\eta N/P_m$ as X axis, where η [Pa·s] is the dynamic viscosity of water, N [s^{-1}] is the rotational velocity and P_m [Pa] is the effective mean contact pressure. Each curve showed a obvious transition of COF from a low and stable region to an increasing region, viz., from hydrodynamic lubrication to mixed lubrication. However, the Stribeck curve of self-mated SiC ceramics sliding in water shifted in the X direction based on different sliding velocities. This means the duty parameter, at which transition happened, was affected by sliding velocity. Therefore, the data obtained from different sliding velocities can't be unified into one curve as supposed by the classic hydrodynamic theory. Different from the Stribeck curve of metal sliding in oil, such as bronze/stainless steel tribopair, the transition point from hydrodynamic lubrication region to mixed lubrication region has almost the same value of duty parameter. Therefore, it can be concluded that the friction of SiC ceramics in water is different from that of metal under oil lubrication. Wong et al. [8] also showed

the Stribeck curves for SiC cylinder sliding on SiC disk in water at different sliding velocities (Fig. 2b). Three lubrication regions, viz., boundary, mixed and hydrodynamic lubrications, were observed in self-mated SiC ceramics, and the COF was the lowest when the duty parameter was 3.5~7 $\times 10^{-9}$ (Table 1). Different from the above result of Wang et al. [7], the Stribeck curve has almost no obvious shift in the X direction based on different sliding velocities, which means the duty parameter at which transition happened was almost unaffected by the sliding velocity. They stated that when the lubrication regime was hydrodynamic lubrication, the COF was not affected by materials and the COF was proportional to the duty parameter. Compared with self-mated Si_3N_4 ceramics and self-mated Al_2O_3 ceramics, the duty parameter corresponding to the minimum COF of the self-mated SiC ceramics was the lowest, which means the self-mated SiC ceramics had greater load carrying capacity. This is due to higher hardness, better thermal shock resistance and thermal conductivity of SiC ceramics. During hydrodynamic lubrication, the COF is low, and the wear rate of SiC ceramics, theoretically, is zero. Jordi et al. [9] measured that the wear rate of SiC ceramics during hydrodynamic lubrication was smaller than 2×10^{-11} $mm^3/N\cdot m$, which is in the range of wear rates in well-lubricated machinery. Further, the wear rate of SiC ceramics during run-in period was a liner function of the COF.

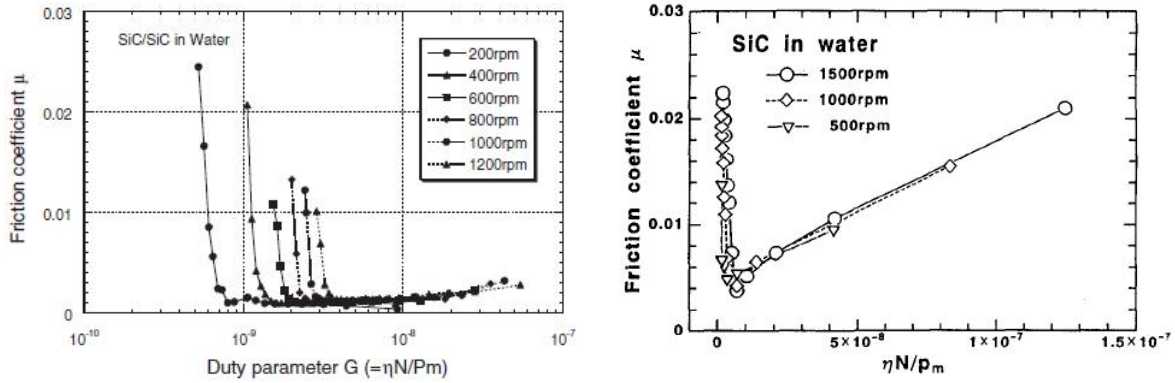

(a) (b)

Fig. 2. Stribeck curves of self-mated SiC sliding in water at different sliding velocities proposed: (a) in Ref. [7] and (b) in Ref. [8].

Table 1 Minimum COF of self-mated SiC ceramics in each sliding velocity [8].

	500 rpm (0.39 m/s)	1000 rpm (0.78 m/s)	1500 rpm (1.17 m/s)
COF_{min}	0.0049	0.0042	0.0038
$\eta N/P_m$	3.48×10^{-9}	6.97×10^{-9}	6.97×10^{-9}

Pressless sintering of B_4C ceramics

Boron carbide (B_4C) ceramics has many outstanding performance, such as extremely high hardness, high melting point, low density, high elastic modulus, high thermoelectromotive force, high chemical resistance, high neutron absorption cross section, high impact, and excellent wear resistance [10-12]. Because of the valuable properties, B_4C ceramics are useful for various industrial applications both at room and high temperatures.

However, it is impossible to sinter pure B_4C ceramics to high densities without additives or high external pressure owing to low self-diffusion coefficient, the strong high covalent bonding of B-C, high resistance to grain boundary sliding, high melting temperature, existence of surface oxide layer and absence of plasticity. It is reported that the covalent bond ratio of boron carbide is up to 93.94%, which is higher than other ceramics, such as SiC(88%), Al_2O_3(33%), ZrO_2(33%) [13]. Pure B_4C ceramics can not be densified more than 80% of theoretical density even at temperature over 2300 °C. Boron carbide of the specified atomic ratios, of which density is up to at least 90% of theoretical density, could only be obtained near the melting point of B_4C. Although fully densified

B_4C ceramics can be fabricated by means of hot-pressing at above 2100 ℃ [14], disadvantages are that directional change of physical performance perpendicular and parallel to the hot pressing direction, high cost, and limit to only relatively simple shapes. Whereas pressureless sintering can avoid the costly diamond machining required to form complicated shapes, and the method of pressureless sintering is suitable for large scale-production. Pressureless sintering is a conventional method by sintering products at atmospheric pressure(0.1 MPa), which is the simplest sintering method. So many researchers have tried to study sintering B_4C ceramics without press but with addition of different kinds of sintering additives and then it was proved that sintering additives can promote the densification of boron carbide under a normal sintering process.

Carbon is often used as a sintering additive to add into B_4C ceramics. The reason is that the eutectic temperature for B_4C-C presented in phase diagram is about 2375 ℃, which is lower than melting point of B_4C. However, carbon-rich B_4C fabricated with an excess carbon of 2wt% could not be densified to higher than 85% of theoretical density at a temperature of up to 2200 ℃, because the free C in carbon-rich B_4C is in the form of non-active graphite [15]. Therefore, carbon should be introduced from outside to B_4C. Usually, carbon can be provided in the form of carbonaceous precursor and amorphous carbon [16-26]. C can also be introduced by in situ chemical reaction between metal carbide and B_4C [27]. Recently, it was reported that carbon can be introduced into B_4C ceramics in the form of graphene platelets [28].

Tribology of B_4C ceramics

B_4C, the third hard material in the known substance, has characteristics of low density (2.52 g/cm^3), good strength, good wear resistance, exceptional hardness (29.1 GPa), high elastic modulus (450 GPa) and good chemical inertness at room temperature [29, 30]. Therefore, B_4C ceramics and their compounds are considered as potential candidates for tribological applications requiring low friction and low wear. Compared with Al_2O_3 ceramics, ZrO_2 ceramics, SiC ceramics and Si_3N_4 ceramics, B_4C ceramics have higher hardness and lower density. Therefore, B_4C ceramics are more suitable to be used in movable or rotatory tribological applications where reduction of weight is of great significance. Because of their high hardness, B_4C ceramics are highly resistant to abrasion and particle erosion. B_4C can be used as wear-resistant materials in both the bulk form and thin coating.

The main application fields of B_4C ceramics as wear-resistant components are mechanical seals, bearings, cutting tools, wheel dressing tools and blast nozzles [31]. Compared with hard metals, B_4C ceramics are more suitable employed as abrasive water-jet nozzle materials when very hard abrasives are used, such as Al_2O_3 [32]. However, the poor friction property, which can cause a lot of energy consumption during friction process, limits the extensive application of B_4C ceramics in the filed of wear resistance. Also, surface damage caused by sliding or particle erosion restricts the service life of triboelements, reducing their reliability and durability. To reduce friction and further reduce wear for B_4C ceramics, many scientific and technological researchers have taken some effective measures [33].

Surface relief structure

Surface relief structure is a well known technique to improve tribological properties of materials [34-36]. Fig.3 shows some artificially formed relief structure by laser processing [37]. Under unlubricated sliding condition, the craters or grooves created by laser can trap wear debris, reducing abrasive wear. Under lubricated sliding condition, these craters or grooves can act as lubricant reservoirs in lubricated regime, extending lubrication. Murzin et al. [38] prepared a non-periodic microrelief structure on SiC ceramics with help of pulse-periodic Nd:YAG laser. The friction coefficient of the SiC ceramics is decreased from 0.146 to 0.099 after the formation of

microrelief structure under unlubricated sliding condition. Wang et al. [39] found surface texture can generate additional hydrodynamic pressure to increase the load carrying capacity for SiC ceramics under water lubricated sliding condition. They also found the surface texture is beneficial to improve the running-in progress to smooth the sliding interface. Therefore, based on the two reasons mentioned above, the SiC ceramics with surface texture showed reduced friction coefficient under lubricated sliding condition. To prepare surface texture on ceramics, laser-fabricated surface texture is an effective method [40, 41].

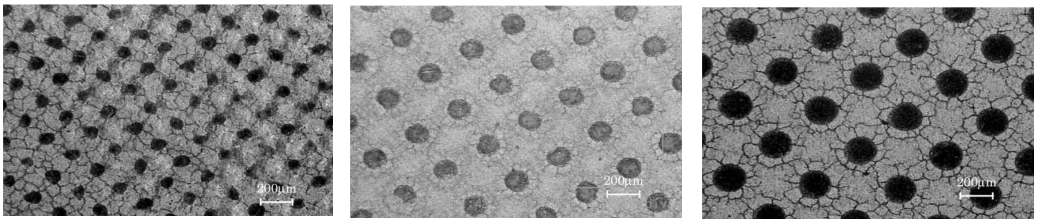

Fig. 3. Artificially formed relief structure by laser processing [37].

Backgrounds of this thesis

There are three backgrounds in this thesis. First, Surface relief structure is a well-known approach to control friction and wear between sliding surfaces. Relief structure is defined as flat and smooth regions interrupted by local depressions. Until now, relief structure is usually produced by laser processing. However, there are some disadvantages for this method, such as large defects induced to ceramics, high cost and complex preparation process. The innovation of this study is that relief structure can be produced by in-situ method. Second, SiC ceramics has been widely used as wear-resistant components. B_4C, as the third hardest material in the world, is a potential material for the application in the field of tribology. To date, reports about B_4C ceramics and B_4C-SiC composite ceramics have been quite limited. Third, for the current typical combination materials of mechanical seals used in pump, SiC ceramics is used as rotating ring, and SiC ceramics or C is used as stationary ring. In order to further reduce the friction and wear of mechanical seal materials, B_4C-SiC composite ceramics was developed to replace SiC ceramics as rotating ring.

On these backgrounds, I aim to evaluate the tribological properties of B_4C-SiC ceramics and B_4C ceramics under both unlubricated and lubricated conditions, to analyze the friction and wear mechanisms.

In part I of this thesis, effect of relief structure on B_4C-SiC composite ceramics with different ratio is studied. Chapter 1 shows that the relief structure can be formed in situ on the surface of B_4C-SiC composite ceramics, and this relief structure has an important effect on tribological properties of B_4C-SiC ceramics. In Chapter 2, we reveal the formation mechanisms of relief structure formed in situ on the surface of ceramics. Chapter 3 compares the influence of surface roughness parameters and surface morphology on friction performance of ceramics. In Chapter 4, we find that the relief structure of B_4C-SiC ceramics was damaged at high load. Chapter 5 shows that the relief structure also has an important effect on B_4C-SiC ceramics sliding under lubricated condition (under going).

In Part II of this thesis, the tribological properties of B_4C-SiC ceramics in water are investigated. In Chapter 6, we have measured the Stribeck curves for SiC, B_4C-SiC, B_4C ceramics under different loads (under going). Chapter 7 shows that water temperature has an important effect on tribological performance of B_4C-SiC ceramics under water-lubricated condition.

In Part III of this thesis, we study the influence of annealing on tribological properties of B_4C, SiC, B_4C-SiC ceramics. In Chapter 8, the tribological properties of B_4C ceramics prepared by pressureless sintering and annealed at different temperatures are studied. We found some results that are different from previous research reported by

other researchers, and a new structural model of the worn surface composition of B_4C ceramics after annealing, which is different from the models put forward by previous works, is proposed. Chapter 9 shows that the formation of α-cristobalite on the annealed SiC ceramics can further lubricate SiC ceramics and shorten run in period. In Chapter 10, we demonstrate that the B_4C-SiC composite can obtain lower friction coefficient by annealing at 1000 ℃, whereas the friction coefficient of B_4C-SiC composite annealed at 1200 ℃ was significantly increased. Chapter 11 compares the friction behaviors of SiC-B_4C composite ceramics with different ratio after annealing.

In Part IV of this thesis, the influence of counterpart materials on tribological properties of B_4C-SiC ceramics is studied. In Chapter 12, we evaluate the effect of counterbody on tribological properties of B_4C-SiC composite ceramics under dry sliding condition. Chapter 13 shows the tribology of B_4C-SiC ceramics under water lubrication: Influence of counterbody.

Objectives of this thesis

The objectives of this study are to find the optimized condition and composition of B_4C based ceramics for mechanical seals by evaluating the tribological properties of B_4C and B_4C-SiC ceramics under both unlubricated and lubricated conditions, and to analyze the friction and wear mechanisms for B_4C based ceramics.

References

[1] F. Li, S. Y. Zhu, J. Cheng, Z. H. Qiao, J. Yang. Tribological properties of Mo and CaF_2 added SiC matrix composites at elevated temperatures. Tribology International,2017,111:46-51.

[2] M. Masuko, A. Suzuki, Y. Sagae, M. Tokoro, K. Yamamoto. Friction characteristics of inorganic or organic thin coatings on solid surfaces under water lubrication. Tribology International,2006,39(12):1601-1608.

[3] B. Buri, S. Busch, H. Kubach, U. Spicher. High injection pressures at the upper load limit of stratified operation in a DISI engine. SAE International Journal of Engines,2010, 2(2),40-47.

[4] P. Andersson, P. Lintula. Load-carrying capability of water-lubricated ceramic journal bearings. Tribology International,1994,27(5):315-321.

[5] W. Zhang, S. Yamashita, H. Kita. Progress in tribological research of SiC ceramics in unlubricated sliding-A review. Materials & Design,2020,190:108528.

[6] Y. Yamamoto, A. Ura. Influence of interposed wear particles on the wear and friction of silicon carbide in different dry atmospheres. Wear,1992,154(1):141-150.

[7] X. L. Wang, K. Kato, K. Adachi. The critical condition for the transition from HL to ML in water-lubricated SiC. Tribology Letters,2004,16(4):253-258.

[8] H. C. Wong, N. Umehara, K. Kato, K. Nii. Fundamental study of water-lubricated ceramic bearing. Proceeding of the Japanese Mechanical Society,1995,61:4027-4032. (in Japanese)

[9] L. Jordi, C. Iliev, T. E. Fischer. Lubrication of silicon nitride and silicon carbide by water: Running in, wear and operation of sliding bearing. Tribology Letters,2004,17(3):367-376.

[10] T. Kumazawa, K. Sekine, A. Matsuoka. Pressureless sintering of boron carbide ceramics. Ceramics,2014,49(2):122-125.

[11] K. Reinmuth, A. Lipp, H. Knoch, K. A. Schwetz. Borhaltige keramische neutronenabsorberwerkstoffe. Journal of Nuclear Materials,1984,124:175-184.

[12] M. Mashhadi, M. R. Saraf, S. Baghshahi. Synthesis of boron carbide powder via carbothermic reaction of boron oxide. International Journal of Engineering Science,2005,16(1):9-14.

[13] L. S. Wang, Y. B. Yang, J. S. Zhang, Y. Fan, F. Wu. Study on the mechanism and kinetic of boron carbide sintering. Journal of Central South University of Technology,1999,30(5):505-508.

[14] M. A. Kuzenkova, P. S. Kislyi, B. L. Grabchuk, N. I. Bodnaruk. The structure and properties of sintered boron carbide. Journal of the Less-Common Metals,1979,67(1):217-223.

[15] W. Zhang, S. Yamashita, H. Kita. Progress in pressureless sintering of boron carbide ceramics-A review. Advances in Applied Ceramics: Structural, Functional and Bioceramics,2019,118(4):222-239.

[16] M. Bougoin, F. Thevenot, J. Dubois, G. Fantozzi. Synthèse et caracterisation de ceramiques denses en carbure de bore. Journal of the Less-Common Metals,1985,114(2):257-271.

[17] K. A. Schwetz, W. Grellner. The influence of carbon on the microstructure and mechanical properties of sintered boron carbide. Journal of the Less-Common Metals,1981,82:37-47.

[18] Y. Y. Li, H. Liu, T. Y. Li, J. Yang, X. Q. Pan, Y. Zhang. Study on pressless sintering of B_4C pellets used in nuclear reactors. Powder Metallurgy Technology,2017,35(1):53-56.

[19] L. S. Wang, B. Y. Yin, Y. C. Fang. Boron carbide material fabricated by carbon-doping activated sintering. Then Chinese Journal of Nonferrous Metal,2002,12(6):1210-1213.

[20] Y. P. Yuan, H. W. Jiang, Y. J. Zheng. Effect of glucose additives on the properties of pressureless-sintered boron carbide. Journal of Mudanjiang Normal University,2016(3):36-38.

[21] H. Suzuki, T. Hase, T. Maruyama. Effect of carbon on sintering of boron carbide. The Ceramic Society of Japan,1979,87(8):430-433.

[22] H. Lee, R. F. Speyer. Hardness and fracture toughness of pressureless-sintered boron carbide (B_4C). Journal of the American Ceramic Society,2002,85(5):1291-1293.

[23] S. L. Dole, S. Prochazka, R. H. Doremus. Microstructural coarsening during sintering of boron carbide. Journal of the American Ceramic Society,1989,72(6):958-966.

[24] S. L. Dole, S. Prochazka. Densification and microstructure development in boron carbide. Ceramic Engineering and Science Proceedings,1985,6(7-8):1151-1160.

[25] R. F. Speyer, H. Lee. Advances in pressureless densification of boron carbide. Journal of Materials Science,2004,39(19):6017-6021.

[26] K. A. Schwetz, L. S. Sigl, L. Pfau. Mechanical properties of injection molded B_4C-C ceramics. Journal of Solid State Chemistry,1997,133:68-76.

[27] L. S. Sigl. Processing and mechanical properties of boron carbide sintered with TiC. Journal of the European Ceramic Society,1998,18(11),1521-1529.

[28] D. Z. Gao, J. Jing, J. C. Yu, X. Guo, Y. B. Zhang, H. Y. Gong, Y. J. Zhang. Graphene platelets enhanced pressureless-sintered B_4C ceramics. Royal Society Open Science,2018,5(4):1-7.

[29] F. Thévenot. Boron carbide- a comprehensive review. Journal of the European Ceramic Society,1990,6(4):205-225.

[30] G.S. Samy, S. T. Kumaran. Measurement and analysis of temperature, thrust force and surface roughness in drilling of AA (6351)-B_4C composite. Measurement,2017,103:1-9.

[31] P. H. Shipway, I. M. Hutchings. The influence of particle properties on the erosive wear of sintered boron carbide. Wear,1991,149:85-98.

[32] K. A. Schwetz, L. S. Sigl, J. Greim, H. Knoch. Wear of boron carbide ceramics by abrasive waterjets. Wear,1995,181-183(part-P1):148-155.

[33] W. Zhang. A review of tribological properties for boron carbide ceramics. Progress in Materials Science,2021,116:100718.

[34] T. Roch, F. Klein, K. Guenther, A. Roch, T. Mühl, A. Lasagni. Laser interference induced nano-crystallized surface swellings of amorphous carbon for advanced micro tribology. Materials Research Express,2014,1(3):035042.

[35] T. Shimizu, T. Kakegawa, M. Yang. Micro-texturing of DLC thin film coatings and its tribological performance under dry sliding friction for microforming operation. Procedia Engineering,2014,81:1884-1889.

[36] R. Capozza, N. Pugno. Effect of surface grooves on the static friction of an elastic slider. Tribology Letters,2015,58(3):35-40.

[37] X. L. Wang, K. Kato, K. Adachi, K. Aizawa. The effect of laser texturing of SiC surface on the critical load for the transition of water lubrication mode from hydrodynamic to mixed. Tribology International,2001,34(10):703-711.

[38] S. P. Murzin, V. B. Balyakin. Microstructuring the surface of silicon carbide ceramic by laser action for reducing friction losses in rolling bearings. Optics & Laser Technology,2017,88:96-98.

[39] X. L. Wang, K. Adachi, K. Otsuka, K. Kato. Optimization of the surface texture for silicon carbide sliding in water. Applied Surface Science,2006,253(3):1282-1286.

[40] Y. L. Zhang, X. G. Zhang, T. H. Wu, Y. B. Xie. Effects of surface texturing on the tribological behavior of piston rings under lubricated conditions. Industrial Lubrication and Tribology, 2016,68(2):158-169.

[41] D. Z. Segu, S. G. Choi, J. H. Choi, S. S. Kim. The effect of multi-scale laser texutured surface on lubrication regime. Applied Surface Science,2013,270(14):58-63.

Part I

Effect of Relief Structure on B_4C-SiC Composite Ceramics with Different Ratio

Chapter 1
Tribological properties of SiC-B_4C ceramics under dry sliding condition

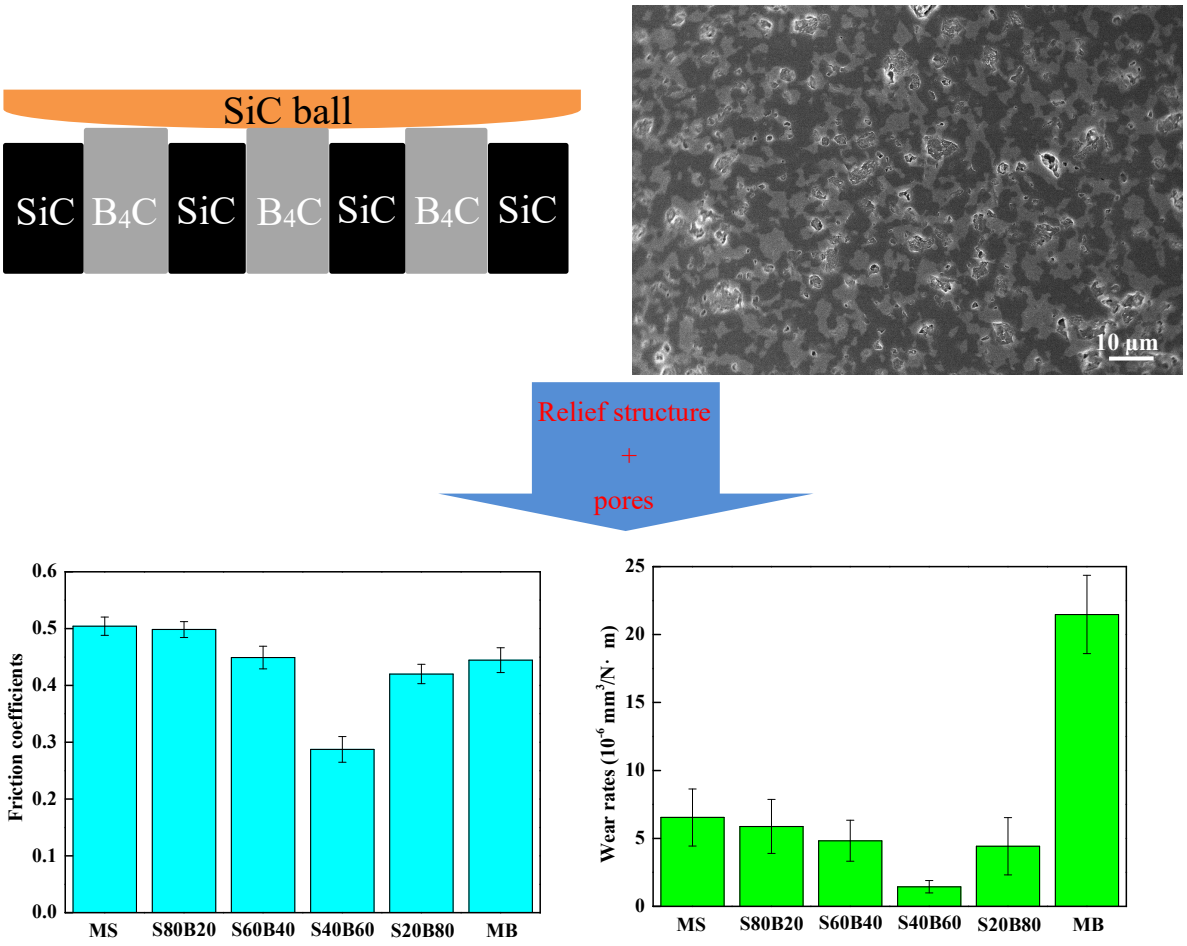

SiC-B_4C ceramic composites with different ratios of SiC to B_4C were produced. The relative density, mechanical properties, initial surface characteristics, dry sliding tribological properties against SiC ball and worn surface characteristics of the SiC-B_4C ceramics were studied. Results of dry sliding tribological tests showed that, 40 wt.%SiC-60 wt.%B_4C ceramic composite had the best tribological properties in SiC-B_4C ceramic composites. A relief structure with height difference of 10-30 nm between B_4C grains and SiC grains is formed after dry sliding. This relief structure, on the one hand, can reduce real contact area on interface, decreasing adhesion effect, and on the other hand, can fix or trap the wear pieces formed on sliding interface during the dry sliding process, reducing the abrasive wear. However, there is a limit to the beneficial influence of decreased adhesion effect and reduced abrasive wear, and an optimum proportion of relief structure. Pores can also fix or trap some wear pieces, reducing the abrasive wear. Under the condition of strong bonding between SiC grains and B_4C grains, the SiC-B_4C ceramic composites with higher porosity can obtain better tribological properties. In addition, it is observed by AFM that the depth of scratch on B_4C grains is shallower than that on SiC grains. Hence, it is demonstrated by micro scale measurement that the wear rate of B_4C is lower than that of SiC in this study.

Contents

1.1. Introduction

B_4C, as the third hardest substance (36 GPa), is a potential material for the application in the field of tribology, such as nozzles, sealing elements, high-speed cutting tools, bearings, owing to its extremely high hardness and low density [1-6]. SiC, another material with high hardness (24 GPa), is also widely used as wear-resistant components [7-12]. For monolithic B_4C ceramics and monolithic SiC ceramics, they have many outstanding physical and chemical properties, however, poor tribological performance has restricted their wide application in the field of tribology.

In order to improve tribological properties of monolithic B_4C ceramics and monolithic SiC ceramics, Li et al. [13-15] and Motealleh et al. [16] added hBN into B_4C ceramics and SiC ceramics, respectively, and the results showed that hBN can improve tribological properties of these monolithic ceramics as an external lubricant. Sedlák et al. [17] and Llorente et al. [18] found that the addition of graphene has slight effect on the friction coefficients of monolithic B_4C ceramics and monolithic SiC ceramics, respectively, however, wear resistance of these monolithic ceramics has been significantly improved. Alexander et al. [19] reported that friction and wear performance of monolithic B_4C ceramics can be improved by adding either carbon fiber or carbon nanotube. Tang et al. [20] and Candelario et al. [21] pointed out that the introduction of carbon fiber and carbon nanotube can reduce the friction and wear for SiC ceramics, respectively. As a whole, the introduction of a suitable second phase can improve the tribological properties for monolithic B_4C ceramics and monolithic SiC ceramics.

To date, the studies on tribological properties of adding B_4C into monolithic SiC ceramics or adding SiC into monolithic B_4C ceramics are limited. Therefore, the aim of the present contribution is to study the tribological properties of SiC-B_4C ceramics under dry sliding condition.

1.2. Experimental procedures

1.2.1. Preparation and characters of the composites

SiC powder (Yakushima Denko, Grade OY-15, average particle size: 0.4 μm, Japan, main impurity O (0.25 wt%)) and B_4C powder (H. C. Starck Gmbh & Co., Grade HS, average particle size: 0.8 μm, Germany, main impurities O (1.2 wt%), N (0.2 wt%), Si (0.1 wt%), Fe (0.03 wt%), Al (0.02 wt%)) were utilized as raw materials to prepare SiC-B_4C ceramic composites. Monolithic SiC ceramics and monolithic B_4C ceramics were also prepared as references for comparison with the tribological properties of composites. In order to promote the sintering of monolithic SiC ceramics, 3 wt.% B_4C was introduced. Additional 3 wt.% carbon black powder (Mitsubishi Chemical, #4000B, average particle size: 20-30 nm, Japan) was added in all cases as a sintering additive. The composition of the SiC-B_4C ceramics and their numbers are shown in Table 1.

Table 1 Composition of the SiC-B_4C ceramic composites (wt.%) and their numbers.

NO.	MS	S80B20	S60B40	S40B60	S20B80	MB
SiC	97	80	60	40	20	0
B_4C	3	20	40	60	80	100
Carbon black	3	3	3	3	3	3

The respective powder batches were milled in ethanol for 24 h using SiC balls. After being mixed, the powder mixtures were pressed into disks at 9.8 MPa and then were cold-isostatically pressed at 196 MPa. The disks were sintered by pressureless sintering technology at 2300 ℃ for 16 h, in Ar atmosphere. The electrical

furnace (Chugai-ro, Inc., Osaka, Japan) composed of graphite heating elements and fibrous insulation was heated at a rate of 10 ℃/min up to 1900 ℃ under vacuum and held for 10 min to introduce pure Ar into the furnace, and then the temperature was raised at a rate of 10 ℃/min up to 2300 ℃. After sintering, the samples were naturally cooled to room temperature. Temperature was monitored using a pyrometer sighted on the graphite crucible in which the samples existed, measuring through a fused silica viewing port mounted on the furnace side wall.

Density was determined by the geometric method from weight and geometric volume of the sintered bodies after polishing the surface of samples, with the relative density and the porosity of the ceramics evaluated. Theoretical density was calculated by the rule of mixtures using 2.51 g/cm^3, 3.21 g/cm^3 and 2 g/cm^3 as densities for B_4C, SiC and carbon black, respectively. Vickers-indentation tests were carried out using a hardness tester (VKH-1, Tokyo Testing Machine, Japan) with a load of P=9.8 N for a dwell time of 10 s. The diagonals (d) and radial-crack diameters (2c) of each indent were measured. Hardness and fracture toughness (K_{IC}) were calculated using $H=1.8544P/d^2$ and $K_{IC}=0.016(E/H)^{0.5}Pc^{-1.5}$, respectively [22]. Elastic modulus E of 390 GPa and 405 GPa was used for B_4C and SiC, respectively. Five indentations were made on the polished surface of each sample.

1.2.2. Friction and wear test

Dry sliding tests of SiC-B_4C ceramics were carried out on a ball-on-disc tribometer (T-18-0162, NANOVEA, US), the schematic image of which is shown in Fig. 1. Disks with size of 29×26×4.5 mm^3 were cut from the SiC-B_4C ceramics. The surfaces were polished down to surface roughness below 0.05 μm. Commercial SiC balls (Sato Tekkou, Japan, Bulk density=3.13 g/cm^3, Hv=22.1 GPa) with 9.5 mm diameter were used as counterparts. The parameters of the dry sliding tribological tests are presented in Table 2.

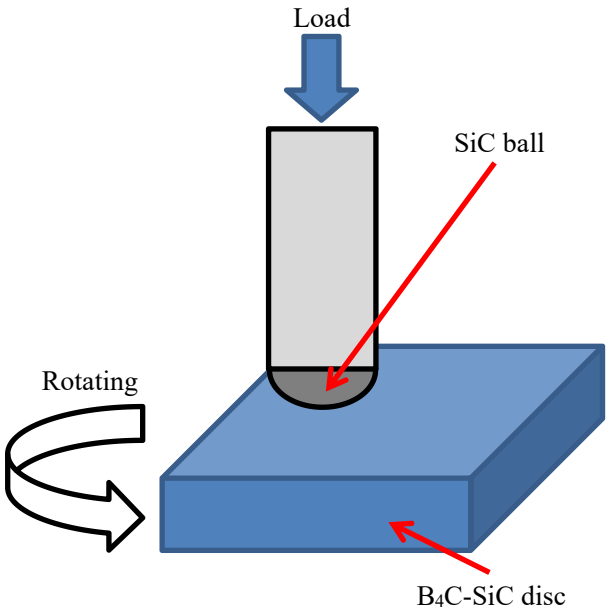

Fig. 1. Schematic image of dry sliding test.

Table 2 Parameters of the dry sliding tribological tests.

Load (N)	Sliding velocity (m/s)	Sliding radius (mm)	Sliding distance (m)	Temperature (℃)	Relative humidity (%)
5	0.1	10	100	25±1	45±5

During the tests, friction coefficients were automatically calculated and recorded by a microprocessor-controlled data acquisition system and the material losses (wear volume of the wear tracks) on

each disk were measured and calculated by a surface profilometer. Wear rates were calculated according to the following equation:

$$WR = V/(Ps)$$

Where WR-the wear rate ($mm^3/N \cdot m$); V-the wear volume (mm^3), P-the normal load (N); s-the sliding distance (m). Three repeated measurements were performed under the same conditions, and the average values were obtained.

Initial surface morphologies of the SiC-B_4C ceramics after polishing and worn surface morphologies of the SiC-B_4C ceramics after dry sliding were observed by SEM (JSM-7500F, JEOL, Japan). The chemical composition on worn surface was analyzed by EDS. Surface profiles were characterized by AFM (SPM9700, SHIMADZU, Japan).

1.3. Results and discussion

1.3.1. Physical properties

The results of the bulk density and relative density/porosity of the SiC-B_4C ceramics are shown in Fig. 2. From Fig. 2, we can see that the bulk density decreases with an increase of B_4C content. In our previous work, it has been determined that the SiC-B_4C ceramic composites were composed of SiC, B_4C and C phases [23]. Because the density of B_4C (2.51 g/cm^3) is lower than that of SiC (3.21 g/cm^3), thereby the increasing B_4C content decreases the bulk density of SiC-B_4C ceramics. Although the bulk density of SiC-B_4C ceramics decreases as B_4C content increases, the relative density/porosity of SiC-B_4C ceramics presents different trend. The relative density of SiC-B_4C ceramics decreases first with the increasing of B_4C content to 60 wt.%, and then slightly increases. Meanwhile, the change of porosity of SiC-B_4C ceramics is contrary to the relative density. The decreased relative density is attributed to the poor sinterability of B_4C. The covalent bond ratio of B_4C is 93.94%, which is significantly higher than other ceramic raw materials, such as ZrO_2 (33%), Al_2O_3 (33%), SiC (88%) [1]. Because of strong high covalent bonding of B-C, low self-diffusion coefficient, absence of plasticity and high resistance to grain boundary of B_4C, therefore, the addition of B_4C restricts the interdiffusion of SiC-B_4C ceramics.

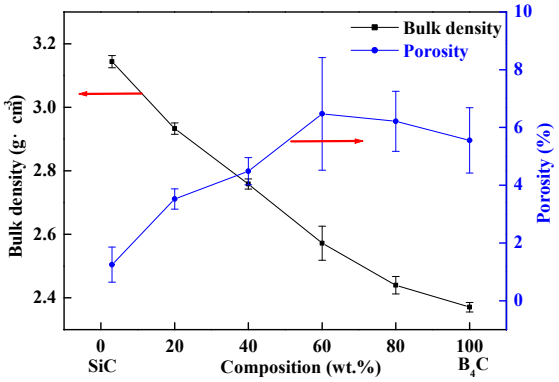

Fig. 2. Bulk density and porosity of the SiC-B_4C ceramics.

The variations in the fracture toughness and the Vickers hardness of the SiC-B_4C ceramics are shown in Fig. 3. It can be seen from Fig. 3 that the changes of both the fracture toughness and the Vickers hardness of SiC-B_4C ceramics are not obvious with the increasing of B_4C content. For the sample of MB, it shows the reduced hardness and improved fracture toughness. The fracture toughness of SiC-B_4C ceramics varies between 3.1 $MPa \cdot m^{1/2}$ and 3.7 $MPa \cdot m^{1/2}$, and the Vickers hardness of SiC-B_4C ceramics varies between 27 GPa and 33 GPa. The hardness of B_4C is higher than that of SiC, therefore, the hardness of SiC-B_4C ceramics slightly increased with the B_4C content increasing up to 40 wt.%. However, when B_4C content exceeds 40 wt.%, excessive porosity results in reduced

hardness of SiC-B_4C ceramics. On the other hand, the reason why the addition of B_4C cannot significantly increase the hardness of SiC-B_4C ceramic composites may be the poor sinterability of B_4C.

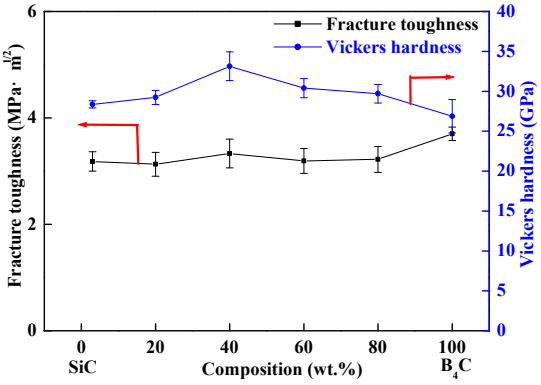

Fig. 3. Fracture toughness and Vickers hardness of the SiC-B_4C ceramics.

1.3.2. Initial surface characteristics of the SiC-B_4C ceramics after polishing

Initial surface morphologies of the SiC-B_4C ceramics after polishing are shown in Fig. 4. It can be seen from Fig. 4 that visible pores increases with the increasing B_4C content, less pores are observed in the SiC-B_4C ceramics when the content of SiC is more than that of B_4C. This observation is consistent with the porosity results in Fig. 2. Additionally, an important discovery reported in our previous work is that a relief structure with height difference of 10-15 nm between SiC and B_4C grains is formed during polishing [23], which is caused by the different hardness between SiC and B_4C, however no relief structure is observed on monolithic ceramics [24]. This relief structure will cause an significant effect on the tribological properties of SiC-B_4C ceramics, which will be discussed in detail later.

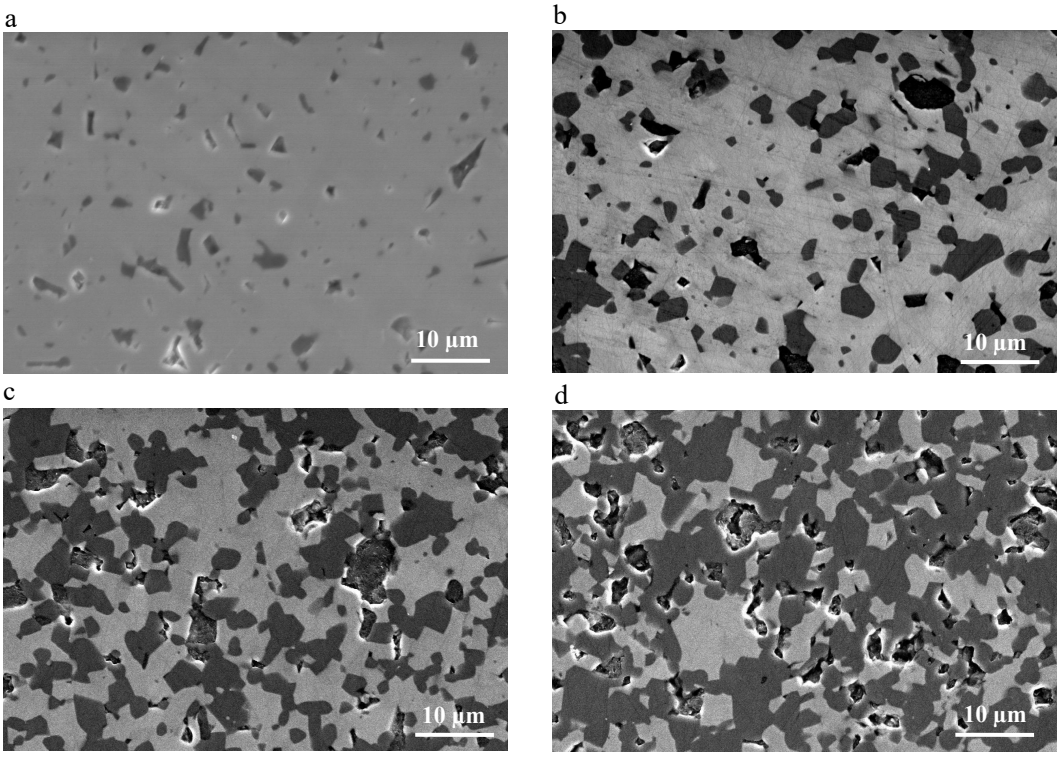

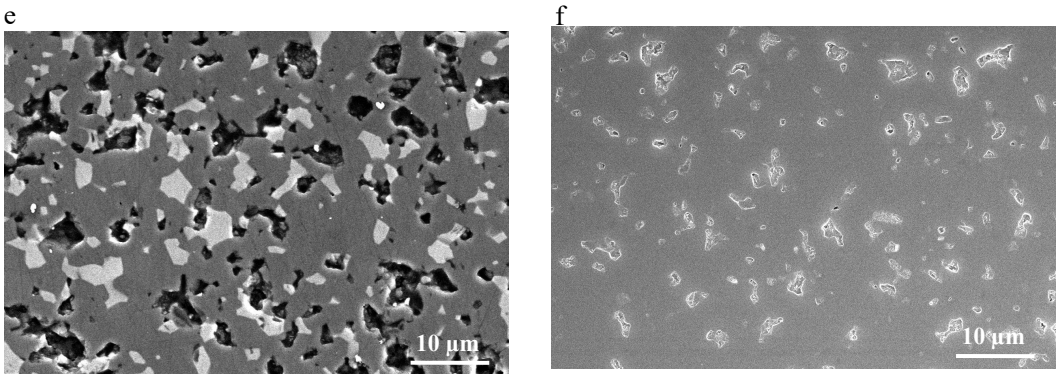

Fig. 4. Initial surface morphologies of the SiC-B_4C ceramics after polishing: (a) MS, (b) S80B20, (c) S60B40, (d) S40B60, (e) S20B80 and (f) MB.

1.3.3. Tribological properties

The steady-state friction coefficients and the wear rates of SiC-B_4C ceramics are presented in Fig. 5. Both the friction coefficient and wear rate decrease first and then increase with the increase of B_4C content. When the content of B_4C is less than 40 wt.%, friction coefficient and wear rate of SiC-B_4C ceramics decrease slowly with an increase of B_4C content. Both friction coefficient and wear rate of SiC-B_4C ceramics show minimum when the content of B_4C is 60 wt.%. When the content of B_4C is higher than 60 wt.%, friction coefficient and wear rate of SiC-B_4C ceramics increase with the increasing B_4C content.

Worn surface morphologies of the SiC-B_4C ceramics after dry sliding are shown in Fig. 6. It can be seen from Fig. 6 that no tribofilm is observed on the worn surfaces of SiC-B_4C ceramic composites, and SiC grains and B_4C grains in the SiC-B_4C ceramic composites can be seen clearly. Moreover, a certain extent of adhesive wear is observed on the worn surface of MS, and obvious scratches are also observed on the worn surface of MS. However, scratches become less and shallower on the worn surfaces of S80B20 and S20B80, and obvious scratches are not even found on the worn surface of S40B60. Further, it can be seen from Fig. 6f that the concentration of O on the worn surface of S40B60 is quite low (0.26 at%), which is considered as an impurity from raw materials. On the one hand, the oxides impurities of raw materials can be removed by the carbon additive during the sintering, and on the other hand, such a low concentration of O means neither SiC grains nor B_4C grains undergo an oxidation reaction during the friction process. Therefore, the SEM images and EDS analysis do not show evidence of triboreactions in this study. Thus, based on the experimental results, the assumption made in ref. 24 concerning the oxidation of SiC grains and B_4C grains under the same test conditions seems unacceptable. In addition, severe adhesive wear is observed on the worn surface of MB. Lörcher et al. [25] pointed out that wear caused by adhesion is greater than that caused by abrasion, which is consistent with the significant increased wear rate of MB in this study. Although the wear mechanism of self-mated B_4C ceramics reported by Li et al. [26] was abrasive wear, it is reasonably believed that wear mechanism is dependent on experimental parameters or counterpart materials [27]. Moreover, tribochemical reactions were observed to occur on the worn surface of B_4C ceramics by some scholars [19,28]. During the friction process, B_4C can react with O_2 to form B_2O_3, and then B_2O_3 may react with moisture to form smooth H_3BO_3 film, which is a well solid lubricant to reduce friction for B_4C ceramic. However, on the one hand, smooth tribofilm was not observed on the worn surface of MB in present study, and on the other hand, the friction coefficient of MB was not reduced. Therefore, tribochemical reactions are not considered to have occurred on MB under the present test conditions.

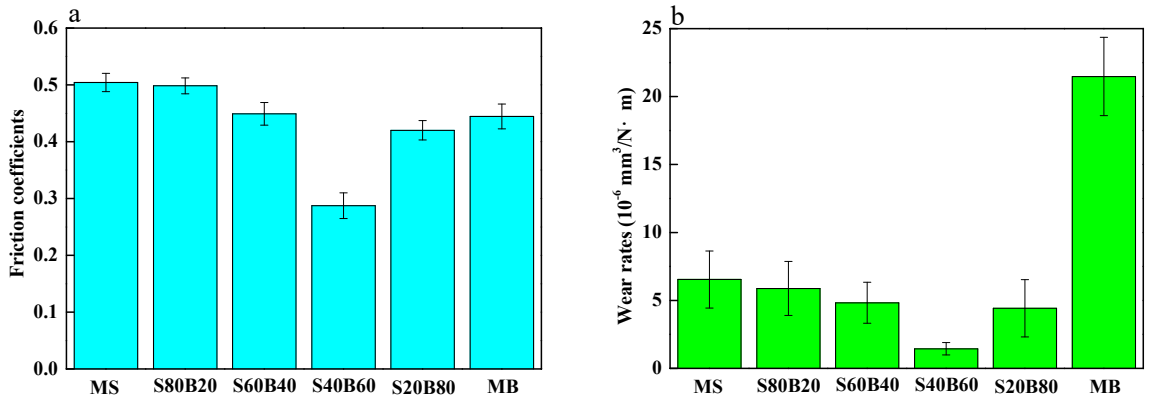

Fig. 5. Steady-state friction coefficients of the SiC-B_4C/SiC tribocouples (a) and wear rates of SiC-B_4C disks (b).

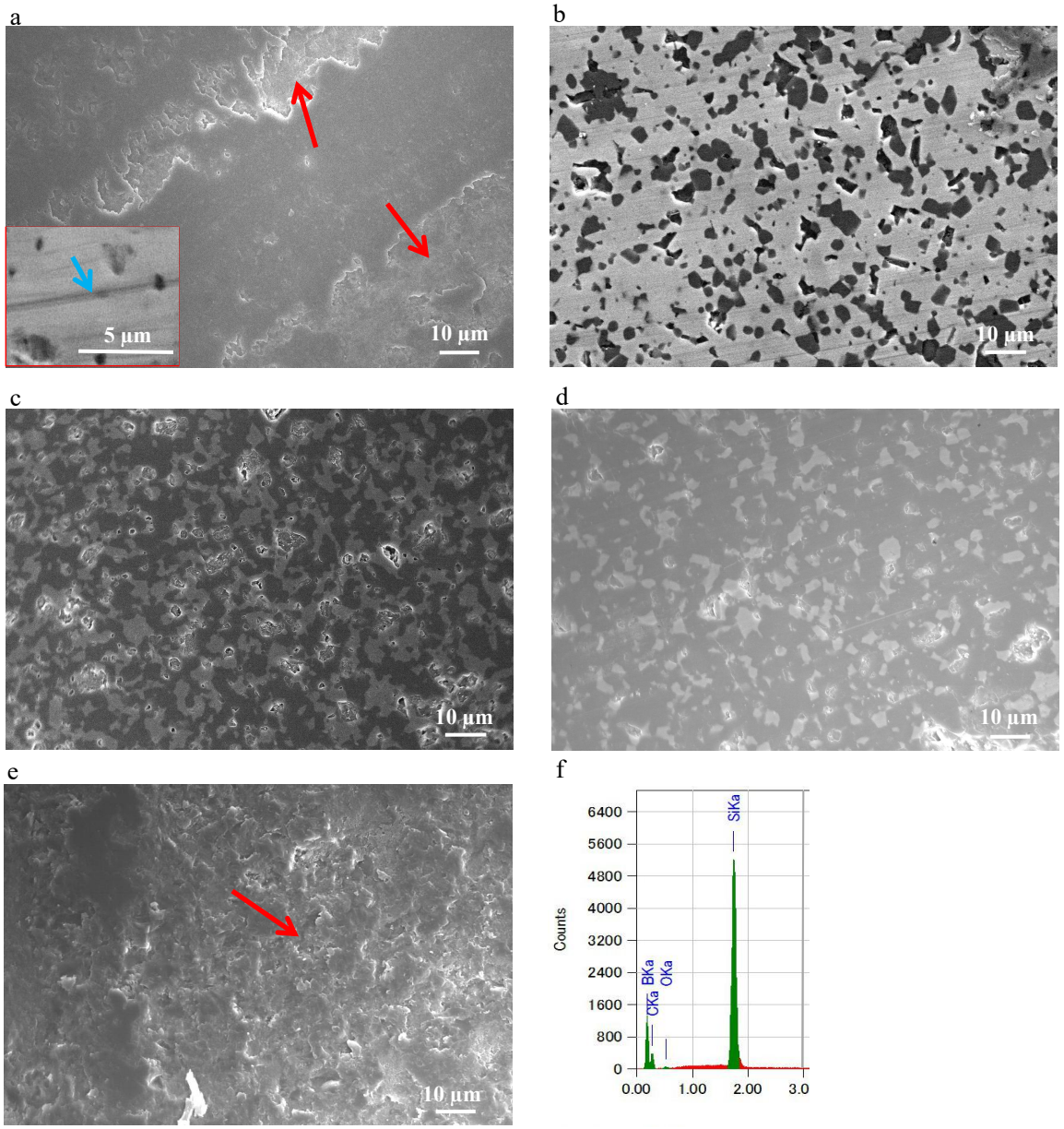

Fig. 6. Worn surface morphologies of the SiC-B_4C ceramics after dry sliding: (a) MS, (b) S80B20, (c) S40B60, (d) S20B80, (e) MB and (f) EDS analysis of Fig. 5(c).

1.3.3.1. The effect of relief structure on the worn surface on SiC-B_4C ceramic composites

Fig. 7 gives the AFM image and the data of sliding track surface profiles corresponding to the four line scans of S40B60 after dry sliding. First, the height difference of relief structure between SiC and B_4C grains is increased to 10-30 nm after dry sliding. This means the relief structure formed on the initial surface of SiC-B_4C ceramic composites after polishing not only can't disappear, but also can continue to increase the height difference during the dry sliding process. Second, it can be measured that the depth of scratch on SiC grains is 2.97 nm, whereas the depth of scratch on B_4C grains is 1.94 nm, which is shallower than that on SiC. Song et al. [29] found the protruding of B_4C particles is higher than those of original SiC particles and secondary SiC particles in the reaction-sintered SiC/B_4C composites after polishing. However, there were no experimental data to explain this phenomenon in their study, and the different protruding was simply attributed to the different hardness of different particles. The observation in this study explains this phenomenon based on the micro scale measurement that the wear rate of B_4C is lower than that of SiC, resulting in higher heights of B_4C grains. Third, this relief structure has an significant influence on the tribological performance of SiC-B_4C ceramics. A model of contact between SiC-B_4C ceramic composites and SiC counterpart is shown in Fig. 8. On the one hand, compared with MS and MB, the samples of S80B20, S60B40, S40B60 and S20B80 with relief structure have a reduced real contact area with counterparts. The reduced real contact area is favorable for decreasing adhesion effect between the SiC-B_4C ceramic composites and the counterparts, which can reduce friction and wear. Therefore, obvious adhesive wear is observed on the worn surfaces of MS and MB (Fig. 6a, e), especially on MB, while the adhesive wear is significantly reduced on the worn surfaces of S80B20 and S20B80 (Fig. 6b, d). Further, the reduced real contact area also means decreased contact points on the sliding interface, reducing the force needed to break these conjunctions. On the other hand, for MS and MB, the wear pieces can move freely and easily on the interface, resulting in the severely abrasive wear, however, for S80B20, S60B40, S40B60 and S20B80, the wear pieces formed during the dry sliding process can be fixed in the valleys of relief structure, which can reduce the abrasive wear on the interface. Therefore, obvious scratches are found on the worn surface of MS (Fig. 6a), whereas less and shallower scratches are found on the worn surfaces of SiC-B_4C ceramic composites with relief structure (Fig. 6b, c and d). More abrasive can result in increased friction and wear for MS and MB. For S20B80, the content of B_4C is more than that in S40B60, which suggests the real contact area is higher and the number of valleys which can fix wear pieces is less than that of S40B60, resulting in the increased friction and wear than those of S40B60. For S80B20 and S60B40, the content of B_4C is lower than that in S40B60, which suggests the real contact area is lower and number of valleys which can fix wear pieces is more than that of S40B60. However, the decreased real contact area means the increased real contact pressure. The positive effects of decreased adhesion effect and reduced number of abrasive from the relief structure are smaller than the negative effect of increased real contact pressure. Therefore, it can be concluded that there is a limit to the beneficial influence of decreased adhesion effect and reduced abrasive wear, and an optimum proportion of relief structure. The relief structure that can improve the tribological properties for SiC ceramics under dry sliding conditions is also observed by Murzin et al. [30,31], however, the relief surface is prepared by a laser treatment. In the present study, the relief structure is formed in situ, which can't cause large defects and contaminant on the surface. In addition, this relief structure is also found by Sang and Jin [32] in reaction-sintered SiC ceramics (SiC with 12 wt.% free Si) owing to the low hardness of free Si. However, on the one hand, the free Si is weakly bonded to the matrix, and on the other hand, the number of valleys in relief structure is fewer, thereby the tribological performance of reaction-sintered SiC ceramics is not improved due to the relief structure. In the present study, it is found that only the appropriate proportion of relief structure can significantly improve the tribological performance of ceramics. The influence of bonding between SiC grains and B_4C grains on tribological properties will be discussed in section 3.3.2.

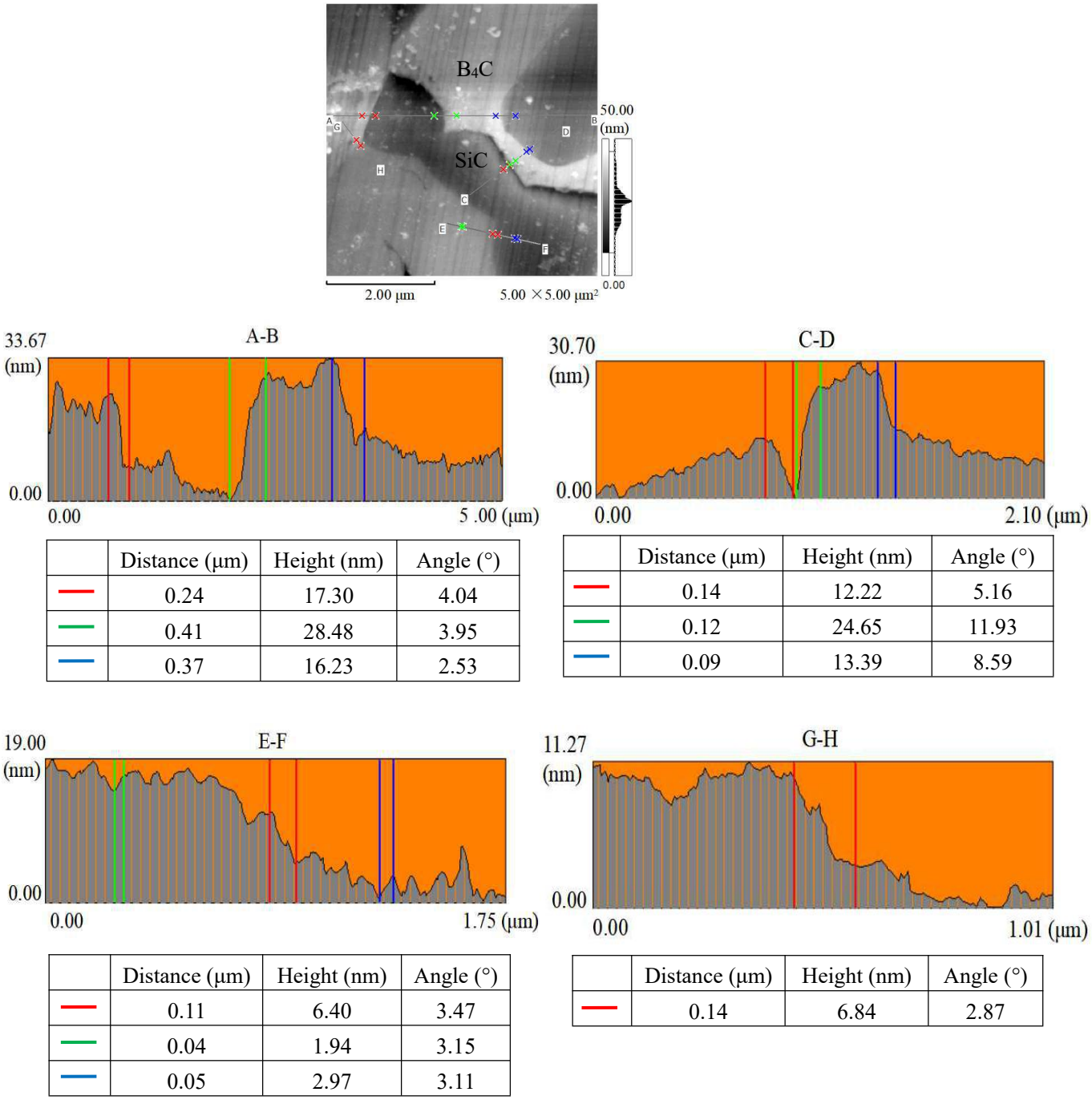

	Distance (µm)	Height (nm)	Angle (°)
	0.24	17.30	4.04
	0.41	28.48	3.95
	0.37	16.23	2.53

	Distance (µm)	Height (nm)	Angle (°)
	0.14	12.22	5.16
	0.12	24.65	11.93
	0.09	13.39	8.59

	Distance (µm)	Height (nm)	Angle (°)
	0.11	6.40	3.47
	0.04	1.94	3.15
	0.05	2.97	3.11

	Distance (µm)	Height (nm)	Angle (°)
	0.14	6.84	2.87

Fig. 7. AFM image and the data of sliding track surface profiles corresponding to the four line scans of S40B60 after dry sliding.

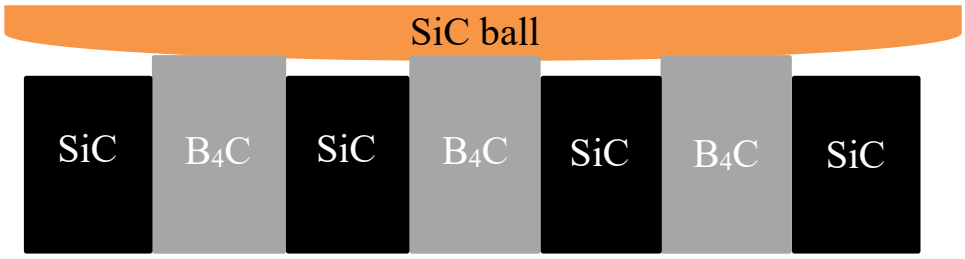

Fig. 8. Model of contact between SiC-B_4C ceramic composites and SiC counterpart.

1.3.3.2. The effect of pores on tribological properties of SiC-B_4C ceramics

From Fig. 2, we have known that the porosity of SiC-B_4C ceramics is increased with the increasing B_4C content. Borrell et al. [33] reported that the ceramics with full densification can obtain a significant reduction of wear rate, whereas lower relative density of the ceramics can lead to a noticeably mass loss during dry sliding. Turatti et al. [34] also found that porosity has an effect on wear resistance of B_4C ceramics produced by pressureless sintering, and the abrasive wear coefficient is lower for B_4C ceramics with lower porosity. In this study, however, the wear rates of samples of S80B20, S60B40, S40B60 and S20B80 with higher porosity are lower than that of MS with lower porosity. One possible reason is owing to the relief structure as mentioned in section 3.3.1. The other possible reason is attributed to the increased porosity. Firstly, compared with the pores in Fig. 4d, it can be seen from Fig. 6c that some wear pieces fills the pores, which means abrasive wear is reduced. Therefore, besides the valleys of relief structure, pores can also fix or trap some wear pieces. Secondly, the sizes of both SiC grains and B_4C grains are larger than that of pores. If grains are pulled out during the dry sliding, these grains can't be fixed or trapped in pores, which means these pores lose the function of reducing abrasive wear. However, it is found in our previous work that SiC grains and B_4C grains in the SiC-B_4C ceramic composites used in this study are firmly bonded due to the clean, no gap grain boundary observed by HRTEM, which can protect SiC grains and B_4C grains from pulling out [23]. Therefore, the wear pieces formed on the sliding interface are produced by micro-cutting, rather than pulling out of whole grains, and the cutting rates on SiC grains and on B_4C grains are different which has been observed in Fig. 7. In summary, under the condition of strong bonding between SiC grains and B_4C grains, the SiC-B_4C ceramic composites with higher porosity can fix or trap more wear pieces, which can reduce abrasive wear, improving the tribological properties for SiC-B_4C ceramic composites.

1.4. Conclusions

SiC-B_4C ceramics with different ratios of SiC to B_4C were produced by pressureless sintering. The relative density, mechanical properties, initial surface characteristics, dry sliding tribological properties against SiC balls and worn surface characteristics of the SiC-B_4C ceramics have been studied. The following results were drawn:

(1) With an increase of B_4C content, the bulk density of SiC-B_4C ceramics decreased, and the relative density of SiC-B_4C ceramics decreased first with the increasing of B_4C content to 60 wt.% and then slightly increased. Meanwhile, the change of porosity of SiC-B_4C ceramics is contrary to the relative density.
(2) The changes of both the fracture toughness and the Vickers hardness of SiC-B_4C ceramics were not obvious with the increasing of B_4C content.
(3) The friction coefficient and wear rate of the 40 wt.%SiC-60 wt.%B_4C/SiC tribocouple were minimum due to optimum proportion of relief structure between B_4C grains and SiC grains formed in situ on the surface, resulting in decreased adhesion effect and reduced abrasive wear.
(4) Pores can also fix or trap some wear pieces, reducing the abrasive wear. Under the condition of strong bonding between SiC grains and B_4C grains, the SiC-B_4C ceramic composites with higher porosity can obtain better tribological properties.
(5) The depth of scratch on B_4C grains was shallower than that on SiC grains. Hence, it is demonstrated by micro scale measurement that the wear rate of B_4C is lower than that of SiC in this study.

1.5. References

[1] W. Zhang, S. Yamashita, H. Kita. Progress in pressureless sintering of boron carbide ceramics-A review. Advances in Applied Ceramics: Structural, Functional and Bioceramics,2019,118(4):222-239.

[2] J. L. Sun, C. X. Liu, J. Tian, B. F. Feng. Erosion behavior of B_4C based ceramic nozzles by abrasive air-jet. Ceramics International,2012,38(8):6599-6605.

[3] F. Rubino, M. Pisaturo, A. Senatore, P. Carlone, T. S. Sudarshan. Tribological characterization of SiC and B_4C manufactured by plasma pressure compaction. Journal of Materials Engineering and Performance,2017,26(11):5648-5659.

[4] F. Findik. Latest progress on tribological properties of industrial materials. Materials & Design,2014,57:218-244.

[5] C. X. Liu, J. L. Sun. Erosion behaviour of B_4C-based ceramic composites. Ceramics International,2010,36(4):1297-1302.

[6] H. Y. Zhu, Y. R. Niu, C. C. Lin, L. P. Huang, H. Ji, X. B. Zheng. Microstructures and tribological properties of vacuum plasma sprayed B_4C-Ni composite coatings. Ceramics International,2013,39(1):101-110.

[7] E. Ciudad, O. Borrero-López, F. Rodríguez-Rojas, A. L. Ortiz, F. Guiberteau. Effect of intergranular phase chemistry on the sliding-wear resistance of pressureless liquid-phase-sintered α-SiC. Journal of the European Ceramic Society,2012,32(2):511-516.

[8] S. Lafon-Placette, K. Delbé, J. Denape, M. Ferrato. Tribological characterization of silicon carbide and carbon materials. Journal of the European Ceramic Society,2015,35(4):1147-1159.

[9] U. Soy, A. Demir, F. Findik. Friction and wear behaviors of Al-SiC-B_4C composites produced by pressure infiltration method. Industrial Lubrication and Tribology,2011,63(5):387-393.

[10] S. K. Sharma, B. V. M. Kumar, Y. W. Kim. Tribology of WC reinforced SiC ceramics: Influence of counterbody. Friction,2019,7(2):129-142.

[11] W. Zhang, S. Yamashita, H. Kita. Progress in tribological research of SiC ceramics in unlubricated sliding-A review. Materials & Design,2020,190:108528.

[12] S. Gupta, S. K. Sharma, B. V. M. Kumar, Y. W. Kim. Tribological characteristics of SiC ceramics sintered with a small amount of yttria. Ceramics International,2015,41(10):14780-14789.

[13] X. Q. Li, Y. M. Gao, W. Pan, Z. C. Zhong, L. C. Song, W. Chen, Q. X. Yang. Effect of hBN content on the friction and wear characteristics of B_4C-hBN ceramic composites under dry sliding condition. Ceramics International,2015,41(3):3918-3926.

[14] X. Q. Li, Y. M. Gao, Q. X. Yang, W. Pan, Y. F. Li, Z. C. Zhong, L. C. Song. Evaluation of tribological behavior of B_4C-hBN ceramic composites under water-lubricated condition. Ceramics International,2015,41(6):7387-7393.

[15] X. Q. Li, Y. M. Gao, W. Pan, X. Wang, L. C. Song, Z. C. Zhong, S. S. Wu. Fabrication and characterization of B_4C-based ceramic composites with different mass fractions of hexagonal boron nitride. Ceramics International,2015,41(1):27-36.

[16] A. Motealleh, A. L. Ortiz, O. Borrero-López, F. Guiberteau. Effect of hexagonal-BN additions on the sliding-wear resistance of fine-grained α-SiC densified with $Y_3Al_5O_{12}$ liquid phase by spark-plasma sintering. Journal of the European Ceramic Society,2014,34(3):565-574.

[17] R. Sedlák, A. Kovalčíková, J. Balko, P. Rutkowski, A. Dubiel, D. Zientara, V. Girman, E. Múdra, J. Dusza. Effect of graphene platelets on tribological properties of boron carbide ceramic composites. International Journal of Refractory Metals & Hard Materials,2017,65:57-63.

[18] J. Llorente, B. Román-Manso, P. Miranzo, M. Belmonte. Tribological performance under dry sliding conditions of graphene/silicon carbide composites. Journal of the European Ceramic Society,2016,36(3):429-435.

[19] R. Alexander, K.V. Ravikanth, R. D. Bedse, T. S. R. Ch. Murthy, K. Dasgupta. Effect of carbon fiber on the tribo-mechanical properties of boron carbide: Comparison with carbon nanotube reinforcement. International Journal of Refractory Metals & Hard Materials,2019,85:105055.

[20] H. L. Tang, X. R. Zeng, X. B. Xiong, L. Li, J. Z. Zou. Mechanical and tribological properties of short-fiber-reinforced SiC composites. Tribology International,2009,42(6):823-827.

[21] V. M. Candelario, R. Moreno, F. Guiberteau, A. L. Ortiz. Enhancing the sliding-wear resistance of SiC nanostructured ceramics by adding carbon nanotubes. Journal of the European Ceramic Society,2016,36(13):3083-3089.

[22] O. Borrero-López, A. L. Ortiz, F. Guiberteau, N. P. Padture. Microstructural design of sliding-wear-resistant liquid-phase-sintered SiC:An overview. Journal of the European Ceramic Society,2007,27(11):3351-3357.

[23] W. Zhang, S. Yamashita, T. Kumazawa, F. Ozeki, H. Hyuga, W. Norimatsu, H. Kita. A study on formation mechanisms of relief structure formed in situ on the surface of ceramics. Ceramics International,2019,45(17):23143-23148.

[24] W. Zhang, S. Yamashita, T. Kumazawa, F. Ozeki, H. Hyuga, H. Kita. Effect of nanorelief structure formed in situ on tribological properties of ceramics in dry sliding. Ceramics International,2019,45(11):13818-13824.

[25] R. Lörcher, R. Telle, G. Petzow. Influence of mechanical and tribochemical properties on the wear behaviour of B_4C-TiB_2-W_2B_5 composites. Materials Science and Engineering A,1988,105-106:117-123.

[26] X. Q. Li, Y. M. Gao, S. Z. Wei, Q. X. Yang, Z. C. Zhong. Dry sliding tribological properties of self-mated couples of B_4C-hBN ceramic composites. Ceramics International,2017,43(1):162-166.

[27] A. Kovalčíková, P. Kurek, J. Balko, J. Dusza, P. Šajgalík, M. Mihaliková. Effect of the counterpart material on wear characteristics of silicon carbide ceramics. International Journal of Refractory Metals and Hard Materials:2014,44: 12-18.

[28] J. K. Sonber, P. K. Limaye, T. S. R. Ch. Murthy, K. Sairam, A. Nagaraj, N. L. Soni, R. J. Patel, J. K. Chakravartty. Tribological properties of boron carbide in sliding against WC ball. International Journal of Refractory Metals & Hard Materials,2015,51:110-117.

[29] S. C. Song, C. G. Bao, K. K. Wang. Studies of microstructure and mechanical properties of SiC/B_4C composites based on reaction sintering. China Sciencepaper,2017,12(4):425-429. (in Chinese)

[30] S. P. Murzin, V. B. Balyakin, A. A. Melnikov, N. N. Vasiliev, P. I. Lichtner. Determining ways of improving the tribological properties of the silicon carbide ceramic using a pulse-periodic laser treatment. Computer Optics,2015,39(1):64-69.

[31] S. P. Murzin, V. B. Balyakin. Microstructuring the surface of silicon carbide ceramic by laser action for reducing friction losses in rolling bearings. Optics & Laser Technology,2017,88:96-98.

[32] K. Z. Sang, Z. H. Jin. Unlubricated friction of reaction-sintered silicon carbide and its composite with nickel. Wear,2000,246(1-2):34-39.

[33] A. Borrell, R. Torrecillas, V. G. Rocha, A. Fernández, V. Bonache, M. D. Salvador. Effect of CNFs content on the tribological behaviour of spark plasma sintering ceramic-CNFs composites.Wear,2012,274-275:94-99.

[34] A. M. Turatti, A. S. Pereira. Wear resistant boron carbide compacts produced by pressureless sintering. Ceramics International,2017,43(11):7970-7977.

Chapter 2
A study on formation mechanisms of relief structure formed in situ on the surface of ceramics

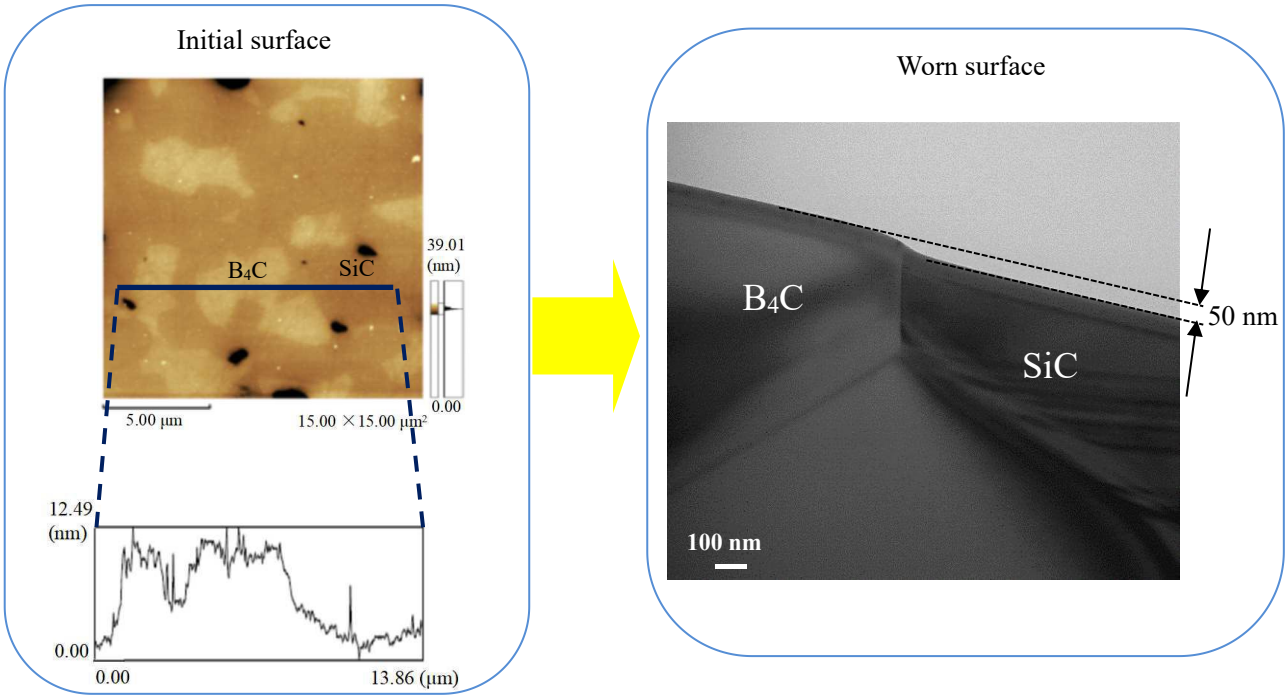

The formation mechanisms of relief structure formed in situ on the surface of B_4C-SiC ceramics were studied. The hardness difference between B_4C and SiC is one of the formation conditions of relief structure. SiC grains are subjected to a preferential wearing owing to their lower hardness as compared to B_4C grains, resulting in the difference of wear rates between B_4C grains and SiC grains. Clean, no gap grain boundary in the B_4C-SiC ceramics, which can make B_4C grains and SiC grains bond firmly protecting them from pulling out, is another formation condition of relief structure.

Contents

2.1. Introduction

The relief structure of the materials has been demonstrated to be effective in improving the tribological properties of materials under both unlubricated friction condition and lubricated friction condition [1-5]. In recent years, laser surface texturing is widely reported to be used to fabricate relief structure for both metals and ceramics [6-10]. The relief structure produced by laser can enhance tribological performance of materials, however, laser route still has some unsatisfactory aspects, such as defects induced by processing, complex preparation process, a gradually disappeared relief structure during wear, etc. In our previous work, both lower wear rate and lower friction coefficient were observed for the B_4C-SiC ceramics, which were ascribed to the relief structure with nanometer size (nanorelief) formed in situ on the surface [11]. However, the formation mechanisms of relief structure formed in situ were not reported in detail.

The aim of this paper is to study the formation conditions and mechanisms of nanorelief structure formed in situ in detail. Nanorelief is defined as that in which the crater depth ranges from 10 nm to 50 nm [11]. For that purpose, we studied the effect of polishing time on nanorelief structure on the ceramic surfaces and studied grain boundaries of the composite ceramics. The nanorelief structures on the ceramic surfaces after different polishing time were measured by AFM (atomic force microscopy). Further, grain boundaries of the composite ceramics were observed by TEM (transmission electron microscope). Ultimately, the aim is to provide theoretical basis for the microstructural design of composite ceramics with relief structure formed in situ.

2.2. Experimental procedure

Commercial high-purity 60wt% B_4C (0.8 μm; HS grade, H.C.Starch GmbH & Co., Germany) powder and submicrometric 40wt% SiC (0.3 μm; Yakushima Denko, Japan) powder were used as raw materials, and 3wt% carbon black (#4000B; Mitsubishi Chemical Corporation, Japan) was used as a sintering additive. The powder blend was pressed into blocks, which were subsequently cold-isostatically pressed. The blocks were sintered at 2300 ℃ for 16 h in flowing argon atmosphere.

After cutting to nominal dimensions of 29 mm × 26 mm × 4.5 mm, the specimens used in this study were subjected to grind. Then, the specimens were polished using diamond slurry with diamond size of 1 μm for 10 min, 20 min, 30 min, 45 min and 60 min, respectively. XRD (Rigaku, Ultima IV) was used to identify phase composition of the B_4C-SiC ceramics. Before and after polishing, SEM (JEOL, JSM-7500F) was used to observe surface morphology of the B_4C-SiC ceramics. AFM was used to observe nanorelief structures of the B_4C-SiC ceramics polished by different time. Then a pin-on-disk tribometer was used to investigate the change of nanorelief structure in dry sliding process. Mating balls of SiC with the radius of 4.75 mm were used for the tests. The dry sliding tests with the distance of 100 m were conducted under a load of 5 N and at a speed of 0.1 m/s in ambient air with the RH 40-50% at room temperature. TEM (HITACHI, H-800) was used to observe cross-sectional worn surface of the B_4C-SiC ceramics, and FIB equipment (HITACHI, FB-2100) was used to prepare samples. TEM (JEOL, JEM-2010F) was used to observe B_4C-SiC grain boundaries to determine the presence of other phases at grain boundaries, and ion milling method was used to prepare samples.

2.3. Results and discussion

Fig. 1 shows the XRD spectrum of the B_4C-SiC ceramics. It can be seen that the phase composition of the B_4C-SiC ceramics are B_4C, SiC and C, and B_4C and SiC are major phases. Fig. 2 shows the backscattered electron (BSE) images of B_4C-SiC ceramic surface before and after polishing. It can be seen that there are pores in the

ceramics because the B_4C-SiC ceramics were prepared by pressureless sintering and the relative density of the ceramics was 97.1%. Compared with the surface topography of the B_4C-SiC ceramics before polishing, smoother surface is observed for the B_4C-SiC ceramics after polishing. Fig. 3 shows typical AFM images and surface profiles of the B_4C-SiC ceramics polished by different time. Fig. 4 shows height difference between B_4C grains and SiC grains as a function of the polishing time. Our previous study showed that the bright areas in Fig. 3 are B_4C grains, the dark areas are SiC grains and the black areas are pores [11]. From Fig. 3 and Fig. 4, it can be observed that the height difference between B_4C grains and SiC grains increased gradually with an increase in polishing time up to 60 min. It is known that the hardness of B_4C which is the third hardest material known in the world is approximately 37 GPa [12], whereas the hardness of SiC is approximately 24 GPa. Because the hardness of SiC is lower than that of B_4C, thus, SiC grains are subjected to a preferential wearing by free diamond particles during the polishing process. The wear rate of SiC grains is higher than that of B_4C grains, therefore, the height difference between B_4C grains and SiC grains increased gradually with the increase of polishing time. The surface roughness after polishing for 60 min is approximately 0.02 μm. After polishing, dry sliding tests were used to investigate the change of nanorelief structure in sliding process.

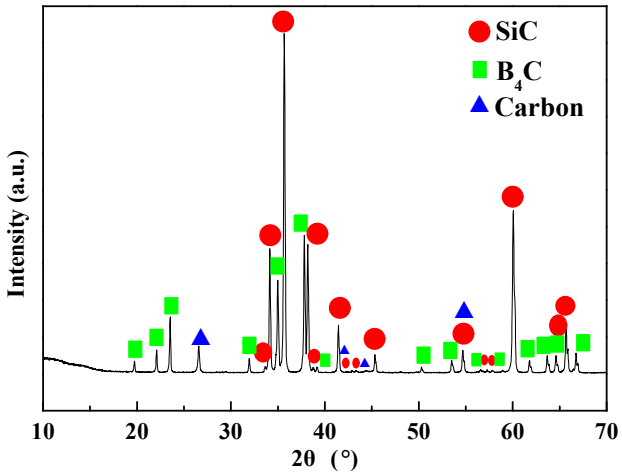

Fig. 1. XRD spectrum of the B_4C-SiC ceramics.

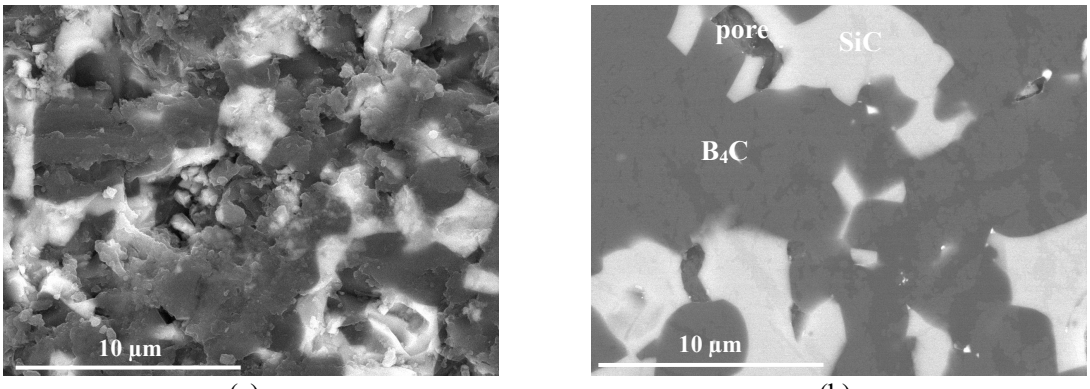

(a) (b)

Fig. 2. BSE images of B_4C-SiC ceramic surface: (a) before polishing and (b) after polishing.

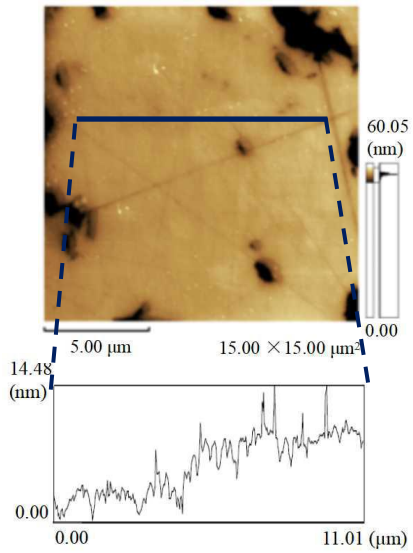
60.05
(nm)
0.00
5.00 μm
15.00 ×15.00 μm²
14.48
(nm)
0.00
0.00
11.01 (μm)

(a)

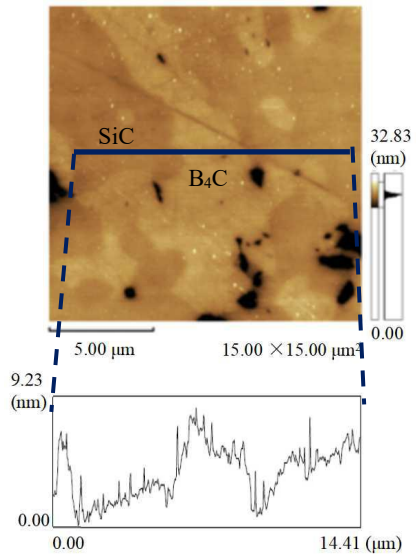
SiC
B4C
32.83
(nm)
0.00
5.00 μm
15.00 ×15.00 μm²
9.23
(nm)
0.00
0.00
14.41 (μm)

(b)

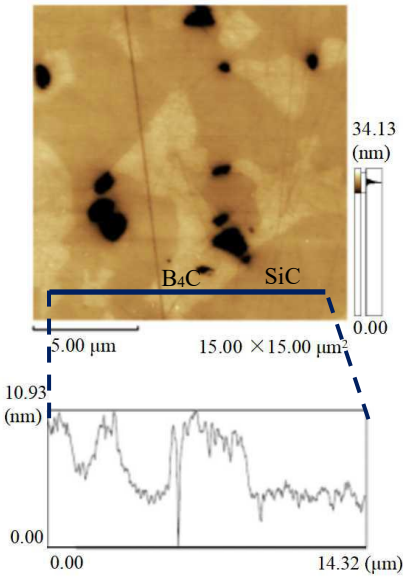
B4C
SiC
34.13
(nm)
0.00
5.00 μm
15.00 ×15.00 μm²
10.93
(nm)
0.00
0.00
14.32 (μm)

(c)

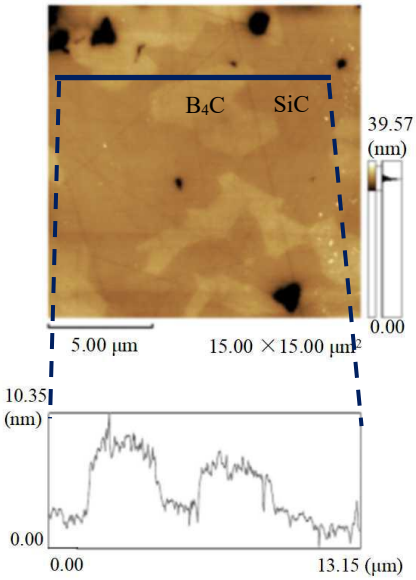
B4C
SiC
39.57
(nm)
0.00
5.00 μm
15.00 ×15.00 μm²
10.35
(nm)
0.00
0.00
13.15 (μm)

(d)

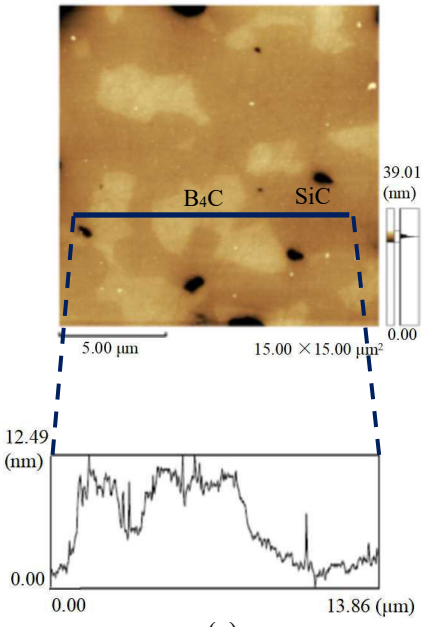
B4C
SiC
39.01
(nm)
0.00
5.00 μm
15.00 ×15.00 μm²
12.49
(nm)
0.00
0.00
13.86 (μm)

(e)

Fig. 3. Typical AFM images and surface profiles of B_4C-SiC ceramics polished by different time: (a) 10 min, (b) 20 min, (c) 30 min, (d) 45 min and (e) 60 min.

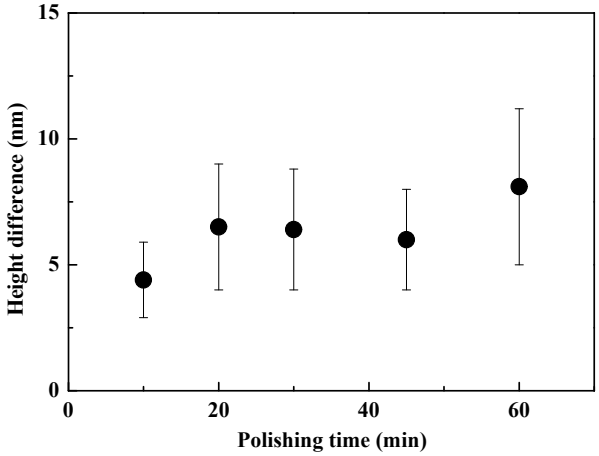

Fig. 4. Height difference between B_4C grains and SiC grains as a function of the polishing time.

Fig. 5 shows cross-sectional worn surface of the B_4C-SiC ceramics after dry sliding. It can be seen that the difference in height between B_4C grains and SiC grains continues to increase up to approximately 50 nm during dry sliding. This phenomenon also can be attributed to the different hardness between B_4C grains and SiC grains. The debris composed of B_4C and SiC was formed during the dry sliding. Similarly, SiC grains in the B_4C-SiC ceramics are further preferentially worn by the wear debirs. Meanwhile, the existence of nanorelief structure after sliding also means nanorelief structure formed in situ cannot disappear during the dry sliding process, which is an outstanding advantage compared with the relief structure fabricated by laser route. In summary, the hardness difference between B_4C grains and SiC grains is one of the reasons for the formation of nanorelief structure of B_4C-SiC ceramics.

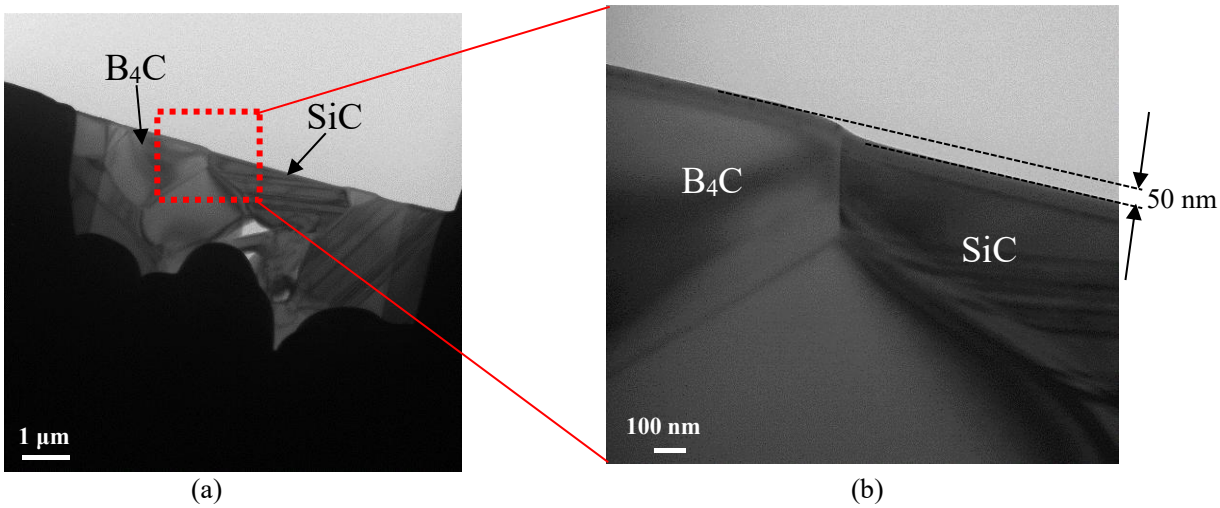

(a) (b)

Fig. 5. TEM images of B_4C-SiC ceramics: (a) cross-sectional worn surface; (b) high magnification.

Fig. 6 and Fig. 7 show the grain boundaries of the sintered B_4C-SiC ceramics in different regions and electron diffraction patterns of B_4C and SiC. As much as we can observe, no gap is observed between B_4C grains and SiC grains. The crystallinity for both SiC and B_4C is good because no hollow pattern is observed in Fig. 6 and Fig. 7. It can be seen from Fig. 6 that the interplanar spacing between B_4C lattice planes and SiC lattice planes is matching, thereby resulting in lattice planes of B_4C crystal directly connect with that of SiC crystal without disordered layer, which means the lattice planes of B_4C and lattice planes of SiC are coherent. Further, the interplanar spacing of

[$\bar{2}$021] in B_4C is the same as that in B_4C near the grain boundary, which means there are no defects at grain boundaries. As a result, clean, no gap grain boundary is formed in the B_4C-SiC ceramics. It is reported that grain boundary phase has an important effect on the tribological performance of ceramics. For monolithic ceramics, Gupta et al. [13] reported that SiC ceramics with different amount of sintering additive of Y_2O_3 have different wear resistant properties. The wear rate of SiC ceramics decreased with an decrease in Y_2O_3 content. Relative large amount of Y_2O_3 rich weak amorphous phase is observed at the grain boundaries when the additive amount of Y_2O_3 is 3wt%, which causes easy pull-out of SiC grains, leading to an increased wear rate. The pull-out and fracture of SiC grains are dominant when SiC ceramics has large amount of amorphous phase at the grain boundary. In contrast, transgranular fracture is observed in the SiC ceramics when the additive amount of Y_2O_3 is 0.2wt% because there is only less secondary phase at the grain boundaries, resulting to an improved wear resistance. Kumar et al. [14] also suggested that amorphous intergranular phase of Y-O-Si-C is detected in the SiC ceramics with sintering additives of AlN+Y_2O_3, whereas the clean grain boundary is found in the SiC ceramics with sintering additives of AlN+Sc_2O_3. Easier nucleation and propagation of microcracks along weak amorphous grain boundaries are the reasons that the SiC ceramics with amorphous intergranular phase has a lower wear resistance. For composite ceramics, Kita et al. [15,16] reported that the addition of ZnO (10wt%) can reduce the coefficient of friction of Al_2O_3 ceramics, however, $ZnAl_2O_4$ phase formed in situ during sintering was worn preferentially and pulled out during lubricated sliding, resulting in an increased wear. Although there is a difference in hardness between Al_2O_3 (Mohs hardness of 9) and $ZnAl_2O_4$ (Mohs hardness of 6.5), the bonding strength between Al_2O_3 grains and $ZnAl_2O_4$ grains is weak, leading to the pull-out of $ZnAl_2O_4$ grains. Therefore, relief structure is expected to be not formed under this condition. Further, the phenomenon of grain pull-out is also observed in SiC-WC composite ceramics [17,18], SiC-graphite nanodispersoids composite ceramics [19] and reaction-sintered SiC-B_4C composite ceramics [20] during sliding or polishing. In regards to the B_4C-SiC composite ceramics prepared in this experiment, the grain boundaries of B_4C-SiC composite ceramics are clean, which suggests that direct contact between B_4C grains and SiC grains occurred and there is no amorphous phase at the grain boundary. This microstructure makes it difficult for SiC grains or B_4C grains to be pulled out of the matrix during the sliding. If SiC grains or B_4C grains are pulled out from the matrix during sliding, on the one hand the relief structure cannot be maintained, and on the other hand the wear rate of the ceramics would be increased. The fact was, however, both the wear rate and friction coefficient of B_4C-SiC ceramics were lower than those of monolithic SiC ceramics, as we observed in the literature [11]. This means the bond between SiC grains and B_4C grains is very strong. In addition, it can be seen from Fig. 7 that the difference of interplanar spacing between B_4C lattice planes and SiC lattice planes is also observed. However, the thickness of the disordered layer caused because of different interplanar spacing between B_4C lattice planes and SiC lattice planes at the grain boundary is less than 1 nm. The disordered layer at the grain boundary is too thin to affect the bonding strength between B_4C grains and SiC grains too much. Therefore, clean, no gap grain boundary is another, the most important reason for the formation of nanorelief structure of B_4C-SiC cermaics.

A schematic diagram of the nanorelief structure formed on the surface of the B_4C-SiC composite ceramics by the in-situ method is shown in Fig. 8. Diamond particles are fixed on the surface of the grinding wheel used for grinding; thus, B_4C particles and SiC particles are ground uniformly together because the hardness of diamond is greater than those of both SiC and B_4C. Further, debris formed during this period is immediately removed from the contact interface. No nanorelief structure is expected to form during this period. However, during polishing under a load, SiC particles, which have lower hardness, are preferentially worn by free diamond particles existing in the slurry, which is the reason for the formation of nanorelief structure. The depth of the nanorelief structure formed during the polishing period is approximately 10 nm. When the B_4C-SiC composite ceramics are slid against their counterpart, SiC particles are further worn out by the mixed wear particles of B_4C and SiC; therefore, the depth of

the nanorelief structure formed during sliding is increased to 30 to 50 nm.

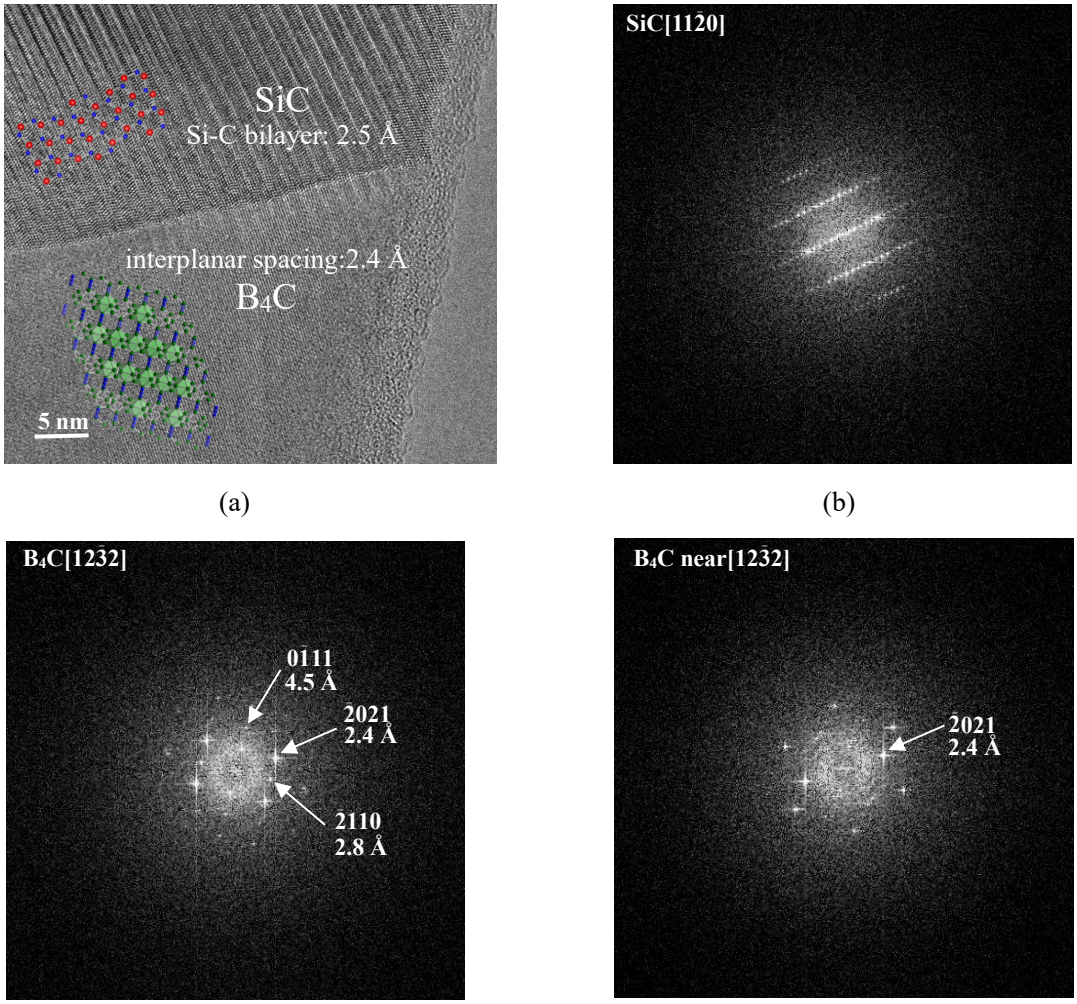

(a) (b)

(c) (d)

Fig. 6. TEM image of B_4C-SiC ceramics (a) as well as electron diffraction patterns and interplanar spacing in SiC (b), B_4C (c) and B_4C near the grain boundary (d).

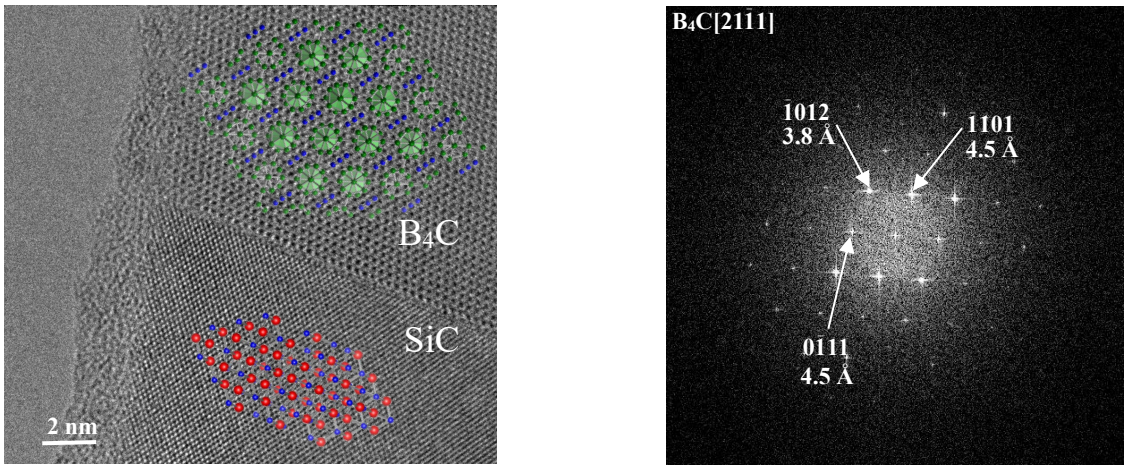

(a) (b)

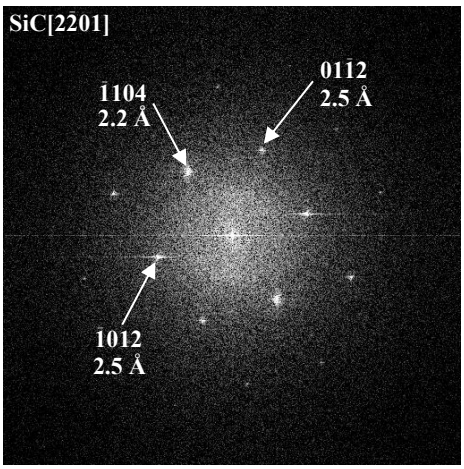

(c)

Fig. 7. TEM image of B_4C-SiC ceramics (a) as well as electron diffraction patterns and interplanar spacing in SiC (b), and B_4C (c).

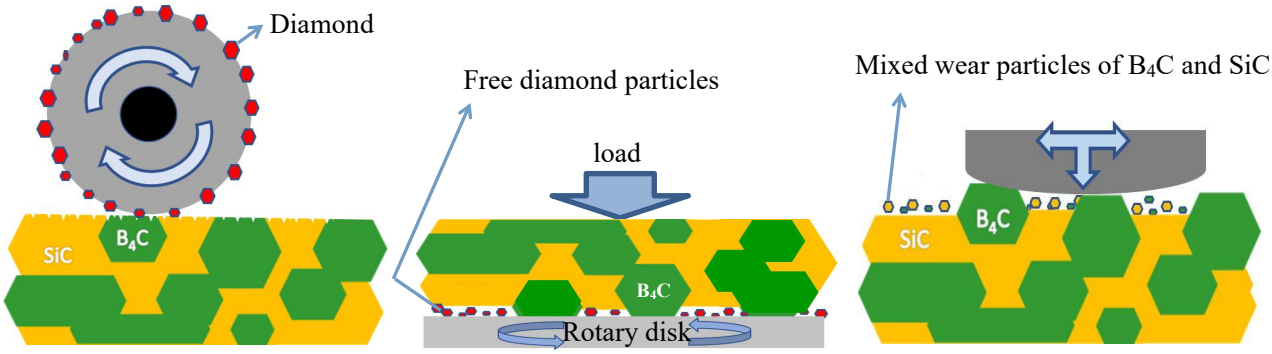

(a) (b) (c)

Fig. 8. Schematic diagram of relief structure formed on B_4C-SiC ceramics during (a) grinding, (b) polishing, and (c) sliding.

2.4. Conclusions

The results presented in this work show the formation mechanisms of relief structure formed in situ on the B_4C-SiC ceramics. Firstly, the hardness difference between B_4C grains and SiC grains is one of the formation conditions of nanorelief structure of B_4C-SiC ceramics. Because the wear rates between B_4C grains and SiC grains are different, SiC grains are subjected to a preferential wearing by free diamond particles during the polishing process and by wear debirs during the dry sliding process. Furthermore, nanorelief structure formed in situ during polishing process cannot disappear during dry sliding process. Secondly, clean, no gap grain boundary in the B_4C-SiC ceramics is another formation condition, which is the most important factor, for nanorelief structure on B_4C-SiC ceramics. Finally, the results obtained in this work give some hints for further investigation of relief structure formed in situ. Whether the relief structure will also be produced under the conditions that other two ceramic materials with different hardness as well as clean, no gap grain boundaries formed after sintering, which needs to be investigated.

2.5. References

[1] K. W. Guo. Effect of sliding speed on tribological characteristics of different surface textures on AISI O1 steel irradiated by Nd:YAG pulsed laser. Ironmaking & Steelmaking,2009,36(1):63-74.

[2] H. Yamakiri, S. Sasaki, T. Kurita, N. Kasashima. Effects of laser surface texturing on friction behavior of silicon nitride under lubrication with water. Tribology International,2011,44(5):579-584.

[3] T. Roch, F. Klein, K. Guenther, A. Roch, T. Mühl, A. Lasagni. Laser interference induced nano-crystallized surface swellings of amorphous carbon for advanced micro tribology. Materials Research Express,2014,1(3):035042.

[4] T. Shimizu, T. Kakegawa, M. Yang. Micro-texturing of DLC thin film coatings and its tribological performance under dry sliding friction for microforming operation. Procedia Engineering,2014,81:1884-1889.

[5] R. Capozza, N. Pugno. Effect of surface grooves on the static friction of an elastic slider. Tribology Letters,2015,58(3):35-40.

[6] S.I. Dolgaev, A.A. Lyalin, G.A. Shafeev, V.V. Voronov. Fast etching and metallization of SiC ceramics with copper-vapor-laser radiation. Applied Physics A (Materials Science Processing),1996,63(1):75-79.

[7] G.A. Shafeev, E.D. Obraztsova, S.M. Pimenov. Laser-assisted etching of diamonds in air and in liquid media. Applied Physics A,1997,65(1):29-32.

[8] A. Blatter, M. Maillat, S.M. Pimenov, G.A. Shafeevc, A.V. Simakin. Lubricated friction of laser micro-patterned sapphire flats. Tribology Letters,1998,4(3-4):237-241.

[9] X. L. Wang, K. Adachi, K. Otsuka, K. Kato. Optimization of the surface texture for silicon carbide sliding in water. Applied Surface Science,2006,253(3):1282-1286.

[10] D. Z. Segu, S. G. Choi, J. H. Choi, S. S. Kim. The effect of multi-scale laser texutured surface on lubrication regime. Applied Surface Science,2013,270(14):58-63.

[11] W. Zhang, S. Yamashita, T. Kumazawa, F. Ozeki, H. Hyuga, H. Kita. Effect of nanorelief structure formed in situ on tribological properties of ceramics in dry sliding. Ceramics International,2019,45(11):13818-13824.

[12] W. Zhang, S. Yamashita, H. Kita. Progress in pressureless sintering of boron carbide ceramics- a review. Advances in Applied Ceramics,2019,118(4):222-239.

[13] S. Gupta, S. K. Sharma, B. V. M. Kumar, Y. W. Kim. Tribological characteristics of SiC ceramics sintered with a small amount of yttria. Ceramics International,2015,41(10):14780-14789.

[14] B. V. M. Kumar, Y. W. Kim, D. S. Lim, W. S. Seo. Influence of small amount of sintering additives on unlubricated sliding wear properties of SiC ceramics. Ceramics International,2011,37(8):3599-3608.

[15] H. Kita, H. Hyuga, K. Yoshida, K. Osumi, T. Iizuka. Enhancement of hydrophilic properties of alumina-based ceramics. Journal of the Ceramic Society of Japan,2006,114(4):347-350.

[16] H. Kita, K. Osumi, T. Iizuka, M. Fukushima, K. Yoshida, H. Hyuga. Changes in microstructure and properties of ZnO-Added Al_2O_3 upon sliding. Journal of the Ceramic Society of Japan,2006,114(7):599-602.

[17] S. K. Sharma, B. V. M. Kumar, Y. W. Kim. Effect of WC addition on sliding wear behavior of SiC ceramics. Ceramics International,2015,41(3):3427-3437.

[18] S. K. Sharma, B. V. M. Kumar, K. Y. Lim, Y. W. Kim, S. K. Nath. Erosion behavior of SiC-WC composites. Ceramics International,2014,40(5):6829-6839.

[19] V. M. Candelario, O. Borrero-López, F. Guiberteau, R. Moreno, A. L. Ortiz. Sliding-wear resistance of liquid-phase-sintered SiC containing graphite nanodispersoids. Journal of the European Ceramic Society,2014,34(10):2597-2602.

[20] S. C. Song, C. G. Bao, K. K. Wang. Studies of microstructure and mechanical properties of SiC/B_4C composites based on reaction sintering. China Sciencepaper,2017,12(4):425-429.

Chapter 3
Influence of surface roughness parameters and surface morphology on friction performance of ceramics

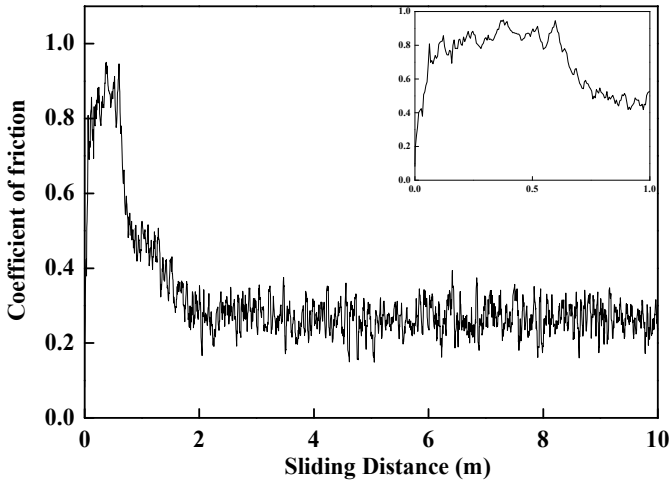

Influence of both surface roughness and surface morphology on frictional behavior of ceramics during run-in period under dry sliding was investigated simultaneously. Similar average surface roughness (Ra=0.01~0.02 μm) was produced for the three ceramics: monolithic boron carbide ceramics, boron carbide-silicon carbide composite ceramics and monolithic silicon carbide ceramics. Surface roughness parameters show some influence on friction processes, however, surface morphology is considered as a more important competitive factor. Lower friction coefficient during run-in period and shorter sliding distance up to the steady state condition were observed for the B_4C-SiC composite ceramics, which has a different surface morphology from those of monolithic B_4C ceramics and monolithic SiC ceramics.

Contents

3.1. Introduction

Advanced structural ceramics as tribo-elements get more and more extensive attention, such SiC ceramics, B_4C ceramics, Si_3N_4 ceramics, Al_2O_3 ceramics, ZrO_2 ceramics and some composite ceramics [1-8]. Therefore, studies on friction property between the two mating surfaces are becoming more and more widely. It is well known that two significant surface characteristics are surface roughness and surface morphology. Initial surface roughness has a significant effect on frictional behavior at the friction interface [9]. Meanwhile, surface morphology also has an important influence on friction processes [10]. It is widely reported that higher initial surface roughness can cause lower friction coefficient and lower initial surface roughness results in higher coefficient of friction [11]. At present, most of research on the influence of surface roughness parameters on tribological properties is focus on average surface roughness (Ra). In fact, other surface roughness parameters also have effects on tribological properties of ceramics. On the other hand, in particular, there are some differences for the surface morphology between composite ceramics and monolithic ceramics after polishing before application. For example, nanorelief structure is found on the surface of B_4C-SiC composite ceramics [12]. Different surface morphologies also have different effects on frictional behavior.

Average surface roughness (R_a) is defined as arithmetic mean of the absolute values of vertical deviation from the mean line through the profile. Although R_a can describe height variations well, other information, such as the shapes, slopes, and sizes of the asperities and the regularity and frequency of their occurrence, can't be provided. It is possible that the profiles have the same R_a values, but different frequencies or different shapes. Thus, surface roughness parameter R_a can't describe contact surface sufficiently. The standard deviation (R_q) is the square root of the arithmetic mean of the square of the vertical deviation from the mean line, which is more sensitive to deviations from mean line than R_a. Average peak-to-valley height (R_z) is defined as the distance between average of the five highest asperities and average of the five lowest valleys. Kurtosis (R_{ku}) represents the probability density sharpness of the profile. For surface profile with a symmetric Gaussian distribution, R_{ku} equals to 3. For surface profile with leptokurtic, R_{ku} is more than 3, and R_{ku} is less than 3 for surface profile with platykurtic. Skewness (R_{sk}) describes the degree of symmetry of the density function and is sensitive to occasional deep valleys or high peaks. For surface profile with the Gaussian distribution, R_{sk} is equal to zero. For surface profile with high peaks or filled valleys, R_{sk} is positive. For surface profile with deep scratches or loss of peaks, R_{sk} is negative. A schematic of surfaces with R_{ku} values higher and lower than 3 and with positive and negative R_{sk} is shown in Fig. 1.

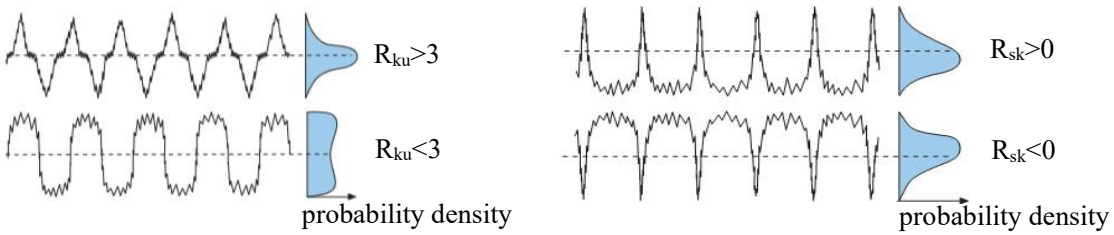

Fig. 1. Schematic of surfaces with R_{ku} values higher and lower than 3 and with positive and negative R_{sk}.

In practical applications, frictional behavior of ceramics is usually affected by both surface roughness and surface morphology. However, the studies focus on frictional property of ceramics by investigating both surface roughness and surface morphology simultaneously are limited. The goal of this work is to study the effects of both surface roughness and surface morphology on frictional behavior of ceramics simultaneously.

3.2. Experimental procedure

In order to investigate effects of surface roughness parameters and surface morphology on the frictional behavior, three different samples were used in this experiment. The composition of the three samples were monolithic B_4C ceramics with sintering additives of 3wt% SiC and 3wt% C (hereafter referred to as B), B_4C-40wt%SiC composite ceramics with a sintering additive of 3wt% C (hereafter referred to as BS) and monolithic SiC ceramics with sintering additives of 3wt% B_4C and 3wt% C (hereafter referred to as S), respectively. To study effects of other roughness parameters (R_z, R_{ku}, R_{sk}) and surface morphology on tribological behavior of samples with similar values of R_a parameter, disc type specimens with nominal dimensions of 29 × 26 × 4.5 mm^3 were polished to have similar average surface roughness (R_a=0.01~0.02 μm) using diamond slurry. Surfaces of the three samples were randomly orientated. Different surface morphology and different R_z, R_{ku} and R_{sk} values were caused for the three samples after polishing. The relative densities of the obtained samples were measured by the Archimedes method. The hardness of the obtained samples were measured by a Vickers hardness instrument. The microstructure of the polished surfaces of the samples was examined by SEM.

Tribological tests were made on a pin-on-disk tribolometer under dry sliding contacts at room temperature of 25±2 ℃. Commercial SiC balls (9.5 mm diameter) were used as counterbodies. The sliding distance for each friction test was set to 100 m, during which the steady state condition were reached. The tests were conducted at speed on 0.1 m/s and under a normal load of 5 N. The relative humidity was about 40-50%. The friciton coefficients were monitored as a function of sliding distance during tests. The roughness profiles of the samples were measured by a surface profilometer.

3.3. Results and discussion

3.3.1. Physical properties and microstructure analysis

Physical properties of the three samples are shown in Table 1. The sample S shows a slightly higher relative density and the sample BS shows a slightly higher hardness. As a whole, the three samples don't show obvious difference in physical properties. The representative micrographs of the polished surfaces of B, BS and S are shown in Fig. 2. Visible pores are observed in all the three samples. Compared with sample B and sample BS, less pores are observed in the sample S, which is consistent with the relative densities measurements.

Table 1 Physical properties of the three samples.

No. of samples	Relative density (%)	Hardness (GPa)
B	95.67	29.7 ± 2.6
BS	97.09	30.4 ± 1.2
S	98.65	27.7 ± 1.0

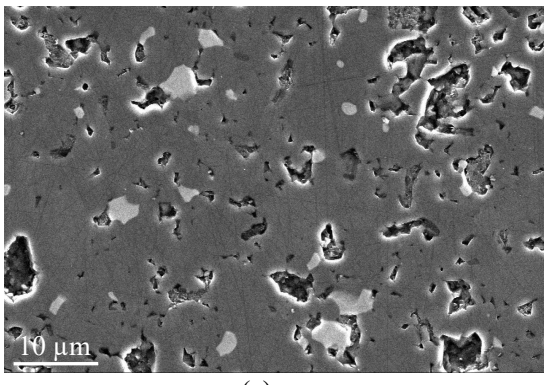

(a)

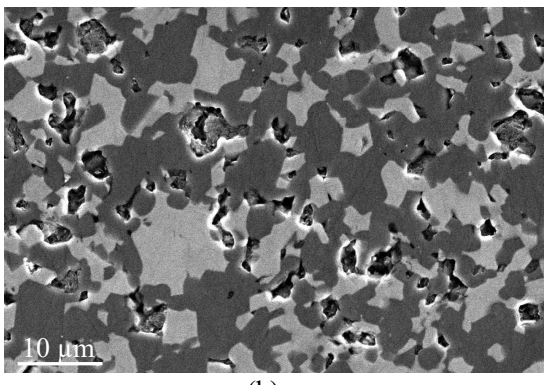

(b)

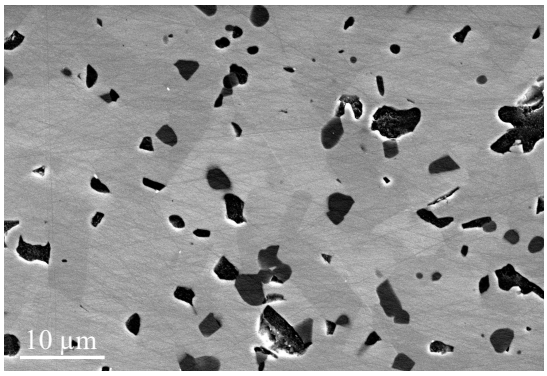

(c)

Fig. 2. Representative micrographs of the polished surfaces: (a) B, (b) BS and (c) S.

3.3.2. Surface roughness parameters and surface morphologies

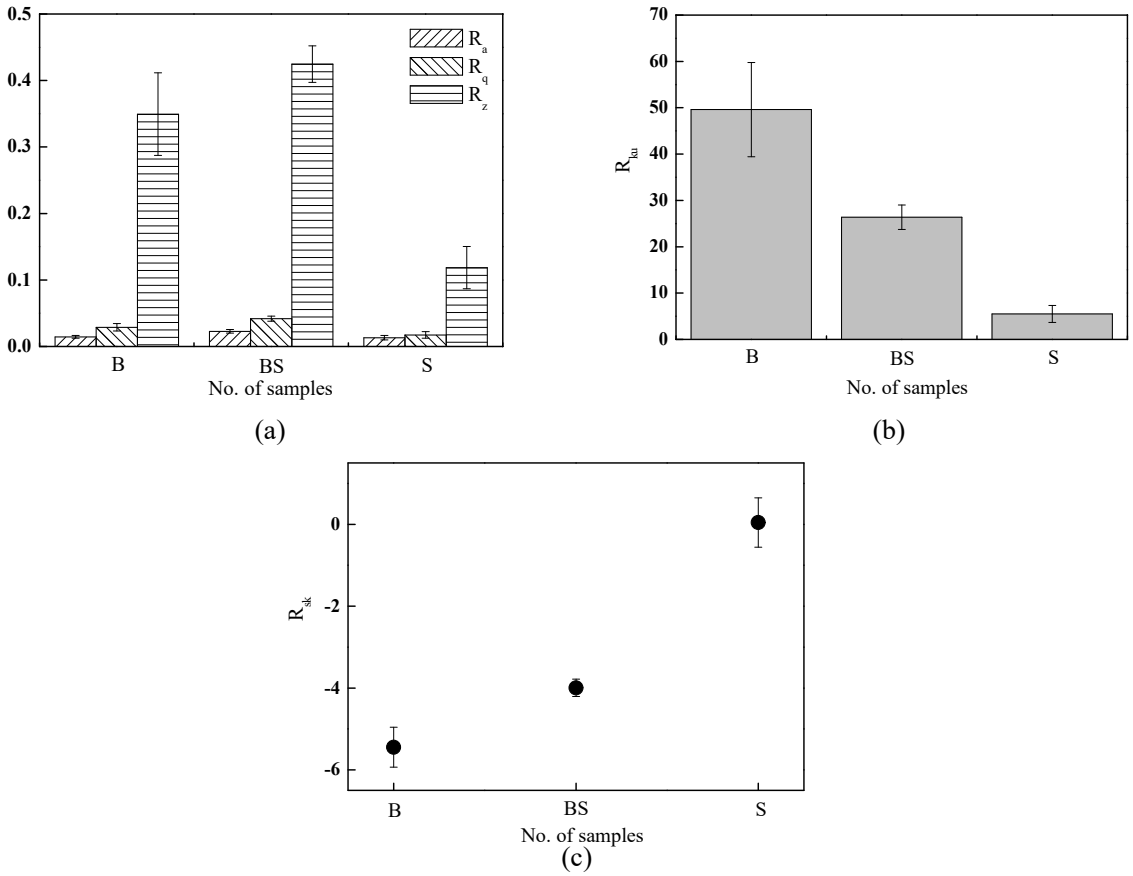

Fig. 3. Surface roughness parameters for polished samples: (a) R_a, R_q and R_z; (b) R_{ku}; (c) R_{sk}.

Different surface roughness parameters (R_a, R_q, R_z, R_{ku}, R_{sk}) for the three samples are shown in Fig. 3. Typical roughness profiles of the three samples after polishing are shown in Fig. 4. Although R_a shows similar values for the three samples, R_z, R_{ku} and R_{sk} exhibit different behaviors. Among the three samples, the sample BS reveals the largest R_z. The larger R_z is probably attributed to the larger pores formed during the sintering process. As for R_{ku} of the three samples, the values for three samples are 49.60, 26.38 and 5.49, respectively. The R_{ku} parameters of all three samples are greater than 3. As for R_{sk} of the three samples, the values for the three samples are -5.45, -3.99 and 0.05, respectively. Except for the sample S, the other two samples reveal negative values of R_{sk} parameter. The value of R_{sk} parameter of the sample S is ≈ 0, which is a characteristic of Gaussian distribution. Moreover, in our

previous work [12], we discovered that nanorelief structure was formed during polishing for B_4C-SiC composite ceramics because of preferential wearing of SiC grains by free diamond particles. The dimple depth is approximately 10 nm after polishing. A schematic diagram for nanorelief structure is shown in Fig. 5. However, the nanorelief structure didn't be observed on the surface for monolithic ceramics.

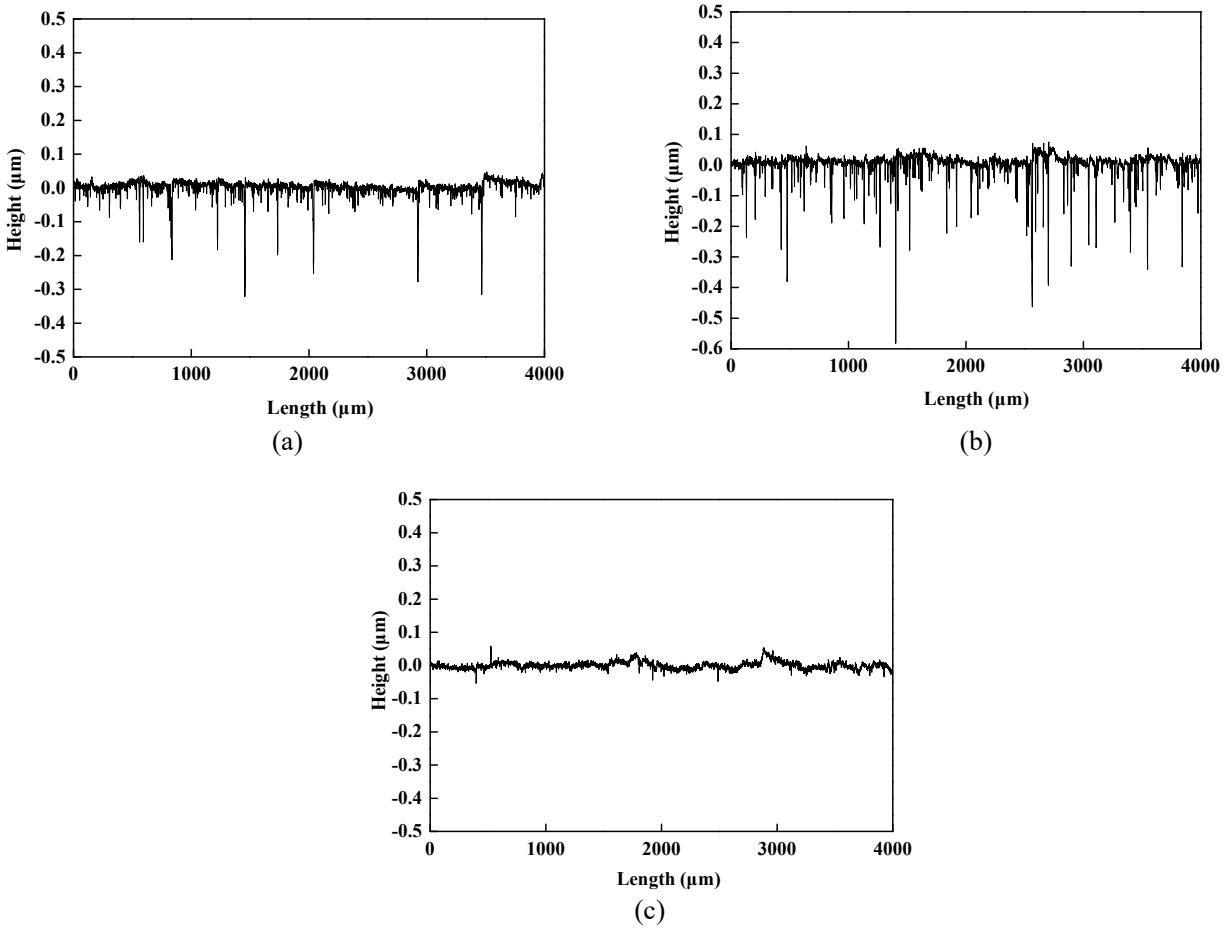

Fig. 4. Typical roughness profiles of the three samples after polishing: (a) B; (b) BS; (c) S.

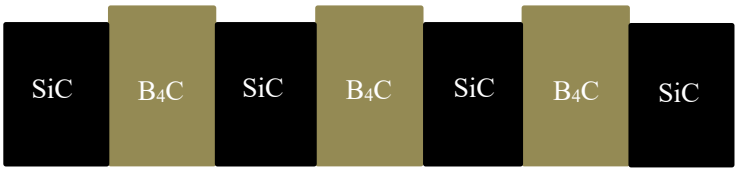

Fig. 5. A schematic diagram for nanorelief structure.

3.3.3. Average coefficients of friction during run-in period

Fig. 6 shows the average coefficients of friction of the three samples during run-in period. Fig. 7 shows the typical curves of friction coefficients of the three samples. It can be seen that the friction coefficients for the three samples reached a peak value of approximately 1.0 during run-in period, and then decreased to a steady state value. A slightly lower maximum friction coefficient for the sample BS was measured during run-in period. Further, the sample BS reveals the lowest coefficient of friction during run-in period (Fig. 6). In general, the friction coefficient of materials during run-in period is associated with the initial surface roughness. Rubino et al. reported that the B_4C ceramics with different surface roughness (R_a=0.9 μm, 1.3 μm, 1.9 μm) exhibited different friction coefficients during run-in period [11]. The B_4C ceramics with higher surface roughness (R_a) showed a slightly

lower friction coefficient. Rubino et al. also stated that for SiC ceramics, the SiC ceramics with initial smoother surface (R_a=0.5 μm) had a higher friction coefficient than that of the SiC ceramics with initial rougher surface (R_a=2.2 μm) during run-in period [11]. The friction coefficient is decided by the asperities and protrusion between the two mating surfaces at the beginning of the test. The rougher surface means a lower number of contact points, which needs a smaller force to break these conjunctions. However, in the present study, the three samples have similar surface roughness (R_a) but different surface morphologies. For monolithic ceramics, it is considered that there is no obvious relief structure after polishing, which has been proved in our previous work [12]. In contrast, the relief structure with the depth of ~10 nm was observed on the B_4C-SiC composite ceramics after polishing [12]. The formation of nanorelief structure on the B_4C-SiC composite ceramics, on the one hand, can reduce the real contact area between the two mating surfaces, and on the other hand, can trap wear particles. The reduced real contact area can decrease adhesion effect between the two mating surfaces, which is beneficial to reduce the coefficient of friction. Meanwhile, wear particles can be trapped in the craters of the nanorelief structure. Although the size of wear particles may larger than the depth of the nanorelief structure and the nanorelief structure can't act as wear particles' traps to reduce friction directly, which is the function of relief structure produced by laser, the wear particles can be hold or fixed on the worn surface by the craters of nanorelief structure and further broken to much smaller pieces. The smaller wear pieces, whose composition may be SiC, B_4C or the mixture of B_4C and SiC, are more easy to be oxidized and lower the coefficient of friction. Conversely, it is difficult for the wear particles to have the same effect on the monolithic B_4C ceramics and the monolithic SiC ceramics during the friction process. The wear particles can move easily and it is hardly for them to stay at the interface during the friction process. Therefore, the sample BS shows the lowest coefficient of friction. In addition, Sedlaček et al. suggested that the surface profile of hardened 100Cr6 ball bearing steel with a higher value of R_{ku} and a more negative R_{sk} can cause a lower friction coefficient [13]. The sample B has a higher value of R_{ku} and a more negative R_{sk} than those of sample BS, however, the sample B reveals a higher coefficient of friction than that of the sample BS. As a result, it can be concluded that surface morphology may have been a competitive factor for coefficient of friction as compared B_4C-SiC composite ceramics with monolithic B_4C ceramics. Furthermore, when compared with monolithic SiC ceramics, monolithic B_4C ceramics has a higher value of R_{ku} and a more negative R_{sk}, resulting in a slightly lower friction coefficient, which is consistent with the result of Sedlaček et al. stated above.

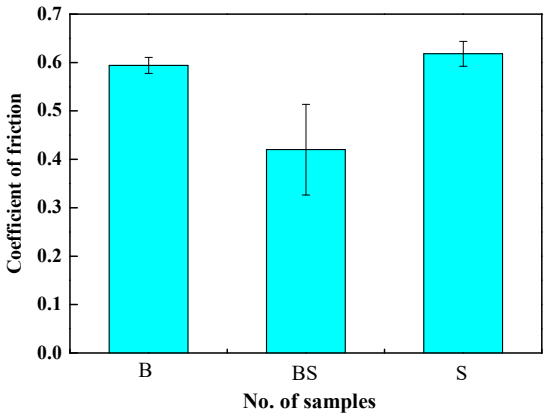

Fig. 6. Average coefficients of friction of the three samples during run-in period.

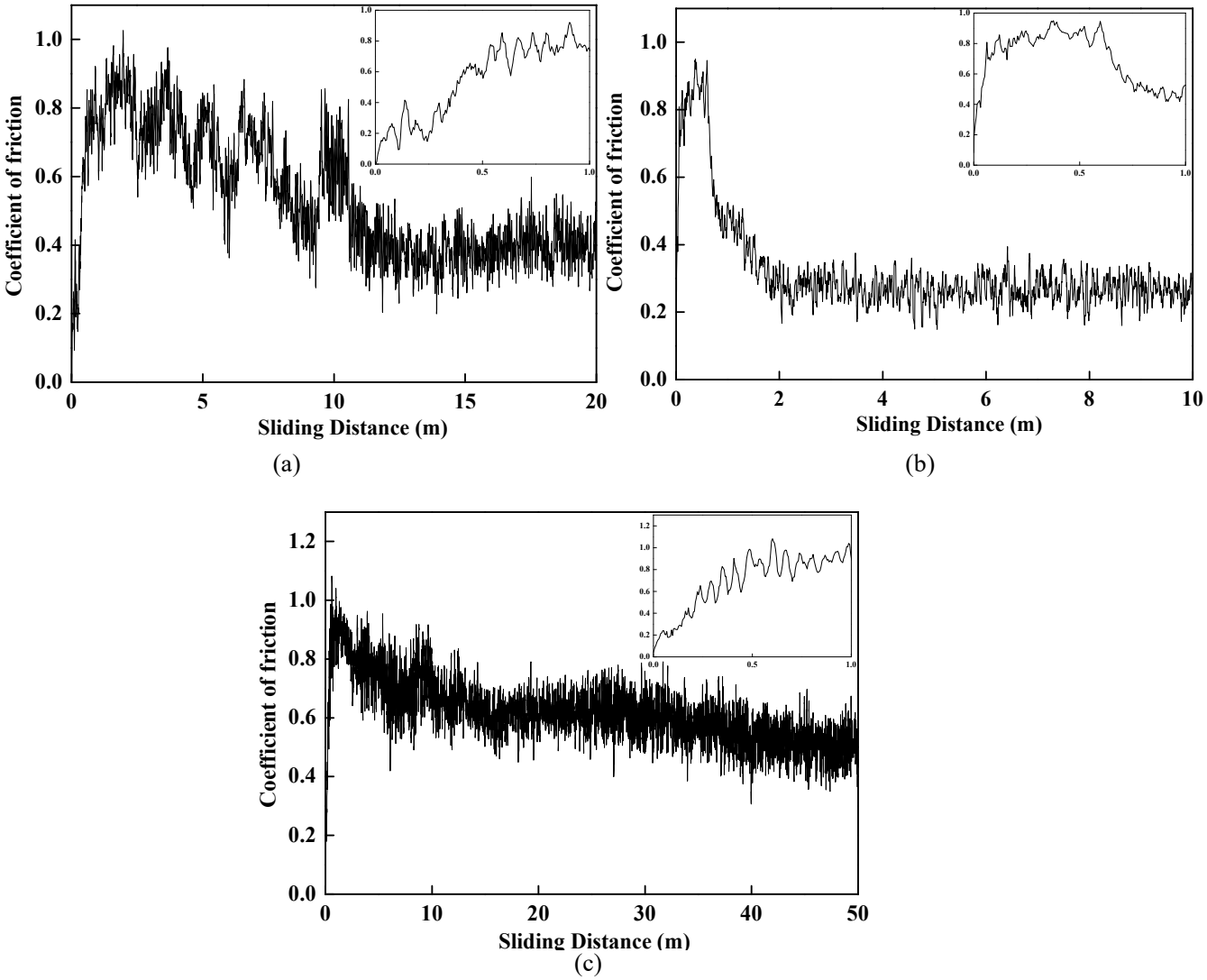

Fig. 7. Typical curves of coefficients of friction of three samples: (a) B; (b) BS; (c) S.

3.3.4. Sliding distance to steady state condition

Fig. 8 shows the sliding distance to steady state condition for the three samples. The characteristic of the steady state condition is that the friction coefficient tends to a constant, and there may be large fluctuations near the constant based on the experimental and material parameters. The sample BS exhibits the shortest sliding distance up to the steady state condition. On numerous occasions, the sliding distance to steady state condition is also associated with the initial surface roughness. Kubiak et al. reported that friction coefficient evolves more quickly to its stable value for smoother surfaces and then remains at that level during friction processes [14]. Sedlaček et al. found that although rougher surfaces have lower friction coefficient, sliding distance when steady state condition is reached, is longer for rougher surfaces [15]. In the present study, the three samples have the similar average roughness (R_a), however, they also show different sliding distance to steady state condition. Compared with the monolithic ceramics, the B_4C-SiC composite ceramics has a different surface morphology. The nanorelief structure is formed on B_4C-SiC ceramics. The reduced adhesion and the trap of wear debris resulting from the nanorelief structure make the coefficient of friction quickly to its stable-state. Furthermore, the sample B and the sample S have similar R_a values but different R_{ku} and R_{sk} values. The surface with higher R_{ku} and lower R_{sk} is easier to cause fast run-in period [13], therefore, the sliding distance is shorter for sample B than that for sample S.

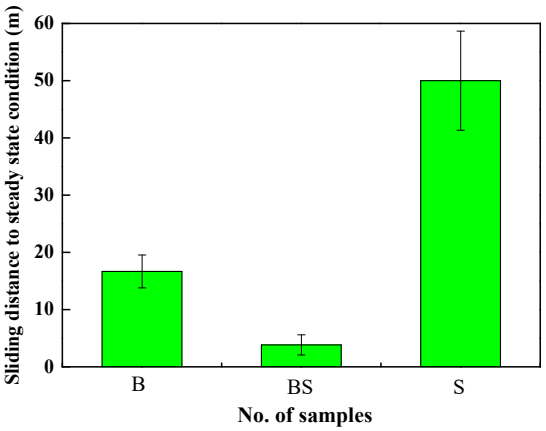

Fig. 8. Sliding distance to steady state condition for the three samples.

Low friction coefficient during run-in period and short sliding distance to steady state condition in unlubricated sliding can result in expansion of the sphere of application of ceramic tribo-elements. Friction is related with the energy consumption. Low friction coefficient during run-in period and short sliding distance to steady state condition mean the decrease in heat generation, which can provide an opportunity to reduce the requirements for the heat transfer. The nanorelief structure formed in situ is used to change the surface morphology, and subsequently to change tribological performance of ceramic. In recent years, the research of ceramics on tribology is not only to improve tribological performance, but also to improve the strength and reduce the cost of manufacturing. Unlike laser-fabricated relief structure, nanorelief structure formed in situ would not reduce the strength of ceramics due to the absence of defects caused by laser. On the other hand, the cost of nanorelief structure formed in situ is significantly lower than that of laser-fabricated relief structure. However, nanorelief structure formed by in-situ method is only confined to composite ceramics at present, whilst nanorelief structure can't be formed in situ on all composite ceramic surfaces. Further research should be focus on the study of the effects of surface roughness parameters and surface morphology on the wear of ceramics during run-in period.

3.4. Conclusions

In this paper, pin-on-disc tests with B_4C disc, B_4C-SiC disc and SiC disc with SiC balls were carried out to study the influence of surface morphology and surface roughness parameters on tribological behavior on the basis of the samples with similar surface roughness (R_a). The main conclusions are as follows:

(1) For friction coefficient during run-in period in dry sliding, surface morphology is considered as a more important competitive factor. The friction coefficient during run-in period for B_4C-SiC composite ceramics with nanorelief structure on the surface is lower than those for monolithic B_4C ceramics and monolithic SiC ceramics, both of which have no nanorelief structure. Compared with the monolithic SiC ceramics, the monolithic B_4C ceramics with a higher R_{ku} and a more negative R_{sk} results in a slightly lower friction coefficient.
(2) For sliding distance to steady state condition in dry sliding, surface morphology also plays an important role. The B_4C-SiC composite ceramics with nanorelief structure on the surface exhibits the shortest sliding distance up to steady state condition. Compared with the monolithic SiC ceramics, the monolithic B_4C ceramics with a higher R_{ku} and a more negative R_{sk} leads to a shorter sliding distance up to steady state condition.

3.5. References

[1] S. Gupta, S. K. Sharma, B. V. M. Kumar, Y. W. Kim. Tribological characteristics of SiC ceramics sintered with a small amount of yttria. Ceramics International,2015,41(10):14780-14789.

[2] X. Q. Li, Y. M. Gao, S. Z. Wei, Q. X. Yang, Z. C. Zhong. Dry sliding tribological properties of self-mated couples of B_4C-hBN ceramic composites. Ceramics International,2017,43:162-166.

[3] W. Zhang, S. Yamashita, H. Kita. Progress in pressureless sintering of boron carbide ceramics- a review. Advances in Applied Ceramics,2019,118(4):222-239.

[4] W. Chen, Y. M. Gao, C. Chen, J. D. Xing. Tribological characteristics of Si_3N_4-hBN ceramic materials sliding against stainless steel without lubrication. Wear,2010,269(3-4):241-248.

[5] H. Kita, K. Osumi, T. Iizuka, M. Fukushima, K. Yoshida, H. Hyuga. Changes in microstructure and properties of ZnO-Added Al_2O_3 upon sliding. Journal of the Ceramic Society of Japan,2006,114(7):599-602.

[6] L. Q. Kong, Q. L. Bi, M. Y. Niu, S. Y. Zhu, J. Yang, W. M. Liu. High-temperature tribological behavior of ZrO_2-MoS_2-CaF_2 self-lubricating composites. Journal of the European Ceramic Society,2013,33(1):51-59.

[7] F. Li, S. Y. Zhu, J. Cheng, Z. H. Qiao, J. Yang. Tribological properties of Mo and CaF_2 added SiC matrix composites at elevated temperatures. Tribology International,2017,111:46-51.

[8] Z. S. Chen, H. J. Li, Q. G. Fu, X. F. Qiang. Tribological behaviors of SiC/h-BN composite coating at elevated temperatures. Tribology International,2012,56:58-65.

[9] J. R. Jiang, R. D. Arnell. The effect of substrate surface roughness on the wear of DLC coatings. Wear,2000,239(1):1-9.

[10] C. Y. Chen, B. H. Wu, C. J. Chung, W. L. Li, C. W. Chien, P. H. Wu, C. W. Cheng. Low-friction characteristics of nanostructured surfaces on silicon carbide for water-lubricated seals. Tribology Letters,2013,51(1):127-133.

[11] F. Rubino, M. Pisaturo, A. Senatore, P. Carlone, T. S. Sudarshan. Tribological characterization of SiC and B_4C manufactured by plasma pressure compaction. Journal of Materials Engineering and Performance,2017,26(7):1-12.

[12] W. Zhang, S. Yamashita, T. Kumazawa, F. Ozeki, H. Hyuga, H. Kita. Effect of nanorelief structure formed in situ on tribological properties of ceramics in dry sliding. Ceramics International,2019,45(11):13818-13824.

[13] M. Sedlaček, B. Podgornik, J. Vižintin. Correlation between standard roughness parameters skewness and kurtosis and tribological behaviour of contact surfaces. Tribology International,2012,48:102-112.

[14] K. J. Kubiak, T. W. Liskiewicz, T. G. Mathia. Surface morphology in engineering applications: Influence of roughness on sliding and wear in dry fretting. Tribology International,2011,44(11):1427-1432.

[15] M. Sedlaček, B. Podgornik, J. Vižintin. Influence of surface preparation on roughness parameters, friction and wear. Wear,2009,266(3):482-487.

Chapter 4
Effects of load on tribological properties of B_4C and B_4C-SiC ceramics sliding against SiC balls

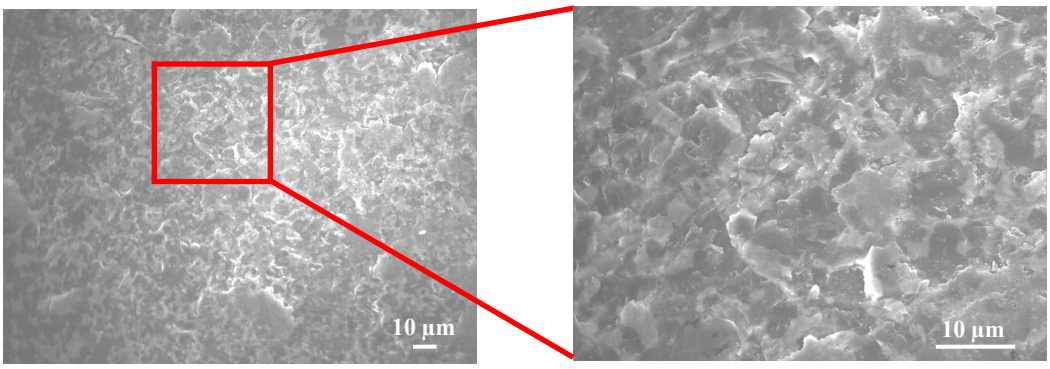

Pressureless sintered B_4C and B_4C-SiC ceramics were subjected to tests of dry sliding against SiC balls at 5 N, 10 N and 20 N. The effects of load on the respective tribological properties of B_4C and B_4C-SiC ceramics were studied. Meanwhile, the tribological properties and friction, wear mechanisms of B_4C and B_4C-SiC ceramics at different loads were compared. Both the friction coefficient and wear rate of B_4C ceramics first decreased and then increased with increases in load, while both the friction coefficient and wear rate of B_4C-SiC ceramics increased with increases in load. At low load, the B_4C-SiC ceramics showed a lower friction coefficient and wear rate. At intermediate load, the B_4C ceramics showed a lower friction coefficient, and no difference between the wear rates of B_4C and B_4C-SiC ceramics was apparent. At high load, the B_4C ceramics showed a lower friction coefficient, while the B_4C-SiC ceramics showed a lower wear rate. With increases in load from 5 N to 20 N for the B_4C ceramics, the wear mechanism changed from adhesive wear to delamination and spalling of tribofilm; for the B_4C-SiC ceramics, meanwhile, the wear mechanism changed from surface polishing and mild abrasion to micro-fracture.

Contents

4.1. Introduction

B_4C and B_4C-based ceramics possess such superior performance characteristics as exceptional hardness, high elastic modulus, low density, good wear resistance and good chemical inertness at room temperature [1,2]. B_4C and B_4C-based ceramics are considered to be potential candidates for tribological applications, such as mechanical seals, bearings, cutting tools, wheel dressing tools and blast nozzles [3-7]. Li et al. [8,9] studied the tribological properties of B_4C-hBN composite ceramics, and obtained a decreased coefficient of friction but increased specific wear rate system as compared to monolithic B_4C ceramics. Alexander et al. [10] investigated a B_4C-carbon nanotube system and obtained a specific wear rate of 1.06×10^{-6} $mm^3/N\cdot m$, which was lower than that of B_4C ceramics. Murthy et al. [11] added ZrO_2 to B_4C ceramics and noted that ZrB_2 formed in situ and that sub-micron-sized round pores formed owing to the formation of CO gas could help to deflect and/or arrest cracks, improving the tribological properties of B_4C ceramics. Among B_4C-based composite ceramics, it has been observed that B_4C-SiC composite ceramics showed better mechanical properties and oxidation resistance as compared to monolithic B_4C ceramics [12-14]. However, little literature is available on the friction and wear performance of B_4C-SiC ceramics [15,16].

It was reported that the tribological behaviors of ceramic materials under dry sliding conditions are complex and dependent on such external factors as humidity, temperature, sliding speed, load, counterpart, and atmosphere [17]. Sharma et al. [18] mentioned that the friction coefficient of SiC ceramics first increased and then decreased and that the specific wear rate decreased with increases in load. Sonber et al. [19] found that the coefficient of friction of B_4C ceramics decreased and the specific wear rate increased with increases in load. Micele et al. [20] pointed out that the specific wear rate of SiC ceramics increased as the sliding speed increased. Gogotsi et al. [21] reported that the coefficient of friction of B_4C ceramics decreased with increases in sliding speed. Murthy et al. [22] and Cao et al. [23] found that both the friction coefficients and specific wear rates of SiC ceramics and B_4C ceramics decreased with increases in humidity, respectively. To date, only a few reports are available on the friction and wear properties of B_4C ceramics and no reports on those of B_4C-SiC ceramics at different loads when other test conditions are the same. Furthermore, in order to explore the potential of B_4C and B_4C-SiC ceramics for applications in the automotive and aerospace industries as tribological structural components such as abrasion resistance linings, exhaust systems for liquid rocket engine turbopumps, and aerospace turbine blades, it is important to evaluate the tribological behaviors of these ceramics at different loads. Therefore, we decided to take a fresh look at the effects of load on the tribological properties of B_4C and B_4C-SiC composite ceramics when slid against SiC balls under dry sliding conditions. The tribological properties of B_4C ceramics and B_4C-SiC ceramics at different loads were also compared, moreover, and their friction and wear mechanisms at different loads were analyzed.

4.2. Experimental procedures

Commercial B_4C powder (Grade HS, H. C. Starck, Germany) and SiC powder (Grade OY-15, Yakushima Denko, Japan) were used as raw materials. The typical characteristics of the B_4C powder and SiC powder based on the manufacturers' data are shown in Table 1. Monolithic B_4C ceramics and B_4C-40 wt% SiC composite ceramics were prepared using a pressureless sintering technique, and carbon black powder (average particle size: 20-30 nm) was used as a sintering additive for the two ceramics. First, each powder mixture was ball-milled for 24 h using SiC balls and ethanol as the milling media. After drying, the powder mixture was pressed into disks, which were then cold-isostatically pressed at 196 MPa. The disks were sintered at 2300 ℃ in an argon atmosphere, and their dwell time was 16 h.

Table 1 Typical characteristics of B_4C powder and SiC powder.

Property	B_4C	SiC
Purity	-	97
Crystal type	-	α
Average particle size (μm)	0.8	0.4
Specific surface area (m^2/g)	18	15
Impurity (wt%)		
Free C	-	0.9
O	1.2	-
N	0.2	-
Fe	0.03	0.08
Si	0.1	-
Al	0.02	0.02
Other	0.2	-
Total boron (wt%)	75.8	-
Total carbon (wt%)	22.3	-
B/C molar ratio	3.8	-

Density was determined using Archimedes' method and the relative density evaluated. Hardness was measured for the polished surfaces by Vickers indentation with a load of 1 kg for a dwell time of 10 s. The lengths of cracks generated by Vickers indentation were measured and the fracture toughness (K_{IC}) was estimated using the formula $K_{IC}=0.016(E/H)^{0.5}Pc^{-1.5}$ [24]. Each measurement was repeated five times, and the data was averaged. The physical and mechanical performances of sintered B_4C ceramics and B_4C-SiC composite ceramics are shown in Table 2. The physical and mechanical performances of commercially available SiC balls based on the manufacturers' data are also shown in Table 2.

Table 2 Physical and mechanical performances of sintered B_4C ceramics, B_4C-SiC composite ceramics and commercially available SiC balls.

Property	B_4C ceramics	B_4C-SiC composite ceramics	SiC balls
Density (g/cm^3)	2.40	2.66	3.15
Relative density (%)	95.7	96.6	98.3
Vickers hardness (GPa)	26.87	30.39	23.80
Fracture toughness ($MPa\cdot m^{1/2}$)	3.66	3.19	-
Bending strength (MPa)	240	390	785
Average grain size (μm)	3-4	B_4C: 2 SiC: 3	-

Dry sliding tests were performed in a ball-on-disc tribometer (T-18-0162, NANOVEA, US). The size of the disk samples was 29×26×4.5 mm^3. The surfaces of the disks were ground and polished to Ra=15-35 nm. Commercially available SiC balls with 9.5 mm diameter were used as counterparts. Before the wear test, both the disk samples and balls were ultrasonically cleaned in acetone. The balls were kept stationary under the applied load to make a track radius of 7 mm, while the disks were rotated at a speed of 0.1 m/s for a sliding distance of 100 m. The tribological tests were carried out at 21±3 ℃ and 45±5 RH in ambient air at three different loads (5 N, 10 N, 20 N).

During the tests, the friction coefficients were automatically calculated and recorded by a microprocessor-controlled data acquisition system. Wear volume losses (ΔV, mm^3) for the disks and balls were evaluated by the following means: for the disks, four cross-sectional areas on the wear tracks, each at 90º with respect to the previous one, were measured using a surface profilometer and the four areas were averaged and multiplied by the wear track length to obtain the ΔV. For the balls, the radius at the wear scars was measured using a microscope and the ΔV was then calculated according to this radius at the wear scars and the original radius of the ball. The specific wear rates (WR, $mm^3/N \cdot m$) of the disks and balls were then calculated according to the following equation:

$$WR = \Delta V/(Ps)$$

where P is the normal load and s is the sliding distance. Three repeated tests were performed for each tribopair. The worn surfaces of the B_4C and B_4C-SiC ceramics were observed and analyzed by SEM and EDS. The wear scars on the SiC balls were observed by microscope.

4.3. Results and discussion

4.3.1. Effects of load on the coefficients of friction of the B_4C and B_4C-SiC ceramics

The coefficients of friction of the B_4C and B_4C-SiC ceramics sliding against SiC balls with a sliding distance at different loads and average coefficients of friction of the B_4C and B_4C-SiC ceramics in a steady-state period at different loads are presented in Fig. 1. An initial run-in period followed by a steady-state period is observed for all the B_4C and B_4C-SiC ceramics sliding against SiC balls at different loads. For the B_4C ceramics, the average coefficient of friction varied in the range of 0.24-0.44 with increases in load from 5 N to 20 N, and larger fluctuations in friction occurred at low load (5 N). The coefficient of friction of the B_4C ceramics first decreased and then increased with increases in load, but the coefficient of friction at high load (20 N) was still lower than that at low load. For the B_4C-SiC ceramics, the average coefficient of friction varied in the range of 0.32-0.48 as the load increased from 5 N to 20 N, and larger fluctuations in friction occurred at low load and high load. The coefficient of friction of the B_4C-SiC ceramics increased with increases in load. At low load, the B_4C-SiC ceramics showed a lower coefficient of friction. At intermediate load (10 N) and high load, the B_4C ceramics exhibited lower coefficients of friction.

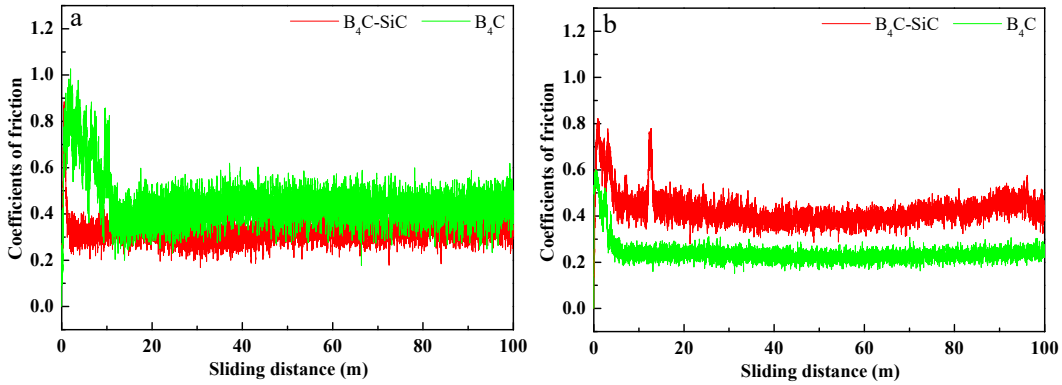

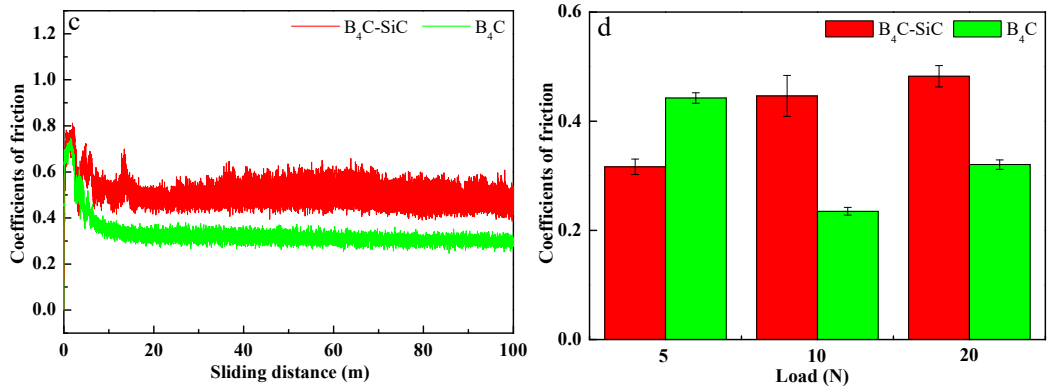

Fig. 1. Coefficients of friction of the B_4C and B_4C-SiC ceramics sliding against SiC balls with sliding distances of (a) 5 N, (b) 10 N and (c) 20 N, and (d) average coefficients of friction of the B_4C and B_4C-SiC ceramics in a steady-state period at different loads.

4.3.2. Effects of load on specific wear rates of the B_4C and B_4C-SiC ceramics

The average specific wear rates of the B_4C and B_4C-SiC ceramics sliding against SiC balls at different loads are shown in Fig. 2a. For the B_4C ceramics, the specific wear rate varied in the range of 11.0-22.4×10^{-6} $mm^3/N·m$ as the load was increased from 5 N to 20 N. The specific wear rate of the B_4C ceramics first decreased and then increased with increases in load, and the specific wear rate of the B_4C ceramics reached its minimum value at a load of 10 N. For the B_4C-SiC ceramics, the specific wear rate varied in the range of 1.3-7.3×10^{-6} $mm^3/N·m$ as the load was increased from 5 N to 20 N. The specific wear rate of the B_4C-SiC ceramics increased with increases in load. The B_4C-SiC ceramics showed a lower specific wear rate at every load, but no difference between the specific wear rates of B_4C ceramics and B_4C-SiC ceramics was apparent at intermediate load.

The average specific wear rates of SiC balls sliding against B_4C and B_4C-SiC ceramics at different loads are presented in Fig. 2b. For SiC balls sliding against B_4C ceramics, the specific wear rate varied in the range of 1.2-3.5×10^{-6} $mm^3/N·m$ as the load was increased from 5 N to 20 N. The specific wear rate of the SiC balls first decreased and then increased with increases in load, and the specific wear rate of the SiC balls reached its minimum value at 10 N. For SiC balls sliding against B_4C-SiC ceramics, the specific wear rate varied in the range of 0.9-3.6×10^{-6} $mm^3/N·m$ as the load was increased from 5 N to 20 N. The specific wear rate of SiC balls increased with increases in load. At low load, SiC balls showed a lower specific wear rate when sliding against the B_4C-SiC ceramics. At intermediate load, SiC balls showed a lower specific wear rate when sliding against the B_4C ceramics. At high load, SiC balls sliding against the B_4C ceramics and the SiC balls sliding against the B_4C-SiC ceramics revealed similar specific wear rates.

The average systematic specific wear rates of B_4C/SiC and B_4C-SiC/SiC tribopairs at different loads are summarized in Fig. 2c. The value of the systematic average specific wear rate of every tribopair is the sum of the B_4C disk's or B_4C-SiC disk's and the corresponding SiC ball's average specific wear rate. For the B_4C/SiC tribopair, the average systematic specific wear rate first decreased and then increased with increases in load, and the average systematic specific wear rate reached its minimum value at a load of 10 N. For the B_4C-SiC/SiC tribopair, the average systematic specific wear rate increased with increases in load. The B_4C-SiC/SiC tribopair showed a lower average systematic specific wear rate at every load, but no difference between the systematic specific wear rates of the B_4C/SiC tribopair and B_4C-SiC/SiC tribopair was apparent at intermediate load.

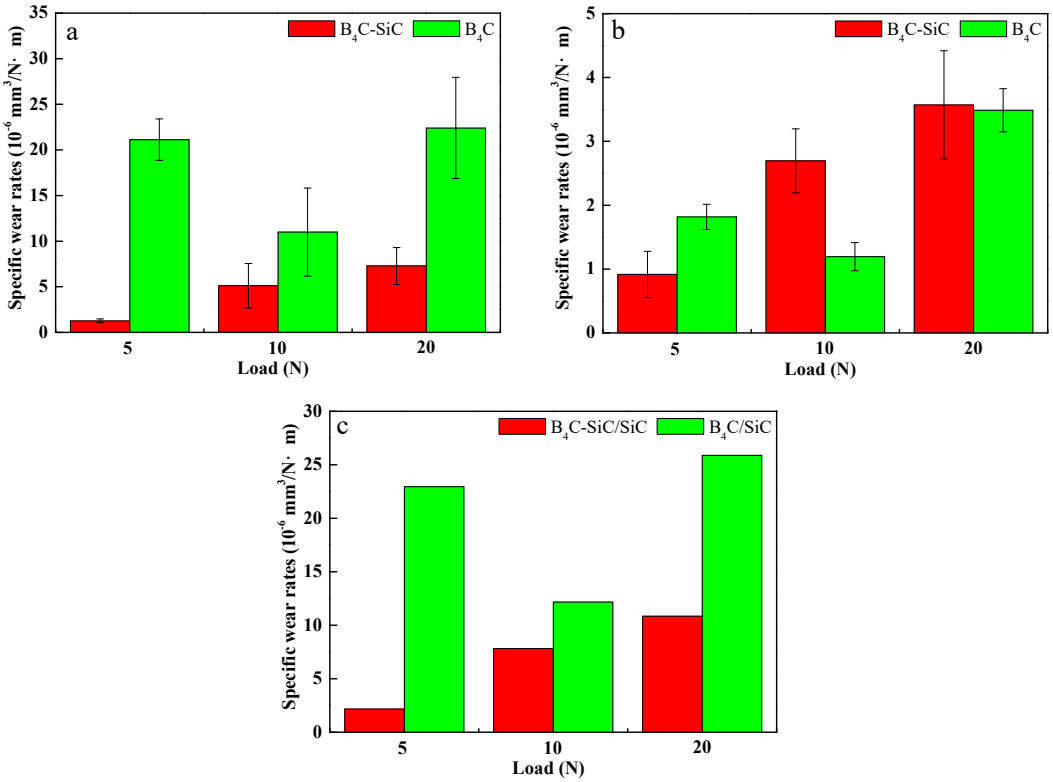

Fig. 2. Average specific wear rates of (a) the B_4C and B_4C-SiC ceramics sliding against SiC balls at different loads, (b) SiC balls sliding against the B_4C and B_4C-SiC ceramics at different loads, and (c) average systematic specific wear rates of the B_4C/SiC and B_4C-SiC/SiC tribopairs at different loads.

4.3.3. Friction and wear mechanisms

SEM images of worn surfaces of the B_4C and B_4C-SiC ceramics at 5 N as well as EDS analyses of the corresponding worn surfaces are presented in Fig. 3. It can be observed that severe adhesive wear was dominant on the B_4C ceramics, and the wear surface was quite rough. EDS analysis of the wear surface of the B_4C ceramics showed the presence of a small amount of oxygen (2.17 at%), which was induced by a tribochemical reaction. Other scholars [19,25] observed that the formation of B_2O_3 or H_3BO_3 induced by a tribochemical reaction could decrease friction on B_4C ceramics, but the coefficient of friction for the B_4C ceramics was not reduced owing to the presence of a small amount of oxide in this study. One possible reason is that there was only a small amount of oxygen, which resulted in formation of too few oxide layers to reduce the coefficient of friction of the B_4C ceramics at 5 N. The other possible reason is that the beneficial influence of the oxide layers was weaker than the deterioration influence of adhesion, resulting in a higher coefficient of friction and specific wear rate for B_4C ceramics. In the case of B_4C-SiC ceramics, the wear surface was quite smooth. Surface polishing and mild abrasion were dominant in the B_4C-SiC ceramics. EDS analysis of the wear surface showed little oxygen (0.43 at%), which was considered to be an impurity from the raw materials. In our previous work [26,27], it was found that a relief structure was formed on the surface of B_4C-SiC ceramics owing to differences in hardness between the B_4C grains and SiC grains under the same experimental conditions. This relief structure can not only decrease the real contact area between the B_4C-SiC ceramics and SiC ball at the sliding interface, reducing the adhesion effect, but can also trap wear pieces formed by mild abrasion, reducing abrasive wear [28]. Therefore, the coefficient of friction and specific wear rate of B_4C-SiC ceramics were lower than those of B_4C ceramics.

The friction and wear mechanisms of B_4C and B_4C-SiC ceramics at 5 N can be further understood by observing the wear scars on their counterpart SiC balls (Fig. 4). Extensive micro-fracture and obvious grooves

were observed on SiC balls sliding against B_4C ceramics, while polishing and slight grooves were observed on SiC balls sliding against B_4C-SiC ceramics. Because of a relief structure on the B_4C-SiC ceramics, on the one hand, the extent of abrasive wear on the SiC balls sliding against B_4C-SiC ceramics was less than that on the SiC balls sliding against B_4C ceramics, while, on the other hand, micro-fracture induced by adhesion was obvious on the SiC balls sliding against B_4C ceramics, whereas no adhesive wear occurred on the SiC balls sliding against B_4C-SiC ceramics. Therefore, due to the severe adhesive wear and abrasive wear on the B_4C/SiC tribopair, the coefficient of friction of the B_4C/SiC tribopair was higher than that of the B_4C-SiC/SiC tribopair, and the specific wear rates of B_4C ceramics and their corresponding SiC balls were higher than those of B_4C-SiC ceramics and their corresponding SiC balls. Lörcher et al. [29] stated that wear caused by adhesion is greater than that caused by abrasion; thus, the specific wear rate of the B_4C ceramics was an order of magnitude higher than that of the B_4C-SiC ceramics.

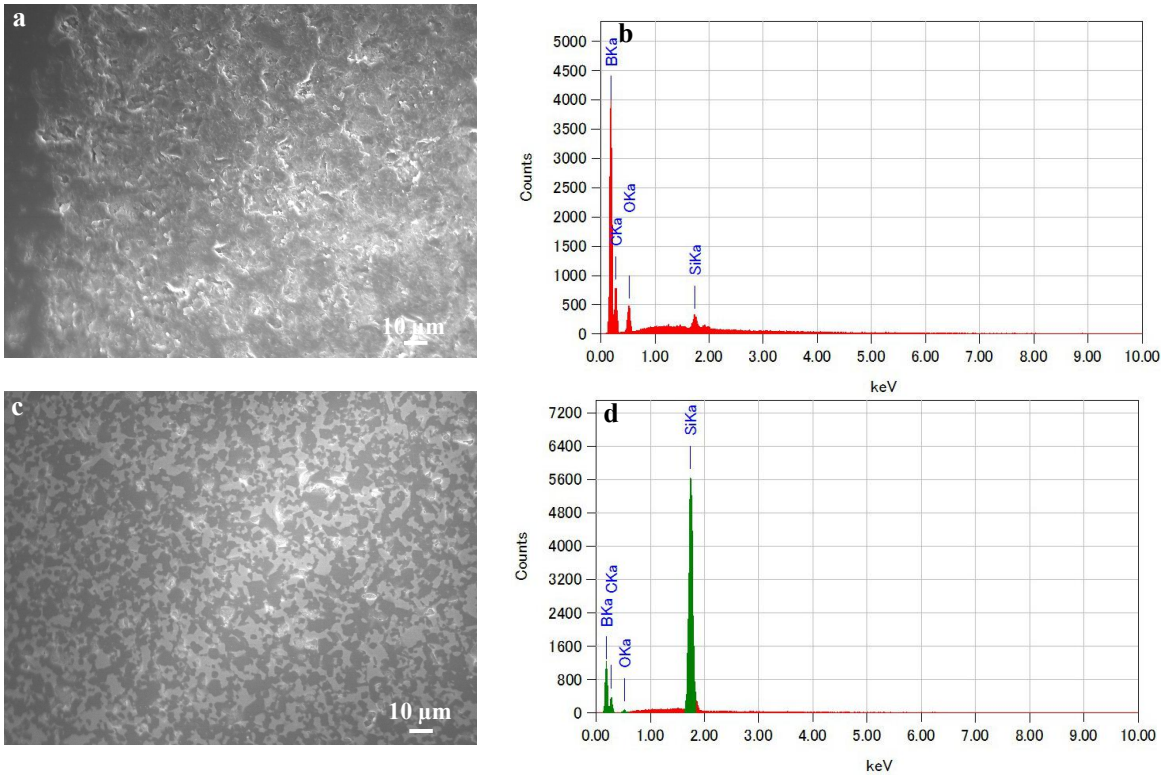

Fig. 3. SEM images of worn surfaces of B_4C (a) and B_4C-SiC (c) ceramics at 5 N. EDS analyses of Fig. 3 (a): (b) and Fig. 3(c): (d).

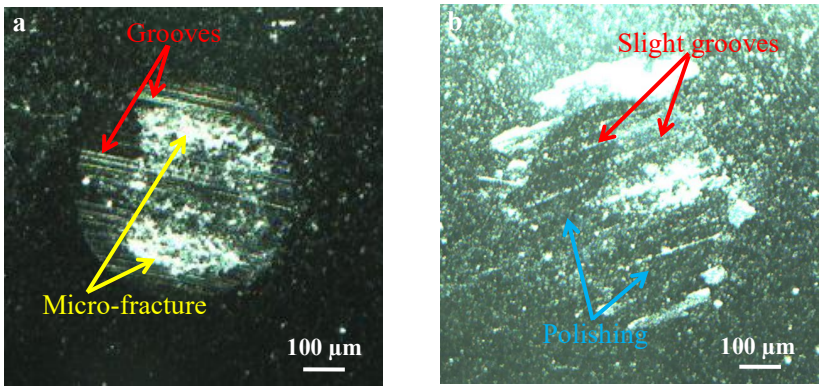

Fig. 4. Microscope images of wear scars on SiC balls after sliding against B_4C (a) and B_4C-SiC (b) ceramics at 5 N.

SEM images of the worn surfaces of B_4C and B_4C-SiC ceramics at 10 N as well as EDS analyses and elemental distributions of the corresponding worn surfaces are presented in Fig. 5. Microscope images of wear scars on SiC balls sliding against B_4C and B_4C-SiC ceramics at 10 N are shown in Fig. 6. Compared with the worn surface of the B_4C ceramics at 5 N, the worn surface of the B_4C ceramics at 10 N had become relatively smooth. The EDS analysis of the worn surfaces of B_4C ceramics showed the presence of a small amount of oxygen (1.50 at%), which means the number of oxide layers formed did not increase with increases in load. Although other scholars [19,25] found that the number of oxide layers formed on B_4C ceramics increased as the load increased, resulting in a gradually decreasing coefficient of friction with increases in load, different results were observed in the present study. The lower coefficient of friction of B_4C ceramics at 10 N than that at 5 N was attributed to greater coverage by tribofilm formed on the worn surface. It can be observed from Fig. 5a that the worn surface of B_4C ceramics at 10 N was covered by more tribofilms compared with that in Fig. 3a. It can be seen from Fig. 4a that obvious grooves were observed on the SiC ball after sliding against B_4C ceramics. It can therefore be inferred that there were some hard wear particles at the interface when the B_4C ceramics were slid at 5 N. When the load was increased to 10 N, however, those wear particles could be crushed into smaller pieces, which can be aggregated together to form a tribofilm and better compacted on the worn surface due to increased frictional heat. According to the results for elemental distributions (Fig. 5c-f), the main composition of tribofilm formed on the worn surface of B_4C ceramics was a mixture of B_4C, SiC and a small amount of silicon oxide. The phenomenon that increased the extent of coverage by forming a protective tribofilm at the interface with increases in load was also observed by Zhu et al. [30] for B_4C coating deposited on a stainless-steel substrate sliding against a WC-Co ball, and the coefficient of friction of the B_4C coating was reduced with increases in the extent of coverage by protective tribofilm. Because of the removal of hard wear particles at the sliding interface of the B_4C/SiC tribopair, no obvious grooves were observed on the SiC ball sliding against B_4C ceramics at 10 N (Fig. 6a), and microfracture was observed only on the SiC ball sliding against B_4C ceramics. On the one hand, abrasive wear was reduced owing to the removal of wear particles, and, on the other hand, the formed tribofilm could not only protect the underlying substrate from further wear, but could also separate and prevent direct contact between the B_4C ceramics and their SiC counterparts, decreasing adhesive wear. Therefore, the coefficient of friction of the B_4C/SiC tribopair at 10 N was lower than that at 5 N, and the specific wear rates of the B_4C ceramics and the corresponding SiC balls at 10 N were lower than those at 5 N. The main wear mechanism of B_4C ceramics changed from adhesive wear at 5 N to delamination of tribofilm at 10 N.

In the case of B_4C-SiC ceramics, it can be observed from Fig. 5g that grain pullout and micro-fracture were observed. B_4C-SiC ceramic is a brittle material, and the fracture of B_4C-SiC ceramic would be increased as the load is increased. Increased fracture was also observed for monolithic SiC ceramics at high load by Cho et al. [31]. Therefore, the grain pullout from the matrix not only resulted in a certain degree of damage to the relief structure of B_4C-SiC ceramic, but it also roughened the worn surface. On the other hand, tribofilm was also found on the B_4C-SiC ceramics. It can be observed from Fig. 5h that the oxygen content (2.73 at%) was slightly increased compare with Fig. 3d. According to the results for elemental distributions (Fig. 5i-l), the main composition of tribofilm formed on the B_4C-SiC ceramics was a mixture of SiC and SiO_2, which was different from the main composition of tribofilm on the B_4C ceramics. The formation of tribofilm induced by tribochemical reaction was beneficial to improving the tribological properties. Therefore, the friction and wear of B_4C-SiC ceramics were controlled by the simultaneous occurrence and competition of mechanical fracture and tribofilm formation. From Fig. 2b, it is known that the specific wear rate of the SiC balls sliding against B_4C-SiC ceramic at 10 N was higher than that at 5 N. It is reported that the wear on SiC ceramics induced by fatigue increased as the load was increased, leading to the formation of a number of wear particles [32,33]. Thus, microfracture was observed on the SiC balls sliding against B_4C-SiC ceramics at 10 N (Fig. 6b). It can be observed from Fig. 6b that obvious grooves

were found on the SiC balls compared with the case in Fig. 4b. Therefore, it was considered that grain pullout from the B_4C-SiC ceramics and the formation of a number of wear particles owing to microfracture of the SiC balls increased abrasive wear. Although some wear particles formed owing to microfracture of SiC balls could be compacted and oxidized to form tribofilm, it was considered that the beneficial influence of this tribofilm was less than the deterioration influence of the microfracture and abrasive wear. Therefore, both the coefficient of friction of the B_4C-SiC/SiC tribopair and the specific wear rates of the B_4C-SiC ceramics and corresponding SiC balls were increased as the load was increased from 5 N to 10 N. The main wear mechanism of B_4C-SiC ceramics changed from surface polishing and mild abrasion at 5 N to surface polishing, mild abrasion and micro-fracture at 10 N.

It can be observed from Fig. 6a that no obvious grooves were formed on the SiC balls sliding against B_4C-SiC ceramics compared with the case in Fig. 6b. This means that abrasive wear had little effect on the B_4C/SiC tribopair at 10 N. Meanwhile, the formed tribofilm can not only protect the underlying B_4C substrate from further wear, but it can also separate and prevent direct contact between the B_4C ceramics and their SiC counterparts, thus decreasing adhesive wear. Therefore, the coefficient of friction of the B_4C/SiC tribopair was lower than that of the B_4C-SiC/SiC tribopair, and no difference between the specific wear rates of B_4C ceramics and B_4C-SiC ceramics was apparent at 10 N.

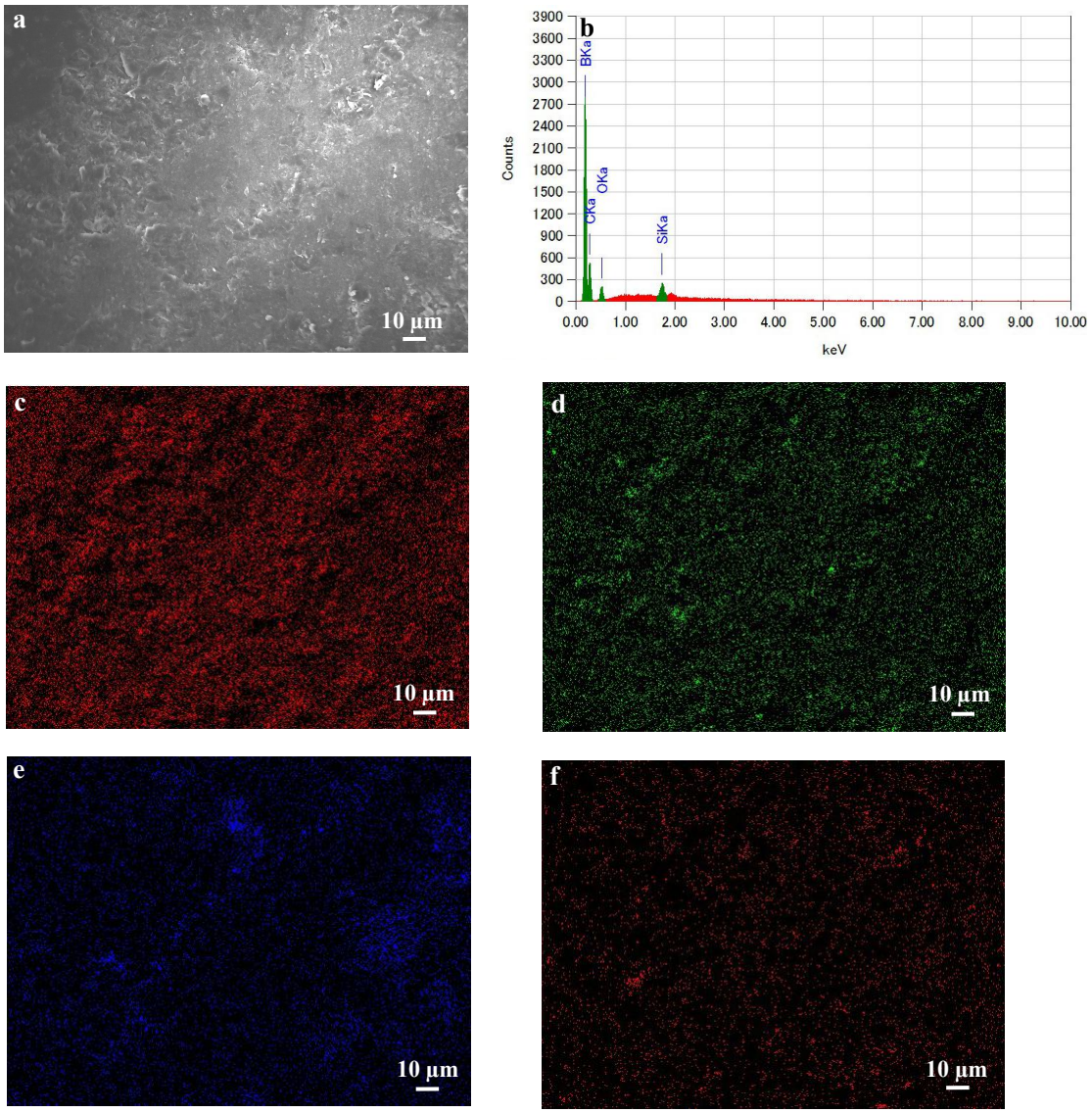

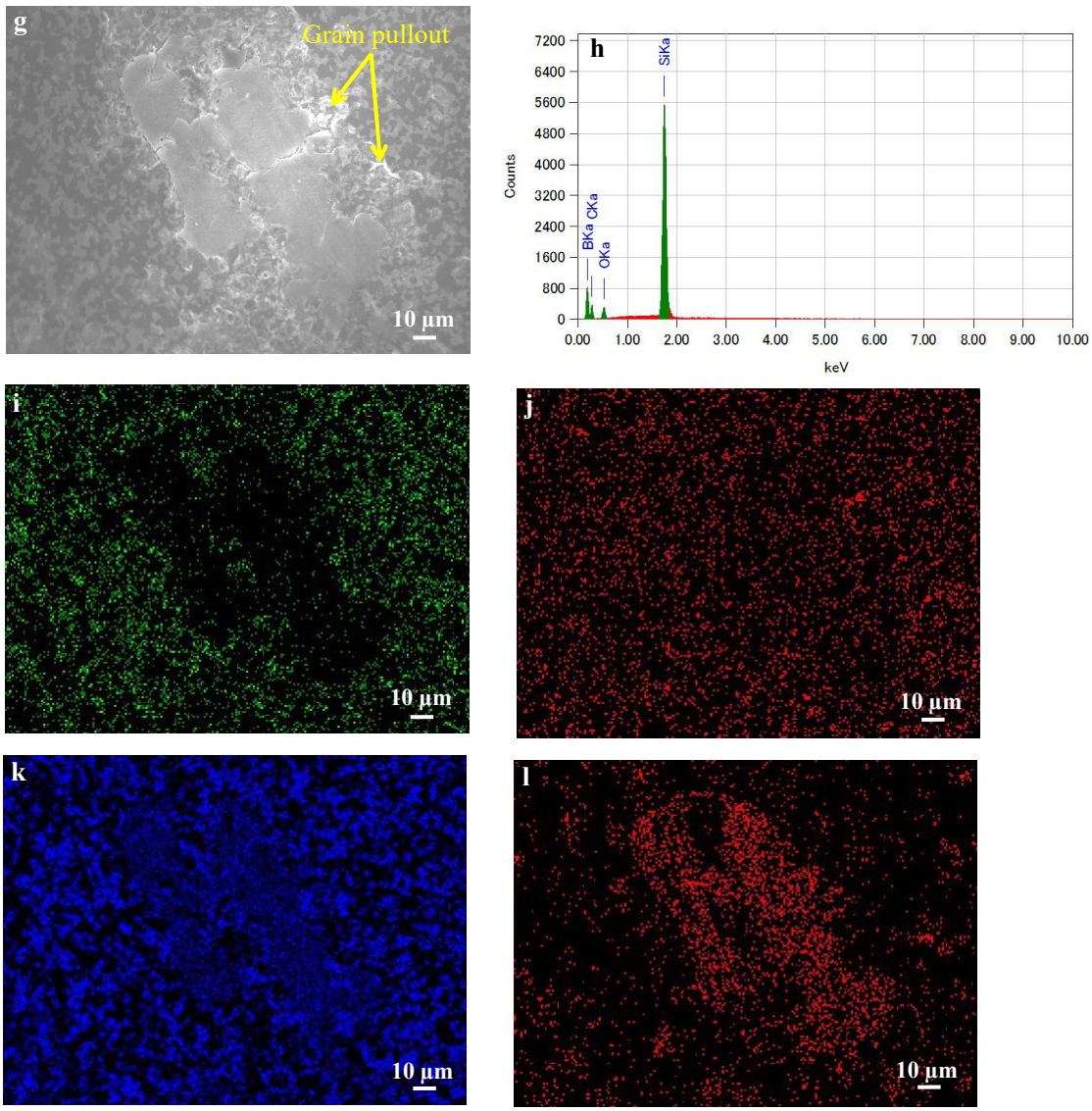

Fig. 5. SEM images of worn surfaces of the B_4C (a) and B_4C-SiC (g) ceramics at 10 N. EDS analyses of Fig. 5 (a): (b) and Fig. 5 (g): (h). Elemental distributions of Fig. 5 (a): (c) B; (d) C; (e) Si; (f) O, and of Fig. 5 (g): (i) B; (j) C; (k) Si; (l) O.

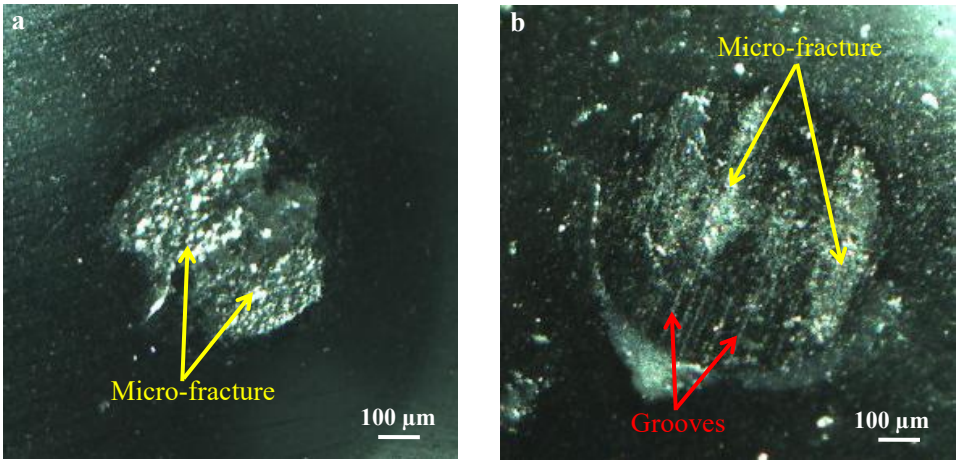

Fig. 6. Microscope images of wear scars on SiC balls after sliding against B_4C (a) and B_4C-SiC (b) ceramics at 10 N.

SEM images of the worn surfaces of B_4C and B_4C-SiC ceramics at 20 N as well as an EDS analysis of the worn surface of the B_4C ceramics are presented in Fig. 7. Microscope images of wear scars on SiC balls after sliding against B_4C and B_4C-SiC ceramics at 20 N are shown in Fig. 8. It can be observed from Fig. 7a that some spalling pits were formed on the B_4C ceramics compared with the worn surface of the B_4C ceramics at 10 N (Fig. 5a). Also, the wear on the corresponding SiC ball was further increased, and traces of abrasive wear were still not found on the wear scars of the SiC ball against B_4C ceramics. The EDS analysis of worn surface of B_4C ceramics showed decreased oxygen content (0.79 at%) at 20 N as compared with at 10 N, which means that increasing the load from 10 N to 20 N still did not promote the tribochemical reaction of B_4C ceramics. It is considered, therefore, that the main composition of tribofilm on the B_4C ceramics at 20 N was similar to that at 10 N. Because of the occurrence of spalling pits, however, which resulted from exceeding the load capacity of the tribofilm, the worn surface was rougher than that at 10 N, but still smoother than that at 5 N. Therefore, the coefficient of friction of B_4C/SiC tribopair was higher at 20 N than at 10 N and lower than at 5 N, and specific wear rates of B_4C ceramics and the corresponding SiC balls were higher at 20 N than at 10 N. The wear on the B_4C ceramics at 20 N was caused mainly by delamination and spalling of tribofilm.

In the case of B_4C-SiC ceramics, it can be observed from Figs. 7c and d that more micro-fracture was found as compared to that at 10 N. Accordingly, the relief structure of B_4C-SiC ceramics was further damaged, and the worn surface was further roughened. On the one hand, the bending force between the tribofilm and B_4C-SiC ceramics could not bear the shear force from friction, causing the exfoliation of some tribofilm. This phenomenon in which tribofilm peeled off as the load increased was also observed by Pan et al. [34] on the worn surface of B_4C-hBN ceramics. On the other hand, the micro-fracture of B_4C-SiC ceramics induced by fatigue was increased, causing more wear particles. Meanwhile, the degree of micro-fracture of the corresponding SiC ball increased progressively as the load was increased from 10 N to 20 N (Fig. 8b), and abrasive wear was still dominant on the wear scars of the SiC ball. Therefore, the coefficient of friction of the B_4C-SiC/SiC tribopair was higher at 20 N than at 10 N, and the specific wear rates of B_4C-SiC ceramics and the corresponding SiC balls were higher at 20 N than at 10 N. The wear on B_4C-SiC ceramics at 20 N was caused mainly by micro-fracture.

Because of the rougher worn surfaces of B_4C-SiC ceramics, the coefficient of friction of the B_4C-SiC/SiC tribopair was higher than that of the B_4C/SiC tribopair. On the other hand, the delamination and spalling of tribofilm on the B_4C ceramics occurred more easily than the grain pullout and fracture on the B_4C-SiC ceramics owing to the clean grain boundaries formed between B_4C grains and SiC grains [27], and the wear on B_4C ceramics was therefore higher than on B_4C-SiC ceramics at 20 N.

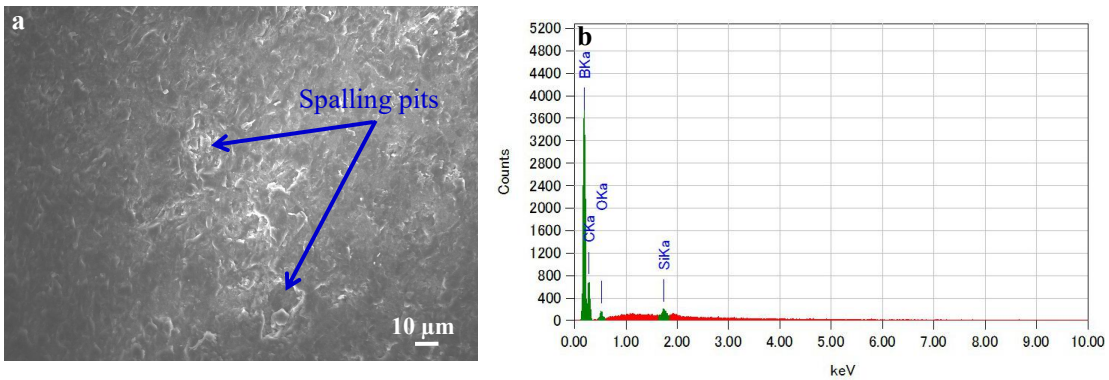

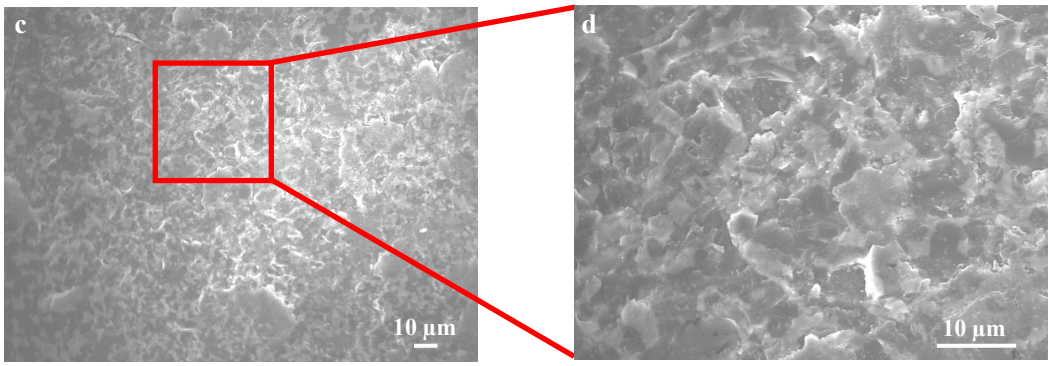

Fig. 7. SEM images of worn surfaces of B_4C (a) and B_4C-SiC (c-d) ceramics at 20 N. An EDS analysis of Fig. 7 (a): (b).

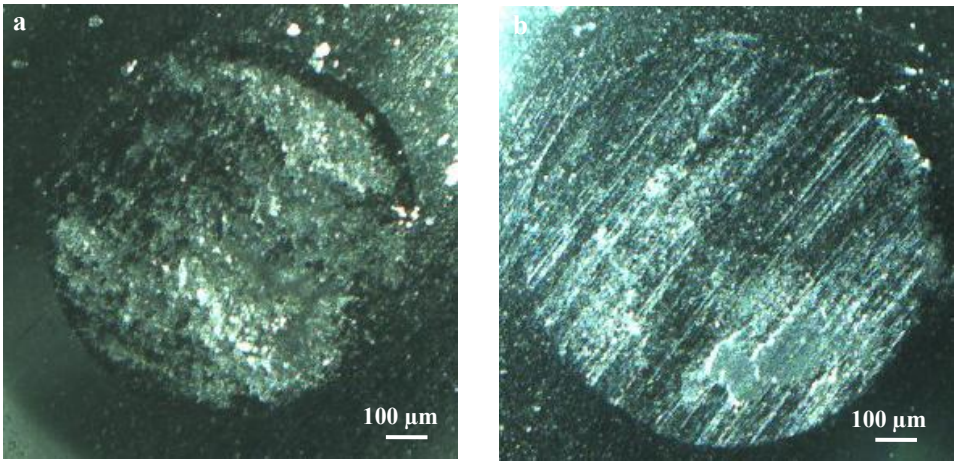

Fig. 8. Microscope images of wear scars on SiC balls after sliding against B_4C (a) and B_4C-SiC (b) ceramics at 20 N.

The major wear types for the B_4C/SiC and B_4C-SiC/SiC tribopairs at different loads are summarized in Table 3. For the B_4C ceramics, the wear mechanism changed from adhesive wear to delamination and spalling of tribofilm as the load was increased from 5 N to 20 N. For the B_4C-SiC ceramics, the wear mechanism changed from surface polishing and mild abrasion to micro-fracture as the load was increased from 5 N to 20 N. At low load, due to the severe adhesive wear and abrasive wear of the B_4C/SiC tribopairs and the beneficial influence of the relief structure on the B_4C-SiC ceramics, the coefficient of friction of the B_4C/SiC tribopair was higher than that of the B_4C-SiC/SiC tribopair, and the specific wear rate of B_4C ceramics was higher than that of B_4C-SiC ceramics. At intermediate load, due to the formation of tribofilm on the B_4C ceramics, adhesive wear and abrasive wear on the B_4C/SiC tribopair were significantly reduced. On the other hand, grain pullout from the B_4C-SiC ceramic matrix and micro-fracture caused deterioration of the relief structure to some extent and roughened the worn surface of the B_4C-SiC ceramics. The coefficient of friction of the B_4C/SiC tribopair was therefore lower than that of the B_4C-SiC/SiC tribopair, and no difference between the specific wear rates of B_4C ceramics and B_4C-SiC ceramics was apparent. At high load, more micro-fracture was caused and the worn surface of B_4C-SiC ceramics further roughened. Thus, the coefficient of friction of the B_4C-SiC/SiC tribopair was higher than that of the B_4C/SiC tribopair. Meanwhile, delamination and spalling of the tribofilm on the B_4C ceramics was increased, which occurred easier than the grain pullout and micro-fracture of B_4C-SiC ceramics, and the specific wear rate of the B_4C ceramics was therefore higher than that of the B_4C-SiC ceramics. Finally, based on the findings of this study, the following design basis and future work can be given for B_4C and B_4C-SiC ceramics sliding against SiC balls under dry sliding conditions: (1) at low load (5 N), B_4C-SiC/SiC tribopairs can show a lower coefficient of

friction and lower systematic specific wear rate; (2) at intermediate load (10 N), B_4C/SiC and B_4C-SiC/SiC tribopairs can reveal similar systematic specific wear rates, as a result of which, from the viewpoint of durability and reliability of a tribosystem, B_4C/SiC tribopairs with a lower coefficient of friction are more suitable for intermediate load; (3) at high load (20 N), B_4C-SiC/SiC tribopairs can exhibit a lower systematic specific wear rate, but a higher coefficient of friction restricts their wide application at high loads. Ways of decreasing the coefficient of friction of B_4C-SiC/SiC tribopairs at high loads should therefore be studied further.

Table 3 Wear types for the B_4C/SiC and B_4C-SiC/SiC tribopairs as a function of load

Load (N)	Tribopairs	
	B_4C/SiC	B_4C-SiC/SiC
5	Adhesive wear, micro-fracture and abrasive wear	Surface polishing and mild abrasion
10	Delamination of tribofilm and micro-fracture	Surface polishing, mild abrasion, micro-fracture and abrasive wear
20	Delamination and spalling of tribofilm and micro-fracture	Micro-fracture and abrasive wear

4.4. Conclusions

B_4C and B_4C-SiC ceramics were studied for dry sliding friction and wear against commercially available SiC balls at 5 N, 10 N and 20 N. The following results were obtained:

(1) When the load was increased from 5 N to 20 N, the average coefficient of friction of the B_4C ceramics varied in the range of 0.24-0.44, while the average coefficient of friction of the B_4C-SiC ceramics varied in the range of 0.32-0.48; the average specific wear rate of the B_4C ceramics varied in the range of 11.0-22.4×10^{-6} $mm^3/N·m$, while the average specific wear rate of the B_4C-SiC ceramics varied in the range of 1.3-7.3×10^{-6} $mm^3/N·m$. Both the coefficient of friction and specific wear rate of the B_4C ceramics first decreased and then increased with increases in load, while both the coefficient of friction and specific wear rate of the B_4C-SiC ceramics increased with increases in load.

(2) At low load, the B_4C ceramics showed a higher coefficient of friction and higher specific wear rate due to severe adhesive wear and abrasive wear, while the B_4C-SiC ceramics exhibited a lower coefficient of friction and lower specific wear rate due to the relief structure. The specific wear rate of the B_4C ceramics was an order of magnitude higher than that of the B_4C-SiC ceramics.

(3) At intermediate load, the B_4C ceramics showed a lower coefficient of friction due to the formation of tribofilm, while the B_4C-SiC ceramics exhibited a higher coefficient of friction due to a certain degree of damage of the relief structure and roughened worn surface. No difference between the specific wear rates of B_4C ceramics and B_4C-SiC ceramics was apparent.

(4) At high load, B_4C-SiC ceramics showed a higher coefficient of friction due to greater micro-fracture. Meanwhile, the delamination and spalling of tribofilm on the B_4C ceramics was increased, occurring more easily than the grain pullout and micro-fracture of B_4C-SiC ceramics. Clearly then, the specific wear rate of B_4C ceramics was higher than that of B_4C-SiC ceramics.

4.5. References

[1] F. Thévenot. Boron carbide- a comprehensive review. Journal of the European Ceramic

Society,1990,6(4):205-225.
[2] W. Zhang, S. Yamashita, H. Kita. Progress in pressureless sintering of boron carbide ceramics-A review. Advances in Applied Ceramics: Structural, Functional and Bioceramics,2019,118(4):222-239.
[3] P. H. Shipway, I. M. Hutchings. The influence of particle properties on the erosive wear of sintered boron carbide. Wear,1991,149:85-98.
[4] J. X. Deng. Erosion wear of boron carbide ceramic nozzles by abrasive air-jets. Materials Science and Engineering A,2005,408(1-2):227-233.
[5] P. H. Shipway, J. J. Hogg. Wear of bulk ceramics in micro-scale abrasion-The role of abrasive shape and hardness and its relevance to testing of ceramic coatings. Wear,2007,263(7):887-895.
[6] A. L. Ortiz, V. M. Candelario, O. Borrero-López, F. Guiberteau. Sliding-wear resistance of pure near fully-dense B_4C under lubrication with water, diesel fuel, and paraffin oil. Journal of the European Ceramic Society,2018,38(4):1158-1163.
[7] W. Pan, Y. M. Gao. Tribological behavior of B_4C/hBN ceramic composites coupled with grey iron under the lubrication of emulsion. Materials Research Express,2018,5(6):066512.
[8] X. Q. Li, Y. M. Gao, W. Pan, Z. C. Zhong, L. C. Song, W. Chen, Q. X. Yang. Effect of hBN content on the friction and wear characteristics of B_4C-hBN ceramic composites under dry sliding condition. Ceramics International,2015,41(3):3918-3926.
[9] X. Q. Li, Y. M. Gao, S. Z. Wei, Q. X. Yang, Z. C. Zhong. Dry sliding tribological properties of self-mated couples of B_4C-hBN ceramic composites. Ceramics International,2017,43(1):162-166.
[10] R. Alexander, K.V. Ravikanth, R. D. Bedse, T. S. R. Ch. Murthy, K. Dasgupta. Effect of carbon fiber on the tribo-mechanical properties of boron carbide: Comparison with carbon nanotube reinforcement. International Journal of Refractory Metals & Hard Materials,2019,85:105055.
[11] T. S. R. Ch. Murthy, S. Ankata, J. K. Sonber, K. Sairam, K. Singh, A. Nagaraj, P. Sengupta, R. D. Bedse, S. Majumdar, V. Kain. Microstructure, thermo-physical, mechanical and wear properties of in-situ formed boron carbide-zirconium diboride composite. Ceramics-Silikáty,2018,62(1):15-30.
[12] B. M. Moshtaghioun, A. L. Ortiz, D. Gómez-García, A. Domínguez-Rodríguez. Toughening of super-hard ultra-fine grained B_4C densified by spark-plasma sintering via SiC addition. Journal of the European Ceramic Society,2013,33(8):1395-1401.
[13] Y. G. Tkachenko, V. F. Britun, É. V. Prilutskii, D. Z. Yurchenko, G. A. Bovkun. Structure and properties of B_4C-SiC composites. Powder Metallurgy and Metal Ceramics,2005,44(3-4):196-201.
[14] Y. L. Zhang, X. G. Song, G. J. Li, Y. M. Zhang. Oxidation behavior research of the SiC/B_4C multiphase ceramics. Applied Mechanics and Materials,2015,727-728:288-291.
[15] W. Zhang, S. Yamashita, T. Kumazawa, F. Ozeki, H. Hyuga, H. Kita. Influence of surface roughness parameters and surface morphology on friction performance of ceramics. Journal of the Ceramic Society of Japan,2019,127(11):837-842
[16] W. Zhang, S. Yamashita, T. Kumazawa, F. Ozeki, H. Hyuga, H. Kita. Study on friction behavior of SiC-B_4C composite ceramics after annealing. Industrial Lubrication and Tribology,2020,72(5):673-679.
[17] W. Zhang, S. Yamashita, H. Kita. Progress in tribological research of SiC ceramics in unlubricated sliding-A review. Materials & Design,2020,190:108528.
[18] S. K. Sharma, B. V. M. Kumar, Y. W. Kim. Effect of WC addition on sliding wear behavior of SiC ceramics. Ceramics International,2015,41(3):3427-3437.
[19] J. K. Sonber, P. K. Limaye, T. S. R. Ch. Murthy, K. Sairam, A. Nagaraj, N. L. Soni, R. J. Patel, J. K. Chakravartty. Tribological properties of boron carbide in sliding againstWC ball. International Journal of Refractory Metals and Hard Materials,2015,51:110-117.
[20] L. Micele, G. Palombarini, S. Guicciardi, L. Silvestroni. Tribological behaviour and wear resistance of a

SiC-$MoSi_2$ composite dry sliding against Al_2O_3. Wear,2010,269(5):368-375.

[21] Y. G. Gogotsi, A. M. Koval'chenko, I. A. Kossko. Tribochemical interactions of boron carbides against steel. Wear,1992,154:133-140.

[22] V. S. R. Murthy, H. Kobayashi, S. Tsurekawa, N. Tamari, T. Watanabe, K. Kato. Influence of humidity and doping elements on the friction and wear of SiC in unlubricated sliding. Tribology International,2004,37(5):353-364.

[23] X. Q. Cao, L. L. Shang, Y. M. Liang, G. G. Zhang, Z. B. Lu, Q. J. Xue. The tribological performances of the boron carbide films tested under wet air and wet N_2 conditions. Tribology Letters,2019,67(3):70.

[24] G. R. Anstis, P. Chantikul, B. R. Lawn, D. B. Marshall. A critical evaluation of indentation techniques for measuring fracture toughness: I, direct crack measurements. Journal of the American Ceramic Society,1981,64(9):533-538.

[25] F. Wu, L. S. Wang, J. S. Zhang, Y. Fan, B. W. Liu, Y. Gao. Tribological properties of hot-pressed boron carbide ceramic. Transactions of Nonferrous Metals Society of China,2001,11(1):119-122.

[26] W. Zhang, S. Yamashita, T. Kumazawa, F. Ozeki, H. Hyuga, H. Kita. Effect of nanorelief structure formed in situ on tribological properties of ceramics in dry sliding. Ceramics International,2019,45(11):13818-13824.

[27] W. Zhang, S. Yamashita, T. Kumazawa, F. Ozeki, H. Hyuga, W. Norimatsu, H. Kita. A study on formation mechanisms of relief structure formed in situ on the surface of ceramics. Ceramics International,2019,45(17):23143-23148.

[28] W. Zhang, S. Yamashita, H. Kita. Tribological properties of SiC-B_4C ceramics under dry sliding condition. Journal of the European Ceramic Society,2020,40(8):2855-2861.

[29] R. Lörcher, R. Telle, G. Petzow. Influence of mechanical and tribochemical properties on the wear behaviour of B_4C-TiB_2-W_2B_5 composites. Materials Science and Engineering A,1988,105-106:117-123.

[30] H. Y. Zhu, Y. R. Niu, C. C. Lin, L. P. Huang, H. Ji, X. B. Zheng. Fabrication and tribological evaluation of vacuum plasma-sprayed B_4C coating. Journal of Thermal Spray Technology,2012,21(6):1216-1223.

[31] S. J. Cho, C. D. Um, S. S. Kim. Wear and wear transition in silicon carbide ceramics during sliding. Journal of the American Ceramic Society,1996,79(5):1247-1251.

[32] X. Dong, S. Jahanmir, L. K. Ives. Wear transition diagram for silicon carbide. Tribology International,1995,28(8):559-572.

[33] T. E. Fischer, Z. Zhu, H. Kim, D. S. Shin. Genesis and role of wear debris in sliding wear of ceramics. Wear,2000,245(1):53-60.

[34] W. Pan, Y. M. Gao, X. Q. Li, S. S. Wu, L. C. Song, Z. C. Zhong. Tribological behavior of B_4C/hBN ceramic composites sliding against gray cast irons without lubrication. Tribology Letters,2015,60(1):10.

Chapter 5
A ceramic with low friction and low wear under water lubrication: B_4C-SiC

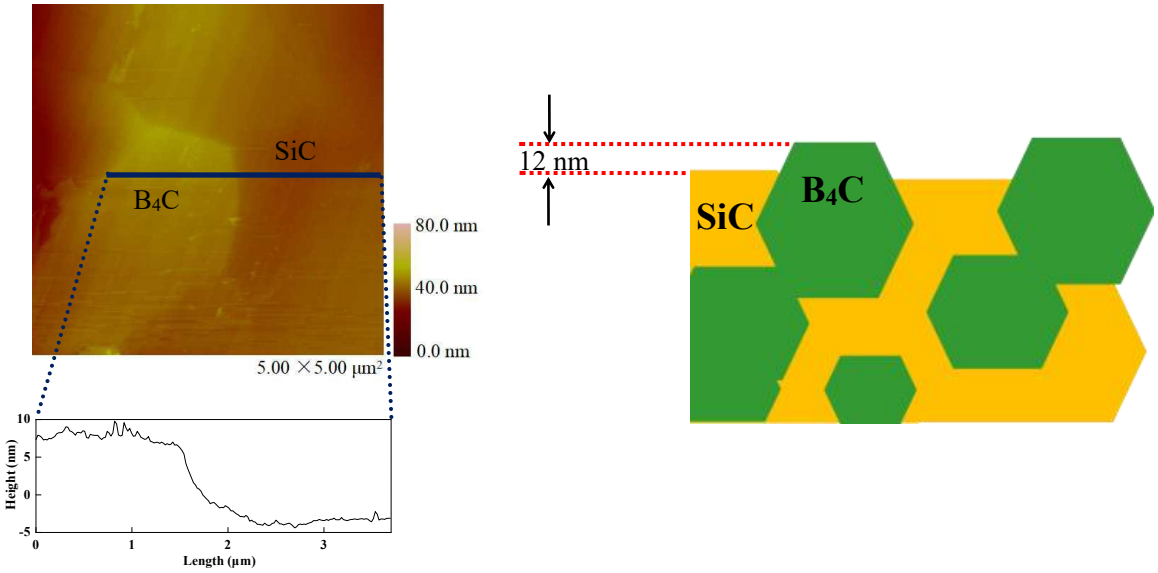

The tribological properties of carbide ceramics (SiC, B_4C-SiC, B_4C) in water were investigated. Compared with traditional SiC ceramics used as mechanical seal materials, B_4C-SiC ceramics exhibit lower friction and wear when sliding against SiC balls under water lubrication. The lower COF of B_4C-SiC ceramics is ascribed to the nano-relief with valleys with depth of 12 nm formed on their friction surfaces under water lubrication. Nano-relief formed by in situ can show beneficial influence similar to micron-relief produced by laser for frictional property of materials under water lubrication. B_4C-SiC ceramics with better tribological properties are expected to replace traditional SiC ceramics as mechanical seal materials under water lubrication. A new design idea that using the microhardness difference between the two phases of composite ceramics to prepare relief in situ on composite ceramic surface to improve the frictional property under water lubrication has been proposed in this study.

Contents

5.1. Introduction

Mechanical seals are mechanical components applied to seal the rotating shaft and the stationary pump cavity. Rotating and stationary rings are the most important components of mechanical seal. The materials of rotating and stationary rings determine the friction, wear and sealing property of the mechanical seals, as well as the service life of mechanical seals. Therefore, the choice of materials for rotating and stationary rings is very important. Generally, the materials with low friction and low wear are suitable for rotating and stationary rings of mechanical seal. Advanced engineering ceramic materials are often selected as mechanical seal materials. On the other hand, ceramics/water combination has gradually replaced metal/oil combination in modern mechanical design due to better environmental sustainability and safer disposal following leakage.

Carbide ceramics have many outstanding characteristics like excellent wear resistance, high hardness, and low density [1-7]. To date, silicon carbide (SiC) ceramics are widely applied as wear-resistant components in mechanical engineering field [8-10]. Compared with another Si-based non-oxide ceramics-silicon nitride (Si_3N_4) ceramics, which also show low friction under water lubrication, SiC ceramics can exhibit lower wear due to higher hardness [11]. Accordingly, SiC ceramics have been successfully used as mechanical seals and bearings [12, 13]. For the current typical combination materials of mechanical seals, especially for the application in harsh conditions, SiC ceramic is used as a rotating ring, and another SiC ceramic is used as a stationary ring [14, 15]. Among carbide ceramics, boron carbide (B_4C) ceramics also have extremely high hardness, which are expected to be potential candidates for tribological applications [16-18]. Further, B_4C has lower density than that of SiC, thus, B_4C and B_4C-based ceramics are considered to be more suitable as movable or rotatory tribo-elements, where the weight reduction has practical significance. Until now, the investigations on tribological behaviors of B_4C and B_4C-based ceramics sliding in water are rather limited [19, 20]. In our previous works [21-25], we found by foundational research that under dry sliding, B_4C-SiC ceramics could exhibit better tribological properties as compared to monolithic SiC or B_4C ceramics under certain conditions. Nonetheless, there is no report on tribological performance of B_4C-SiC ceramics under lubrication condition. How about the tribological performance of B_4C-SiC ceramics under water lubrication?

Although SiC ceramics are successfully used as mechanical seals, are SiC ceramics the best materials for mechanical seals? To further decrease friction and wear for the materials used as mechanical seals, new materials should be developed. Meanwhile, to expand the application of carbide ceramics, the tribological properties of carbide ceramics under water lubrication should be studied. Therefore, the aim of this study is to develop new materials suitable for mechanical seals working in water environment, and to compare tribological properties of other carbide ceramics (B_4C and B_4C-SiC ceramics) with traditional SiC ceramics used as mechanical seals under water lubrication.

5.2. Experimental procedures

For preparation of the carbide ceramics, B_4C powder (purity: 98%; average particle size: 0.8 μm) and SiC powder (purity: 97%; average particle size: 0.4 μm) were chosen as starting materials, and carbon black (purity:99%; average particle size: 20-30 nm) was used as a sintering aid. The compositions of the carbide ceramics and their numbers are presented in Table 1. The powder mixtures were mixed in ethanol using SiC balls for 24 h, and then were pressed into discs, followed by cold-isostatically pressing at a pressure of 196 MPa. The discs were sintered using an electrical furnace via pressureless sintering at the temperature of 2300 ℃ for a dwell time of 3 h, in argon atmosphere.

Table 1 Compositions of the carbide ceramics (wt%) and their numbers.

Specimens	SiC	B_4C	C
MS	98	2	5
S80B20	80	20	5
S60B40	60	40	5
S40B60	40	60	5
S20B80	20	80	5
MB	0	100	5

Bulk density of specimens was measured using Archimedes' method, with the relative density evaluated. The macrohardness and fracture toughness were tested by Vickers' indentation with an applied load of 10 kg for a dwell time of 10 s. Each test was repeated seven times. The properties of the carbide ceramics are presented in Table 2.

Table 2 Properties of the carbide ceramics.

Specimens	Bulk density (g/cm^3)	Relative density (%)	Hardness (Gpa)	Fracture toughness ($MPa \cdot m^{1/2}$)
MS	3.11	97.28	27.5	2.96
S80B20	2.95	97.18	30.1	2.92
S60B40	2.78	96.22	33.7	3.20
S40B60	2.64	96.15	30.3	3.13
S20B80	2.53	96.43	29.9	3.19
MB	2.40	95.71	27.7	3.60

Water-lubricated sliding friction and wear tests were performed in a ball-on-disc machine (T-18-0162, Nanovea, US), as schematically shown in Fig. 1. The disc specimens with a size of 27 × 27 × 2.7 mm^3 were taken from the carbide ceramics, and the final roughness (Ra) after grinding and polishing was less than 0.06 μm. Before test, all discs and balls were washed using ethanol in an ultrasonic bath for 20 min. During the test, the friction surfaces were submerged in deionized water all the time. The parameters of water-lubricated sliding tests are summarized in Table 3. The coefficient of friction (COF) was measured by the machine directly. The wear rate was calculated with the equation of WR=ΔV/SL, where ΔV is wear volume, S is sliding distance, and L is normal load. The wear volumes (ΔV) of carbide ceramics and balls were calculated from surface profile traces across the wear track and from wear scars, respectively.

SEM was used to observe the friction surface morphologies of carbide ceramics. The friction surface compositions of carbide ceramics were analyzed by XPS. The friction surface images and profile were characterized using AFM. Water samples with filtration after sliding tests were investigated by ICP-AES.

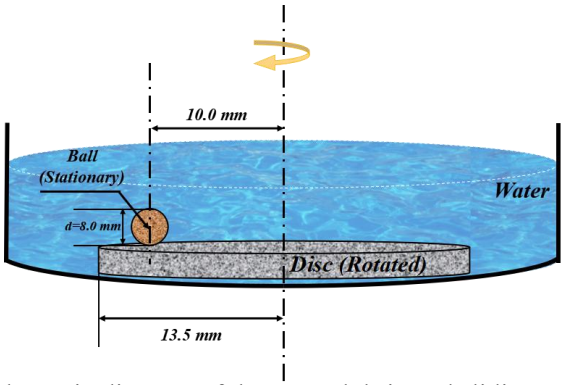

Fig. 1. Schematic diagram of the water-lubricated sliding tests.

Table 3 Parameters of water-lubricated sliding friction and wear tests.

Parameters	Conditions
Counterbody	Commercially available SiC ball (roughness (Ra): 0.05 μm)
Load (N)	20
Sliding velocity (m/s)	0.1
Friction distance (m)	1000
Sliding radius (mm)	10
Ambient temperature (°C)	20-23.5

5.3. Results and discussion

Fig. 2 reveals the experimental curves of COF of carbide ceramics vs. friction distance under water lubrication and average COF of carbide ceramics. The experimental curves of COF of carbide ceramics first gradually decrease with increase in friction distance, and then enter into steady state. In addition, the average COFs of MB and B_4C-SiC ceramics are lower than that of MS, and the average COFs of B_4C-SiC ceramics are lower than that of MB. Fig. 3 presents the wear rates of carbide ceramics, SiC balls against carbide ceramics, and sum of carbide ceramics and balls (systematic wear rate). The wear rates of B_4C-SiC ceramics are lower than those of MS and MB, and MB exhibits the highest wear rate. Meanwhile, the wear rates of SiC balls gradually decrease with increase in B_4C content of the carbide ceramics. As to the systematic wear rates, the systematic wear rates of B_4C-SiC ceramics are lower as compared to MS and MB, and S40B60 exhibits the lowest systematic wear rate. On the whole, the B_4C-SiC ceramics exhibit better tribological properties than those of MS and MB under water lubrication.

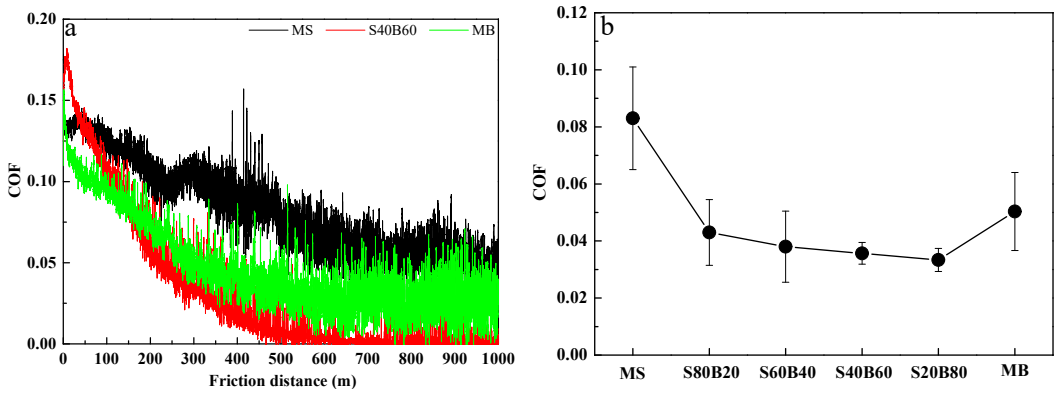

Fig. 2. COF of carbide ceramics vs. friction distance (a), and average COF of carbide ceramics (b).

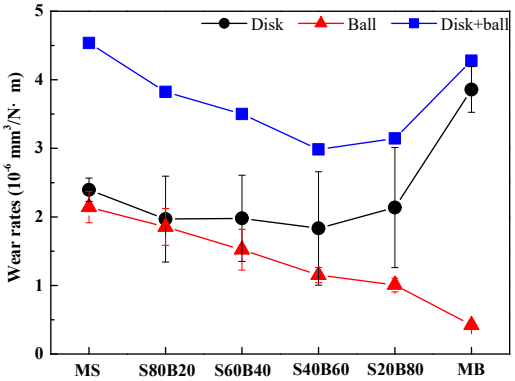

Fig. 3. Wear rates of carbide ceramics, SiC balls against carbide ceramics, and sum of carbide ceramics and balls (systematic wear rate).

The friction surface morphologies of carbide ceramics are shown in Fig. 4. In B_4C-SiC ceramics, the black areas are B_4C particles, and the gray areas are SiC particle. For MS, a small amount of B_4C particles, which are used as a sintering aid, are observed. For B_4C-SiC ceramics, B_4C and SiC particles can be seen clearly, and no tribolayer can be found. For MB, no secondary particles are observed due to its nature of single phase. All the friction surfaces of carbide ceramics are relatively smooth, no grain pull-out or fracture are found. The compositions of the friction surfaces of carbide ceramics are analyzed by XPS, as shown in Fig. 5. For the symmetrical Si_{2p} spectra with a binding energy of 99.7-99.9 eV of MS and S40B60, they are attributed to SiC [26]. For the symmetrical B_{1S} peaks with a binding energy of 187.5 eV of S40B60 and MB, they correspond to B_4C [27, 28]. It is reported that the SiO_2 tribochemical layer, which is the product of tribochemical reaction of SiC ceramics, would be formed on the friction surface, leading to the reduced COF for SiC ceramics [29-32]. However, in this study, neither silicon oxide/hydroxide nor boron oxide/hydroxide exists on the friction surfaces of carbide ceramics. Therefore, it can be concluded that the better frictional property of B_4C-SiC ceramics are not caused by oxide tribochemical layer.

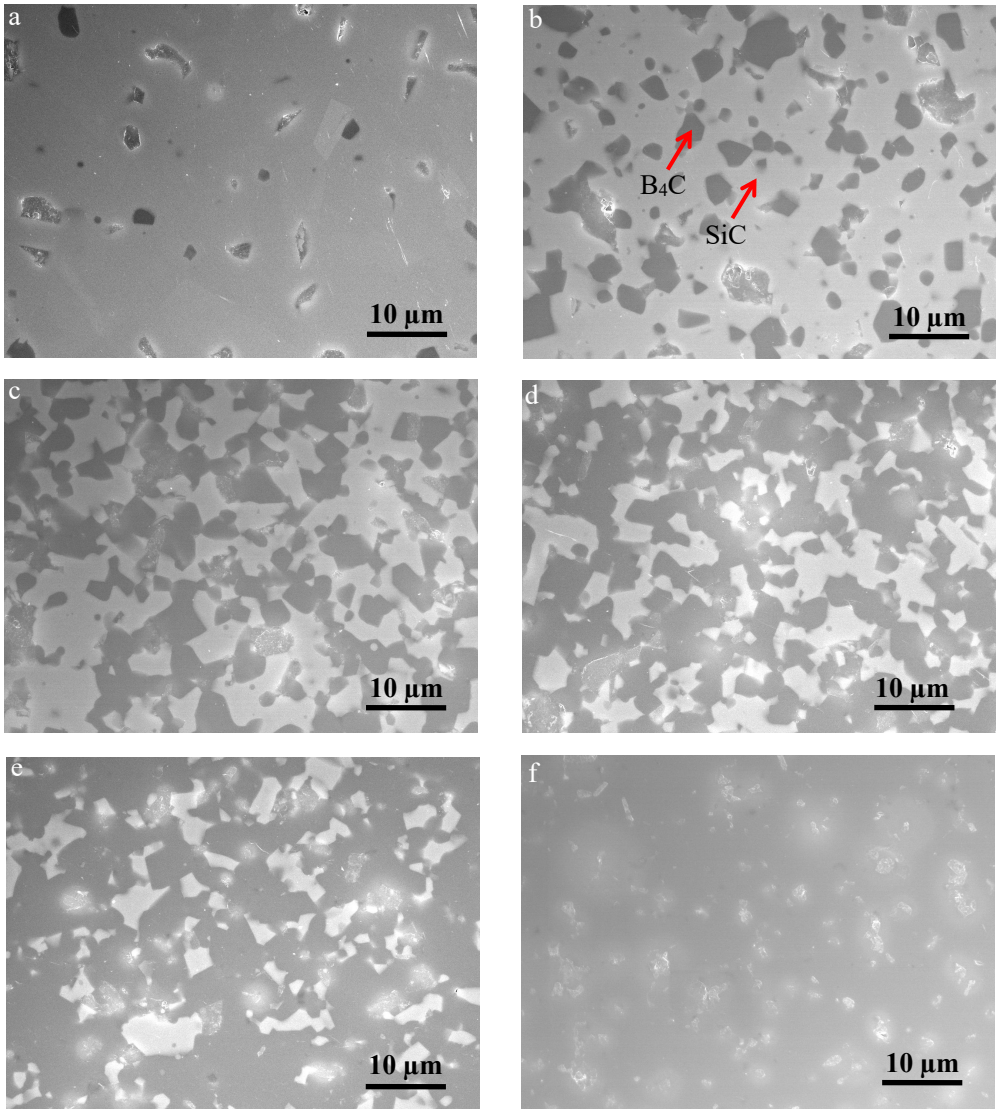

Fig. 4. Friction surface morphologies of carbide ceramics: (a) MS, (b) S80B20, (c) S60B40, (d) S40B60, (e) S20B80, and (f) MB.

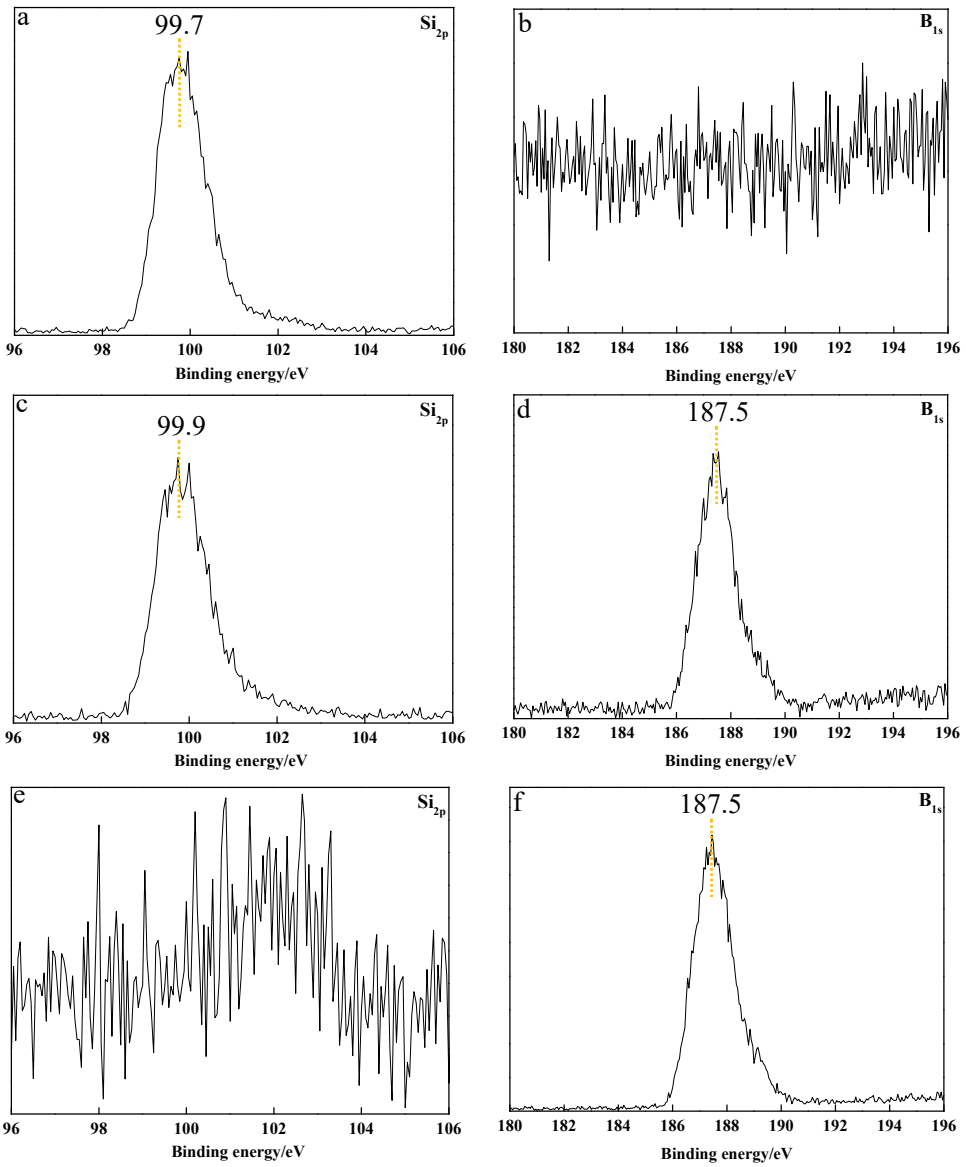

Fig. 5. XPS results of the friction surfaces of carbide ceramics: (a-b) MS, (c-d) S40B60, and (e-f) MB.

AFM image of friction surface of S60B40 and the corresponding image binarized by surface elevation difference are shown in Fig. 6. The red areas in Fig. 6(b) are convex, and the gray areas are recessed. The ratio of the convex areas, which is calculated by image analysis using default threshold of the software "ImageJ", is about 43.5%, which is close to the volume fraction of B_4C (46.0%) in S60B40. Therefore, it can be concluded that the higher particles on the B_4C-SiC ceramic friction surfaces are B_4C particles. The AFM image of friction surface of S40B60 and the surface profile corresponding to line scan across the friction surface are shown in Fig. 7. The surface elevation difference can also be observed on the friction surface of S40B60. In our previous work, we found that the relief with a depth of less than 10 nm is formed on the B_4C-SiC ceramic surface after polishing [33]. This is because that B_4C grains have a higher microhardness as compared to SiC grains, thereby SiC particles are preferentially worn by free diamond particles during polishing. From Fig. 7, it can be seen that the relief still exists on the B_4C-SiC ceramic friction surface after friction under water lubrication, and the elevation difference between B_4C particles and SiC particles is approximate 12 nm. It is widely reported that the relief produced via laser with a depth of micron size (micron-relief structure) on surface of materials can significantly improve tribological properties for materials under lubrication [34-38], the mechanisms of which are as follows: (1) lubricants can be stored in the dimples to keep continuous lubrication for friction surface [39]; and (2) additional hydrodynamic

pressure can be generated to enhance the load carrying capacity [40], which indicates that materials can work with low friction in a wider load range. In this study, the B_4C-SiC ceramic surfaces with relief structure with nano size (nano-relief structure) after friction under water lubrication is observed, whose schematic diagram is shown in Fig. 8. The diameter of water molecule is 0.4 nm, thus the B_4C-SiC ceramics with nano-relief can store more water in the valleys with depth of 12 nm on the friction surface as compared to MS and MB. We consider that the benefits from the micron-relief structure also applies to the nano-relief structure. This indicates that the nano-relief structure on surface is favorable for decreasing friction and increasing load carrying capacity for B_4C-SiC ceramics. The COF range of carbide ceramics is 0.03-0.09, thereby the carbide ceramics are sliding under mixed lubrication, which means there is still a certain degree of solid-solid contact on the friction surfaces between carbide ceramics and SiC counterbody. On the one hand, the water stored in the valleys of nano-relief can provide continuous lubrication to the B_4C-SiC ceramic friction surfaces; on the other hand, load carrying capacity of B_4C-SiC ceramics is expected to be improved by this nano-relief, making B_4C-SiC ceramics exhibit lower COF under higher loads (20 N) than those of MS and MB. However, for MS, although there are secondary B_4C particles, which are used as a sintering aid, on the friction surface, the amount of B_4C particles is too low to form effective nano-relief structure for MS. For MB, there are no secondary particles in it, thereby, there is no relief structure formed by the difference in microhardness between the two phases on its surface. Therefore, the COFs of MS and MB are higher as compared to B_4C-SiC ceramics, and the higher COF of MS than that of MB is attributed to self-mated tribopair [41].

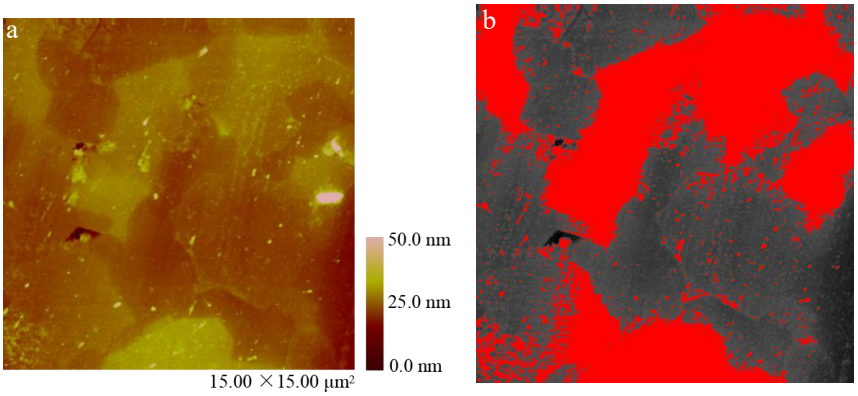

Fig. 6. AFM image of friction surface of S60B40 (a), and the corresponding image binarized by surface elevation difference (b).

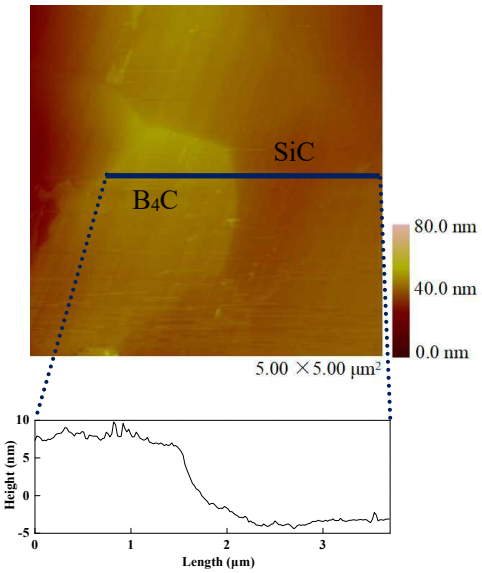

Fig. 7. AFM image of friction surface of S40B60 and the surface profile corresponding to line scan across the

friction surface.

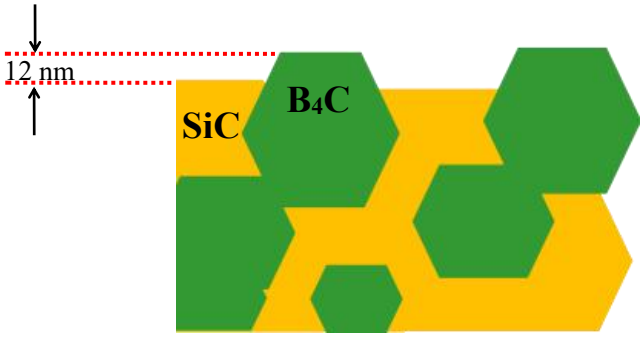

Fig. 8. Schematic diagram of B_4C-SiC ceramic friction surface with relief with nano size (nano-relief structure).

All in all, the lower COF of B_4C-SiC ceramics is ascribed to nano-relief on the friction surface. Although micron-relief produced by laser can also improve frictional property for SiC ceramics [37], there are some disadvantages for this method: (1) the preparation process is complex; (2) the cost is high; (3) large defects are induced for ceramics; (4) ring-like heat influenced areas around dimples caused by heat accumulation effect from the laser can result in the formation of crack and unsmooth surface in the heat affected zone, which can prevent the SiC ceramic surface from becoming smooth; and (5) the residual bulges around the dimple rims produced by the heat are needed to remove after laser treatment. Compared with micron-relief on SiC ceramics produced artificially by laser processing, nano-relief can be formed on B_4C-SiC ceramic surface in situ, and this nano-relief will be durable on the friction surface during friction under water lubrication. Nano-relief formed by in situ can not only show beneficial influence similar to micron-relief produced by laser for frictional property of materials under water lubrication, but also avoid the disadvantages of micro-relief. Therefore, B_4C-SiC ceramics with lower friction and lower wear are expected to replace traditional SiC ceramics to be used as mechanical seal materials under water lubrication. Meanwhile, a new design idea that using the microhardness difference between the two phases of composite ceramics to prepare relief in situ on composite ceramic surface to improve the frictional property under water lubrication has been proposed in this study.

To clarify the wear mechanism of carbide ceramics, the concentration of Si and B elements in the water samples after carbide ceramics sliding in water is analyzed by ICP-AES, whose results are shown in Fig. 9. Both Si and B are detected in the water samples. With increasing B_4C content in the carbide ceramics, the concentration of Si in water gradually decreases, whereas the concentration of B gradually increases. This indicates that both SiC and B_4C have undergone the tribochemical reactions. The tribochemical reactions of SiC can be expressed as follows [30, 42]:

$$SiC + 2H_2O = SiO_2 + CH_4 \quad (1)$$

$$SiO_2(s) + 2H_2O(l) = H_4SiO_4\ (aq) \quad (2)$$

The tribochemical reaction of B_4C can be expressed as follow [43]:

$$B_4C + 12H_2O = 4H_3BO_3 + C + 6H_2 \quad (3)$$

As a result, tribochemical wear is one of the wear mechanisms of the carbide ceramics. On the other hand, some narrow, shallow grooves can be observed on the friction surface of S60B40 (Fig. 6(a)), thus the mechanical wear of the carbide ceramics is mainly achieved by micro-cutting. Therefore, the wear mechanisms of carbide ceramics are mechanical wear and tribochemical wear. The macrohardness of B_4C-SiC ceramics is higher than those of MS and MB (Table 2). The material with higher hardness can exhibit better wear resistance [44, 45], thereby, the mechanical wear of B_4C-SiC ceramics is lower as compared to MS and MB under mixed lubrication. For MS and MB, their macrohardness is similar (Table 2), however, the wear rate of MB is higher than that of MS (Fig. 2). This phenomenon is caused by the different tribochemical wear between MS and MB. For MS/SiC tribopair, the wear rate of MS disc is similar with that of SiC ball, therefore, it is considered that about half of the concentration

of Si in water comes from the tribochemical reactions of SiC ball. Accordingly, the concentration of Si in water coming from the tribochemical reactions of MS is about 0.5 mg/L, which is lower than that of B in water from the tribochemical reaction of MB. This suggests that the tribochemical reactions of MS is weaker than that of MB, i.e., B_4C grains are subjected to more tribochemical wear than that of SiC grains. Therefore, MB exhibits the highest wear rate. Although the B_4C grains in B_4C-SiC ceramics are subjected to stronger tribochemical wear as compared to SiC grains in B_4C-SiC ceramics, the microhardness of B_4C is higher than that of SiC. For B_4C grains in B_4C-SiC ceramics, it is considered that the beneficial influence from higher microhardness to resist mechanical wear is more than the deteriorated influence from stronger tribochemical wear. As a result, B_4C grains exhibit a higher height than that of SiC grains on the B_4C-SiC ceramic friction surfaces. Finally, the wear rate of SiC ball gradually decreases when sliding against carbide ceramics with increase in B_4C content, which is caused by the gradually reduced chemical similarity between carbide ceramics and SiC balls.

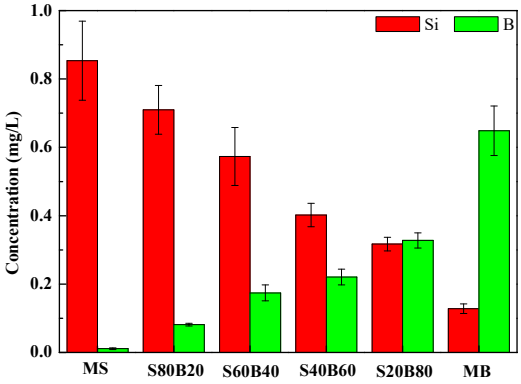

Fig. 9. Concentration of Si and B elements in the water samples after carbide ceramics sliding in water.

5.4. Conclusions

In this study, the tribological properties of carbide ceramics (SiC, B_4C-SiC, B_4C) in water were investigated. The following results can be obtained:

(1) B_4C-SiC ceramics exhibit lower COF and wear as compared to monolithic SiC and B_4C ceramics when sliding against SiC balls under water lubrication.

(2) The lower COF of B_4C-SiC ceramics is ascribed to the nano-relief with valleys with depth of 12 nm formed on their friction surfaces under water lubrication. Nano-relief formed by in situ can show beneficial influence similar to micron-relief produced by laser for frictional property of materials under water lubrication.

(3) B_4C-SiC ceramics with lower friction and wear are expected to replace traditional SiC ceramics as mechanical seal materials under water lubrication.

5.5. References

[1] W. Zhang, S. Yamashita, H. Kita. Self lubrication of pressureless sintered SiC ceramics. Journal of Materials Research and Technology,2020,9(6):12880-12888.

[2] V. Brizmer, Y. Kligerman, I. Etsion. A laser surface textured parallel thrust bearing. Tribology Transactions,2003,46(3):397-403.

[3] W. Zhang, S. Yamashita, H. Kita. Progress in pressureless sintering of boron carbide ceramics-A review. Advances in Applied Ceramics: Structural, Functional and Bioceramics,2019,118(4):222-239.

[4] A. L. Ortiz, V. M. Candelario, O. Borrero-López, F. Guiberteau. Sliding-wear resistance of pure near

fully-dense B_4C under lubrication with water, diesel fuel, and paraffin oil. Journal of the European Ceramic Society,2018,38(4):1158-1163.

[5] W. Zhang, S. Yamashita, T. Kumazawa, F. Ozeki, H. Hyuga, H. Kita. Study on friction behavior of SiC-B_4C composite ceramics after annealing. Industrial Lubrication and Tribology,2020,72(5):673-679.

[6] W. Zhang, S. Yamashita, H. Kita. Effect of counterbody on tribological properties of B_4C-SiC composite ceramics. Wear,2020,458-459:203418.

[7] Y. G. Tkachenko, B. L. Grabchuk, N. I. Bodnaruk, V. V. Sychev. Friction and wear of boron carbide at temperatures in the range 20-1500 °C. Soviet Powder Metallurgy & Metal Ceramics,1977,16(7):541-543.

[8] X. Wang, K. Kato, K. Adachi. Running-in effect on the load-carrying capacity of a water-lubricated SiC thrust bearing. Proceedings of the Institution of Mechanical Engineers, Part J: Journal of Engineering Tribology,2005,219:117-124.

[9] W. Zhang, S. Yamashita, H. Kita. Progress in tribological research of SiC ceramics in unlubricated sliding-A review. Materials & Design,2020,190:108528.

[10] J. J. Chen, Q. C. Sun, W. Y. Chen, S. Y. Zhu, W. S. Li, J. Cheng, J. Yang. High-temperature tribological behaviors of ZrO2/h-BN/SiC composite under air and vacuum environments. Tribology International,2021,154:106748.

[11] P. Andersson, P. Lintula. Load-carrying capability of water-lubricated ceramic journal bearings. Tribology International,1994,27(5):315-321.

[12] X. L. Wang, K. Kato, K. Adachi, K. Aizawa. Loads carrying capacity map for the surface texture design of SiC thrust bearing sliding in water. Tribology International,2003,36(3):189-197.

[13] X. L. Wang, K. Kato. Improving the anti-seizure ability of SiC seal in water with RIE texturing. Tribology Letters,2003,14(4):275-280.

[14] H. Tomizawa, T. E. Fischer. Friction and wear of silicon nitride and silicon carbide in water: hydrodynamic lubrication at low sliding speed obtained by tribochemical wear. ASLE Transactions,1987,30(1):41-46.

[15] H. Nagasaka, K. Ito, J. Mori, T. Shimizu, S. Sasaki. Tribological properties of polycrystalline diamond films prepared by hot-filament chemical vapor deposition methods. Proceedings of the 16th International Conference on Nanotechnology, IEEE, 2016.

[16] X. Q. Li, Y. M. Gao, L. C. Song, Q. X. Yang, S. Z. Wei, L. You, Y. C. Zhou, G. S. Zhang, L. J. Xu, B. Yang. Influences of hBN content and test mode on dry sliding tribological characteristics of B4C-hBN ceramics against bearing steel. Ceramics International,2018,44(6):6443-6450.

[17] W. Zhang, S. Yamashita, T. Kumazawa, F. Ozeki, H. Hyuga, H. Kita. Tribological properties of B_4C ceramics prepared by pressureless sintering and annealed at different temperatures. Tribology Transactions,2020,63(4):672-682.

[18] W. Zhang. A review of tribological properties for boron carbide ceramics. Progress in Materials Science,2021,116:100718.

[19] X. Q. Li, Y. M. Gao, Q. X. Yang, W. Pan, Y. F. Li, Z. C. Zhong, L. C. Song. Evaluation of tribological behavior of B_4C-hBN ceramic composites under water-lubricated condition. Ceramics International,2015,41(6):7387-7393.

[20] X. Q. Li, Y. M. Gao, Q. X. Yang. Sliding tribological performance of B_4C-hBN composite ceramics against AISI 321 steel under distilled water condition. Ceramics International,2017,43(17):14932-14937.

[21] W. Zhang, S. Yamashita, H. Kita. Tribological properties of SiC-B_4C ceramics under dry sliding condition. Journal of the European Ceramic Society,2020,40(8):2855-2861.

[22] W. Zhang, S. Yamashita, T. Kumazawa, F. Ozeki, H. Hyuga, H. Kita. Effect of nanorelief structure formed in situ on tribological properties of ceramics in dry sliding. Ceramics International,2019,45(11):13818-13824.

[23] W. Zhang, S. Yamashita, H. Kita. A study of B_4C-SiC composite for self-lubrication. Journal of the American

Ceramic Society, DOI: 10.1111/jace.17584.
[24] W. Zhang, S. Yamashita, H. Kita. Effects of load on tribological properties of B_4C and B_4C-SiC ceramics sliding against SiC balls. Journal of Asian Ceramic Societies,2020,8(3):586-596.
[25] W. Zhang, S. Yamashita, T. Kumazawa, F. Ozeki, H. Hyuga, H. Kita. Influence of surface roughness parameters and surface morphology on friction performance of ceramics. Journal of the Ceramic Society of Japan,2019,127(11):837-842.
[26] W. F. A. Besling, A. Goossens, B. Meester, J. Schoonman. Laser-induced chemical vapor deposition of nanostructured silicon carbonitride thin films. Journal of Applied Physics,1998,83(1):544-553.
[27] X. Q. Li, Y. M. Gao, W. Pan, Z. C. Zhong, L. C. Song, W. Chen, Q. X. Yang. Effect of hBN content on the friction and wear characteristics of B_4C-hBN ceramic composites under dry sliding condition. Ceramics International,2015,41(3):3918-3926.
[28] P. D. Cuong, H. S. Ahn, E. S. Yoon, K. H. Shin. Effects of relative humidity on tribological properties of boron carbide coating against steel. Surface and Coatings Technology,2006,201(7):4230-4235.
[29] J. G. Xu, K. Kato. Formation of tribochemical layer of ceramics sliding in water and its role for low friction. Wear,2000,245(1-2):61-75.
[30] M. Chen, K. Kato, K. Adachi. The difference in running-in period and friction coefficient between self-mated Si_3N_4 and SiC under water lubrication. Tribology letters,2001,11(1):23-28.
[31] M. Chen, K. Kato, K. Adachi. The comparisons of sliding speed and normal load effect on friction coefficients of self-mated Si_3N_4 and SiC under water lubrication. Tribology International,2002,35(3):129-135.
[32] C. Y. Chen, B. H. Wu, C. J. Chung, W. L. Li, C. W. Chien, P. H. Wu, C. W. Cheng. Low-friction characteristics of nanostructured surfaces on silicon carbide for water-lubricated seals. Tribology letters,2013,51:127-133.
[33] W. Zhang, S. Yamashita, T. Kumazawa, F. Ozeki, H. Hyuga, W. Norimatsu, H. Kita. A study on formation mechanisms of relief structure formed in situ on the surface of ceramics. Ceramics International,2019,45(17):23143-23148.
[34] K. W. Guo. Effect of sliding speed on tribological characteristics of different surface textures on AISI O1 steel irradiated by Nd:YAG pulsed laser. Ironmaking & Steelmaking,2009,36(1):63-74.
[35] T. Shimizu, T. Kakegawa, M. Yang. Micro-texturing of DLC thin film coatings and its tribological performance under dry sliding friction for microforming operation. Procedia Engineering,2014,81:1884-1889.
[36] R. Capozza, N. Pugno. Effect of surface grooves on the static friction of an elastic slider. Tribology Letters,2015,58(3):35-40.
[37] X. L. Wang, K. Kato, K. Adachi, K. Aizawa. The effect of laser texturing of SiC surface on the critical load for the transition of water lubrication mode from hydrodynamic to mixed. Tribology International,2001,34(10):703-711.
[38] M. Geiger, S. Roth, W. Becker. Influence of laser-produced microstructures on the tribological behaviour of ceramics. Surface and Coatings Technology,1998,100-101:17-22.
[39] M. Wakuda, Y. Yamauchi, S. Kanzaki, Y. Yasuda. Effect of surface texturing on friction reduction between ceramic and steel materials under lubricated sliding contact. Wear,2003,254(3-4):356-363.
[40] S. Sasaki. Elucidation and control of tribology by numerical simulation and surface analysis.2018,211-213.
[41] Guicciardi S, Sciti D, Melandri C, Pezzotti G. Dry sliding wear behavior of nano-sized SiC pins against SiC and Si_3N_4 discs. Wear,2007,262(5-6):529-535.
[42] J. D. Rimstidt, H. L. Barnes. The kinetics of silica-water reactions. Geochimica et Cosmochimica Acta,1980, 44(11):1683-1699.
[43] W. Zhang, X. Y. Chen, S. Yamashita, M. Kubota, H. Kita. Effect of water temperature on tribological

performance of B_4C-SiC ceramics under water lubrication.(in press)

[44] W. X. Li, L. X. Ma, J. Chen. Abrasion resistance of boron carbide ceramic. Journal of Harbin University of Commerce (Natural Sciences Edition),2010,26(6):753-754. (in Chinese)

[45] J. E. Zorzi, C. A. Perottoni, J. A. H. da Jornada. Hardness and wear resistance of B_4C ceramics prepared with several additives. Materials Letters,2005,59(23):2932-2935.

Part II

Tribological Properties of B_4C-SiC Ceramics in Water

Chapter 6
Frictional characteristics of carbide ceramics in water

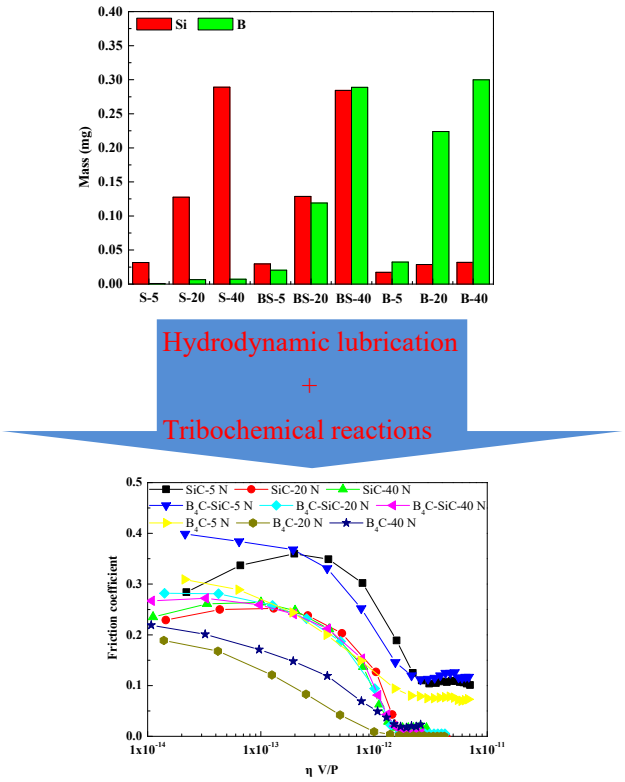

Frictional characteristics of carbide ceramics (SiC, B_4C-SiC, B_4C) in water against SiC balls were measured over a wide range of test conditions. Carbide ceramics can obtain hydrodynamic lubrication with low friction coefficient at 20 and 40 N, however, carbide ceramics can't obtain hydrodynamic lubrication with low friction coefficient at 5 N. Carbide ceramics exhibit lower friction coefficients at 20 and 40 N than those at 5 N in each lubrication regime. Carbide ceramics can exhibit wider application range with low friction at high loads (20 and 40 N). The low friction of carbide ceramics is achieved by the combination of hydrodynamic lubrication and tribochemical reactions. The products of tribochemical reactions of carbide ceramics improve the viscosity of water at or near the worn surfaces of carbide ceramics, promoting the hydrodynamic lubrication for carbide ceramics. B_4C ceramic shows lower friction coefficients than those of SiC and B_4C-SiC ceramics in boundary lubrication and mixed lubrication at 20 and 40 N.

Contents

6.1. Introduction

Reducing pollution released to environment has become an vital basis for mechanical design. Accordingly, ceramics/water combination has gradually replaced metal/oil combination. On the other hand, for energy-saving, low frictional materials are required. Among advanced engineering ceramic materials, carbide ceramics are considered to be promising materials for tribological applications, such as mechanical seals, sliding bearings and thrust bearings, because of their low density, good wear resistance, and low friction in water [1-7]. In particular, SiC ceramics have been successfully used as mechanical seals and bearings. For the current typical combination materials of mechanical seals used in pump, SiC ceramic is used as a rotating ring, and SiC ceramic or carbon is used as a stationary ring [8-10]. SiC ceramic could show very low friction coefficient when sliding against itself in water [11-13]. In carbide ceramics, in addition to SiC ceramics, B_4C ceramics, as the third hard material, are also expected to be potential candidates for tribological applications [14-16]. Several investigations on tribological properties of B_4C ceramics sliding in water have been reported [17, 18], however, those experimental results were obtained only within a certain narrow range of experimental conditions. Furthermore, recently, it is observed that under certain conditions, B_4C-SiC composite ceramics exhibited better tribological properties than those of monolithic SiC and B_4C ceramics under dry sliding [19-24]. However, there is no report on tribological properties of B_4C-SiC ceramics under water lubrication. To expand the application of carbide ceramics under water lubrication and to meet the actual design needs of carbide ceramics as mechanical seals and bearing, the frictional characteristics of carbide ceramics in water need to be measured over a wide range of test conditions.

On the other hand, until now, there is still a heated debate on lubrication mechanisms responsible for the low friction of non-oxide ceramics sliding in water. Tomizawa and Fischer [9], Muratov et al. [25] and Jordi et al. [26] stated that hydrodynamic lubrication alone is responsible for the low friction of SiC ceramics and Si_3N_4 ceramics sliding in water, and water film could sustain the whole weight. In contrast, Xu and Kato [27], Chen et al. [28, 29] and Chen et al. [30] proposed that the low friction of SiC and Si_3N_4 ceramics is achieved by the combination of hydrodynamic lubrication and boundary lubrication by products of the tribochemical reactions. There have been many investigations on lubrication mechanisms for Si based non-oxide ceramics, in spite of a big academic debate, however, reports on lubrication mechanisms of B_4C and B_4C based ceramics are limited.

Therefore, the purpose of this study is to investigate the fundamental frictional property for carbide ceramics in water under a wide range of sliding conditions, and to compare the frictional property of carbide ceramics under different lubrication regimes by comparing their Stribeck curves. The effect of load on lubrication regime was clarified. The lubrication mechanisms for carbide ceramics were also discussed.

6.2. Experiment

Friction tests were performed in a stationary ball in contact with a rotated disc, as schematically shown in Fig. 1. Three kinds of carbide ceramics (SiC, B_4C-SiC and B_4C), whose properties and phase compositions are shown in Table 1 and Fig. 2, respectively, were slid against commercially available SiC balls. The size of carbide ceramics is 75 mm × 75 mm × 8 mm. Friction tests were carried out at room temperature (25-27.5 ℃) in air. During the tests, the friction surfaces were submerged in deionized water all the time. Before friction tests, all specimens were cleaned by washing in ethanol in an ultrasonic bath for 15 min. The test conditions are summarized in Table 2. Friction coefficients were automatically calculated and recorded by a microprocessor-controlled data acquisition system.

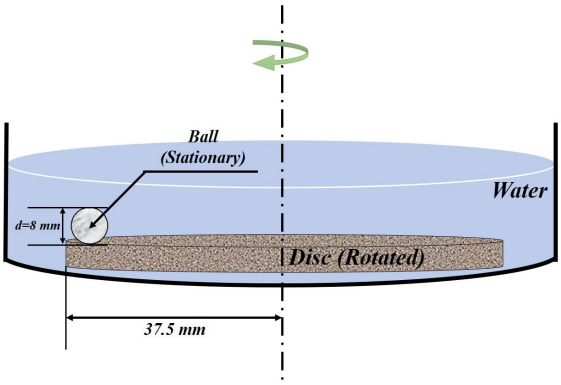

Fig. 1. Schematic diagram of the friction test.

Table 1 Properties of the carbide ceramics.

Material	SiC	B_4C-SiC	B_4C
Production technique	Pressureless sintering	Pressureless sintering	Pressureless sintering
Sintering additives	3wt%B_4C, 3wt%C	3wt%C	3wt%C
Bulk density (g/cm^3)	3.13	2.66	2.40
Relative density (%)	98.4	96.6	95.7
Average hardness (GPa)	28.3	30.4	26.9
Average fracture toughness (MPa·m$^{1/2}$)	3.2	3.2	3.7
Bending strength (MPa)	250	390	240
Surface roughness (Ra, μm)	0.06	0.10	0.09

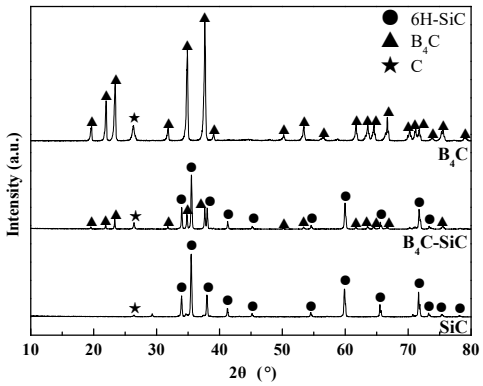

Fig. 2. XRD patterns of the carbide ceramics.

Table 2 The friction test conditions.

Sliding speed (m/s)	0.005-1.6
Revolution speed (rpm)	1.33-424.41
Load (N)	5-40
Sliding radius (mm)	34.5-36
Sliding time for each sliding speed (min)	10

The surface morphologies of carbide ceramics were observed by SEM equipped with EDS. The compositions of worn surfaces of carbide ceramics were analyzed by XPS. Water samples with filtration after friction tests were investigated by ICP-AES.

6.3. Results

6.3.1. Effects of sliding speed and load on friction coefficients of carbide ceramics

Friction coefficients as a function of sliding speed for SiC, B_4C-SiC, and B_4C ceramics at 5, 20, and 40 N are shown in Fig. 3 - Fig. 5. The upper curves are for increasing sliding speed, and the lower curves are for decreasing sliding speed. During the stage of increasing sliding speed, generally, the friction coefficients of carbide ceramics first decrease and then stay at a stable value with increase in sliding speed. During the stage of decreasing sliding speed, the friction coefficients of carbide ceramics gradually return to the initial high values with decrease in sliding speed. Friction can stay low at sliding speed above 0.5 m/s for the carbide ceramics. When the sliding speed is greater than 0.5 m/s, the friction coefficients of carbide ceramics during the stage of increasing sliding speed are almost the same as those during the stage of decreasing sliding speed. When the sliding speed is less than 0.5 m/s, for SiC and B_4C-SiC ceramics, the friction coefficients during the stage of decreasing sliding speed are obviously less than those during the stage of increasing sliding speed; However, in case of B_4C ceramic, the friction coefficients during the stage of decreasing sliding speed are similar with those during the stage of increasing sliding speed. Furthermore, the friction coefficients of carbide ceramics at 20 and 40 N is smaller than those at 5 N at the same sliding speed.

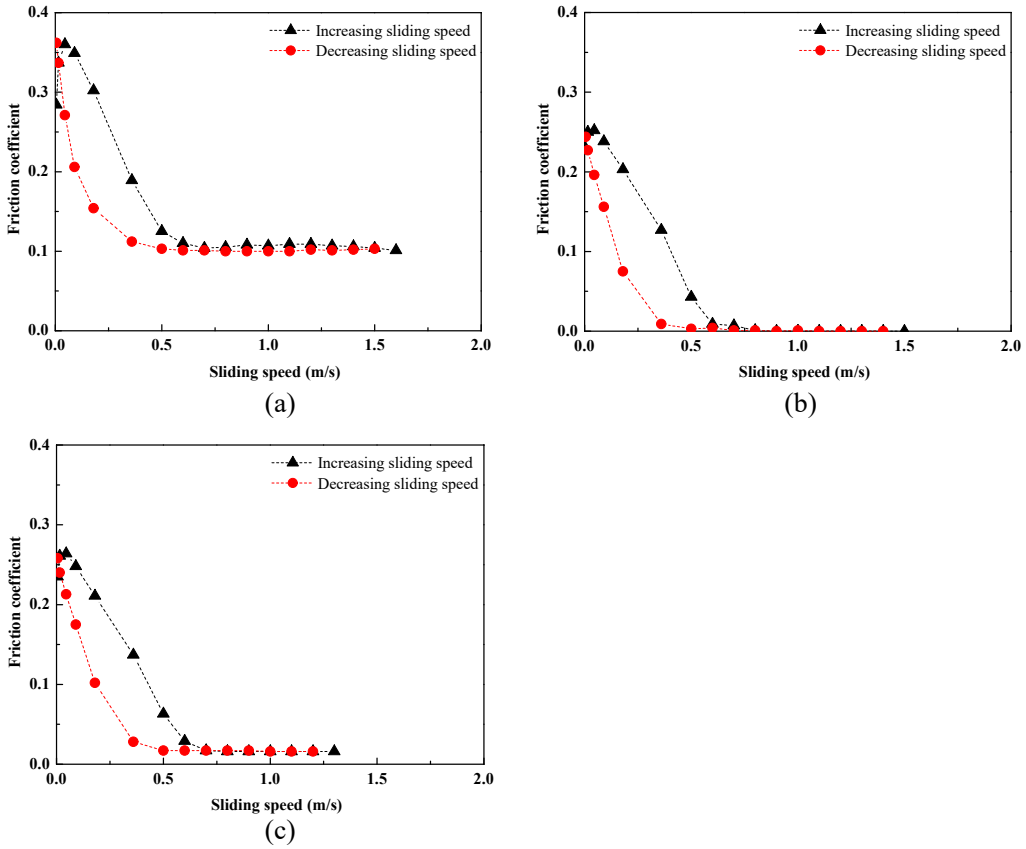

Fig. 3. Friction coefficient as a function of sliding speed for SiC ceramic at: (a) 5 N, (b) 20 N, and (c) 40 N (The upper curve was measure with increasing sliding speed, and the lower curve was measure with decreasing sliding speed).

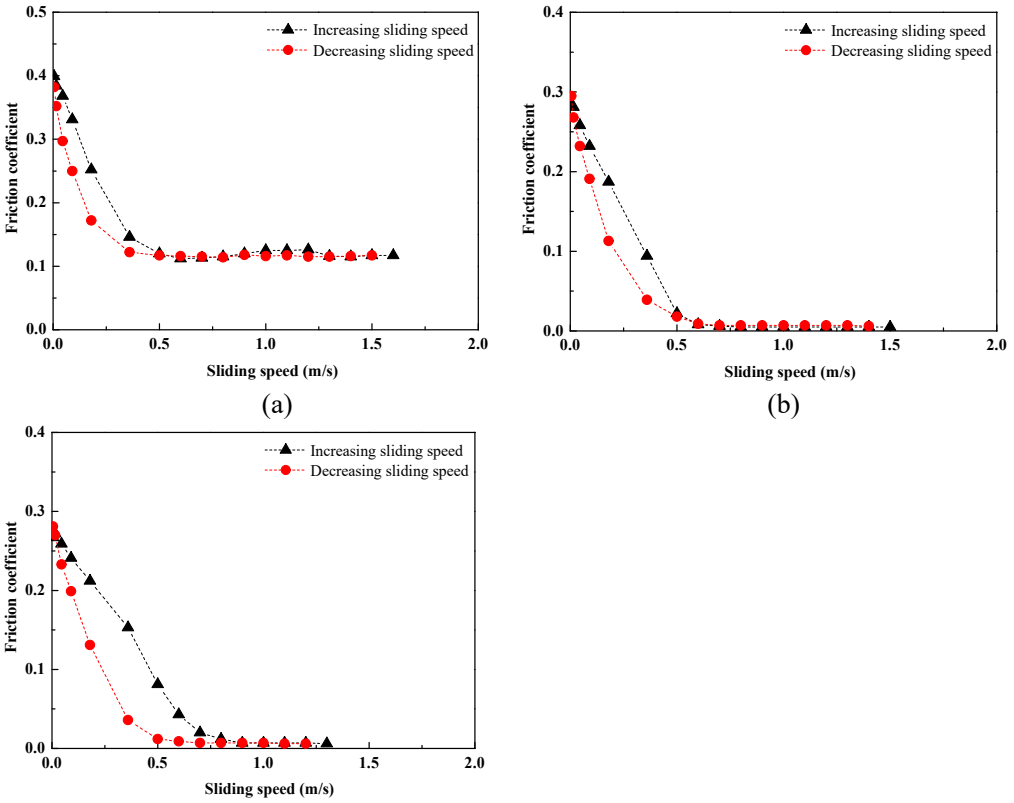

Fig. 4. Friction coefficient as a function of sliding speed for B_4C-SiC ceramic at: (a) 5 N, (b) 20 N, and (c) 40 N (The upper curve was measure with increasing sliding speed, and the lower curve was measure with decreasing sliding speed).

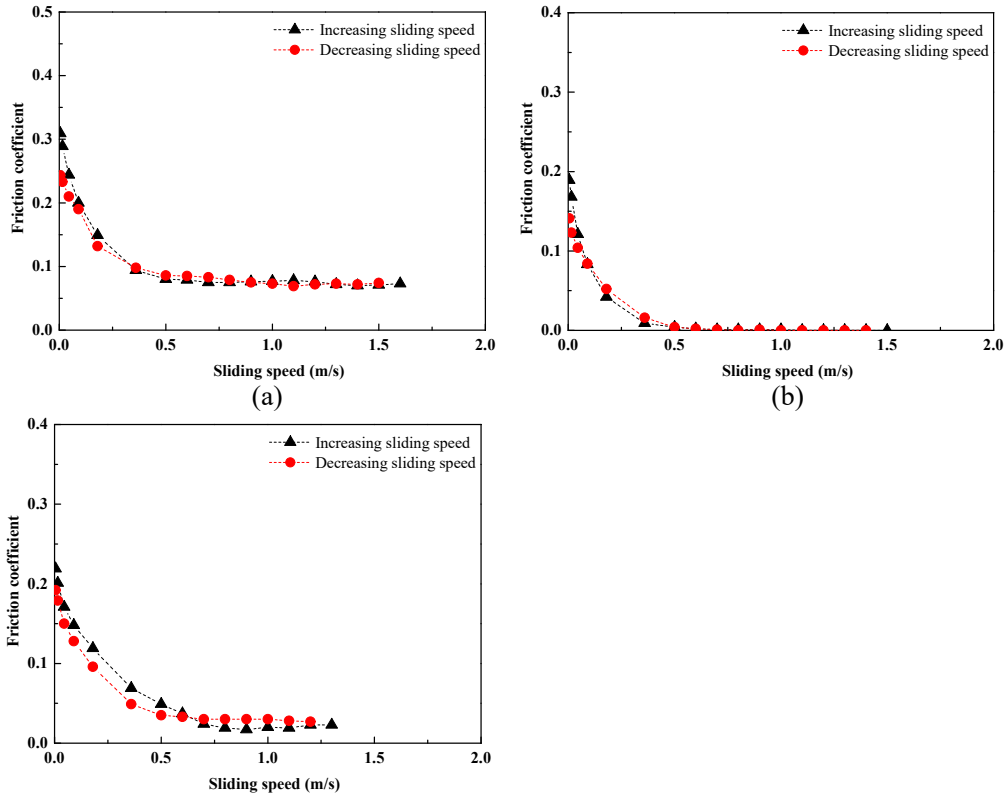

Fig. 5. Friction coefficient as a function of sliding speed for B_4C ceramic at: (a) 5 N, (b) 20 N, and (c) 40 N (The upper curve was measure with increasing sliding speed, and the lower curve was measure with decreasing sliding

speed).

6.3.2. Stribeck curves of carbide ceramics in water

In order to investigate the lubrication regime of carbide ceramics, Stribeck curves of carbide ceramics sliding in water at 5, 20, and 40 N are drawn, as shown in Fig. 6. Stribeck factor ηV/P is used in these figures, where η [Pa·s] is the viscosity of water, V [rps] is the revolution speed, P [Pa] is mean contact pressure. In each figure, there are three curves obtained at the loads of 5, 20 and 40 N, respectively. Every curve of the carbide ceramics can show three different lubrication regimes clearly, viz., from hydrodynamic lubrication to boundary lubrication via mixed lubrication. According to the results in Fig. 6, three findings can be found. First, the carbide ceramics can obtain hydrodynamic lubrication with low friction coefficient at 20 and 40 N, however, the carbide ceramics can't obtain hydrodynamic lubrication with low friction coefficient at 5 N. Second, the carbide ceramics exhibit lower friction coefficients at 20 and 40 N than those at 5 N in each lubrication regime. Third, for carbide ceramics sliding in water, the transition points from hydrodynamic lubrication to mixed lubrication shift to the left along the X axis with increase in load from 5 N to 20 and 40 N. This means that the carbide ceramics can exhibit wider application range with low friction at high loads.

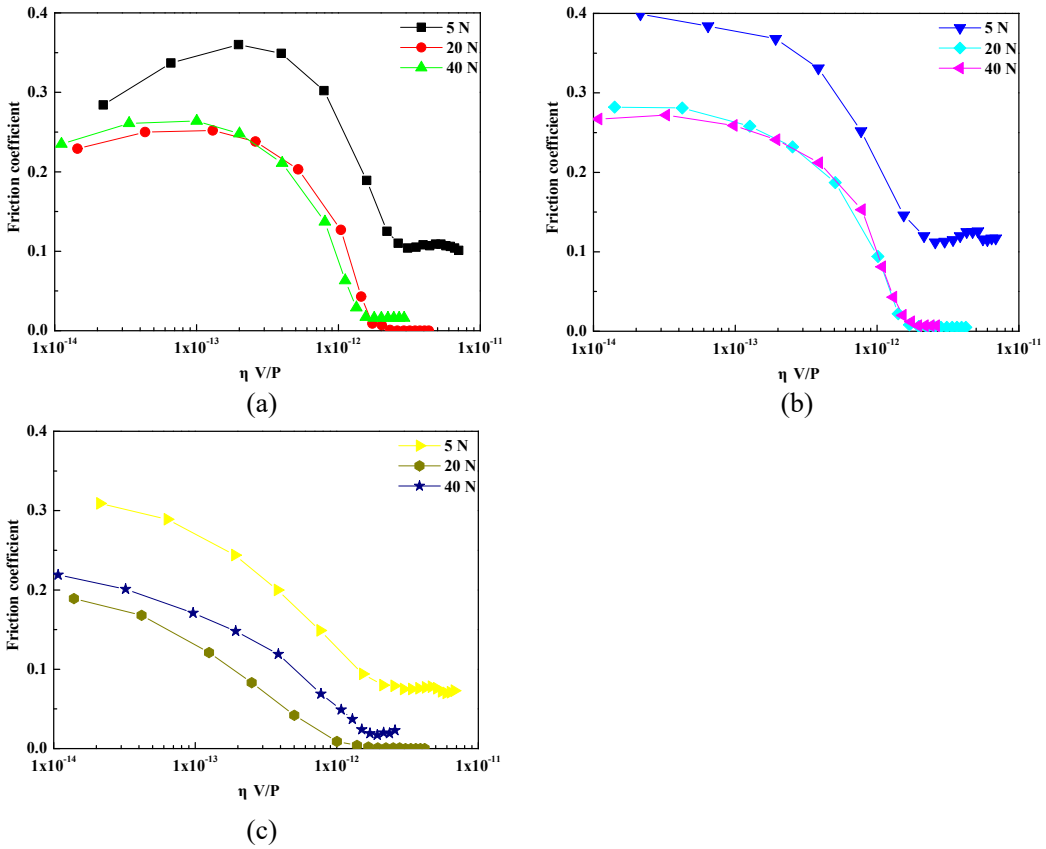

Fig. 6. Stribeck curves of carbide ceramics sliding in water at the given normal loads of 5, 20, and 40 N: (a) SiC, (b) B_4C-SiC, and (c) B_4C.

To compare the results of the three carbide ceramics sliding in water shown in Fig. 6, the Stribeck curves of carbide ceramics are combined in Fig. 7. At 5 N, B_4C ceramic exhibits lower friction coefficient than those of SiC and B_4C-SiC ceramics in different lubrication regimes. Compared with SiC ceramic, B_4C-SiC ceramic exhibits lower friction coefficient in mixed lubrication, but higher friction coefficient in boundary lubrication. The friction coefficients of SiC and B_4C-SiC ceramics are similar in hydrodynamic lubrication. At the loads of 20 and 40 N,

B_4C ceramic shows lower friction coefficient than those of SiC and B_4C-SiC ceramics in boundary lubrication and mixed lubrication. SiC ceramic exhibits slightly lower friction coefficients than those of B_4C-SiC ceramic in boundary lubrication, and the friction coefficients of SiC and B_4C-SiC ceramics are similar in mixed lubrication. The three carbide ceramics have similar friction coefficients in hydrodynamic lubrication. In summary, B_4C ceramic exhibits better frictional property as sliding against SiC ball in water at different loads as compared to SiC and B_4C-SiC ceramics.

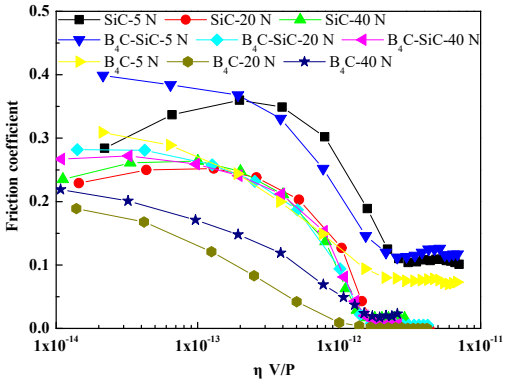

Fig. 7. Variation of Stribeck curve with materials.

6.3.3. Surface morphologies of carbide ceramics

In order to better compare the worn surfaces of different carbide ceramics, the surface morphologies of carbide ceramics outside the wear track after sliding in water are first shown in Fig. 8. Many pores are observed on the initial surfaces of carbide ceramics. The worn surface morphologies of carbide ceramics after sliding at different loads are presented in Fig. 9-Fig. 11. On the whole, the worn surfaces of carbide ceramics become smoother than the initial surfaces outside the wear tracks. In case of SiC ceramic, there are still some pores on the worn surfaces after sliding at different loads. In case of B_4C-SiC and B_4C ceramics, there are still some pores on their worn surfaces after sliding at 5 N. However, the visible pores on the worn surfaces are reduced after sliding at 20 and 40 N. It is found that a number of pores are filled with carbon, and the number of pores on the worn surfaces decreases with increase in load due to the increased formation amount of carbon with increase in load.

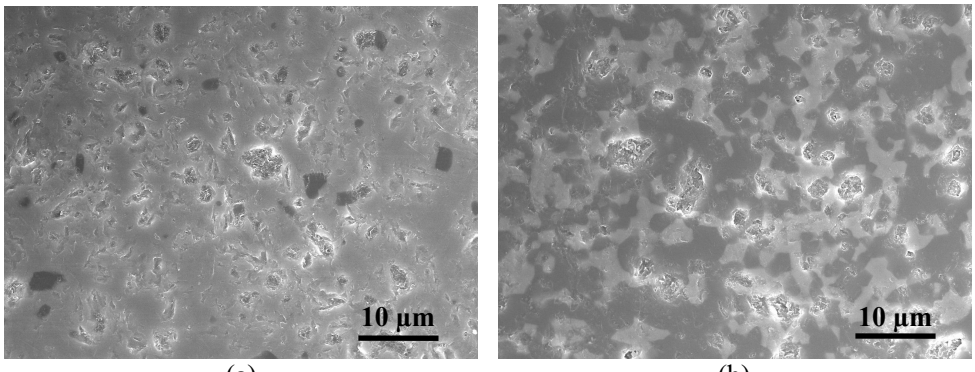

(a) (b)

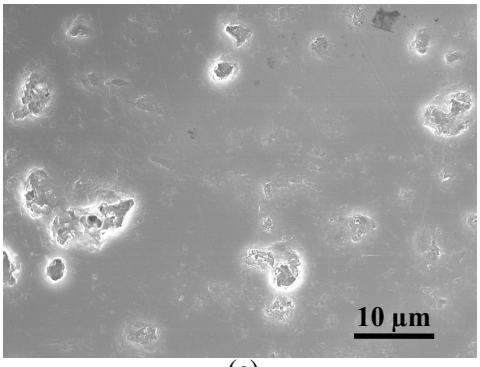

(c)

Fig. 8. Surface morphologies of carbide ceramics outside the wear track after sliding in water: (a) SiC, (b) B_4C-SiC, (c) B_4C.

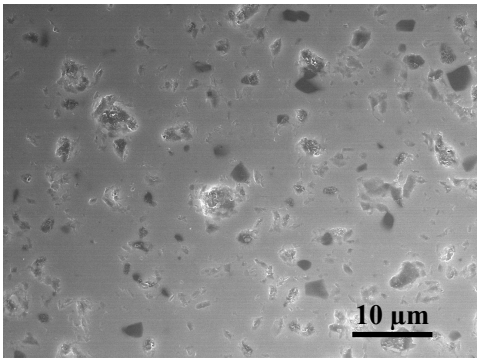

(a)

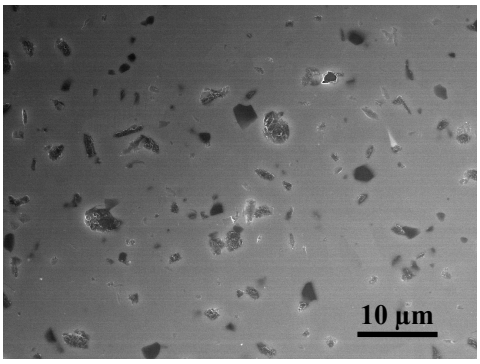

(b)

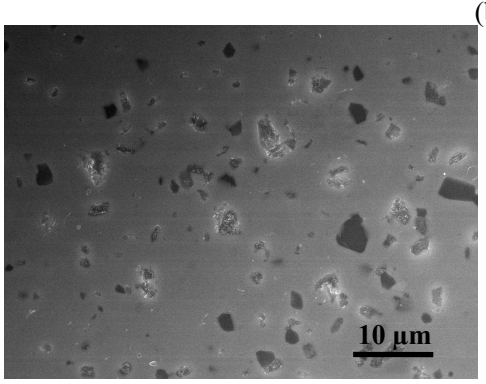

(c)

Fig. 9. Worn surface morphologies of SiC ceramic at: (a) 5 N, (b) 20 N, and (c) 40 N.

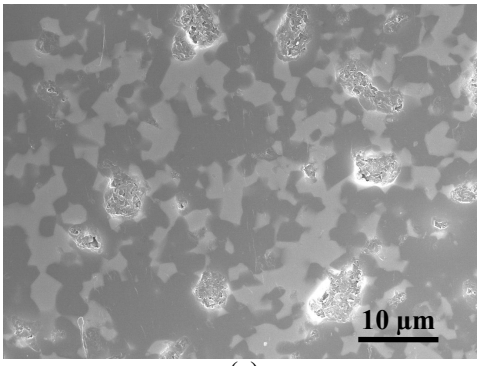

(a)

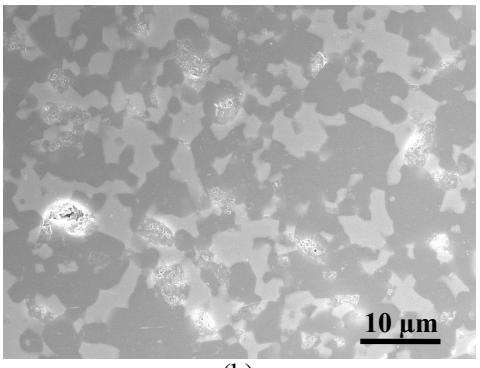

(b)

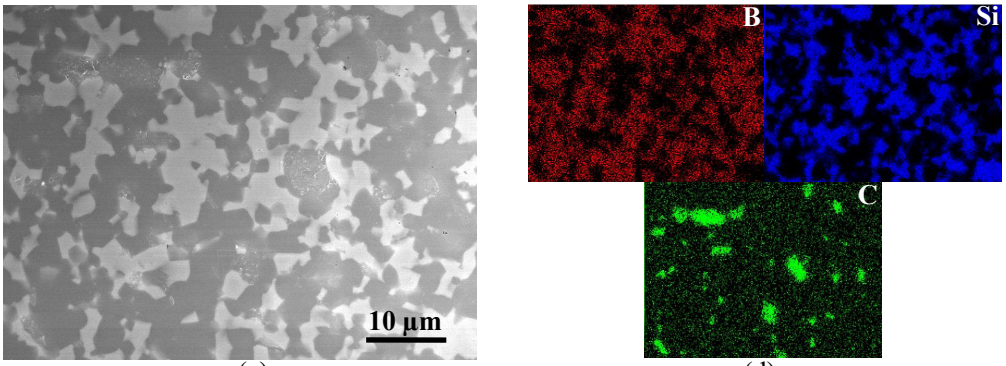

(c) (d)

Fig. 10. Worn surface morphologies of B_4C-SiC ceramic at: (a) 5 N, (b) 20 N, and (c) 40 N and elemental distribution of (c): (d).

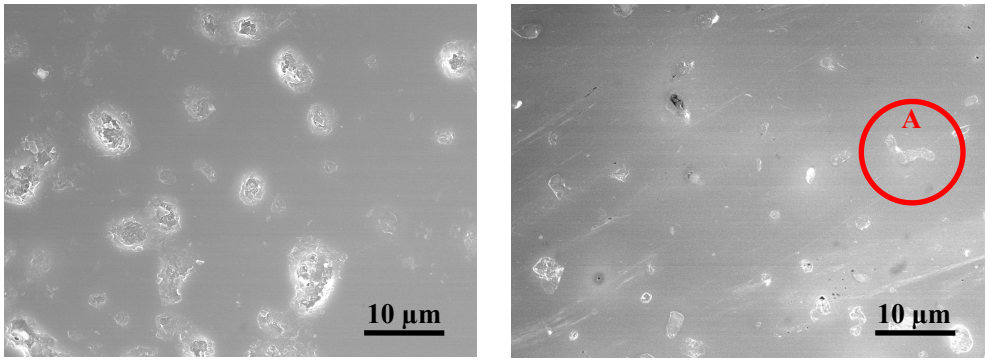

(a) (b)

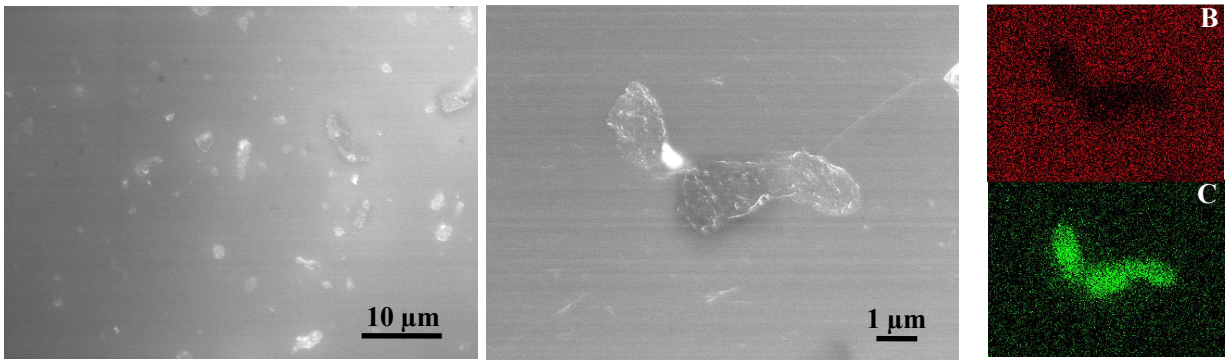

(c) (d) (e)

Fig. 11. Worn surface morphologies of B_4C ceramic at: (a) 5 N, (b) 20 N, (c) 40 N, and (d) an enlarged view of area A in (b) and elemental distribution of (d): (e).

6.3.4. Oxide compositions on worn surfaces of carbide ceramics

XPS was employed to analyze the compositions of worn surfaces of carbide ceramics, as shown in Fig. 12 - Fig. 14. In case of SiC and B_4C-SiC ceramics after sliding at 5 N, the Si_{2p} spectrum can be fitted with two peaks by Gaussian function: the main peak with a binding energy of 99.8-100.3 eV belongs to SiC and the binding energy of 101.3-101.6 eV is attributed to SiO_2 [31]. In case of SiC and B_4C-SiC ceramics at 20 and 40 N, the symmetrical Si_{2p} peak with a binding energy of 99.9-100.2 belongs to SiC. In case of B_4C-SiC and B_4C ceramics after sliding at different loads, the symmetrical B1s peak with a binding energy of 187.4-187.6 eV corresponds to B_4C [32, 33]. For the SiC ceramic, no B_{1s} peak can be detected on the worn surfaces, and SiO_2 only exists on the worn surface at 5 N. For the B_4C-SiC ceramic, only silicon oxide exists on the worn surface at 5 N, no boron oxide or hydroxide exists on the worn surfaces. For the B_4C ceramic, neither silicon oxide nor boron oxide exists on the

worn surfaces.

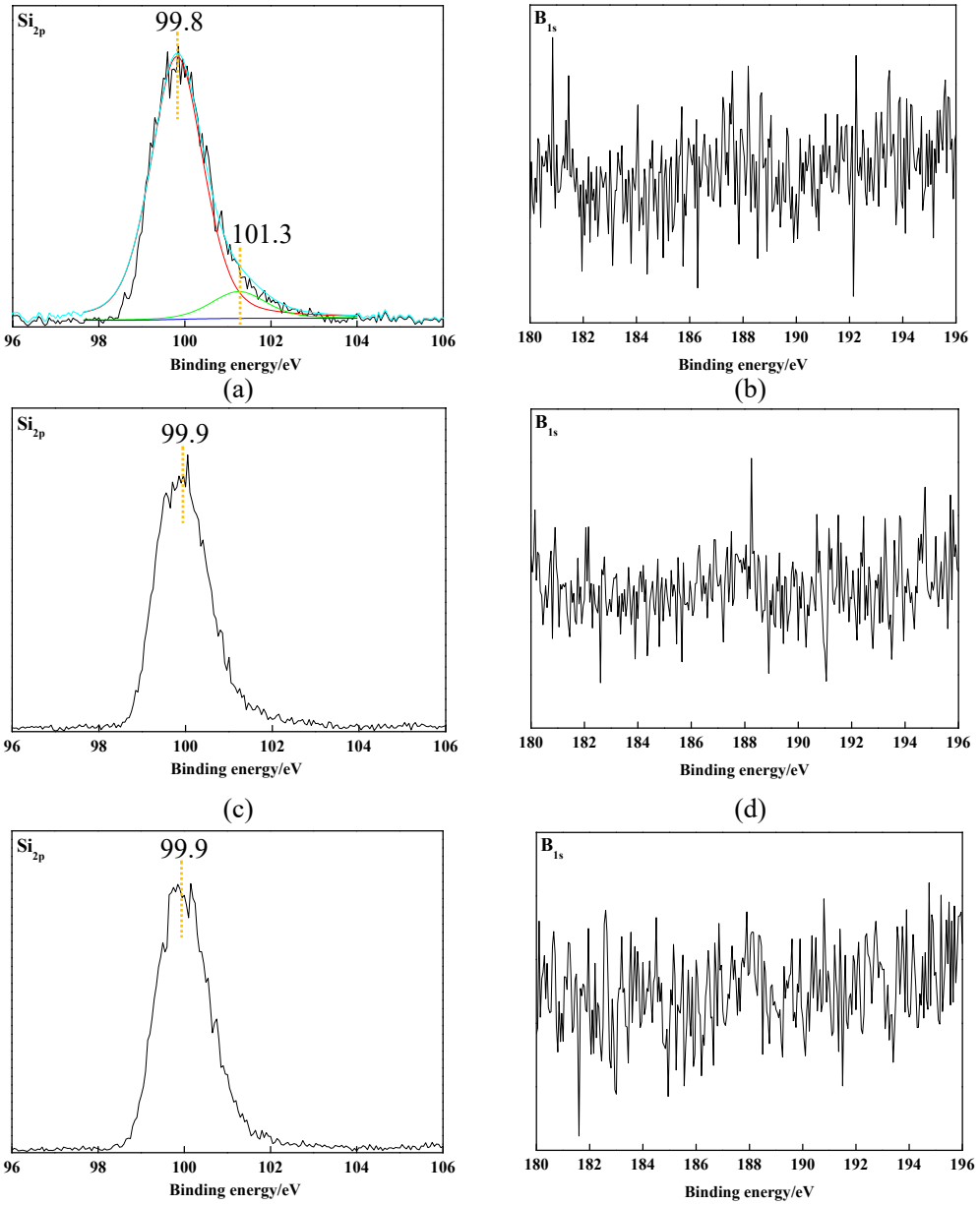

Fig. 12. XPS results of the worn surfaces of SiC ceramic at: (a-b) 5 N, (c-d) 20 N, and (e-f) 40 N.

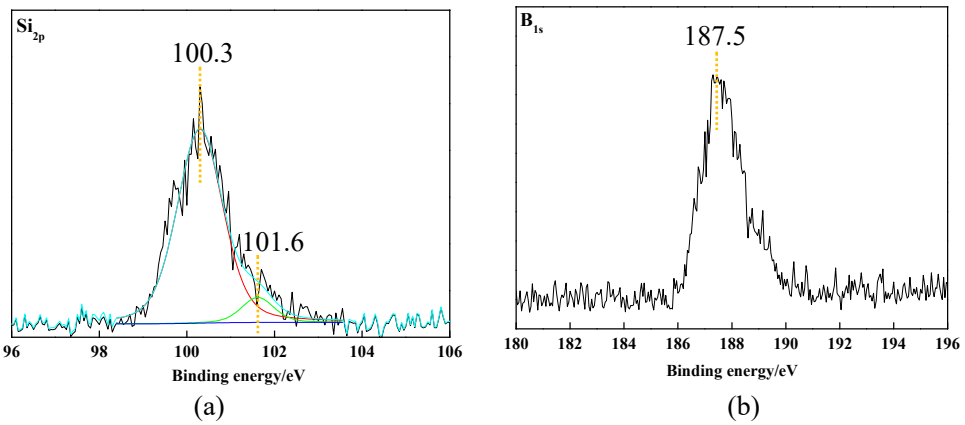

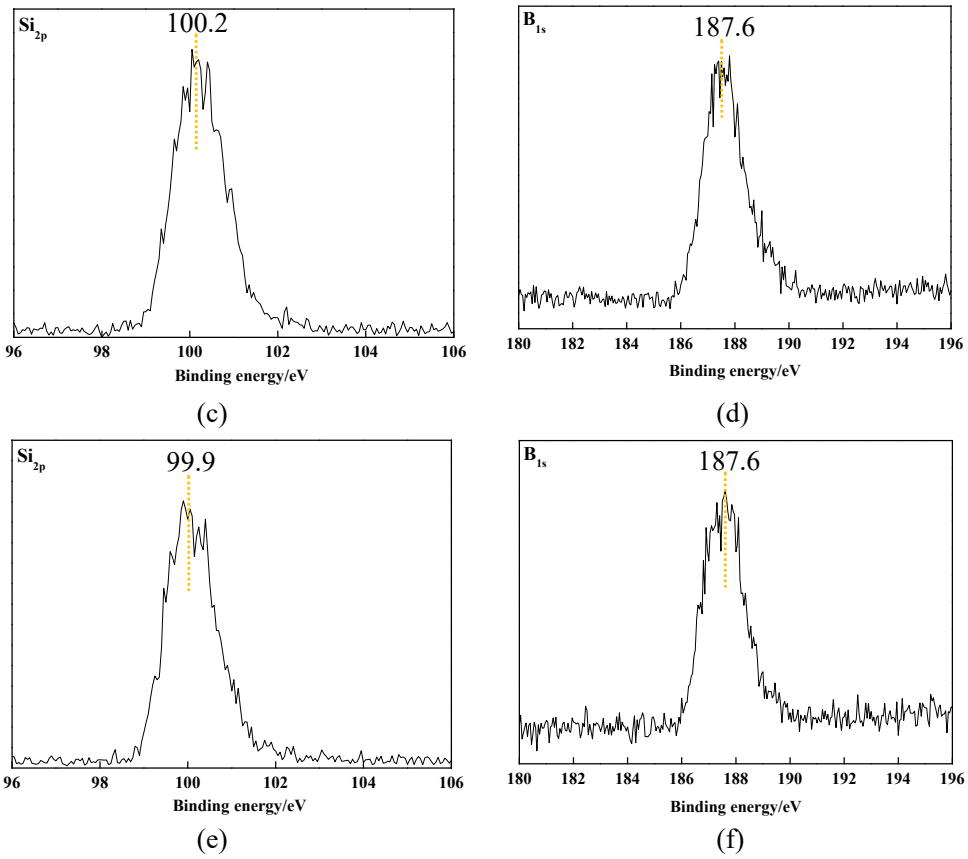

Fig. 13. XPS results of the worn surfaces of B_4C-SiC ceramic at: (a-b) 5 N, (c-d) 20 N, and (e-f) 40 N.

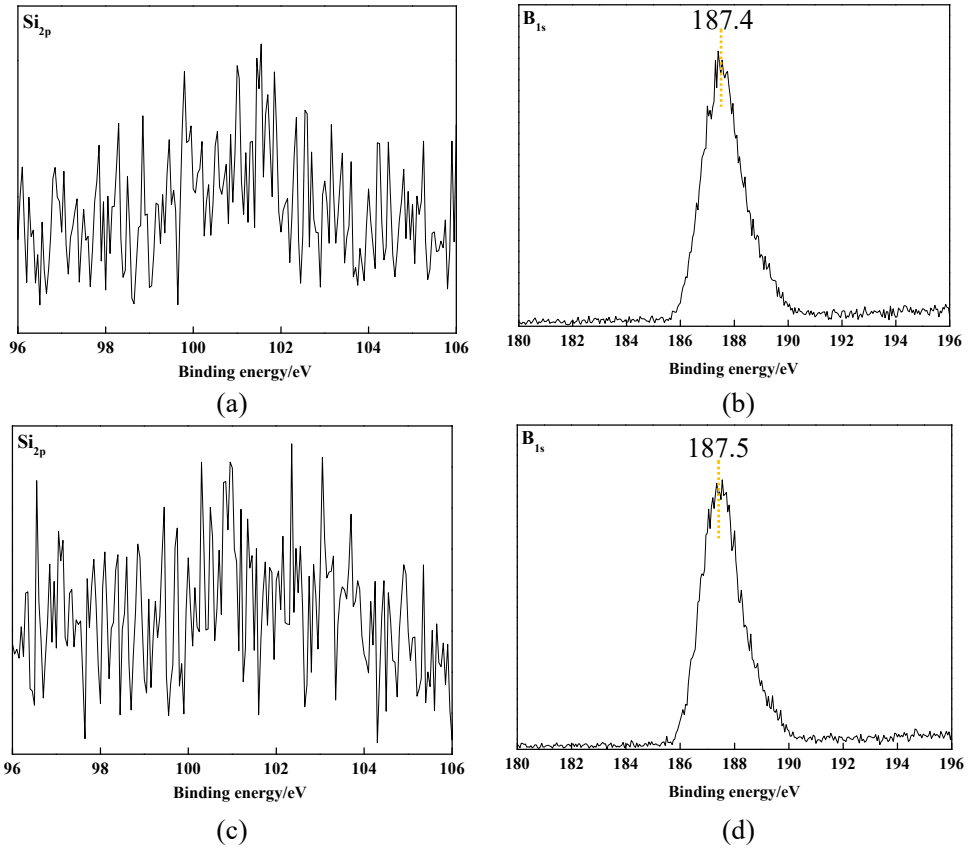

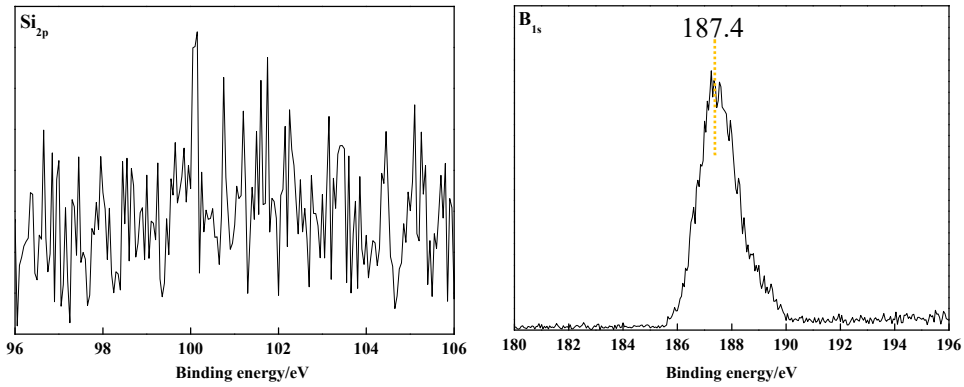

(e) (f)

Fig. 14. XPS results of the worn surfaces of B_4C ceramic at: (a-b) 5 N, (c-d) 20 N, and (e-f) 40 N.

6.3.5. Amounts of Si and B elements in the water samples

ICP-AES was employed to analyze the amounts of Si and B elements in the water samples after carbide ceramics sliding in water to check tribochemical reactions of carbide ceramics, and the result is shown in Fig. 15. For the SiC ceramic, the amount of Si element in water increases significantly with increase in load, and the trace amount of B element in water is attributed to the sintering additive. For the B_4C-SiC ceramic, both Si and B elements increase significantly with increase in load. For the B_4C ceramic, the amount of B element in water increases significantly with increase in load, and the Si element in water comes from tribochemical reaction of counterpart.

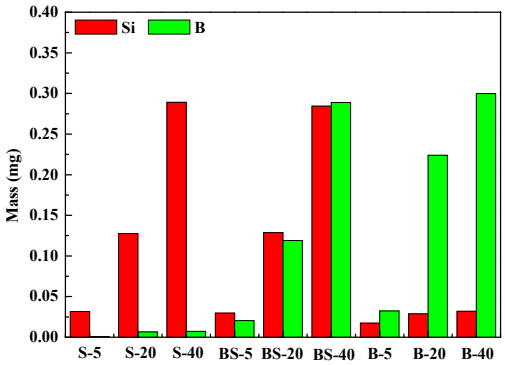

Fig. 15. Amounts of Si and B elements in the water samples after carbide ceramics sliding in water (S-5, S-20, S-40, BS-5, BS-20, BS-40, B-5, B-20 and B-40 in the figure represent carbide ceramics-load, i.e., S, BS, and B correspond to SiC, B_4C-SiC, and B_4C, respectively; 5, 20, and 40 correspond to 5 N, 20 N, and 40 N, respectively).

6.4. Discussion

In this study, it is observed that for carbide ceramics, the friction coefficients gradually return to the initial high values with decrease in sliding speed during the stage of decreasing sliding speed (Fig. 3 - Fig. 5). Jordi et al. [26] also did the similar investigation for SiC and Si_3N_4 ceramics, and they also found that the friction coefficients of SiC and Si_3N_4 ceramics returned to high values with decrease in sliding speed during the stage of decreasing sliding speed. Then they came to a conclusion that the lubrication was purely hydrodynamic, the reason of which was that a chemical form of lubrication would result in low friction at all sliding speeds. However, we put forward a different opinion through this research. On the one hand, according to the ICP result (Fig. 15), the tribochemical reactions of carbide ceramics sliding in water have been established. For SiC, it has been widely reported that the

tribochemical reactions are expressed as follows [28, 34]:

$$SiC + 2H_2O = SiO_2 + CH_4 \quad (1)$$

$$SiO_2(s) + 2H_2O(l) = H_4SiO_4\ (aq) \quad (2)$$

For B_4C, combined with ICP result (Fig. 15) and observation of worn surfaces of carbide ceramics containing B_4C (Fig. 10 and Fig. 11), we propose the following tribochemical reactions based on the presence of residual carbon on the worn surfaces of B_4C-SiC and B_4C ceramics:

$$B_4C + 12H_2O = 4H_3BO_3 + C + 6H_2 \quad (3)$$

or:

$$B_4C + 6H_2O = 2B_2O_3 + C + 6H_2 \quad (4)$$

$$B_2O_3 + 3H_2O = 2H_3BO_3 \quad (5)$$

Therefore, it can be concluded that the carbide ceramics occurred tribochemical reactions when sliding in water, but the extent depends on the load. On the other hand, the carbide ceramics can obtain hydrodynamic lubrication with low friction coefficient at 20 and 40 N, however, the carbide ceramics can't obtain hydrodynamic lubrication with low friction coefficient at 5 N. According to Fig. 15, it has been known that the tribochemical reactions of carbide ceramics are strongly dependent on the load. When the load is 5 N, the tribochemical reactions of carbide ceramics are relatively weak. When the loads are 20 and 40 N, a large amount of Si and B elements are detected in the water, which means that both SiC and B_4C occurred strong tribochemical reactions according to the reactions (1) to (5). For carbide ceramics, they can't obtain hydrodynamic lubrication with low friction coefficient at 5 N, which is attributed to low extent of tribochemical reactions. This suggests that hydrodynamic lubrication alone caused by the increase of sliding speed can't make carbide ceramics obtain low friction. Therefore, we consider that the low friction of carbide ceramics is achieved by the combination of hydrodynamic lubrication and tribochemical reactions. This conclusion is consistent with the conclusion put forward by Xu and Kato [27], Chen et al. [28, 29] and Chen et al. [30]. Because of stronger tribochemical reactions of carbide ceramics at high loads, the carbide ceramics exhibit lower friction coefficients at 20 and 40 N than those at 5 N in each lubrication regime, and the carbide ceramics can exhibit wider application range with low friction at high load.

How does the tribochemical reaction affect the friction coefficient of carbide ceramics? Xu and Kato [27], Chen et al. [28, 29] and Chen et al. [30] proposed that the product of tribochemical reactions of SiC and Si_3N_4 ceramics is SiO_2, and this SiO_2 tribochemical layer produced on the worn surface reduced the friction for SiC and Si_3N_4 ceramics. However, in this study, SiO_2 is only detected on the worn surfaces of SiC and B_4C-SiC ceramics at 5 N, no SiO_2 is detected on the worn surfaces of SiC and B_4C-SiC ceramics at 20 and 40 N, which is caused by the fact that the reaction (2) is promoted by high loads. Further, no boron oxide or hydroxide exists on the worn surfaces of B_4C ceramic at any load. It is noteworthy that no SiO_2 exists on the worn surfaces of B_4C ceramic, even under a load of 40 N. This means that no transfer film of SiO_2 is produced on the worn surfaces of B_4C ceramic, although SiC ball is used as the counterpart material. Although SiO_2 is detected on the worn surfaces of SiC and B_4C-SiC ceramics at 5 N, SiC and B_4C-SiC ceramics can't obtain hydrodynamic lubrication with low friction coefficient at 5 N. Meanwhile, no silicon oxide or boron oxide is detected on the worn surfaces of carbide ceramics at 20 and 40 N, however, they can obtain hydrodynamic lubrication with low friction coefficient at 20 and 40 N. Based on these observations, we do not believe that the low friction of carbide ceramics is caused by the oxide layer formed due to the tribochemical reactions. Although the conclusion we considered that the low friction of carbide ceramics is achieved by the combination of hydrodynamic lubrication and tribochemical reactions is consistent with the conclusion put forward by Xu and Kato [27], Chen et al. [28, 29] and Chen et al. [30], the mechanism of tribochemical reaction for the low friction of carbide ceramics we considered is different from that for the low friction of Si based non-oxide ceramics put forward by the above researchers. We consider that when the carbide ceramics slide in water, on the one hand, silicic acid/SiO_2 and/or boric acid formed due to tribochemical reactions can be acted as a lubricant to reduce stress concentration and friction; and on the other

hand, when silicic acid/SiO_2 and boric acid are dissolved in water, the viscosity of water at or near the worn surfaces of carbide ceramics is improved, promoting the hydrodynamic lubrication for carbide ceramics. The latter assumption can be demonstrated by the results in Fig. 3 - Fig. 5. When the sliding speed is less than 0.5 m/s, the difference in friction coefficients between the stage of increasing sliding speed and the stage of decreasing sliding speed at the same sliding speeds is the most obvious for SiC ceramic, followed by B_4C-SiC ceramic, and lastly B_4C ceramic. This phenomenon is caused by the different viscosity of water at or near the worn surfaces of carbide ceramics. On the one hand, the viscosity of silicic acid is higher than that of boric acid, and on the other hand, some SiO_2 that is not dissolved in water can form clusters of silica gel [13], which can further increase the viscosity of water at or near the worn surfaces of carbide ceramics containing SiC. Therefore, for SiC ceramic sliding during the stage of decreasing sliding speed, when the sliding speed is less than 0.5 m/s, the viscosity of water at or near the worn surfaces is still higher because the water with higher viscosity containing silicic acid and silica gel formed during the hydrodynamic lubrication regime is not easy to disperse. As a result, the friction coefficients of carbide ceramics containing SiC during the stage of decreasing sliding speed are lower than those during the stage of increasing sliding speed as the sliding speed is less than 0.5 m/s, especially for SiC ceramic. However, for B_4C ceramic sliding during the stage of decreasing sliding speed, because B_2O_3 is easily soluble in water and the viscosity of the H_3BO_3 formed is lower, thus boric acid formed during the hydrodynamic lubrication regime is easy to disperse in water when the sliding speed is less than 0.5 m/s. This means that the viscosity of water at or near the worn surfaces of B_4C ceramic is lower. As a result, the friction coefficients of B_4C ceramic during the stage of decreasing sliding speed are similar with those during the stage of increasing sliding speed as the sliding speed is less than 0.5 m/s.

Moreover, many pores are observed on the initial surfaces of carbide ceramics. For the carbide ceramics containing B_4C, a number of pores are filled with the residual carbon formed due to tribochemical reaction of B_4C at 20 and 40 N. For SiC ceramic, there are still some pores on the worn surfaces at different loads. Tomizawa and Fischer [9] reported that pores formed during the sintering could act as fluid reservoirs, which could not only prolong the lubrication time but also improve the hydrodynamic pressure. However, in this study, it is found that carbide ceramics containing B_4C with more pores at 5 N don't exhibit better frictional property than that of carbide ceramics containing B_4C with fewer pores at 20 and 40 N. Also, the SiC ceramic with more pores show similar transition points from hydrodynamic to mixed lubrication with those of carbide ceramics containing B_4C with fewer pores at 20 and 40 N. Therefore, it can be concluded that pores have little effect on the frictional property of carbide ceramics, and pores are not the reason for the low friction coefficient of carbide ceramics under high loads. As to the residual carbon formed on the worn surfaces of carbide ceramics containing B_4C because of the tribochemical reaction of B_4C, because the SiC ceramic without residual carbon on the worn surfaces exhibits the similar friction coefficients with those of B_4C-SiC ceramic with residual carbon on the worn surfaces in different lubrication regimes at 20 and 40 N, thereby it can be inferred that the residual carbon formed due to the tribochemical reaction of B_4C has little effect on the frictional property of carbide ceramics containing B_4C. Finally, the three carbide ceramics have similar friction coefficients in hydrodynamic lubrication regime at 20 and 40 N, however, B_4C ceramic shows lower friction coefficient than those of SiC and B_4C-SiC ceramics in boundary lubrication and mixed lubrication at 20 and 40 N. In boundary and mixed lubrication regimes, there is still solid-solid contact on the sliding interface between carbide ceramics and SiC counterpart. Guicciardi et al. [35] pointed out that SiC ceramics exhibited higher friction coefficient in the case of self-mated than in the case of non self-mated under dry sliding. Therefore, the lower friction coefficient of B_4C ceramic in boundary lubrication and mixed lubrication is attributed to non self-mated. For carbide ceramics containing SiC, the higher friction coefficient in boundary lubrication and mixed lubrication is caused by chemical similarity between carbide ceramics containing SiC and SiC counterparts.

6.5. Conclusions

In this study, the frictional characteristics of carbide ceramics (SiC, B_4C-SiC, B_4C) in water against SiC balls were measured over a wide range of test conditions. The following results are obtained:

(1) Carbide ceramics can obtain hydrodynamic lubrication with low friction coefficient at 20 and 40 N, however, carbide ceramics can't obtain hydrodynamic lubrication with low friction coefficient at 5 N. Carbide ceramics exhibit lower friction coefficients at 20 and 40 N than those at 5 N in each lubrication regime. Carbide ceramics can exhibit wider application range with low friction at high loads (20 and 40 N).
(2) The low friction of carbide ceramics is achieved by the combination of hydrodynamic lubrication and tribochemical reactions.
(3) The products of tribochemical reactions of carbide ceramics improve the viscosity of water at or near the worn surfaces of carbide ceramics, promoting the hydrodynamic lubrication for carbide ceramics.
(4) B_4C ceramic shows lower friction coefficients than those of SiC and B_4C-SiC ceramics in boundary lubrication and mixed lubrication at 20 and 40 N.
(5) Both pores formed during the sintering and the residual carbon formed due to the tribochemical reaction of B_4C have little effect on the frictional property of carbide ceramics.

6.6. References

[1] X. L. Wang, K. Kato. Improving the anti-seizure ability of SiC seal in water with RIE texturing. Tribology Letters,2003,14(4):275-280.
[2] X. L. Wang, K. Kato, K. Adachi, K. Aizawa. Loads carrying capacity map for the surface texture design of SiC thrust bearing sliding in water. Tribology International,2003,36(3):189-197.
[3] V. Brizmer, Y. Kligerman, I. Etsion. A laser surface textured parallel thrust bearing. Tribology Transactions,2003,46(3):397-403.
[4] W. Zhang, S. Yamashita, H. Kita. Self lubrication of pressureless sintered SiC ceramics. Journal of Materials Research and Technology,2020,9(6):12880-12888.
[5] I. Etsion, G. Halperin, V. Brizmer, Y. Kligerman. Experimental investigation of laser surface textured parallel thrust bearing. Tribology Letters,2004,17(2):295-300.
[6] X. Wang, K. Kato, K. Adachi. Running-in effect on the load-carrying capacity of a water-lubricated SiC thrust bearing. Proceedings of the Institution of Mechanical Engineers, Part J: Journal of Engineering Tribology,2005,219:117-124.
[7] W. Zhang, S. Yamashita, H. Kita. Progress in tribological research of SiC ceramics in unlubricated sliding-A review. Materials & Design,2020,190:108528.
[8] T. S. P. Chang, S. Wu. Friction characteristics of carbon versus silicon carbide under stepwise loading conditions. Tribology Transactions,1996,39(2):338-345.
[9] H. Tomizawa, T. E. Fischer. Friction and wear of silicon nitride and silicon carbide in water: hydrodynamic lubrication at low sliding speed obtained by tribochemical wear. ASLE Transactions,1987,30(1):41-46.
[10] H. Nagasaka, K. Ito, J. Mori, T. Shimizu, S. Sasaki. Tribological properties of polycrystalline diamond films prepared by hot-filament chemical vapor deposition methods. Proceedings of the 16th International Conference on Nanotechnology, IEEE, 2016.
[11] S. Kitaoka, T. Tsuji, T. Katoh, Y. Yamaguchi, K. Kashiwag. Tribological characteristics of SiC ceramics in high-temperature and high-pressure water. Journal of the American Ceramic Society,1994,77(7):1851-1856.

[12] M. Chen, K. Kato, K. Adachi. Friction and wear of self-mated SiC and Si_3N_4 sliding in water. Wear,2001,250(1-12):246-255.

[13] R. S. Gates, S. M. Hsu. Tribochemistry between water and Si_3N_4 and SiC: Induction time analysis. Tribology Letters,2004,17(3):399-407.

[14] W. Zhang, S. Yamashita, H. Kita. Progress in pressureless sintering of boron carbide ceramics-A review. Advances in Applied Ceramics: Structural, Functional and Bioceramics,2019,118(4):222-239.

[15] W. Zhang. A review of tribological properties for boron carbide ceramics. Progress in Materials Science,2021,116:100718.

[16] W. Zhang, S. Yamashita, T. Kumazawa, F. Ozeki, H. Hyuga, H. Kita. Tribological properties of B_4C ceramics prepared by pressureless sintering and annealed at different temperatures. Tribology Transactions,2020,63(4):672-682.

[17] X. Q. Li, Y. M. Gao, Q. X. Yang, W. Pan, Y. F. Li, Z. C. Zhong, L. C. Song. Evaluation of tribological behavior of B_4C-hBN ceramic composites under water-lubricated condition. Ceramics International,2015,41(6):7387-7393.

[18] X. Q. Li, Y. M. Gao, Q. X. Yang. Sliding tribological performance of B_4C-hBN composite ceramics against AISI 321 steel under distilled water condition. Ceramics International,2017,43(17):14932-14937.

[19] W. Zhang, S. Yamashita, H. Kita. Tribological properties of SiC-B_4C ceramics under dry sliding condition. Journal of the European Ceramic Society,2020,40(8):2855-2861.

[20] W. Zhang, S. Yamashita, T. Kumazawa, F. Ozeki, H. Hyuga, H. Kita. Effect of nanorelief structure formed in situ on tribological properties of ceramics in dry sliding. Ceramics International,2019,45(11):13818-13824.

[21] W. Zhang, S. Yamashita, H. Kita. A study of B_4C-SiC composite for self-lubrication. Journal of the American Ceramic Society, DOI: 10.1111/jace.17584.

[22] W. Zhang, S. Yamashita, H. Kita. Effects of load on tribological properties of B_4C and B_4C-SiC ceramics sliding against SiC balls. Journal of Asian Ceramic Societies,2020,8(3):586-596.

[23] W. Zhang, S. Yamashita, T. Kumazawa, F. Ozeki, H. Hyuga, H. Kita. Influence of surface roughness parameters and surface morphology on friction performance of ceramics. Journal of the Ceramic Society of Japan,2019,127(11):837-842.

[24] W. Zhang, S. Yamashita, H. Kita. Effect of counterbody on tribological properties of B_4C-SiC composite ceramics. Wear,2020,458-459:203418.

[25] V. A. Muratov, T. Luangvaranunt, T. E. Fischer. The tribochemistry of silicon nitride: effects of friction, temperature and sliding velocity. Tribology International,1998,31(10):601-611.

[26] L. Jordi, C. Iliev, T. E. Fischer. Lubrication of silicon nitride and silicon carbide by water: Running in, wear and operation of sliding bearing. Tribology Letters,2004,17(3):367-376.

[27] J. G. Xu, K. Kato. Formation of tribochemical layer of ceramics sliding in water and its role for low friction. Wear,2000,245(1-2):61-75.

[28] M. Chen, K. Kato, K. Adachi. The difference in running-in period and friction coefficient between self-mated Si_3N_4 and SiC under water lubrication. Tribology letters,2001,11(1):23-28.

[29] M. Chen, K. Kato, K. Adachi. The comparisons of sliding speed and normal load effect on friction coefficients of self-mated Si_3N_4 and SiC under water lubrication. Tribology International,2002,35(3):129-135.

[30] C. Y. Chen, B. H. Wu, C. J. Chung, W. L. Li, C. W. Chien, P. H. Wu, C. W. Cheng. Low-friction characteristics of nanostructured surfaces on silicon carbide for water-lubricated seals. Tribology letters,2013,51:127-133.

[31] W. F. A. Besling, A. Goossens, B. Meester, J. Schoonman. Laser-induced chemical vapor deposition of nanostructured silicon carbonitride thin films. Journal of Applied Physics,1998,83(1):544-553.

[32] X. Q. Li, Y. M. Gao, W. Pan, Z. C. Zhong, L. C. Song, W. Chen, Q. X. Yang. Effect of hBN content on the

friction and wear characteristics of B_4C-hBN ceramic composites under dry sliding condition. Ceramics International,2015,41(3):3918-3926.

[33] P. D. Cuong, H. S. Ahn, E. S. Yoon, K. H. Shin. Effects of relative humidity on tribological properties of boron carbide coating against steel. Surface and Coatings Technology,2006,201(7):4230-4235.

[34] J. D. Rimstidt, H. L. Barnes. The kinetics of silica-water reactions. Geochimica et Cosmochimica Acta,1980, 44(11):1683-1699.

[35] Guicciardi S, Sciti D, Melandri C, Pezzotti G. Dry sliding wear behavior of nano-sized SiC pins against SiC and Si_3N_4 discs. Wear,2007,262(5-6):529-535.

Chapter 7
Effect of water temperature on tribological performance of B_4C-SiC ceramics under water lubrication

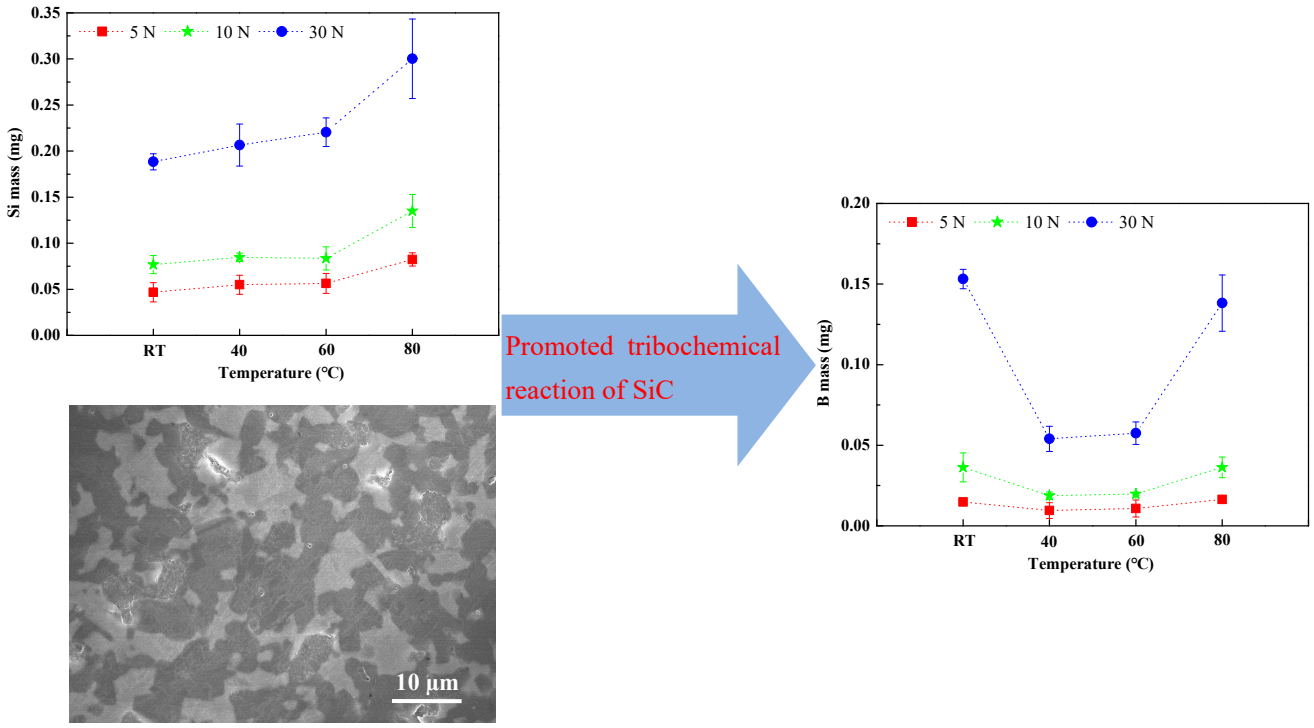

The tribological performance of B_4C-SiC ceramics under water lubrication at different water temperatures was studied. The wear mechanisms of B_4C-SiC ceramics sliding in water are expected to be mechanical wear and tribochemical wear. There is only SiO_2 film on the wear surfaces of B_4C-SiC discs after sliding under different loads, and there is no boron oxide or hydroxide on the wear surfaces of B_4C-SiC discs when the water temperature varied between room temperature and 60 ℃. The tribochemical reaction of B_4C in B_4C-SiC ceramics is discovered. The products of tribochemical reaction of B_4C in B_4C-SiC ceramics are H_3BO_3 and C, and the residual carbon will be left on the wear surface. B_4C-SiC/SiC tribopairs can obtain the lowest friction coefficients and systematic wear rates as sliding in water at water temperature between 40 ℃ and 60 ℃, which is attributed to the promoted tribochemical reaction of SiC in B_4C-SiC ceramics, rather than the tribochemical reaction of B_4C in B_4C-SiC ceramics. More SiO_2 film is gradually formed on the wear surfaces as the sliding distance increases, which can cover or protect more B_4C grains. The formation of more SiO_2 film results in the reduced friction coefficient, tribochemical wear, and mechanical wear for B_4C-SiC ceramics.

Contents

7.1. Introduction

Energy saving and emission reduction is one of the most important tasks in the current social development. In traditional mechanical design, metal/oil is considered as a good combination due to the high viscosity of oil lubricant. However, the leakage of oil lubricant would cause environmental pollution. At present, ceramic/water combination has partially replaced metal/oil combination as friction elements. For example, SiC ceramics have been widely used as sliding bearings and mechanical seals [1-5]. The ceramic/water combination has the following advantages: (1) It will not pollute the environment; (2) It can simplify machines working in water and make maintenance easier because the process fluid is used as a lubricant; (3) For non-oxide ceramics, water is not only a lubricant but also a necessary substance for tribochemical reaction [6-8].

Among ceramic materials, SiC ceramics and B_4C ceramics are expected to be good candidates for tribological applications in water because of their extremely high hardness [9-12]. Many researchers have done a lot of investigations on tribological performance under water-lubricated conditions for SiC ceramics and B_4C ceramics. Wang et al. [13] stated that SiC ceramics can show low friction under water-lubricated conditions, and revealed that the key of this phenomenon is tribochemical reaction of SiC. The product SiO_2 of tribochemical reaction forms a film on the sliding interface, which is effective in decreasing friction as two surfaces begin to contact, especially in the low sliding speed range. Gates and Hsu [14] found that SiO_2 formed due to the tribochemical reaction of SiC can react with water to form silicic acid, which can be acted as a lubricant. Jordi et al. [15] mentioned that the low friction of SiC ceramics sliding in water is achieved by hydrodynamic lubrication alone, and the water film sustains the whole weight. Matsuda et al. [16] noted that the self-mated SiC ceramics would exhibit different tribological behaviors when they slid in water from sea, river, ground, and deionized at room temperature. The largest friction coefficient is found in seawater, while the smallest in deionized water. The largest wear rate is found in deionized water, while the smallest in seawater. Moreover, Li et al. [17] noted that a B_2O_3 film is formed on the wear surface of B_4C-hBN ceramics, which is resulting from the tribochemical reaction of hBN. This B_2O_3 film can protect the wear surface of B_4C-hBN ceramics and can facilitate the wear surface to smooth. Li et al. [18] also pointed out that both the friction coefficient and wear rate of B_4C ceramics reduce with increase in BN content as sliding in water, which was ascribed to the flat wear surface of B_4C ceramics because of hydrolysis of BN phase. Recently, we found that B_4C-SiC ceramics show better tribological performance as compared to SiC ceramics and B_4C ceramics under unlubricated sliding [19-24]. As a new potential candidate material for tribological applications, however, to date, there is no report evaluating the tribological performance of B_4C-SiC ceramics under water lubrication. Does B_4C-SiC ceramics also have tribochemical reactions when they slide in water? If any, are the tribochemical reaction products silicon oxide or hydroxide, boron oxide or hydroxide, or their mixture? On the other hand, as mentioned above, water from different sources will have different effects on the tribological performance of ceramics in water. Then, it is natural to associate whether different water temperatures will also have different effects on the tribological properties of ceramics. Some researchers found that the friction and wear of SiC ceramics and Al_2O_3 ceramics will be increased when sliding in water at 120 ℃ and 300 ℃ [25, 26], corresponding saturated vapor pressures of 0.2 and 8.53 MPa, respectively, however, those are tribological behaviors of ceramics in high-temperature, high-pressure water. Until now, the tribological performance of ceramics sliding in water at different water temperatures under atmospheric pressure has not been studied yet.

In this article, we report the influence of water temperature on the tribological performance of B_4C-SiC ceramics sliding under different loads in water under atmospheric pressure (0.1 MPa).

7.2. Experimental procedures

B_4C-SiC ceramics with a weight ratio of 60:40 were prepared by pressureless sintering method. Carbon black was used as a sintering additive, whose mass fraction was 3 wt%. The powder mixture was first mechanical milled by using SiC balls and then sintered at 2300 ℃ for 16 h in the protection of Ar gas. The properties of the resulting B_4C-SiC ceramics are presented in Table 1. More details about performance testing methods can be found in our previous work [20]. The specimens were polished, and the final surface roughness was 10-25 nm.

Table 1 Properties of the sintered B_4C-SiC ceramics.

Property	Value
Relative density (%)	93.9
Bulk density (g/cm^3)	2.62
Average hardness (GPa)	30.4
Average fracture toughness (MPa·m$^{1/2}$)	3.2

Water-lubricated sliding tests of the B_4C-SiC ceramics were performed on a ball-on-disc tester (T-18-0162, NANOVEA, US) in ambient conditions (22-25 ℃), whose schematic diagram is presented in Fig. 1. The water used here was deionized water, whose conductivity was 0.09 μS/cm (determined at 25 ℃). During the test, the contact surfaces were submerged in deionized water all the time. The B_4C-SiC ceramics with a dimension of 25 × 25 × 6 mm^3 were used as discs. The SiC balls, with a diameter of 9.5 mm, were commercially available. Before tests, both the discs and balls were ultrasonically cleaned with ethanol for 10 min. The water-lubricated sliding tests were conducted at four different water temperatures: room temperature (RT, about 20-22 ℃), 40 ℃, 60 ℃, 80 ℃. A circle heater was used to heat the water. The following test conditions were used: normal load 5-30 N, sliding speed 0.06 m/s, sliding distance 500 m, and sliding radius 7 mm. Friction coefficients were continuously recorded. Wear volumes on discs and balls were calculated from the surface profile traces across the wear track and from the wear scar, respectively. The specific wear rates were calculated by the wear volume divided by the normal load and sliding distance. Three repeated tests were carried out for each tribopair under the same conditions.

Wear surface topographies of B_4C-SiC ceramics were observed by SEM (JEOL, JSM-7500F). Wear surface composition was investigated by XPS (THERMO SCIENTIFIC, ESCALAB250Xi). Concentrations of Si element and B element in water samples after sliding tests were analyzed after filtration by ICP-AES (HITACHI, SPS7800).

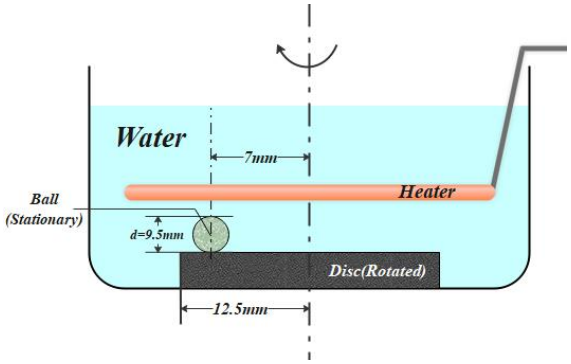

Fig. 1. Schematic diagram of ball-on-disc sliding friction and wear tests in water.

7.3. Results

The friction coefficient curves of the B_4C-SiC/SiC tribopairs as a function of sliding distance in water at

different water temperatures are shown in Fig. 2. When the water temperature is RT, the friction coefficients of B_4C-SiC/SiC tribopairs are relatively stable with increasing of the sliding distance after the run-in period under different loads. When the water temperatures are 40 ℃ and 60 ℃, the friction coefficients of B_4C-SiC/SiC tribopairs decrease continuously with increasing of the sliding distance under different loads. However, when the water temperature is 80 ℃, the friction coefficients of B_4C-SiC/SiC tribopairs no longer drop to lower values under different loads, whose friction behavior is similar to that in RT water.

The average friction coefficients and the complete set of the specific wear rates of the B_4C-SiC/SiC tribopairs sliding in water at different water temperatures are presented in Fig. 3. With water temperature increasing from RT to 60 ℃, in general, the friction coefficients of tribopairs at water temperatures of 40 ℃ and 60 ℃ are lower than those at RT (Fig. 3(a)). However, when the water temperature is 80 ℃, the friction coefficients of B_4C-SiC/SiC tribopairs under different loads are higher than those at RT. Further, the difference in friction coefficients of B_4C-SiC/SiC tribopairs between 5 N and 10 N at different water temperatures is not obvious, and the friction coefficients of B_4C-SiC/SiC tribopairs under 30 N exhibit the lowest values at different water temperatures. It can be found from Fig. 3(b) that, with water temperature increasing from RT to 80 ℃, the specific wear rates of B_4C-SiC disc decrease first and then increase, and the B_4C-SiC disc exhibits lower specific wear rates when the water temperature is between 40 ℃ and 60 ℃. As to the mating SiC balls, they reveal a different wear behavior from the B_4C-SiC disc with water temperature increasing. The changes in specific wear rates of SiC balls are not obvious with water temperature increasing from RT to 60 ℃, however, the specific wear rates of SiC balls increase significantly when the water temperature increases to 80 ℃ (Fig. 3(c)). Accordingly, the systematic wear rates of B_4C-SiC/SiC tribopairs under different loads at water temperatures of 40 ℃ and 60 ℃ are lower than those at the water temperature of RT (Fig. 3(d)). Nonetheless, when the water temperature increases to 80 ℃, the systematic wear rates of B_4C-SiC/SiC tribopairs under different loads are increased (Fig. 3(d)), which are higher than those at the water temperature of RT.

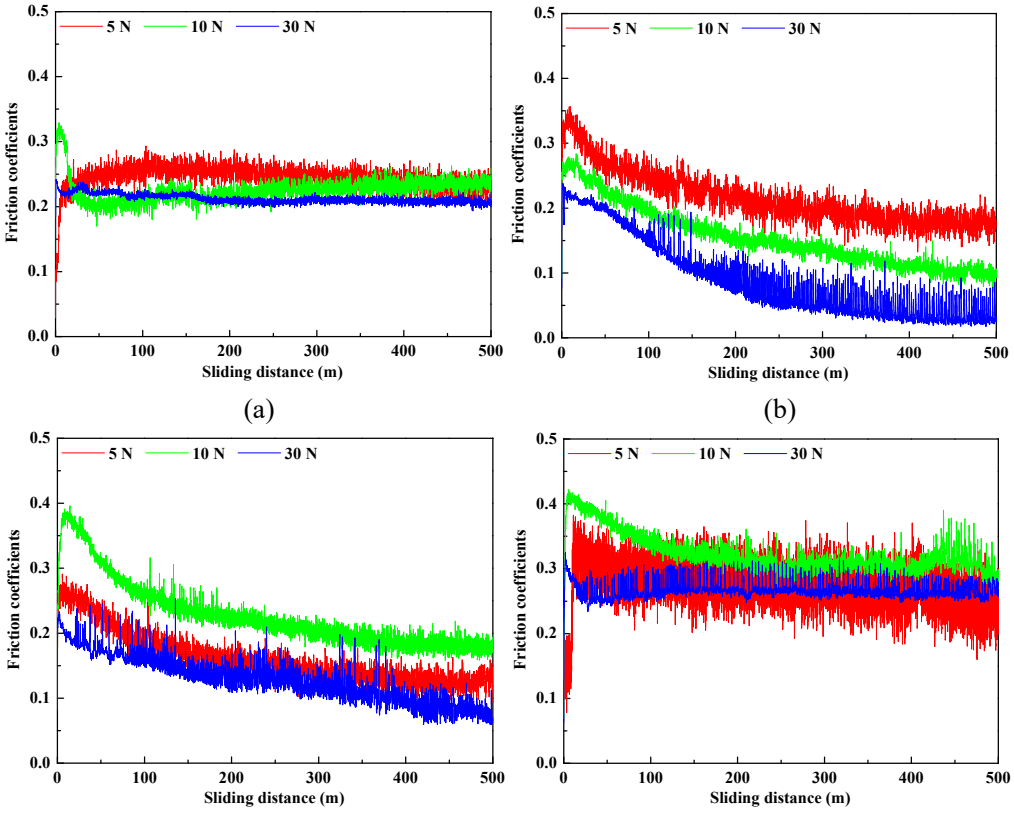

Fig. 2. Friction coefficients of the B_4C-SiC/SiC tribopairs vs sliding distance in water at: (a) RT, (b) 40 ℃, (c) 60 ℃, (d) 80 ℃.

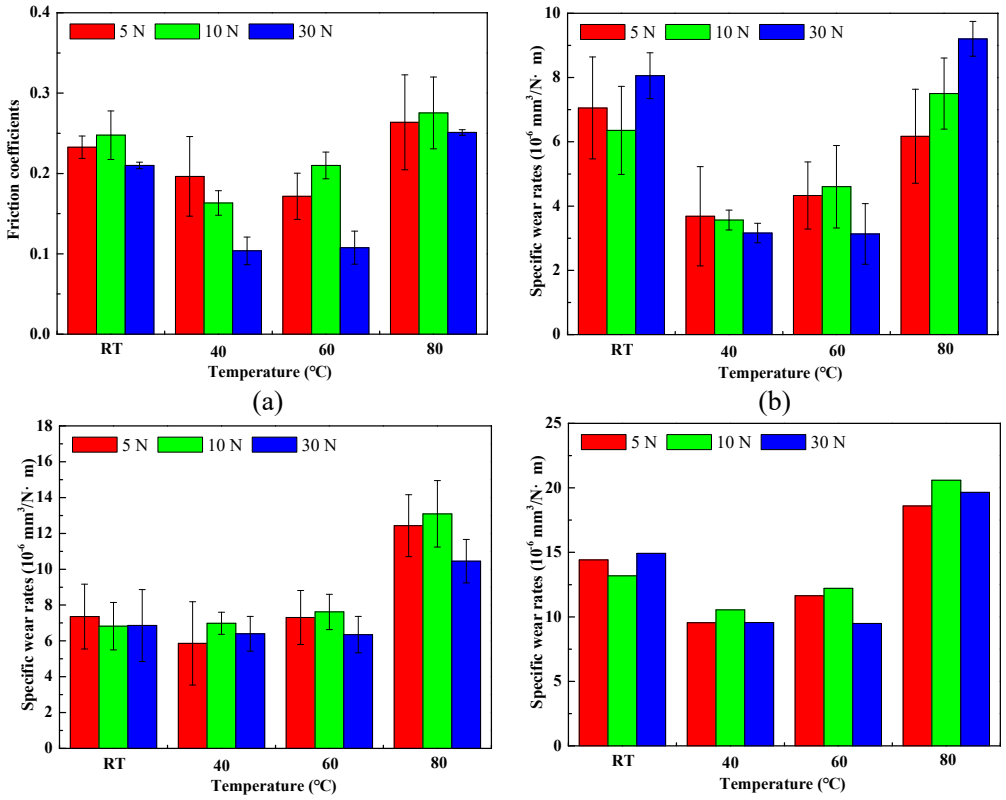

Fig. 3. Average friction coefficients of the B_4C-SiC/SiC tribopairs (a), specific wear rates of the B_4C-SiC discs (b), specific wear rates of mating SiC balls (c), and systematic specific wear rates of B_4C-SiC/SiC tribopairs (d) sliding in water at different water temperatures.

XPS was used to analyze wear surfaces of the B_4C-SiC discs under different loads in water at different water temperatures, with the results shown in Figs. 4-7. For the B_{1s} peaks, they can't be decomposed, and the B_{1s} binding energy in the range of 186.8-187.9 eV can be assigned to B_4C [27]. For the Si_{2p} peaks, through a curve fitting procedure, the Si_{2p} peaks in Figs. 4-6 can be decomposed into two peaks, however, the Si_{2p} peaks in Fig. 7 can't be decomposed. The Si_{2p} binding energy of 99.6-100.5 eV can be assigned to SiC [28], and the Si_{2p} binding energy of 100.7-101.8 eV can be assigned to SiO_2 [28]. Therefore, it can be concluded that neither boron oxide nor hydroxide exists on the wear surfaces after B_4C-SiC discs sliding under different loads in water at different water temperatures, and SiO_2 only exists on the wear surfaces after B_4C-SiC discs sliding under different loads in water at water temperatures of RT, 40 ℃ and 60 ℃. No SiO_2 exists on the wear surfaces after B_4C-SiC discs sliding under different loads in water at the water temperature of 80 ℃.

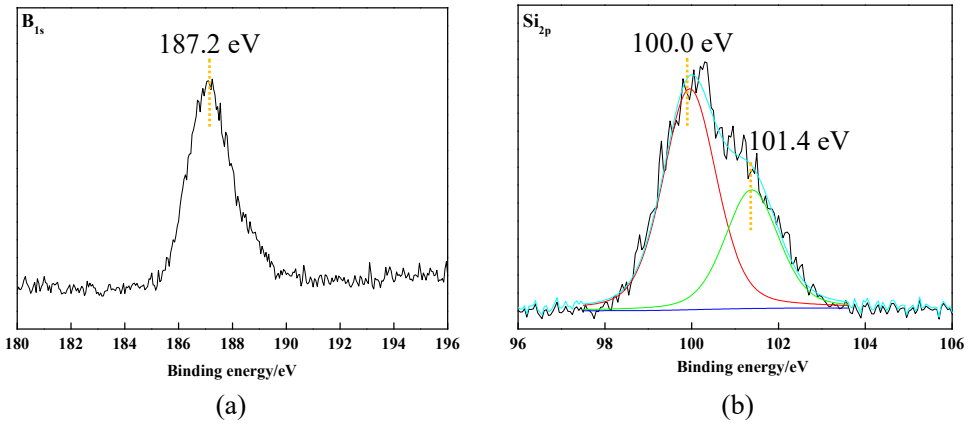

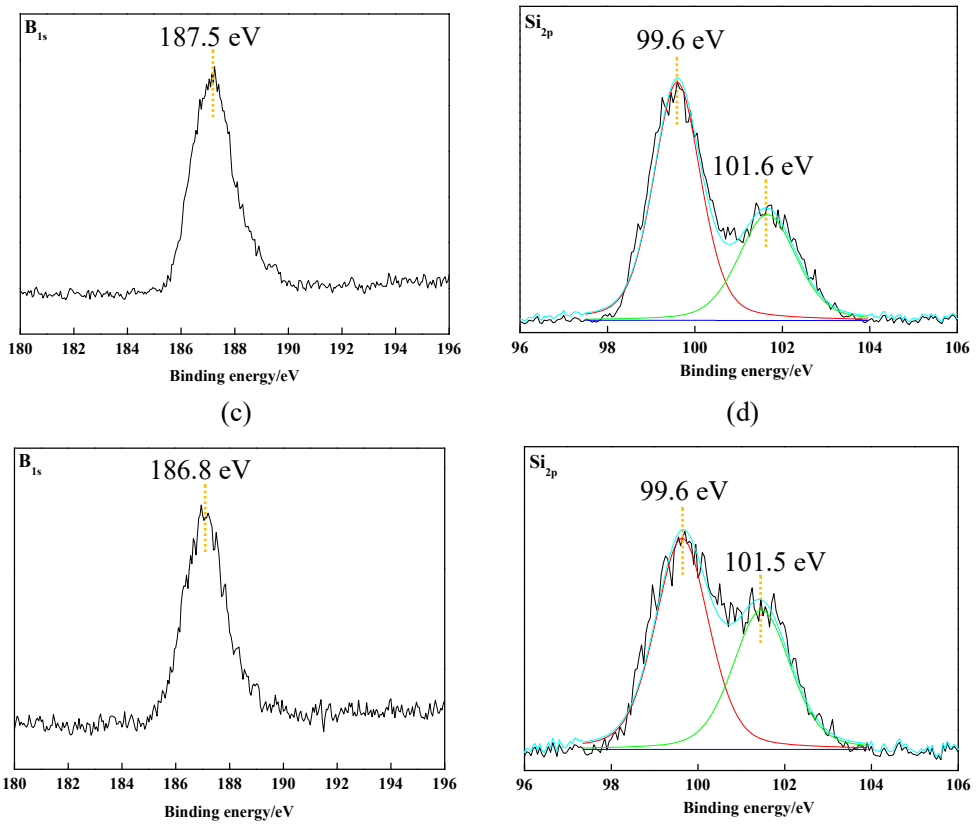

Fig. 4. XPS results of wear surfaces of B_4C-SiC disc in water at RT under different loads: (a-b) 5 N, (c-d) 10 N, (e-f) 30 N.

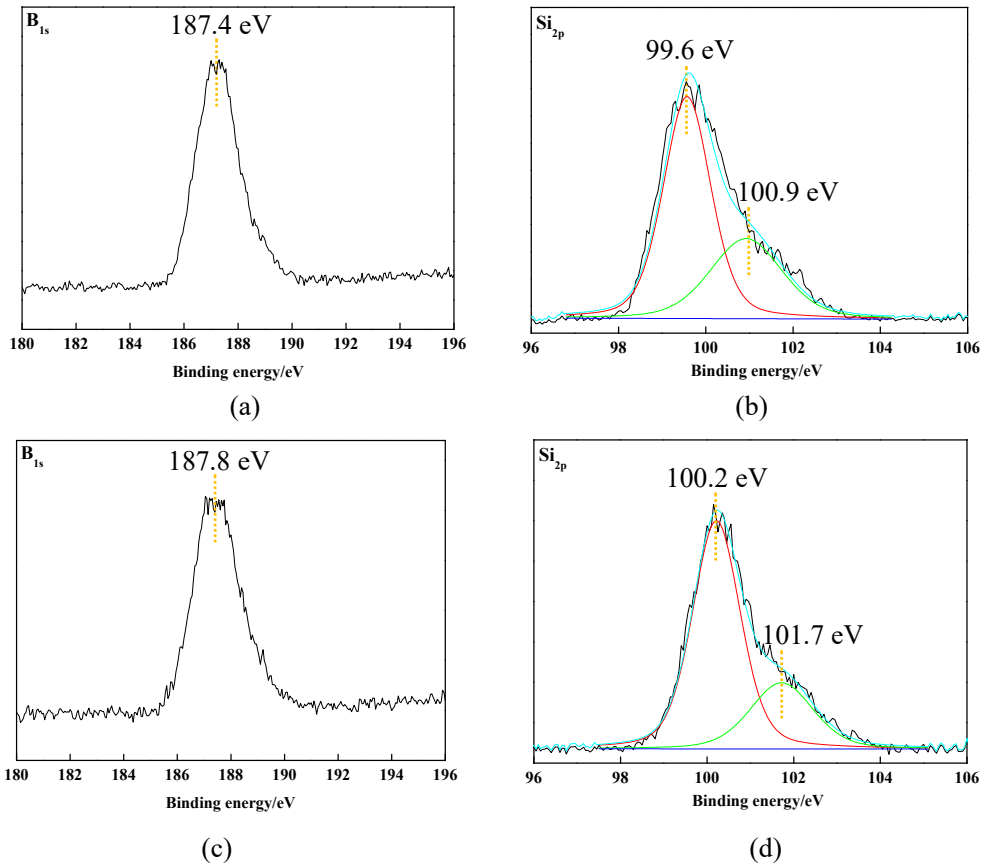

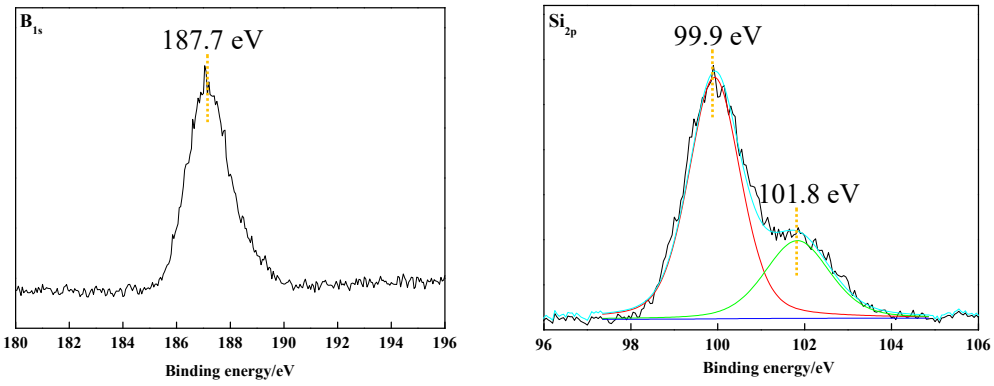

(e) (f)

Fig. 5. XPS results of wear surfaces of B_4C-SiC disc in water at 40 ℃ under different loads: (a-b) 5 N, (c-d) 10 N, (e-f) 30 N.

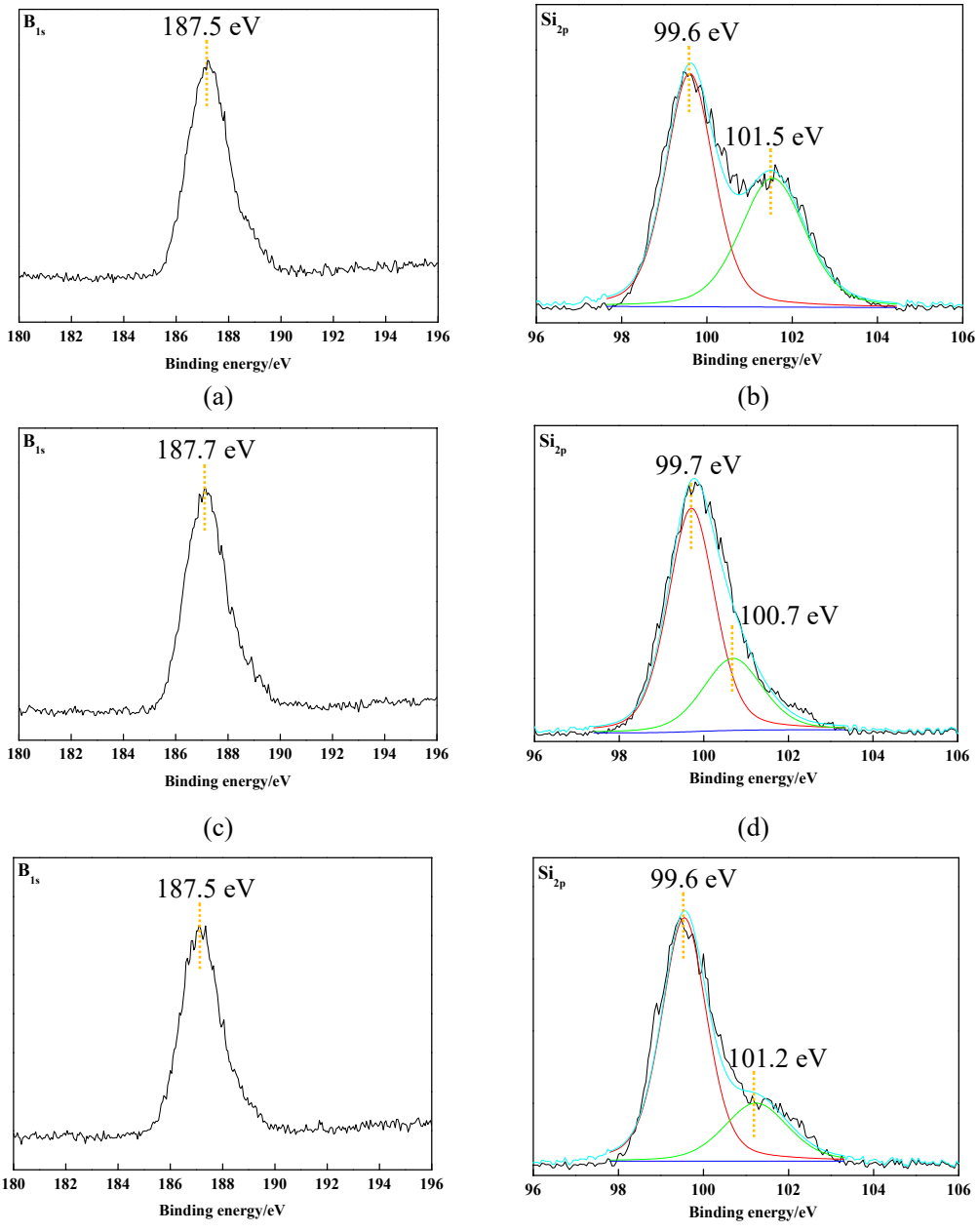

Fig. 6. XPS results of wear surfaces of B_4C-SiC disc in water at 60 ℃ under different loads: (a-b) 5 N, (c-d) 10 N, (e-f) 30 N.

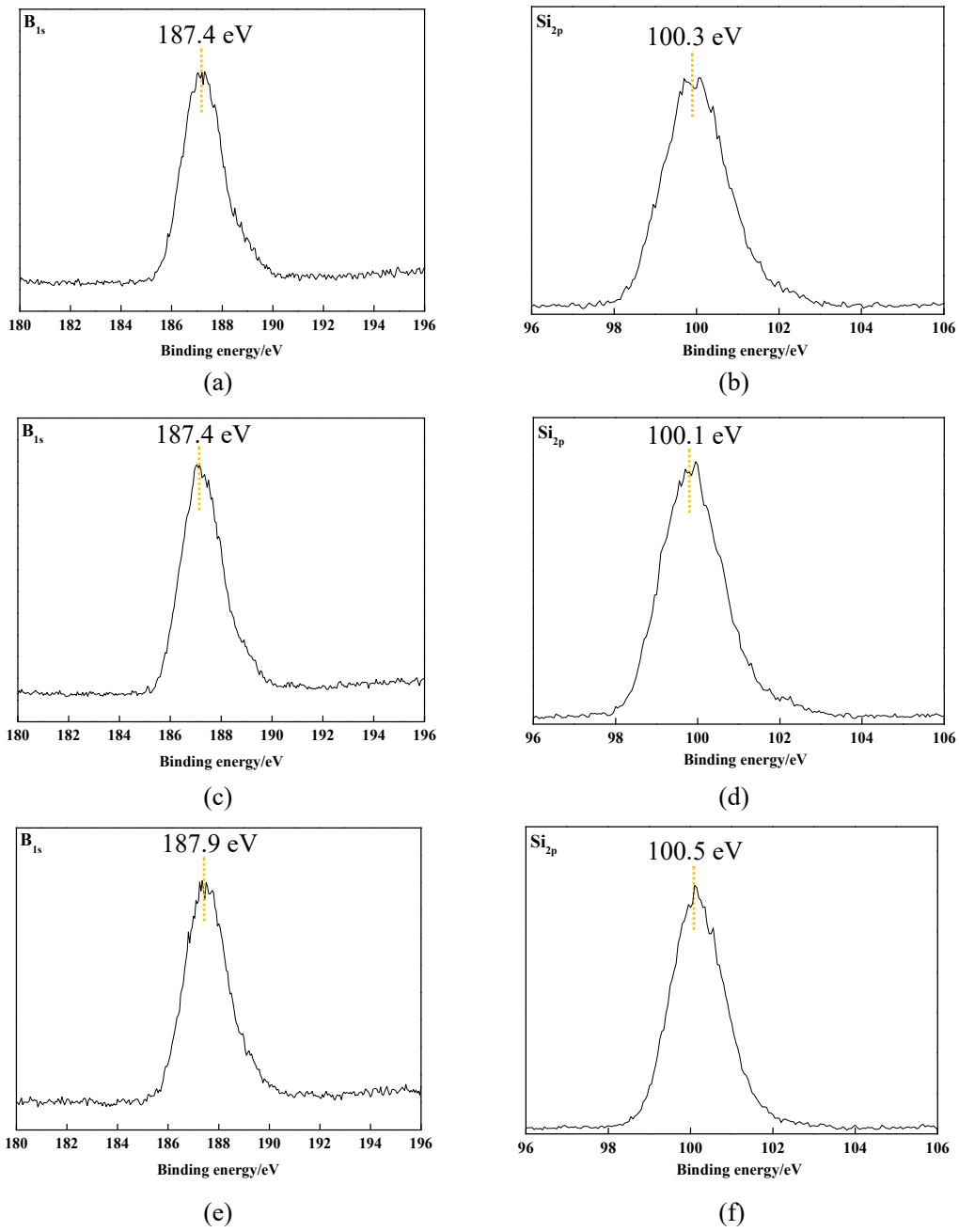

Fig. 7. XPS results of wear surfaces of B_4C-SiC disc in water at 80 ℃ under different loads: (a-b) 5 N, (c-d) 10 N, (e-f) 30 N.

To check the tribochemical reactions of B_4C-SiC/SiC tribopairs sliding under different loads in water at different water temperatures, the water samples were collected after the sliding. The concentrations of Si and B elements in the water samples were tested by ICP-AES. Because the remaining water amounts were different after B_4C-SiC/SiC tribopairs sliding in water at different water temperatures, the mass of Si and B elements in the water samples were calculated, respectively, and the results are presented in Fig. 8. Both Si mass and B mass increase with the increase of load at each water temperature. Further, for the Si element in water, when the water temperature increases from RT to between 40 ℃ and 60 ℃, the Si mass in water slightly increases under different loads. For the B element in water, when the water temperature is between 40 ℃ and 60 ℃, the values of B mass in water under different loads are lower than those at RT. When the water temperature is 80 ℃, both Si mass and B mass in water increase.

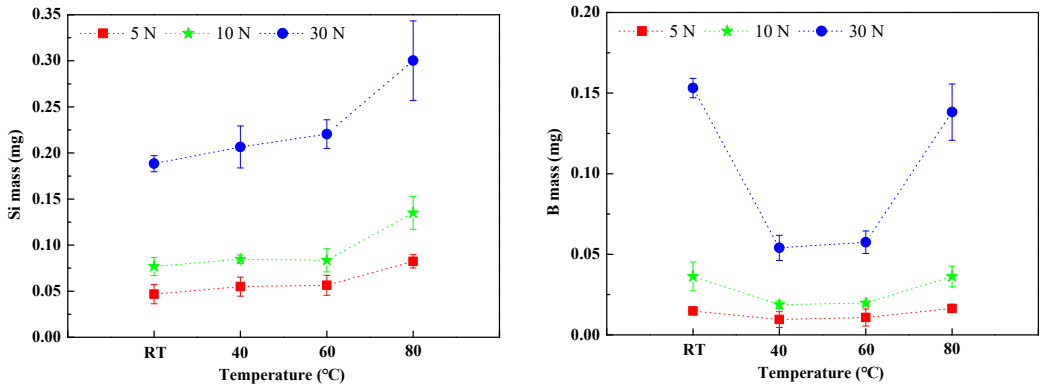

(a) (b)

Fig. 8. Amounts of Si and B elements in the water samples tested by ICP-AES after B_4C-SiC/SiC tribopairs sliding under different loads in water at different water temperatures: (a) Si, and (b) B.

The wear surface morphologies of B_4C-SiC discs after sliding under the load of 30 N in water at different water temperatures are presented in Fig. 9. When the water temperature is RT, some scratches can be found on the wear surface (Fig. 9(a)). Combined with the XPS result in Fig. 4(f), it has known that there is SiO_2 film on the wear surface of the B_4C-SiC disc. However, the SiO_2 film can't be seen clearly on the wear surface, which may be attributed to its small amount. When the water temperature is between 40 °C and 60 °C, it can be observed clearly that there is a thin film on the wear surface (Fig. 9(b)). Combined with XPS results in Fig. 5(f) and Fig. 6(f), it has known that this thin film is SiO_2 film. When the water temperature is 80 °C, however, almost no film can be found on the wear surface, and some scratches can be seen (Fig. 9(c)).

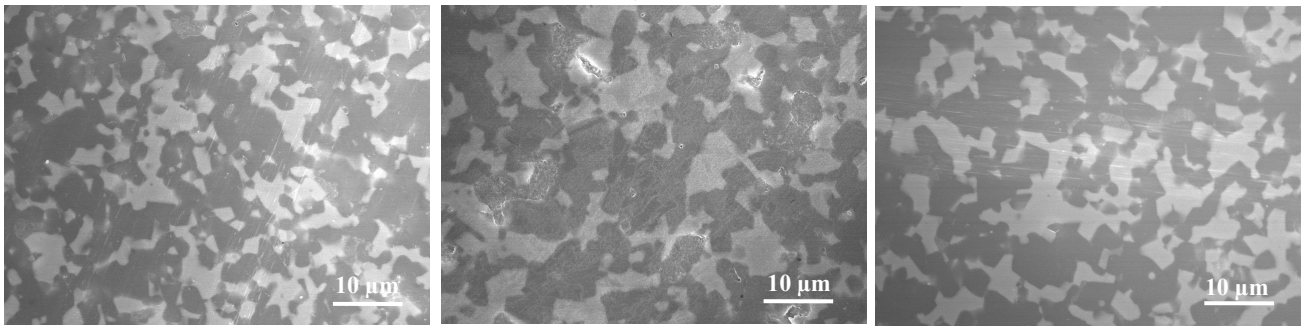

(a) (b) (c)

Fig. 9. Wear surfaces of B_4C-SiC discs after sliding under the load of 30 N in water at different water temperatures: (a) RT, (b) 60 °C, and (c) 80 °C.

7.4. Discussion

For the B_4C-SiC/SiC tribopairs sliding under different loads in water at the water temperature of RT, the friction coefficient of tribopair at 30 N is slightly lower than those at 5 N and 10 N, and the specific wear rate of the B_4C-SiC disc at 30 N is slightly higher than those at 5 N and 10 N. According to the XPS results shown in Fig. 4, it is known that there is only SiO_2 film on the wear surfaces after B_4C-SiC discs sliding under different loads, and there is no H_3BO_3 or B_2O_3 on the wear surfaces of B_4C-SiC discs. For monolithic SiC ceramics sliding in water, many researchers found that the tribochemical reaction of SiC can be induced by friction at room temperature [6, 29, 30], which can be expressed as follow:

$$SiC + 2H_2O = SiO_2 + CH_4 \quad (1)$$

Therefore, in this study, for the B_4C-SiC ceramics, the SiC in B_4C-SiC ceramics also underwent tribochemical reaction. Also, the amount of SiO_2 formed increases with increasing of the load because the increased load is

beneficial to promote tribochemical reaction of SiC due to the increased friction heat. Then partial SiO_2 can be dissolved in water. Thus, Si element in the water samples after B_4C-SiC/SiC tribopairs sliding under different loads can be detected by ICP, and the amount of Si element in water increases with increasing of the load due to more SiO_2 formed with increasing of the load (Fig. 8(a)). Meanwhile, the SiO_2 that is not dissolved in water exists on the wear surface of the B_4C-SiC disc, which has been detected by XPS (Fig. 4). For monolithic B_4C ceramics sliding in water, Li et al. [18] observed that B element exists in the water sample after sliding against AISI 321 steel in RT water, however, the formation mechanism of which was not given. In this study, we also observed that the B element exists in the water sample when B_4C-SiC ceramics sliding against SiC balls. We consider that the formation of B element in water is attributed to the tribochemical reaction of B_4C, which can be achieved by a one-step reaction, as follow:

$$B_4C + 12H_2O = 4H_3BO_3 + C + 6H_2 \quad (2)$$

or two-step reactions, as follows:

$$B_4C + 6H_2O = 2B_2O_3 + C + 6H_2 \quad (3)$$

$$B_2O_3 + 3H_2O = 2H_3BO_3 \quad (4)$$

H_3BO_3 formed by tribochemical reaction of B_4C can be dissolved completely in water, thus, no H_3BO_3 is found on the wear surfaces of B_4C-SiC discs, but B element is present in water. This assumption can be demonstrated by the presence of residual carbon on the wear surface, as shown in Fig. 10. Although 3 wt% carbon black is used as a sintering additive in B_4C-SiC ceramics and there is a small amount of C in the resulting B_4C-SiC ceramics [31], this spotted residual carbon can't be observed on the initial surface of B_4C-SiC ceramics [23]. Conversely, many spotted residual carbon is observed on the wear surface of the B_4C-SiC disc after sliding in water at the water temperature of RT (Fig. 9(a)). Therefore, the residual carbon on the wear surface of the B_4C-SiC disc is considered to be formed by the tribochemical reaction of B_4C. Furthermore, although Li et al. [17] found that B_2O_3 can exist on the wear surface of B_4C-20 wt%hBN ceramics, in this study, neither boron oxide nor hydroxide exists on the wear surfaces of B_4C-SiC discs after sliding at any load, as shown in Fig. 4. Moreover, some scratches are found on the wear surface of the B_4C-SiC disc, thus, micro-cutting is the main way of mechanical wear for B_4C-SiC ceramics. The wear mechanisms of B_4C-SiC ceramics sliding in RT water are expected to be mechanical wear and tribochemical wear.

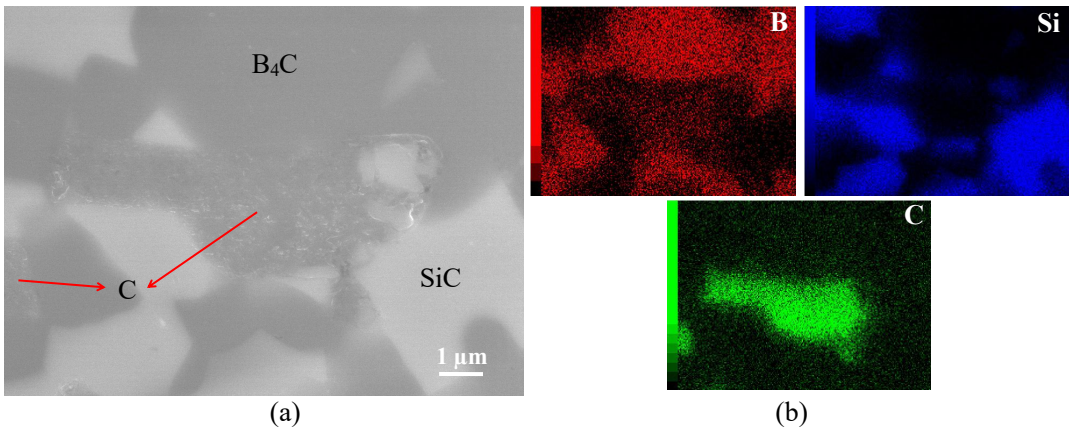

Fig. 10. Wear surface of B_4C-SiC disc after sliding at 10 N in RT water (a), and elemental distributions (b).

For the B_4C-SiC/SiC tribopairs sliding under different loads in water when the water temperature is between 40 °C and 60 °C, both the friction coefficients and specific wear rates of B_4C-SiC discs are lower than those at RT, and the friction coefficients and specific wear rates of B_4C-SiC discs at 30 N are lower than those at 5 and 10 N. It has been known from Fig. 2(b) and (c) that the friction coefficients of the B_4C-SiC/SiC tribopairs continuously decreases with sliding distance increasing. According to the XPS results (Fig. 5 and Fig. 6), when the water temperature increases to between 40 °C and 60 °C, there is still no boron oxide or hydroxide on the wear surfaces

of B_4C-SiC discs under different loads, and only SiO_2 films exist on the wear surfaces of B_4C-SiC discs under different loads. Also, this SiO_2 film can be observed clearly by SEM after the B_4C-SiC disc sliding against SiC ball under the load of 30 N in water at 60 ℃ (Fig. 9(b)). Therefore, it is logical to infer that the increased water temperature promotes the tribochemical reaction of SiC in B_4C-SiC ceramics, rather than B_4C in B_4C-SiC ceramics. When the water temperature increases from RT to between 40 ℃ and 60 ℃, more SiO_2 film is gradually formed on the wear surface of the B_4C-SiC disc as the sliding distance increases, leading to a gradual decrease in friction coefficient with sliding distance increasing. Accordingly, the area of wear surface of B_4C-SiC disc covered by SiO_2 film increases gradually with the sliding distance increases. This means that more B_4C grains are covered or protected by this SiO_2 film formed because of the promoted tribochemical reaction of SiC grains, which reduces the tribochemical reaction of B_4C grains. Thus, the reduced mass of B elements in the water samples after B_4C-SiC/SiC tribopairs sliding under different loads in water at water temperatures of 40 ℃ and 60 ℃ are observed (Fig. 8(b)). The tribochemical wear of B_4C-SiC ceramics is controlled by the simultaneous occurrence and competition of the promoted tribochemical reaction of SiC in B_4C-SiC ceramics and the inhibited tribochemical reaction of B_4C in B_4C-SiC ceramics. However, the SiO_2 film formed due to tribochemical reaction of SiC is not easily soluble in water, which is different from H_3BO_3, and only partial SiO_2 can be dissolved in water. Therefore, the promoted tribochemical reaction of SiC in B_4C-SiC ceramics can't significantly increase tribochemical wear of B_4C-SiC ceramics, which can be demonstrated by the result in Fig. 8(a) and by the observation in Fig. 9(b). As a result, the tribochemical wear of the B_4C-SiC discs sliding in water between 40 ℃ and 60 ℃ under different loads is reduced. Meanwhile, the mechanical wear of B_4C-SiC discs can also be reduced to a certain extent by this increased SiO_2 film. Therefore, the specific wear rates of B_4C-SiC discs sliding in water between 40 ℃ and 60 ℃ under different loads are lower than those at RT. Furthermore, the friction coefficients of B_4C-SiC/SiC tribopairs sliding in water between 40 ℃ and 60 ℃ under different loads are also reduced by this increased SiO_2 film. For the improved tribological performance of B_4C-SiC ceramics sliding in water between 40 ℃ and 60 ℃, it is very interesting to note that the decreased friction and wear of B_4C-SiC ceramics are caused by the tribochemical reaction of SiC in B_4C-SiC ceramics, rather than the tribochemical reaction of B_4C in B_4C-SiC ceramics.

For the B_4C-SiC/SiC tribopairs sliding under different loads in water at the water temperature of 80 ℃, both the friction coefficients of tribopairs and the specific wear rates of B_4C-SiC discs and mating SiC balls increase again. First, according to the XPS results shown in Fig. 7, there is still no boron oxide or hydroxide on the wear surfaces of B_4C-SiC discs under different loads. Second, different from the XPS results at water temperatures of RT, 40 ℃ and 60 ℃, it can be seen that no SiO_2 exists on the wear surfaces of B_4C-SiC discs after sliding under different loads in water at 80 ℃ (Fig. 7). It is considered that the dissolution rate of SiO_2 is faster than its formation rate in water at 80 ℃, thereby, the SiO_2 film formed because of the tribochemical reaction of SiC in B_4C-SiC ceramics is completely dissolved in water, and no SiO_2 film is on the wear surfaces of B_4C-SiC discs under different loads. B_4C and SiC particles can be observed clearly on the wear surface (Fig. 9(c)). Because neither SiO_2 film nor B_2O_3 film covers on the wear surfaces of B_4C-SiC discs, B_4C-SiC discs directly contact with SiC balls and water, leading to the increased friction coefficient, mechanical wear, and tribochemical wear.

In summary, it is found in this study that for the B_4C-SiC/SiC tribopairs sliding under different loads in water at RT, the wear mechanisms of B_4C-SiC ceramics are expected to be mechanical wear and tribochemical wear. There is only SiO_2 film on the wear surfaces of B_4C-SiC discs after sliding under different loads, and there is no boron oxide or hydroxide on the wear surfaces of B_4C-SiC discs. The tribochemical reaction of B_4C was found. After the tribochemical reaction of B_4C in B_4C-SiC ceramics, residual carbon will be left on the wear surface. When the water temperature increases to between 40 ℃ and 60 ℃, the tribochemical reaction of SiC in B_4C-SiC ceramics is promoted, and more SiO_2 film is gradually formed on the wear surfaces as the sliding distance

increases, which can cover or protect more B_4C grains, causing the reduced tribochemical reaction of B_4C grains. Meanwhile, the mechanical wear of B_4C-SiC ceramics can also be reduced to a certain extent by this increased SiO_2 film. Thereby, the reduced friction and wear of B_4C-SiC ceramics sliding in water at water temperature between 40 ℃ and 60 ℃ are attributed to the promoted tribochemical reaction of SiC in B_4C-SiC ceramics, rather than the tribochemical reaction of B_4C in B_4C-SiC ceramics. When the water temperature is further increased to 80 ℃, because the SiO_2 film formed because of the tribochemical reaction of SiC in B_4C-SiC ceramics is completely dissolved in water, and no SiO_2 film is on the wear surfaces of B_4C-SiC discs, thus, the friction coefficients and specific wear rates of B_4C-SiC discs increase. As a whole, when the B_4C-SiC/SiC tribopairs sliding in water at water temperature between 40 ℃ and 60 ℃, the B_4C-SiC/SiC tribopairs can obtain the lowest friction coefficients and systematic wear rates. The mechanism of B_4C-SiC ceramics with low friction and low wear sliding in water at water temperature between 40 ℃ and 60 ℃ is revealed in this paper.

7.5. Conclusions

The tribological performance of B_4C-SiC ceramics under water lubrication at different water temperatures was studied. The following results are obtained:

(1) Mechanical wear and tribochemical wear are the wear mechanisms of B_4C-SiC ceramics sliding in water.
(2) There is only SiO_2 film on the wear surfaces of B_4C-SiC discs after sliding under different loads, and there is no boron oxide or hydroxide on the wear surfaces of B_4C-SiC discs when the water temperature varied between RT and 60 ℃.
(3) The products of tribochemical reaction of B_4C in B_4C-SiC ceramics are H_3BO_3 and C, and the residual carbon will be left on the wear surface.
(4) B_4C-SiC/SiC tribopairs can obtain the lowest friction coefficients and systematic wear rates as sliding in water at water temperature between 40 ℃ and 60 ℃, which is attributed to the promoted tribochemical reaction of SiC in B_4C-SiC ceramics, rather than the tribochemical reaction of B_4C in B_4C-SiC ceramics. More SiO_2 film is gradually formed on the wear surfaces as the sliding distance increases, which can cover or protect more B_4C grains. The formation of more SiO_2 film results in the reduced friction coefficient, tribochemical wear, and mechanical wear for B_4C-SiC ceramics.
(5) B_4C-SiC/SiC tribopairs can't obtain low friction coefficients and systematic specific wear rates as sliding in water at the water temperature of 80 ℃, which is attributed to the fact that the SiO_2 film formed because of the tribochemical reaction of SiC in B_4C-SiC ceramics is completely dissolved in water and no SiO_2 film is on the wear surfaces of B_4C-SiC discs.

7.6. References

[1] T. K. Guha, B. Basu. Microfracture and limited tribochemical wear of silicon carbide during high-speed sliding in cryogenic environment. Journal of the American Ceramic Society,2010,93(6):1764-1773.
[2] K. Kanda, S. Tazawa,T. Urano, S. Kobayashi,K. Adachi. The possibility of both low friction and low leakage by surface texture of mechanical seals in blood. Tribology Letters,2020, 68(2),65.
[3] A. K. Bałata, J. Mazur. Effect of carbon nanoparticle reinforcement on mechanical and thermal properties of silicon carbide ceramics. Ceramics International,2018,44(9):10273-10280.
[4] W. Zhang, S. Yamashita, H. Kita. Progress in tribological research of SiC ceramics in unlubricated sliding-A review. Materials & Design,2020,190:108528.

[5] W. Zhang, S. Yamashita, H. Kita. Self lubrication of pressureless sintered SiC ceramics. Journal of Materials Research and Technology,2020,9(6):12880-12888.

[6] M. Chen, K. Kato, K. Adachi. The difference in running-in period and friction coefficient between self-mated Si_3N_4 and SiC under water lubrication. Tribology letters,2001,11(1):23-28.

[7] H. Tomizawa, T. E. Fischer. Friction and wear of silicon nitride and silicon carbide in water: hydrodynamic lubrication at low sliding speed obtained by tribochemical wear. ASLE Transactions,1987,30(1):41-46.

[8] W. L. Zhang, C. Schröder, B. Schlüter, M. Knoch, J. Dusza, R. Sedlák, R. Mülhaupt, A. Kailer. Effect of mechanochemically functionalized multilayer graphene on the tribological properties of slicon carbide/graphene nanocomposites in aqueous environment. Tribology Letters,2018,66(4),121.

[9] S. K. Sharma, B. V. M. Kumar, Y. W. Kim. Tribological behavior of silicon carbide ceramics - A review. Journal of the Korean Ceramic Society,2016,53(6):581-596.

[10] W. Zhang, S. Yamashita, T. Kumazawa, F. Ozeki, H. Hyuga, H. Kita. Tribological properties of B_4C ceramics prepared by pressureless sintering and annealed at different temperatures. Tribology Transactions,2020,63(4):672-682.

[11] W. Zhang. A review of tribological properties for boron carbide ceramics. Progress in Materials Science,2021,116,100718.

[12] W. Zhang, S. Yamashita, H. Kita. Progress in pressureless sintering of boron carbide ceramics-A review. Advances in Applied Ceramics: Structural, Functional and Bioceramics,2019,118(4):222-239.

[13] X. L. Wang, K. Kato, K. Adachi. The critical condition for the transition from HL to ML in water-lubricated SiC. Tribology Letters,2004,16(4):253-258.

[14] R. S. Gates, S. M. Hsu. Tribochemistry between water and Si_3N_4 and SiC: Induction time analysis. Tribology Letters,2004,17(3):399-407.

[15] G. Vigil, Z. H. Xu, S. Steinberg, J. Israelachvili. Interactions of silica surfaces. Journal of Colloid and Interface Science,1994,165(2):367-385.

[16] M. Matsuda, K. Kato, A. Hashimoto. Friction and wear properties of silicon carbide in water from different sources. Tribology Letters,2011,43(1):33-41.

[17] X. Q. Li, Y. M. Gao, Q. X. Yang, W. Pan, Y. F. Li, Z. C. Zhong, L. C. Song. Evaluation of tribological behavior of B_4C-hBN ceramic composites under water-lubricated condition. Ceramics International,2015,41(6):7387-7393.

[18] X. Q. Li, Y. M. Gao, Q. X. Yang. Sliding tribological performance of B_4C-hBN composite ceramics against AISI 321 steel under distilled water condition. Ceramics International,2017,43(17):14932-14937.

[19] W. Zhang, S. Yamashita, T. Kumazawa, F. Ozeki, H. Hyuga, H. Kita. Effect of nanorelief structure formed in situ on tribological properties of ceramics in dry sliding. Ceramics International,2019,45(11):13818-13824.

[20] W. Zhang, S. Yamashita, H. Kita. Tribological properties of SiC-B_4C ceramics under dry sliding condition. Journal of the European Ceramic Society,2020,40(8):2855-2861.

[21] W. Zhang, S. Yamashita, H. Kita. Effects of load on tribological properties of B_4C and B_4C-SiC ceramics sliding against SiC balls. Journal of Asian Ceramic Societies,2020,8(3):586-596.

[22] W. Zhang, S. Yamashita, T. Kumazawa, F. Ozeki, H. Hyuga, H. Kita. Influence of surface roughness parameters and surface morphology on friction performance of ceramics. Journal of the Ceramic Society of Japan,2019,127(11):837-842.

[23] W. Zhang, S. Yamashita, H. Kita. Effect of counterbody on tribological properties of B_4C-SiC composite ceramics. Wear,2020,458-459:203418.

[24] W. Zhang, S. Yamashita, H. Kita. A study of B_4C-SiC composite for self-lubrication. Journal of the American Ceramic Society. DOI: 10.1111/jace.17584.

[25] S. Kitaoka, Y. Yamaguchi, Y. Takahashi. Tribological characteristics of α-alumina in high-temperature water.

Journal of the American Ceramic Society,1992,75(11):3075-3080.

[26] S. Kitaoka, T. Tsuji, T. Katoh, Y. Yamaguchi, K. Kashiwag. Tribological characteristics of SiC ceramics in high-temperature and high-pressure water. Journal of the American Ceramic Society,1994,77(7):1851-1856.

[27] X. Q. Li, Y. M. Gao, W. Pan, Z. C. Zhong, L. C. Song, W. Chen, Q. X. Yang. Effect of hBN content on the friction and wear characteristics of B_4C-hBN ceramic composites under dry sliding condition. Ceramics International,2015,41(3):3918-3926.

[28] W. F. A. Besling, A. Goossens, B. Meester, J. Schoonman. Laser-induced chemical vapor deposition of nanostructured silicon carbonitride thin films. Journal of Applied Physics,1998,83(1):544-553.

[29] R. S. Gates, S. M. Hsu. Tribochemistry between water and Si_3N_4 and SiC: Induction time analysis. Tribology Letters,2004,17(3):399-407.

[30] M. Yoshimura, J. Kase, S. Sōmiya. Oxidation of SiC powder by high-temperature, high-pressure H_2O. Journal of Materials Research,1986,1(1):100-103.

[31] W. Zhang, S. Yamashita, T. Kumazawa, F. Ozeki, H. Hyuga, W. Norimatsu, H. Kita. A study on formation mechanisms of relief structure formed in situ on the surface of ceramics. Ceramics International,2019,45(17):23143-23148.

Part III

The Influence of Annealing on Tribological Properties of B_4C, SiC, B_4C-SiC Ceramics

Chapter 8
Tribological properties of B_4C ceramics prepared by pressureless sintering and annealed at different temperatures

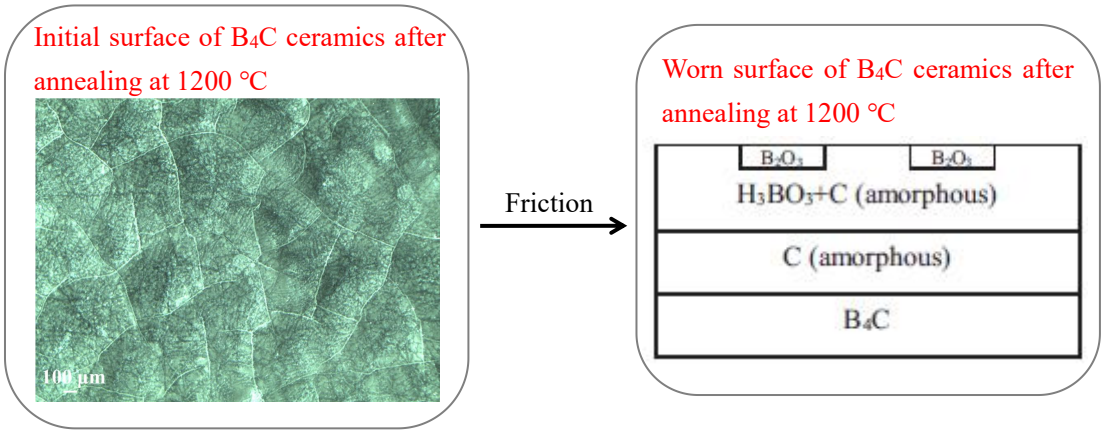

B_4C ceramics were fabricated by pressureless sintering, and the tribological behaviors of B_4C ceramics without and with a postannealing treatment at different temperatures were investigated. It was found that the pores of B_4C ceramics prepared by pressureless sintering might cause large fluctuations in the coefficient of friction but did not increase the coefficient of friction. A B_2O_3 layer was not formed on the B_4C ceramics after annealing at 700 ℃, whereas an H_3BO_3 layer was formed on the B_4C ceramics after annealing at 1000 and 1200 ℃, respectively. B_4C ceramics obtained a favorable self-lubricating property after annealing at 1000 or 1200 ℃ because of the formation of an H_3BO_3 layer during the annealing treatment. B_4C ceramics annealed at 1200 ℃ exhibited the best self-lubricating properties, with the lowest coefficient of friction of approximately 0.08. The friction and wear mechanisms of B_4C ceramics without and with a postannealing treatment are discussed in detail.

Contents

8.1. Introduction

Advanced structural ceramics, such as Al_2O_3 ceramics, ZrO_2 ceramics, Si_3N_4 ceramics, and SiC ceramics, have been widely used for tribo-elements due to their good wear resistance, high hardness, and strength [1-4]. Compared with other ceramics, B_4C ceramics exhibit ultrahigh hardness (the third hardest known material), a high elastic modulus, and low density. Therefore, B_4C ceramics are suitable for use as grinding wheels, die tips, blasting nozzles, polishing media for hard materials, and as a potential material for mechanical seals [5].

However, the poor sinterability of B_4C ceramics due to their high melting point and the strong high covalent bonding of B-C limits their wide application. In order to fabricate B_4C ceramics with high density, many sintering techniques, such as hot isostatic pressing sintering [6, 7], hot pressing sintering [8, 9], pressureless sintering [10-13], spark plasma sintering [14, 15], pulsed electric current sintering [16-18], and plasma pressure compaction sintering [19], have been employed. Although B_4C ceramics with good performance can be obtained using the above-mentioned sintering methods, pressureless sintering is a sintering technology that can realize industrial application of B_4C ceramics because pressureless sintering is suitable to prepare B_4C ceramics with complex shapes and/or large sizes and is a simple and lowcost process. At present, studies focused on the tribological properties of B_4C ceramics are rather limited and mainly focus on B_4C ceramics fabricated by other sintering method. Little research has been done on the friction and wear performance of B_4C ceramics prepared by pressureless sintering.

B_4C ceramics have excellent wear resistance; however, they cannot provide low friction for sliding interfaces. The friction behavior of self-mated B_4C in atmosphere has been investigated by Umeda et al. [20]. The coefficient of friction was 0.95 at a relative humidity of 10%. Li et al. [21] tested the friction behavior of self-mated B_4C at room temperature and achieved a coefficient of friction of 0.59. The coefficient of friction of B_4C ceramics is high, which can cause a lot of energy loss. Therefore, it is necessary to develop B_4C ceramics with a low coefficient of friction. Research in limited studies has mainly focused on improving the tribological performance by adding a secondary phase, such as graphene platelets [22], carbon nanotubes [23], hexagonal boron nitride [24], and silicon carbide [25, 26]. In fact, the self-lubrication of B_4C ceramics can be achieved by annealing treatment. Tests carried out by Erdemir et al. [27] showed that an H_3BO_3 layer can be formed on the oxidized surface of B_4C ceramics prepared by hot pressing via annealing treatment. However, the friction and wear mechanisms of B_4C ceramics annealed at high temperatures have not been explored in detail. Furthermore, no obvious wear of B_4C ceramics annealed at 800 °C was observed after dry sliding tests against a zirconia pin at a load of 5 N and a sliding distance of 250 m. In this investigation, the results, which are different from those of previous research, regarding the wear of B_4C ceramics after annealing are provided. Further, a new structural model of the worn surface composition of B_4C ceramics after annealing, which is different from the models put forward by previous works, is proposed.

In this study, the aims are to investigate the (1) friction and wear properties of B_4C ceramics fabricated by pressureless sintering; (2) self-lubricating mechanism of B_4C ceramics annealed at high temperatures; and (3) failure mechanism of lubricating layer under long sliding distances. This investigation could provide some useful information for the application of B_4C ceramics as mechanical seals to improve conformability of a sliding surface under an initial state of sliding.

8.2. Experimental procedures

High-purity B_4C powder (Fe: 0.02 wt%, Si: 0.08 wt%, Al: <0.01 wt%) was used as the starting material to prepare B_4C ceramics. SiC of 3 wt% and carbon black of 3 wt% were added as sintering additives. B_4C ceramics were fabricated by a pressureless sintering technique. The grain size of B_4C powder is approximately 0.8 μm. The

grain sizes of SiC and carbon black are approximately 0.3 μm and 24 nm, respectively.

The preparation process is described as follows. First, the starting materials were mixed by ball milling for 24 h at a rotational speed of 60 rpm. Then the mixture was die pressed, followed by cold isostatic pressing at 490 MPa to form blocks. The blocks were fired to 2220 ℃ in an argon atmosphere. The heating rate to the sintering temperature was 10 ℃/min and the holding time was 4 h. Then the samples were cooled to room temperature. Postannealing heat treatment of B_4C ceramics was performed at 700, 1000, and 1200 ℃ for 1 h.

The density of the B_4C ceramics sintered by pressureless sintering was tested by the Archimedes method. The hardness and fracture toughness were measured by a Vickers diamond pyramidal indenter, using a normal load of 1 kg and a dwell time of 10 s. The measurements were conducted five times, and the data reported are mean values. The mechanical properties of the B_4C ceramics obtained by pressureless sintering are provided in Table 1.

Table 1 Mechanical properties of the B_4C ceramics obtained by pressureless sintering.

Property	Value
Bulk density (g/cm^3)	2.37
Relative density (%)	93.3
Average hardness (GPa)	27.6
Average fracture toughness (MPa·m$^{1/2}$)	3.7

The friction and wear tests were conducted under dry sliding conditions using a T-18-0162 ball-on-disc tribometer. SiC balls with a radius of 5mm were chosen as the counterpart. The properties of the SiC ball are shown in Table 2. The friction and wear tests were carried out at a load of 5 N and velocity of 0.1 m/s, conditions that are similar to the operating condition of the mechanical seal. The sliding distance was 1,000 m. All tests were carried out at ambient temperature (approximately 23 ℃) in open air at 30% relative humidity.

Table 2 Properties of the SiC ball.

Property	Value
Bulk density (g/cm^3)	3.15
Relative density (%)	98.3
Hardness (GPa)	23.8
Elastic modulus (GPa)	426

Wear volumes (ΔV) of the discs and balls were calculated by means of the following: for the disc, four cross-sectional areas of the wear track, each at 90° with respect to the previous one, were measured using a surface profilometer and then ΔV was calculated according to the average cross-sectional area and the wear track length; for the ball, two perpendicular diameters of the wear scar were measured using a microscope and then ΔV was calculated according to the average diameter and radius of ball. The specific wear rates of the discs and balls were calculated by the wear volume (ΔV) divided by the applied load and sliding distance. Three repeated measurements were performed under the same condition, and the average values were obtained.

Scanning electron microscopy (SEM) and microscopy were used to study the morphologies of the worn surfaces. The phase compositions of the initial surfaces without and with annealing heat treatments and the worn surfaces after sliding were examined by Raman spectroscopy. The spectroscope used a green laser at 532 nm with an output power of 10 mW focused to a spot size of 4 mm.

8.3. Results

Figure 1 shows the Raman spectra of the surfaces of B_4C ceramics without heat treatment and with heat treatment at different temperatures. The Raman peaks at 271, 319, 479, 532, 715, 824, 991, and 1084 cm^{-1}, which appear in the samples without heat treatment and those heat treated at 700 and 1000 ℃, coincide with the Raman shifts of B_4C [28-32]. The Raman peak at 790 cm^{-1} appearing in the sample heat treated at 1000 ℃ and the peak at 971 cm^{-1} appearing in the samples without heat treatment and those heat treated at 700 and 1000 ℃ are in agreement with the Raman shifts of SiC [33]. The Raman peak at 1354 cm^{-1} appearing in the samples without heat treatment and those heat treated at 700, 1000, and 1200 ℃ and the Raman peak at 1581 cm^{-1} appearing in the samples without heat treatment and those heat treated at 700 and 1000 ℃ are in agreement with the Raman shifts of carbon [27]. The Raman peaks at 212, 500, 881, and 1164 cm^{-1} appearing in the samples heat treated at 1000 and 1200 ℃ coincide with the Raman shifts of H_3BO_3 [27, 34]. This indicates the formation of H_3BO_3 on the B_4C ceramics after heat treatment at 1000 and 1200 ℃. Figure 2 shows the optical micrographs of the surfaces of B_4C ceramics heat treated at 1000 and 1200 ℃. It can be seen from Fig. 2a that some substances that appear to be scaly are formed on the B_4C ceramics heat treated at 1000 ℃. Based on the results of the Raman spectra in Fig. 1, it can be proved that this scaly substance is H_3BO_3. However, it appears that an H_3BO_3 layer was not completely formed on the surface of B_4C ceramics after heat treatment at 1000 ℃. In contrast, it can be seen from Fig. 2b that the macroscopic level substance with a scaly form—that is, an H_3BO_3 layer—was completely formed on the whole surface of B_4C ceramics after heat treatment at 1200 ℃.

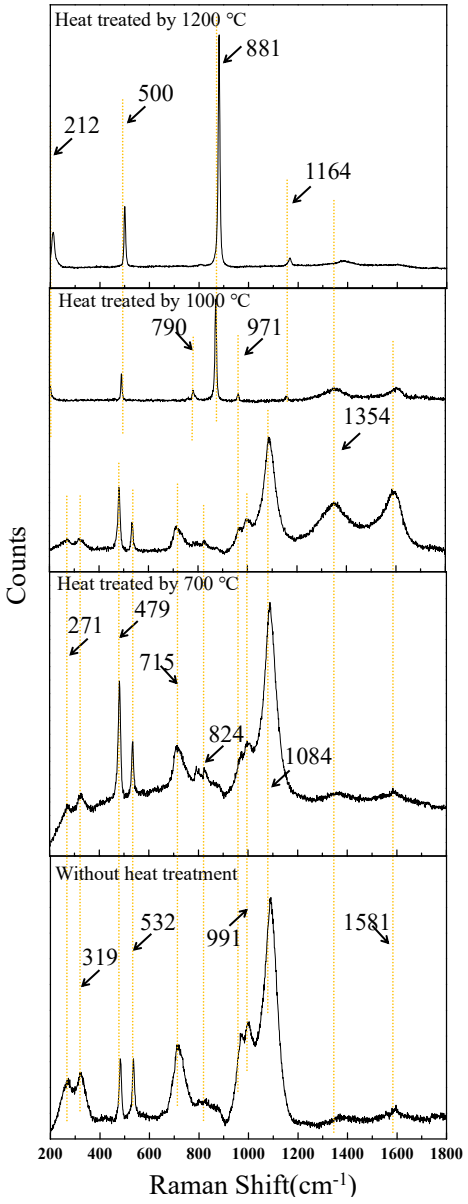

Fig. 1. Raman spectra of the surfaces of B_4C ceramics without heat treatment and heat treatment at 700, 1000, and 1200 °C. Two spectra in one sample indicate that the composition depends on the position of the surface.

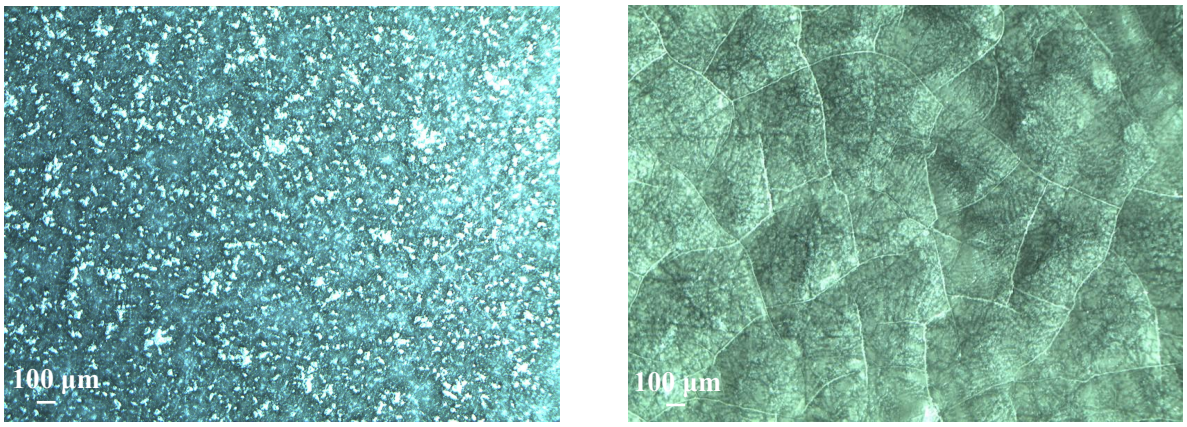

(a) (b)

Fig. 2. Optical micrographs of the surfaces of B_4C ceramics heat treated at (a) 1000 °C and (b) 1200 °C.

Figure 3 shows the variations in the coefficient of friction as a function of sliding distance for samples without heat treatment and those heat treated at different temperatures. It can be seen that the coefficient of friction of the sample without heat treatment is approximately 0.58 during the steady state; with an increase in heat treatment temperature to 700 °C, the coefficient of friction did not change significantly (approximately 0.57); with a further increase in heat treatment temperature to 1000 °C, the sample provides a stable coefficient of friction of approximately 0.2; at a high heat treatment temperature of 1200 °C, the sample displays an excellent self-lubricating performance with a coefficient of friction of around 0.08. As a whole, the coefficient of friction of B_4C ceramics can be significantly decreased when the heat treatment temperature is higher than 1000 °C. The coefficient of friction of the sample heat treated at 1200 °C is the lowest.

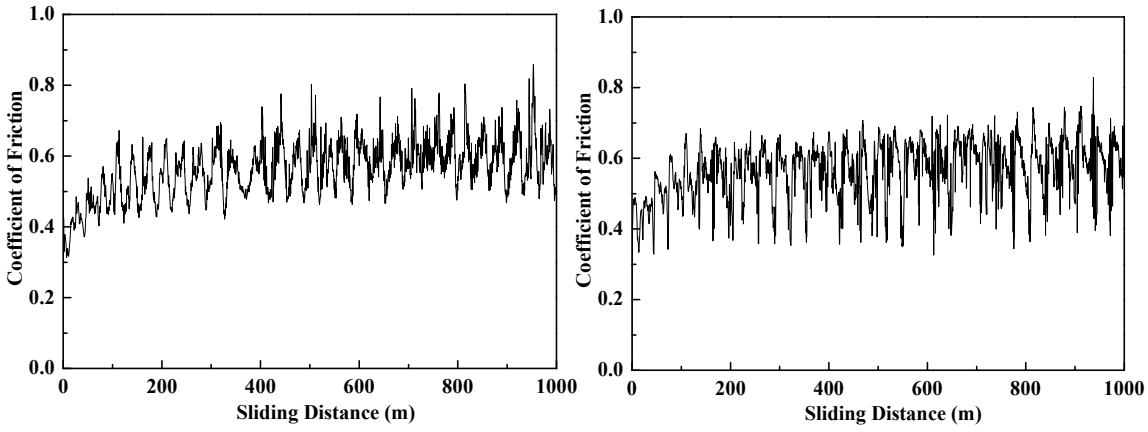

(a) (b)

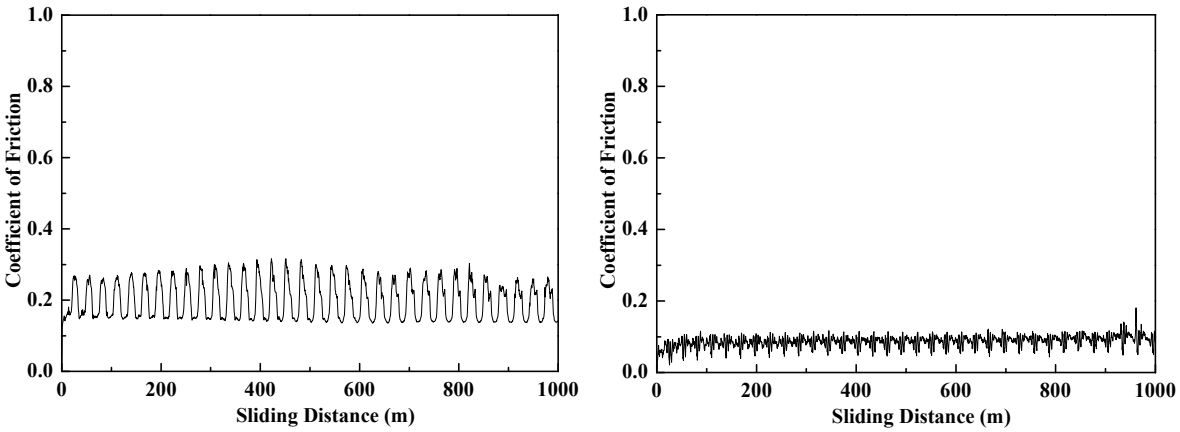

Fig. 3. Variations in the coefficient of friction as a function of sliding distance for samples (a) without heat treatment; (b) heat treated at 700 ℃; (c) heat treated at 1000 ℃; and (d) heat treated at 1200 ℃.

Table 3 shows the specific wear rates of both B_4C discs without heat treatment and those heat treated at different temperatures and SiC balls mated to the corresponding B_4C discs. For the discs, the wear rates of the sample without heat treatment and the sample heat treated at 700 ℃ are of the same order of magnitude, and the wear rates of the sample heat treated at 1000 ℃ and the sample heat treated at 1200 ℃ are of the same order of magnitude. The wear rate of the B_4C disc increases with an increase in heat treatment temperature, and the wear rate drastically increases when the heat treatment temperature is higher than 1000 ℃. For the balls, the wear rate trend is different from that of the discs. The wear rate of the ball sliding against the disc heat treated at 700 ℃ is one order of magnitude higher than that of the ball sliding against the disc without heat treatment. However, the wear rate of the balls gradually decreases when the heat treatment temperatures of discs are higher than 1000 ℃. Furthermore, it can be observed that the wear rates of the discs are lower than those of the mated balls when the disc did not undergo post heat treatment and the disc was heat treated at 700 ℃. The opposite is noticed when the discs were heat treated at temperatures higher than 1000 ℃.

Table 3 Specific wear rates of the discs and balls mated to the corresponding B_4C discs.

	Heat treatment temperatures of B_4C ceramics (℃)	Wear rate ($mm^3/N·m$)
B_4C disc	Without	2.31×10^{-7}
	700	4.31×10^{-7}
	1000	1.48×10^{-5}
	1200	3.05×10^{-5}
SiC ball	Without	4.17×10^{-7}
	700	2.23×10^{-6}
	1000	2.98×10^{-7}
	1200	Without obvious wear

For B_4C discs, the wear rate of the sample without heat treatment is 2.31×10^{-7} $mm^3/N·m$, and it increases to 4.31×10^{-7} $mm^3/N·m$ after heat treated at 700 ℃. The wear rate dramatically increases to 1.48×10^{-5} mm3/N·m and 3.05×10^{-5} mm3/N·m when the annealing temperature is 1000 and 1200 ℃, respectively. The wear rate of the sample without heat treatment is the lowest; however, the wear rate rises to the highest value when the heat treatment temperature rises to 1200 ℃. For the SiC balls, the wear rate of the ball sliding against the disc without heat treatment is 4.17×10^{-7} mm3/N·m, and it increases to 2.23×10^{-6} mm3/ N·m when the ball slides against the disc heat treated at 700 ℃ and then drops to 2.98×10^{-7} mm3/N·m when the ball slides against the disc heat treated

at 1000 ℃. No obvious wear is observed on the SiC ball when the ball slides against the disc heat treated at 1200 ℃.

As a whole, the B_4C ceramic heat treated at 1200 ℃ exhibits the lowest coefficient of friction of 0.08 but the highest wear rate of 3.05×10^{-5} mm3/N·m. The B_4C ceramics can display a self-lubricating performance when the ceramic is heat treated at temperatures higher than 1000 ℃.

Figure 4 shows the optical micrographs of the wear tracks of B_4C ceramics without heat treatment and those heat treated at 700, 1000, and 1200 ℃. Figure 5 shows the SEM images of the worn surfaces of B_4C ceramics without heat treatment and those heat treated at 700 and 1000 ℃ and the elemental distributions on the worn surface of B_4C ceramic heat treated at 1000 ℃. It can be seen from Figs. 4a and 4b that the worn surfaces of B_4C ceramics without heat treatment and those heat treated at 700 ℃ show similar characteristic. Typical plough zones can be seen on the worn surfaces for both samples. However, the width of the wear track of B_4C ceramic heat treated at 700 ℃ is larger than that of B_4C ceramic without heat treatment. Further observations exhibit the difference between the worn surface of B_4C ceramic without heat treatment and the worn surface of B_4C ceramic heat treated at 700 ℃ (Figs. 5a and 5b). As seen in Fig. 5a, the worn surface of B_4C ceramic without heat treatment is smoother, and little brittle fracture is observed. However, for the sample heat treated at 700 ℃ (Fig. 5b), a debris layer covers the worn surface, and large holes are observed. As seen in Fig. 4c, a scaly substance can be observed on the surface. Further, it can be observed clearly at the macroscopic level from Fig. 4d that the scaly substance still exists on the worn surface after sliding. The SEM image and elemental distribution of B_4C ceramic heat treated at 1000 ℃ in Figs. 5c-5f indicate that the worn surface is composed of a mixture of an O-rich phase and a C-rich phase, and a B phase uniformly disperses on the worn surface.

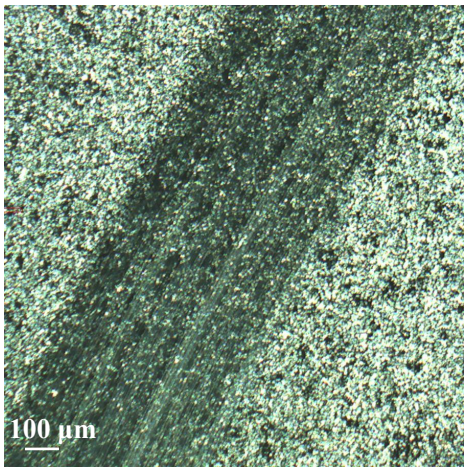

(a)

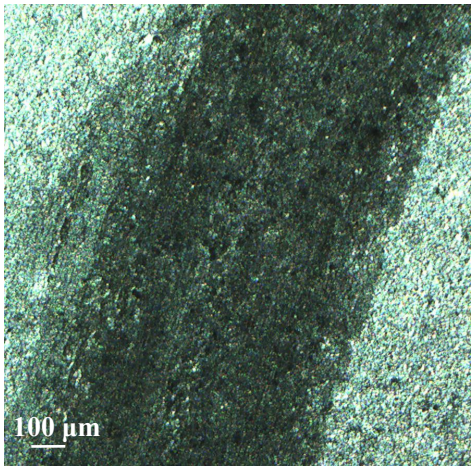

(b)

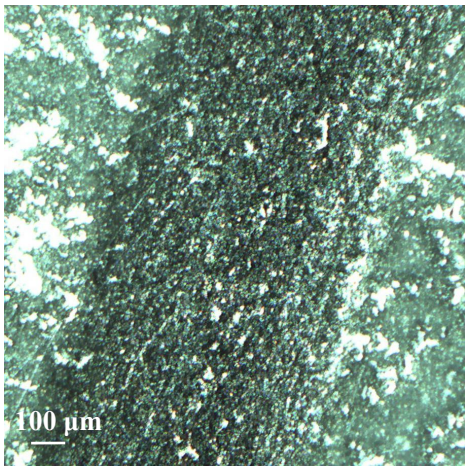

(c)

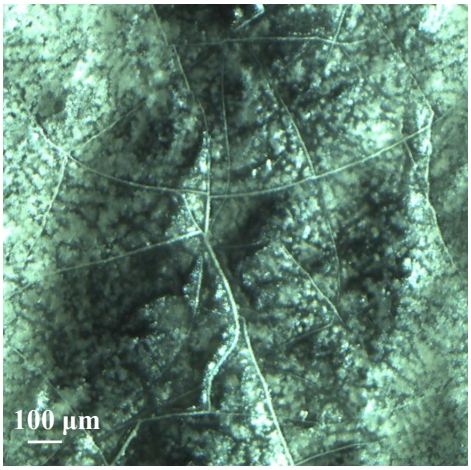

(d)

Fig. 4. Metallograhps showing the wear tracks of (a) B_4C disc without heat treatment; (b) B_4C disc heat treated at 700 °C; (c) B_4C disc heat treated at 1000 °C; and (d) B_4C disc heat treated at 1200 °C.

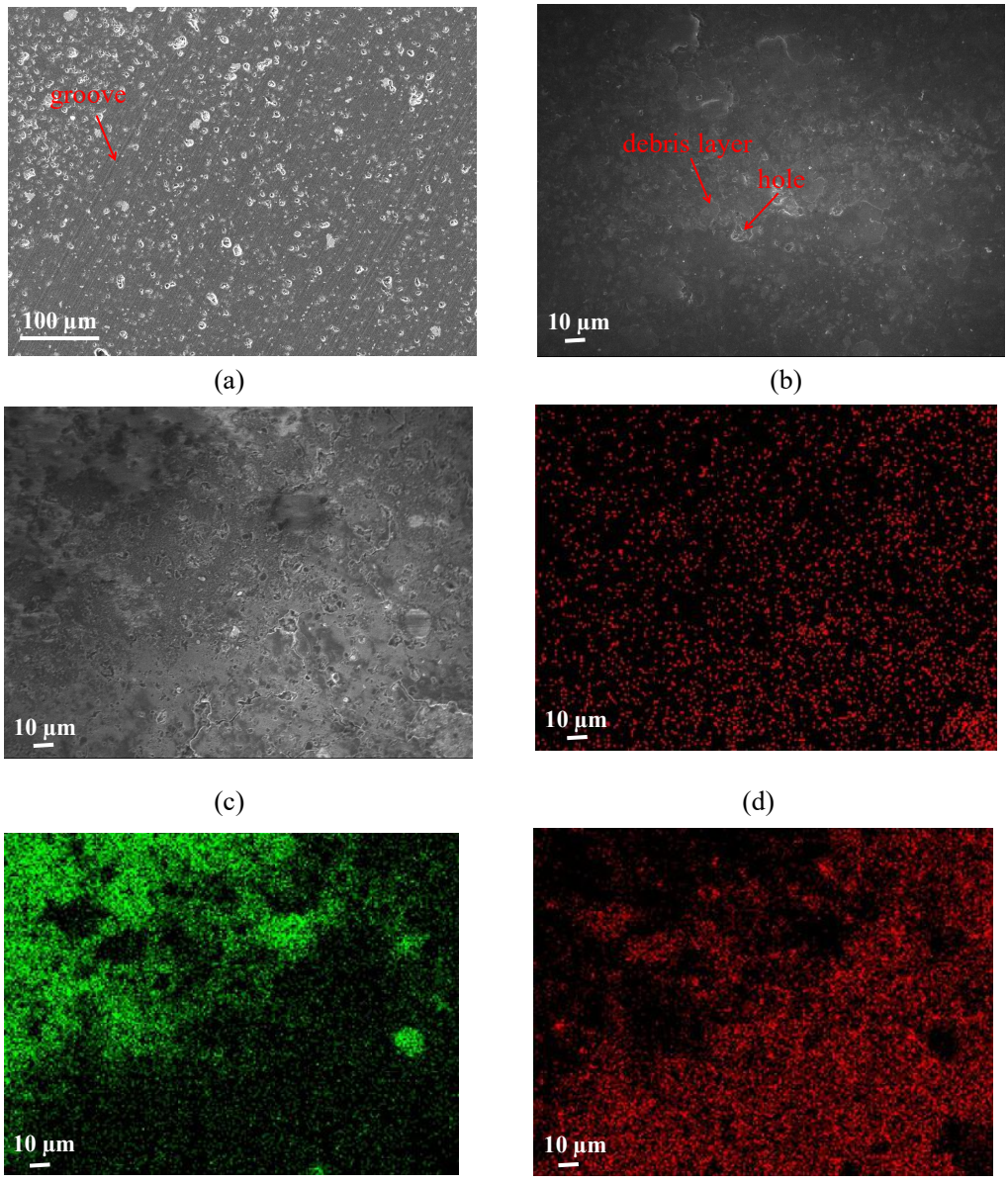

Fig. 5. SEM images of worn surface of (a) B_4C disc without heat treatment; (b) B_4C disc heat treated at 700 °C; and (c) B_4C disc heat treated at 1000 °C and elemental distribution of (c): (d) B; (e) O; and (f) C.

The worn surfaces of the SiC balls sliding against B_4C discs without heat treatment and those heat treated at 700 and 1000 °C are shown in Fig. 6. All balls exhibit abraded grooves. It can be observed that the SiC ball sliding against the B_4C disc heat treated at 700 °C has the maximum wear diameter, which is in agreement with its maximum wear rate, shown in Table 3.

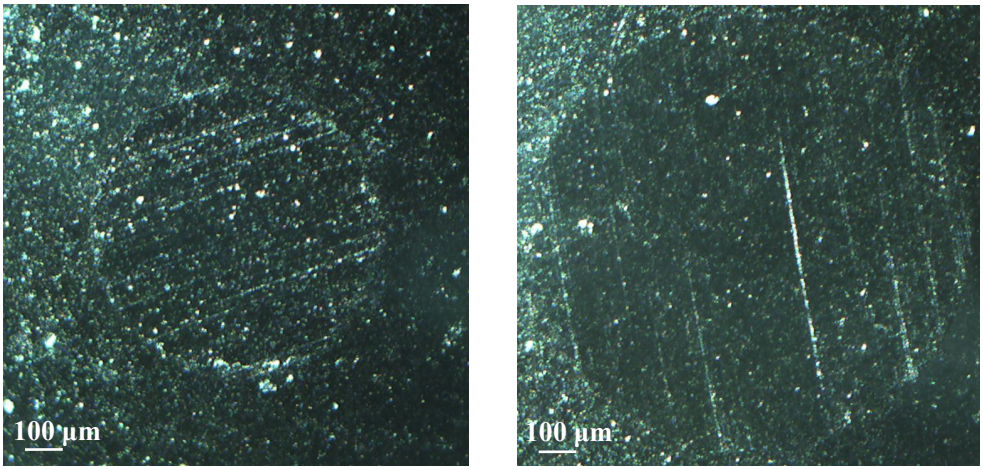

(a) (b)

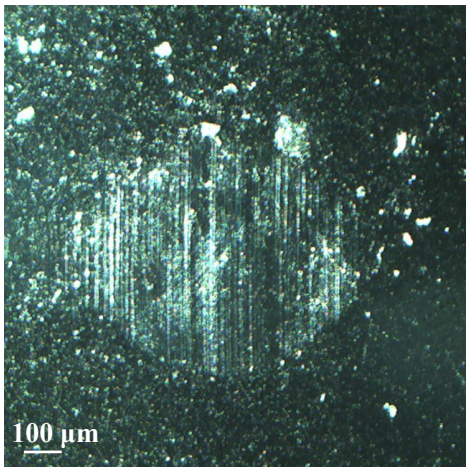

(c)

Fig. 6. Metallograhps showing the wear scars of the SiC balls sliding against B_4C discs: (a) without heat treatment, (b) heat treated at 700 ℃; and (c) heat treated at 1000 ℃.

The Raman spectra of the worn surfaces of B_4C ceramics without heat treatment and with heat treatment at different temperatures are shown in Fig. 7. Compared with the Raman spectra of the initial surfaces of B_4C ceramics without heat treatment and with heat treatment at different temperatures shown in Fig. 1, there is no appreciable difference between the worn surfaces and initial surfaces for the B_4C ceramics without heat treatment and those heat treated at 700 and 1000 ℃. Combined with the result of the elemental distribution analysis of the worn surface of B_4C ceramics heat treated at 1000 ℃ shown in Figs. 5d-5f, it can be demonstrated that the O-rich phase is H_3BO_3 and the C-rich phase is B_4C. The two Raman spectra observed in the B_4C ceramic heat treated at 1000 ℃ are in agreement with the observation by SEM. This means that a B_4C phase and H_3BO_3 phase coexist on the worn interface, the compositions of which are the same as those of the initial surface of the B_4C ceramic after heat treatment at 1000 ℃. However, for the B_4C ceramic heat treated at 1200 ℃, an interesting observation was noted. The Raman peak at 806 cm^{-1} representing B_2O_3 [35] can be observed. Further, Raman peaks at 1350 and 1594 cm^{-1} representing carbon appear.

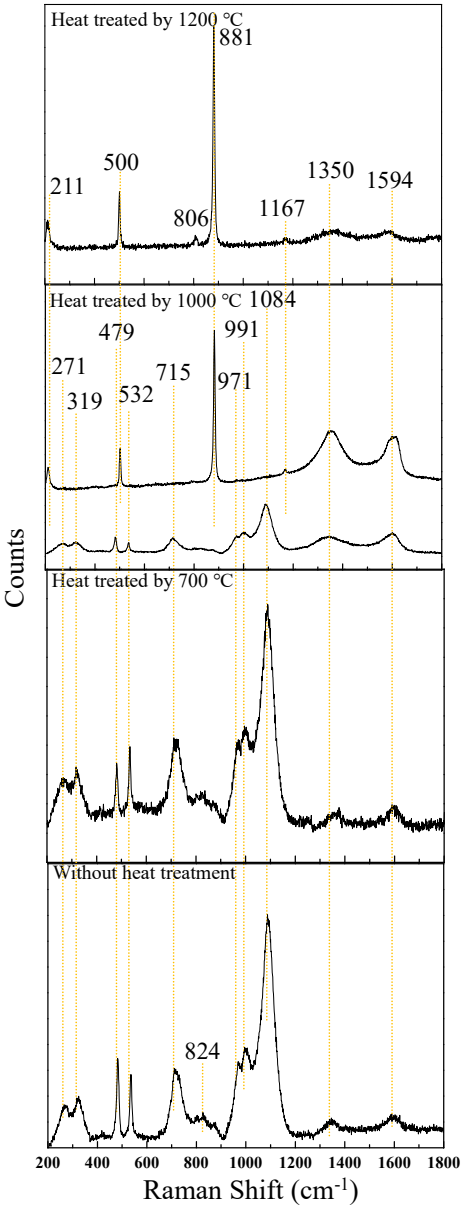

Fig. 7. Raman spectra of the worn surfaces of B_4C ceramics without heat treatment and those heat treated at 700, 1000, and 1200 °C. Two spectra in one sample indicate that the composition depends on position of the surface.

8.4. Discussion

For the B_4C ceramics without post heat treatment, large fluctuations in the coefficient of friction were observed at the steady state. This phenomenon has also been observed for the B_4C ceramics prepared by hot press sintering [36] and plasma pressure compaction sintering [19]. It was reported that the layers of compounds (H_3BO_3, B_2O_3, and B_2O) can be formed on the worn surface by tribochemical reactions during sliding [36, 37]. The formation and subsequent breaking of these layers on the worn surface cause large fluctuations in the coefficient of friction. However, these layers of oxides were not be found on the worn surface after sliding under the selected test conditions as shown in Figs. 5a and 7. In fact, there is no obvious difference between the Raman spectra of the initial surface and the worn surface. The large fluctuations in this experiment may be correlated with greater pore formation during the pressureless sintering process (Fig. 5a). In addition, the commonly reported coefficient of friction for B_4C ceramics prepared by hot press sintering varies from 0.4 to 0.8, based on the experimental and material parameters [22, 38, 39]. The relative density of the B_4C ceramics (93.3%) prepared in this experiment is

lower than that of B_4C ceramics fabricated by hot pressed sintering (>99.0%) [38], and more pores exist in B_4C ceramics fabricated by pressureless sintering; however, the pores are small and uniformly distributed. These pores, therefore, might only cause large fluctuations in the coefficient of friction but do not increase the coefficient of friction during the steady state. Because obvious cutting traces can be observed on the worn surface of B_4C ceramics, microcutting controlled wear is considered as the main wear mechanism.

For the B_4C ceramics heat treated at 700 °C, the coefficient of friction is ≈0.57, a value similar to that of B_4C ceramics without heat treatment. B_4C is stable only up to 600 °C, as reported in previous literature [40]. Erdemir et al. [41] also pointed out that a super-slippery H_3BO_3 film can form on a B_4C substrate after heating the B_4C above 600 °C in open air. However, boron oxides were not be detected after heat treatment at 700 °C (Fig. 1) in this experiment. This is probably explained by the addition of SiC. No significant reduction in the coefficient of friction for B_4C ceramics can be attributed to the absence of the formation of an oxide layer. Further, the wear of B_4C ceramics proceeds mainly by mechanical damage, and the observed severity of damage is consistent with the wear measurement.

For the B_4C ceramics heat treated at 1000 °C, the coefficient of friction is much lower than that of B_4C ceramics without heat treatment and that heat treated at 700 °C but still shows certain fluctuations. From Figs. 1 and 2a, it can be seen that an H_3BO_3 layer formed on the surface of B_4C ceramics after heat treatment. However, the H_3BO_3 layer is not completely formed on the surface of B_4C ceramics and a B_4C phase still can be detected, which may be attributed to the insufficient heat treatment temperature. Moreover, a trace of carbon was observed on the initial surface after heat treatment, which may come from the residual carbon after the oxidation of B atoms in B_4C. It is well known that H_3BO_3 is a kind of crystal with a layered structure, and the atomic layers are 0.318 nm apart. The atomic layers are held together only by the weak van der Waal forces, resulting in easy shearing. The reduced coefficient of friction is expected to be due to the lubrication effect of H_3BO_3. Although H_3BO_3 with layered structure is easily sheared and can provide a low coefficient of friction for B_4C ceramics, it can be observed from Table 3 that the wear rate of B_4C ceramics drastically increases when the annealing temperature is up to 1000 °C, which is ascribed to the formation of an H_3BO_3 layer. It is considered that H_3BO_3 is easily worn off due to its layered structure with a weak bonding force, causing greater wear for B_4C ceramics after heat treatment at 1000 °C. It was reported by Erdemir et al. [27] that the wear of B_4C ceramics with an H_3BO_3 film heat treated at 800 °C for 1 h was so low that it was difficult to measure after dry sliding tests against a ZrO_2 pin at at load of 5 N and sliding distance of 250 m. In contrast, it is observed that the wear of B_4C ceramics is significantly increased when an H_3BO_3 layer forms on the surface of B_4C ceramics under the selected test conditions in this study.

For the B_4C ceramics heat treated at 1200 °C, the coefficient of friction is ≈0.08. One of the most prominent features is that the coefficient of friction becomes relative smooth, and no significant fluctuations are observed. As shown in Figs. 1 and 2b, the surface layer is nearly totally composed of H_3BO_3. Further, a scaly H_3BO_3 layer still exists on the worn surface after sliding, as shown in Fig. 4d, which can also be demonstrated by Fig. 7. The reduced coefficient of friction and no large fluctuations can be attributed to the complete formation of an H_3BO_3 layer on the whole B_4C ceramic surface at a heat treatment temperature of 1200 °C as well as to the fact that H_3BO_3 layer is not worn out during wear. In addition, it can be observed from Fig. 7 that B_2O_3 appears on the worn surface. The formation of B_2O3 may be expressed by the following reactions:

$$2H_3BO_3 = B_2O_3 + 3H_2O(g) \quad (1)$$

$$2H_3BO_3 = B_2O_3 + 3H_2O(1). \quad (2)$$

The temperature dependence of the Gibbs free energies of reactions (1) and (2) calculated using the software MALT is shown in Fig. 8. It can be noted that both reactions (1) and (2) cannot proceed spontaneously at room temperature because the Gibbs free energies are greater than 0. However, the reactions can be accelerated due to the friction heat during sliding. Reaction (1) for the production of gaseous water (vapor) is more stable than reaction (2). Therefore, B_2O_3 may be produced by reaction (1). In addition, H_3BO_3 is easily worn off due to the

layered structure with a weak bonding force; thus, a further increased wear rate is attributed to dual effects of mechanical wear and tribochemical wear. Moreover, Raman peaks of carbon are observed. It was reported by Narushima et al. [31] that C was enriched in the borosilicate layer near the oxide/B_4C-(25-60 mol%)SiC composite interface after oxidation at 800-1500 ℃. Combined with the result in Fig. 1, a trace of carbon is also observed on the surface of B4C ceramics heat treated at 1200 ℃. Therefore, it is considered that the carbon content gradually increases with an increase in oxide layer depth, and carbon is enriched in the H_3BO_3 layer near the oxide layer/B_4C substrate interface. Gogotsi et al. [42] reported that a graphite layer was formed under the B_2O_3 layer after annealing at 1200 ℃ for B_4C ceramics. B_2O_3 as well as graphite with low-energy shear planes provided low friction for B_4C ceramics after annealing. Erdemir et al. [27] stated that an H_3BO_3 layer was formed above the B_2O_3 layer after annealing at 800 ℃ for B_4C ceramics, and this H_3BO_3 layer was responsible for the reduction in the coefficient of friction of B_4C ceramics. Further, graphite formed after annealing was considered to have a beneficial synergistic effect on friction. However, in this study, a graphite phase was not detected, and carbon detected by Raman spectroscopy (Fig.7) only represents amorphous carbon. The structural schematics of worn surfaces of B_4C ceramics after annealing proposed by Gogotsi et al. [42] and Erdemir et al. [27] are shown in Figs. 9a and 9b, respectively. In this study, we propose a new structural model of the worn surface composition of B_4C ceramics after annealing at 1200 ℃, as shown in Fig. 9c, which is different from those proposed by Gogotsi et al. [42] and Erdemir et al. [27].

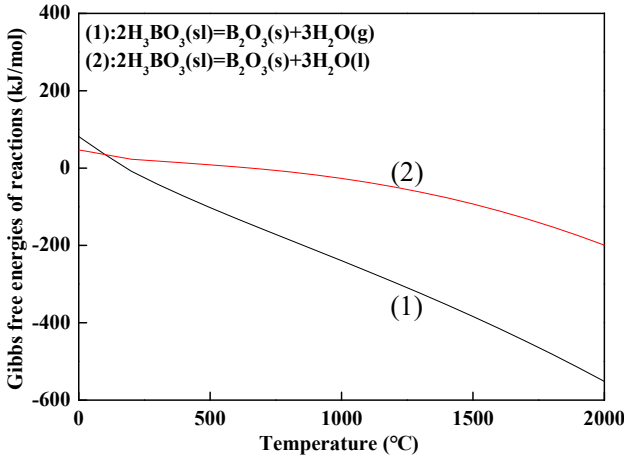

Fig. 8. Gibbs free energies for reactions (1) and (2) as a function of temperature.

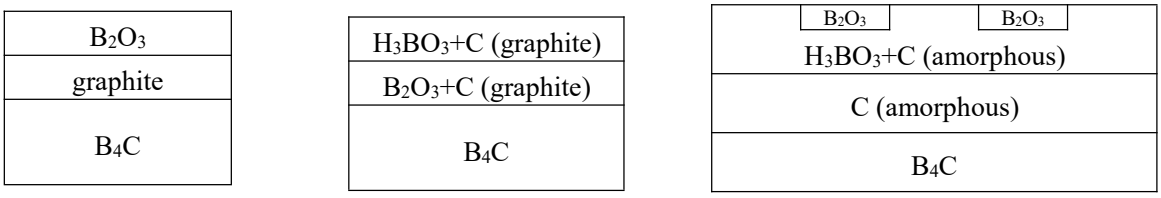

(a) (b) (c)

Fig. 9. Structural schematics of the worn surfaces of B_4C ceramics after annealing proposed in (a) Gogotsi et al. [42], (b) Erdemir et al. [27], and (c) this study.

8.5. Conclusions

In this study, the tribological behaviors of B_4C ceramics fabricated by pressureless sintering and B_4C ceramics heat treated at 700, 1000, and 1200 ℃ were investigated. The following conclusions are made:

(1) The pores of B_4C ceramics prepared by pressureless sintering might cause large fluctuations in the coefficient of friction but did not increase the coefficient of friction.
(2) A B_2O_3 layer was not detected on the B4C ceramics after annealing at 700 ℃, whereas an H_3BO_3 layer was formed on the B_4C ceramics after annealing at 1000 and 1200 ℃ due to oxidation reactions.
(3) B_4C ceramics obtained a favorable self-lubricating property after annealing at 1000 or 1200 ℃ because of the formation of an H_3BO_3 layer during the annealing treatment. B_4C ceramics heat treated at 1200 ℃ exhibited the best self-lubricating property, with the lowest coefficient of friction of approximately 0.08. However, the wear rate of B_4C ceramics increased with an increase in annealing temperature.
(4) The wear mechanisms of B_4C ceramics with an H_3BO_3 layer included dual effects of mechanical wear and tribochemical wear.

8.6. References

[1] L. Q. Kong, Q. L. Bi, S. Y. Zhu, J. Yang, W. M. Liu. Tribological properties of $ZrO_2(Y_2O_3)$-Mo-BaF_2/CaF_2 composites at high temperatures. Tribology International,2012,45(1):43-49.

[2] W. Zhang, Y. L. Han. Progress of investigation on thermal shock resistance of Al_2O_3-based ceramics. Journal of ceramics,2008,29(2):193-198.

[3] M. Maros B., A. K.Németh, Z. Károly, E. Bódis, Z. Maros, O. Tapasztó, K. Balázsi. Tribological characterisation of silicon nitride/multilayer graphene nanocomposites produced by HIP and SPS technology. Tribology International,2016,93:269-281.

[4] S. K. Sharma, B. V. M. Kumar, Y. W. Kim. Effect of WC addition on sliding wear behavior of SiC ceramics. Ceramics International,2015,41(3):3427-3437.

[5] W. Zhang, S. Yamashita, H. Kita. Progress in pressureless sintering of boron carbide ceramics- a review. Advances in Applied Ceramics,2019,118(4):222-239.

[6] K.A.Schwetz, L.S.Sigl, L.Pfau. Mechanical properties of injection molded B_4C-C ceramics. Journal of Solid State Chemistry,1997,133:68-76.

[7] L.S.Sigl.Processing and mechanical properties of boron carbide sintered with TiC.Journal of the European Ceramic Society,1998,18(11):1521-1529.

[8] K.Sairam, J.K.Sonber, T.S.R.Ch.Murthy, C.Subramanian, R.C.Hubli, A.K.Suri. Development of B_4C-HfB_2 composites by reaction hot pressing.International Journal of Refractory Metals and Hard Materials,2012,35 (1):32-40.

[9] X. R. Zhang, Z. X. Zhang, W. M. Wang, J. H. Shan, H. W. Che, J. B. Mu, G. S. Wang. Microstructure and mechanical properties of B_4C-TiB_2-SiC composites toughened by composite structural toughening phases. Journal of the American Ceramic Society,2017,100(7):3099-3107.

[10] Y. Y. Li, H. Liu, T. Y. Li, J. Yang, X. Q. Pan, Y. Zhang. Study on pressless sintering of B_4C pellets used in nuclear reactors. Powder Metallurgy Technology,2017,35(1):53-56.

[11] D. Z. Gao, J. Jing, J. C. Yu, X. Guo, Y. B. Zhang, H. Y. Gong, Y. J. Zhang. Graphene platelets enhanced pressureless-sintered B_4C ceramics. Royal Society Open Science,2018,5(4):1-7.

[12] X. G. Li, D. L. Jiang, J. X. Zhang, Q. L. Lin, Z. M. Chen, Z. R. Huang. Pressureless sintering of boron carbide with Cr_3C_2 as sintering additive. Journal of the European Ceramic Society,2014,34(5):1073-1081.

[13] L. Ma, J. C. Yu, X. Guo, Y. J. Zhang, H. Y. Gong. Pressureless densification and properties of TiB_2-B_4C composite ceramics with Ni as additives. Micro ＆ Nano Letters,2018,13(7):1-4.

[14] D. Pan, S. F. Li, X. Zhang, B. Pan, S. Y. Zhou, Y. B. Fu. Effect of graphite content on properties of B_4C-W_2B_5 ceramic composites by in situ reaction of B-Gr-WC. Journal of the American Ceramic Society,2018,101:3617-3626.

[15] S. Eqtesadi, A. Motealleh, F. H. Perera, P. Miranda, A. Pajares, R. Wendelbo, F. Guiberteau, A. L. Ortiz. Fabricating geometrically-complex B_4C ceramic components by robocasting and pressureless spark plasma sintering.Scripta Materialia,2018,145:14-18.

[16] Z. Liu, D. Wang, J. Li, Q. Huang, S. Ran. Densification of high-strength B_4C-TiB_2 composites fabricated by pulsed electric current sintering of TiC-B mixture.Scripta Materialia,2017,135:15-18.

[17] D. L. Ren, Q. H. Deng, J. Wang, J. S. Yang, Y. B. Li, J. Q. Shao, M. Li, J. Zhou, S. L. Ran, S. Y. Du, Q. Huang. Synthesis and properties of conductive B_4C Ceramic composites with TiB_2 grain network.Journal of the American Ceramic Society,2018,101:1-7.

[18] D. L. Ren, Q. H. Deng, J. Wang, Y. B. Li, M. Li, S. L. Ran, S. Y. Du, Q. Huang. Densification and mechanical properties of pulsed electric current sintered B_4C with in situ synthesized Al_3BC obtained by the molten-salt method. Journal of the European Ceramic Society,2017,37(15):1-8.

[19] F. Rubino, M. Pisaturo, A. Senatore, P. Carlone, T. S. Sudarshan. Tribological characterization of SiC and B_4C manufactured by plasma pressure compaction. Journal of Materials Engineering & Performance,2017,26(7):1-12.

[20] K. Umeda, Y. Enomoto, A. Mitsui, K. Mannami. Friction and wear of boride ceramics in air and water. Wear,1993,169(1):63-68.

[21] X. Q. Li, Y. M. Gao, W. Pan, Z. C. Zhong, L. C. Song, W. Chen, Q. X. Yang. Effect of hBN content on the friction and wear characteristics of B_4C-hBN ceramic composites under dry sliding condition. Ceramics International,2015,41(3):3918-3926.

[22] R. Sedlák, A. Kovalčíková, J. Balko, P. Rutkowski, A. Dubiel. D. Zientara, V. Girman, E. Múdra, J. Dusza. Effect of graphene platelets on tribological properties of boron carbide ceramic composites. International Journal of Refractory Metals & Hard Materials,2017,65:57-63.

[23] R. Alexander, K.V. Ravikanth, R. D. Bedse, T. S. R. Ch. Murthy, K. Dasgupta. Effect of carbon fiber on the tribo-mechanical properties of boron carbide: Comparison with carbon nanotube reinforcement. International Journal of Refractory Metals & Hard Materials,2019,85:105055.

[24] X. Q. Li, Y. M. Gao, S. Z. Wei, Q. X. Yang, Z. C. Zhong. Dry sliding tribological properties of self-mated couples of B_4C-hBN ceramic composites. Ceramics International,2017,43:162-166.

[25] W. Zhang, S. Yamashita, T. Kumazawa, F. Ozeki, H. Hyuga, H. Kita. Effect of nanorelief structure formed in situ on tribological properties of ceramics in dry sliding. Ceramics International,2019,45(11):13818-13824.

[26] W. Zhang, S. Yamashita, T. Kumazawa, F. Ozeki, H. Hyuga, H. Kita. Influence of surface roughness parameters and surface morphology on friction performance of ceramics. Journal of the Ceramic Society of Japan,2019,127(11):837-842.

[27] A. Erdemir, C. Bindal, C. Zuiker, E. Savrun. Tribology of naturally occurring boric acid films on boron carbide. Surface and Coatings Technology,1996,86-87(2):507-510.

[28] D. R. Tallant, T. L. Aselage, A. N. Campbell, D. Emin. Boron carbide structure by Raman spectroscopy. Physical Review B Condensed Matter,1989,40(8):5649-5656.

[29] U. Kuhlmann, H. Werheit. Improved Raman effect studies on boron carbide($B_{4.3}C$). Physica Status Solidi(B),1993,175:85-92.

[30] C. Kunka, A. Awasthi, G. Subhash. Evaluating boron-carbide constituents with simulated Raman spectra. Scripta Materialia,2017,138:32-34.

[31] T. Narushima, T. Goto, M. Maruyama, H. Arashi, Y. Iguchi. Oxidation of boron carbide-silicon carbide composite at 1073 to 1773K. Materials Transactions,2003,44(3):401-406.

[32] X. Q. Yan, W. J. Li, T. Goto, M. W. Chen. Raman spectroscopy of pressure-induced amorphous boron carbide. Applied Physics Letters,2006,88:131905.

[33] S. Nakashima, H. Harima. Raman investigation of SiC polytypes. Physica Status Solidi A,1997,162(1):39-64.

[34] K. Krishnan. The Raman spectrum of boric acid. Proceedings of the Indian Academy of Sciences-Section A,1963,57(2):103-108.

[35] F. L. Galeener, A. E. Geissberger. Raman studies of B_2O_3 glass structure:$^{10}B \rightarrow ^{11}B$ isotopic substitution. Journal de Physique Colloques,1982,43(C9):343-346.

[36] F. Wu, L. S. Wang, J. S. Zhang, Y. Fan, B. W. Liu, Y. Gao. Tribological properties of hot-pressed boron carbide ceramic. Transactions of Nonferrous Metals Society of China,2001,11(1):119-122.

[37] P. Larsson, N. Axén, S. Hogmark. Tribofilm formation on boron carbide in sliding wear. Wear,1999,236(1-2):73-80.

[38] X. Q. Li, Y. M. Gao, W. Pan, X. Wang, L. C. Song, Z. C. Zhong, S. S. Wu. Fabrication and characterization of B_4C-based ceramic composites with different mass fractions of hexagonal boron nitride. Ceramics International,2015,41(1):27-36.

[39] X. Q. Li, Y. M. Gao, L. C. Song, Q. X. Yang, S. Z. Wei, L. You, Y. C. Zhou, G. S. Zhang, L. J. Xu, B. Yang. Influences of hBN content and test mode on dry sliding tribological characteristics of B_4C-hBN ceramics against bearing steel. Ceramics International,2018:44:6443-6450.

[40] D. H. Riu, R. Choi, H. E. Kim, E. S. Kang. Oxidation behaviour and strength of B_4C-30 wt% SiC composite materials. Journal of Materials Science,1995,30(15):3897-3902.

[41] A. Erdemir, C. Bindal, G. R. Fenske. Formation of ultralow friction surface films on boron carbide. Applied Physics Letters,1996,68(12):1637-1639.

[42] Y. G. Gogotsi, A. M. Koval'chenko, I. A. Kossko. Tribochemical interactions of boron carbides against steel. Wear,1992,154(1):133-140.

Chapter 9
Self lubrication of pressureless sintered SiC ceramics

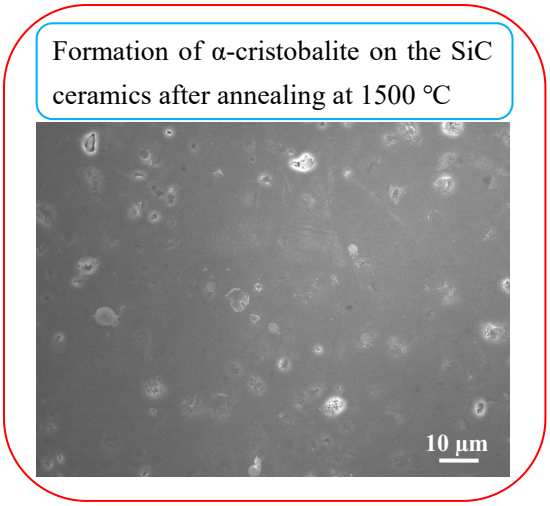

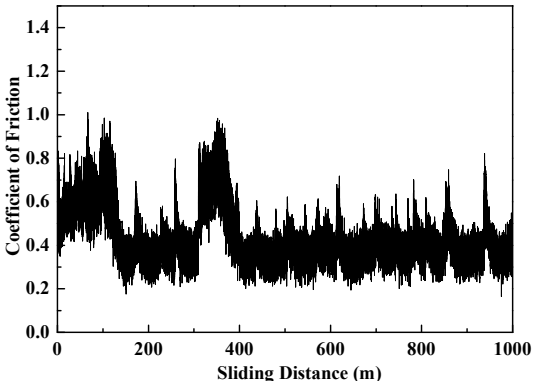

The self lubrication of SiC ceramics prepared by pressureless sintering was investigated by annealing at different temperatures in air. It was found that low coefficient of friction can be obtained for SiC ceramics by annealing, and the coefficient of friction of SiC ceramics decreased with the increase of annealing temperature. The SiC ceramics with annealing at 1500 ℃ revealed the best self lubricating property, with the coefficient of friction of 0.4, while the coefficient of friction of SiC ceramics without annealing was as high as 0.7. The SiC ceramics with annealing at 1000 ℃ can show self lubrication over a long sliding distance without increasing wear. The formation of α-cristobalite on the annealed SiC ceramics can further lubricate SiC ceramics and shorten run in period. Self lubrication mechanism of SiC ceramics with annealing is considered that on the one hand, the formation of silicon oxide layers after annealing can reduce the number of SiC grains directly exposed to the sliding interface in the early stage of the sliding, decreasing the number of hard SiC wear particles formed on the sliding interface; and on the other hand, silicon oxide wear particles generated by the wear of the silicon oxide layers formed by annealing can be used as solid lubricant.

Contents

9.1. Introduction

SiC ceramics with high hardness (24 GPa), low density (3.2 g/cm^3), high thermal conductivity (100 W·(m·K)$^{-1}$) and good thermal stability at elevated temperatures are widely applied in engineering field [1-5]. In particular, SiC ceramics are considered as potential candidates for tribological applications, such as high-speed cutting tools, bearings, nozzles, mechanical seals, etc. [6-8].

Many scholars have done a lot of research on the frictional properties of SiC ceramics. Kumar et al. [9] reported that the coefficient of friction of SiC/SiC pair was 0.59 at the load of 1 N, and the coefficient of friction decreased to 0.23 as the load increased to 13 N. The primary cause for the reduced coefficient of friction was the formation of thick tribo-layers and needle-like debris that can roll during sliding. Andersson and Blomberg [10] pointed out the coefficient of friction of self-mated SiC could increase from 0.5 to 0.8 when the testing speed increased from 0.6 m/s to 2 m/s. The increased coefficient of friction was attributed to the severely fracture of worn surface. Micele et al. [11] found the coefficient of friction of SiC-$MoSi_2$/Al_2O_3 pair changed in the range of 0.55-0.70 when the load varied between 15 N and 50 N and the sliding speed varied between 0.5 m/s and 2 m/s. Furthermore, the tribological behaviors of SiC/SiC and SiC/Al_2O_3 pairs in the temperature range of 20-400 ℃ were tested by Boch et al. [12], and the coefficients of friction were 0.45 and 0.65, respectively. Takadoum et al. [13] showed that the coefficient of friction of SiC/SiC pair was 0.65 when the relative humidity was 20%, Murthy et al. [14] noted that the coefficient of friction of β-SiC/α-SiC pair was 0.8 when the relative humidity was 30%, and the coefficients of friction of both SiC/SiC pair and β-SiC/α-SiC pair reduced with relative humidity increasing, resulting from the gradual formation of a viscous tribo-layer on the worn surfaces due to oxidation and hydrolysis reactions. Also, SiC/SiC pair exhibited higher coefficient of friction (0.6-0.7) in vacuum or N_2 atmosphere [15,16]. From above literatures, it can be seen that the coefficient of friction of SiC ceramics is higher under unlubricated sliding condition. Higher coefficient of friction, on the one hand, can greatly deteriorate the durability and reliability of tirbosystem, and on the other hand, can cause a lot of energy loss.

In order to reduce coefficient of friction of SiC ceramics, adding a second phase into SiC ceramics is an effective method. Zhang et al. [17-19] found that adding B_4C into SiC ceramics can form relief structure on the surface of SiC-B_4C ceramics, which can not only reduce real contact area on the sliding interface but also fix or trap wear pieces, resulting in the reduced coefficient of friction for SiC ceramics. However, the SiC-B_4C ceramics would reveal higher coefficient of friction at high load owing to the destruction of relief structure on the worn surface [20]. Moreover, Zhou et al. [21] researched the frictional behavior of SiC-graphite/SiC pair and found that the coefficient of friction reduced to 0.14 when the amount of graphite particles was 20vol%. Tang et al. [22] investigated the effect of addition of short carbon fibers on tribological behavior of SiC ceramics and observed that the coefficient of friction of SiC-carbon fibers/SiC pair decreased to 0.22 when the addition was 53vol%. Chen et al. [23] studied frictional property of SiC ceramics with the addition of hBN at high temperatures, and they found that SiC-hBN/SiC pair revealed a lower friction coefficient than that of SiC/SiC pair at 800 ℃. However, these good solid lubricants can only reduce friction coefficient for SiC ceramics until they are pulled out from the SiC matrix during the severe wear stage, while they can't effectively reduce friction coefficient during the initial, mild wear stage owing to their relative small area exposed to sliding surface, which suggests that SiC ceramics containing solid lubricants are only suitable for the applications that impose severe wear conditions. Further, the frictional behaviors of these solid lubricants are strongly affected by environment where they work, and they can't show low friction in vacuum or dry nitrogen [24,25].

Annealing in air is another method to reduce friction coefficient for non-oxide ceramics. Gogotsi et al. [26] found that the coefficient of friction of B_4C/steel pair decreased from 0.8 to 0.23 after the B_4C ceramics were annealed at 1200 ℃×0.5 h, which was ascribed to the formation of self-lubricating layers composed of B_2O_3 and

graphite. However, the friction coefficient of the annealed B_4C ceramics was found to increase with longer sliding times, which was attributed to the gradual wear of those self-lubricating layers. In contrast, Erdemir et al. [27-29] and Zhang et al. [30] reported that H_3BO_3 layers were produced on the B_4C ceramics after annealing in air at 800 ℃ and 1200 ℃, respectively. The friction coefficients of the annealed B_4C ceramics sliding against different counterpart materials could be kept at low values (0.04-0.08) over a long sliding distance (600-1000 m) until the end of the experiments. Also, Zhang et al. [31] noted that H_3BO_3 can also be formed on B_4C-SiC composite ceramics after annealing at 1000 ℃, and the resulting ceramics can display low friction coefficients over a long sliding distance of 1000 m. As a result, there is a big controversy on the effect of annealing on the self lubrication of B_4C ceramics in the literature. In addition, a large number of studies have found that SiO_2 formed on the worn surface of SiC ceramics during sliding due to the tribochemical reaction can effectively reduce friction for SiC ceramics [9,13]. However, this tribochemical reaction usually occurs at high load or high humidity in the atmosphere where there is the presence of oxygen. Therefore, SiC triboelements will suffer great friction when they work in low-load or low-humidity air environment and inert atmosphere. If SiC ceramics are used in these environments, annealing in air before application is an effective way to reduce friction for SiC ceramics. Yamamoto and Ura [32] found that SiO_2 layer was produced on SiC ceramics after annealing in air at 1000 ℃×1 h. Compared with the coefficient of friction (0.6-0.8) of SiC ceramics without annealing, the coefficient of friction of annealed SiC ceramics was kept as low as 0.2 in Ar until the end of the experiments. However, the annealed SiC ceramics could only show a low friction coefficient (0.1) during the initial stage when the test was performed in air, then the coefficient of friction was increased, which was attributed to roughened worn surface owing to the further promoted oxidation during the sliding process. In the present study, we found some results that are different from the previous conclusions proposed by Yamamoto and Ura [32]. Further, Yamamoto and Ura [32] only investigated the tribological properties of SiC ceramics after annealing at 1000 ℃, in the present study, we studied the tribological properties of SiC ceramics after different annealing temperatures.

In this study, the aims are to investigate that (i) surface analyses of SiC ceramics after annealing in air at different temperatures; (ii) friction and wear properties of SiC ceramics after annealing at different temperatures in air; (iii) self lubrication mechanism of SiC ceramics after annealing.

9.2. Experimental procedures

Commercial SiC powder (Grade OY-15, Yakushima Denko, Japan) was used as the raw material to fabricate SiC ceramics. To promote the sintering of SiC ceramics, B_4C (Grade HS, H. C. Starck, Germany) of 3 wt% and carbon black (#4000B; Mitsubishi Chemical; Japan) of 3 wt% were added as sintering additives. SiC ceramics were fabricated by the pressureless sintering technique. First, the starting materials were ball-milled for 24 h using SiC balls and ethanol as the milling media. After being dried, the powder mixture was pressed into disks and then were cold-isostatically pressed at 196 MPa. The disks were sintered at 2300 ℃ for 16 h in argon atmosphere. Finally, the samples were cooled to room temperature. After sintering, the samples were polished to obtain a surface roughness (Ra) of less than 10 nm. The post annealing treatments in air of SiC ceramics were done at 1000 ℃, 1200 ℃ and 1500 ℃ for 1 h, respectively. The SiC ceramic without annealing was denoted as S0, while the SiC ceramics with annealing at 1000 ℃, 1200 ℃ and 1500 ℃ were denoted as S1000, S1200, and S1500, respectively.

The density of pressureless sintered SiC ceramics was tested by Archimedes method. Vickers-indentation tests were carried out on the polished samples to evaluate their hardness and fracture toughness (K_{IC}). Additional details of these test procedures were described elsewhere [18]. The measurements were conducted 5 times, and the data obtained were the mean values. The mechanical properties of pressureless sintered SiC ceramics are shown in

Table 1.

Table 1 Mechanical properties of pressureless sintered SiC ceramics.

Property	Value
Bulk density (g/cm^3)	3.13
Relative density (%)	98.4
Average hardness (GPa)	28.3
Average fracture toughness (MPa·m$^{1/2}$)	3.2

The dry sliding tests were performed in a T-18-0162 ball-on-disk tribometer (Nanovea, US). Commercially available SiC balls with a diameter of 9.5 mm were used as counterbodies. The properties of SiC ball was described elsewhere [30]. The tests were performed at a load of 5 N and a sliding velocity of 0.1 m/s with wear track radius of 7 mm. A long sliding distance was set to 1000 m. All tests were conducted at ambient temperature (approximately 20 ℃) in open air of 29-36% relative humidity. Coefficients of friction were automatically calculated and recorded by a microprocessor-controlled data acquisition system. Wear volumes of disks and balls were calculated by measuring cross-sectional areas of the wear track on the disks and by measuring the diameter of the worn scar on the balls, respectively. The specific wear rates were calculated by the wear volume divided by the applied load and sliding distance. Three repeated measurements were performed under the same conditions, and the average values were obtained.

The surfaces of the SiC ceramics without and with annealing were observed and analyzed by SEM and EDS. The wear scars of the SiC balls were observed by microscope. Phase compositions of the initial surfaces of the SiC ceramics without and with annealing were detected by Raman spectroscopy. The spectroscope used a green laser at 532 nm with an output power of 10 mW focused to a spot size of 4 μm. The roughness profiles and cross-sectional areas on wear track of samples were measured using a surface profilometer.

9.3. Results and discussion

9.3.1. Characteristic of surfaces of SiC ceramics without and with annealing treatments

Fig. 1 shows the typical SEM images of initial surfaces of SiC ceramics without and with different annealing treatments, EDS analyses and elemental distributions of the corresponding surfaces. It can be seen from Fig. 1a-c that some visible pores are observed on the surface of S0, and B_4C particles are dispersed in the SiC matrix. The oxygen content in S0 is very low, which is considered as an impurity from raw materials. When the SiC ceramics were annealed at 1000 ℃, CO_2 and/or CO gas would be formed owing to oxidation reaction of SiC. Therefore, more visible pores are observed on the surface of S1000 (Fig. 1d). Meanwhile, the oxygen content on the surface of S1000 was increased (Fig. 1e), and the formed silicon oxide was uniformly distributed on the surface of S1000 and there was still some unoxidized SiC on the surface of S1000 (Fig. 1f-h). This means that silicon oxide and SiC coexist on the surface of S1000. When the SiC ceramics were annealed at 1200 ℃, the oxygen content on the surface of S1200 was dramatically increased (Fig. 1j), and the number of visible pores became relative small (Fig. 1i). The possible reason is that more silicon oxide was formed on the surface of S1200 with the increase of annealing temperature, and formed silicon oxide softened at the high temperature, increasing the surface density. Further, compared with the concentration of oxygen and carbon on the surface of S1000 (Fig. 1g, h), the concentration of oxygen on the surface of S1200 increased and the concentration of carbon decreased (Fig. 1l, m), which means the area of the formed silicon oxide was increased. When the SiC ceramics were annealed at 1500 ℃, the oxidation degree of the surface of S1500 was further increased (Fig. 1o), and the number of visible pores was

further reduced (Fig. 1n).

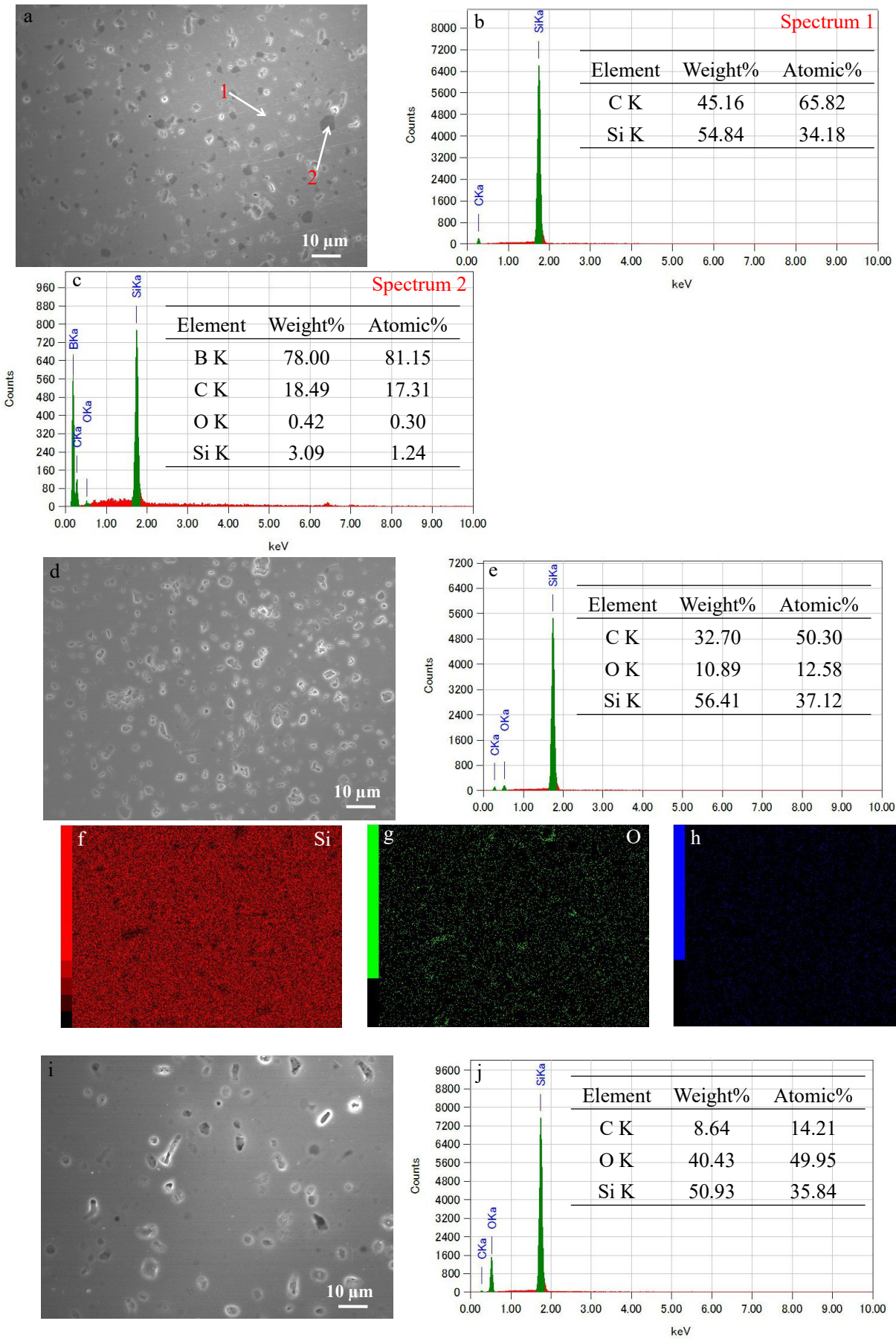

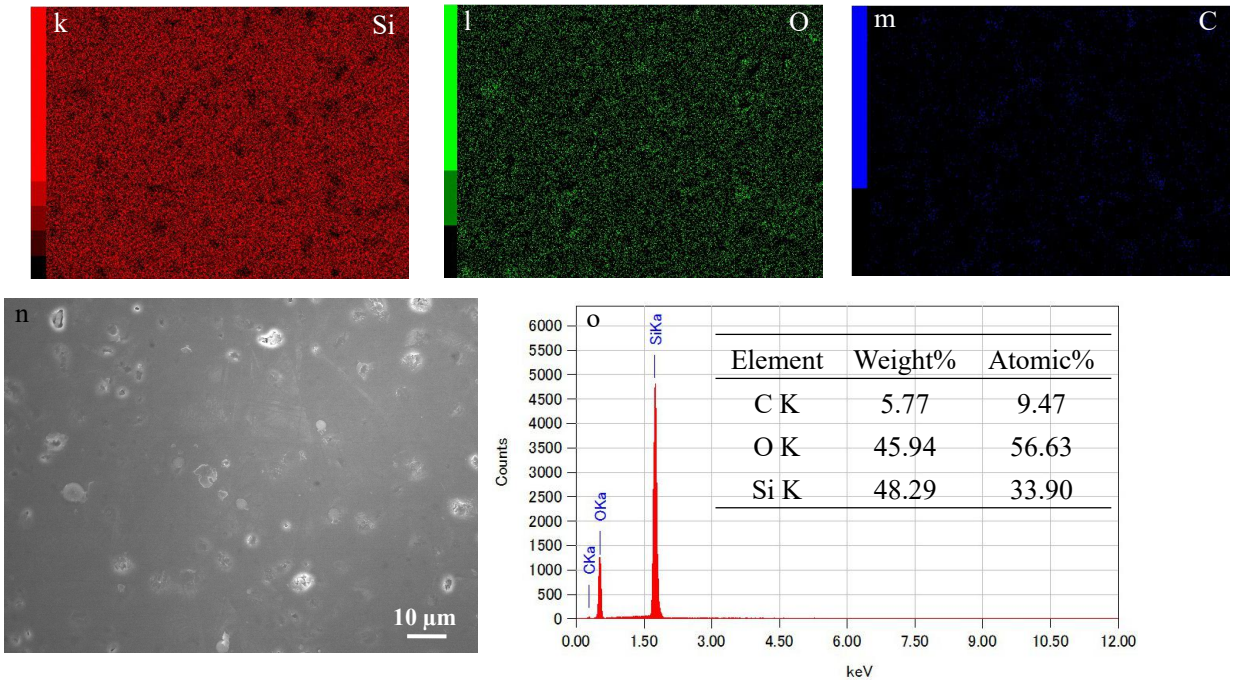

Fig. 1. SEM images of initial surfaces of samples: (a) S0, (d) S1000, (i) S1200, (n) S1500; EDS point analyses of Fig. 1(a): (b) and (c); EDS analyses of Fig. 1(d): (e), of Fig. 1(i): (j), of Fig. 1(n): (o); Elemental distributions of Fig. 1(d): (f)-(h), of Fig. 1(i): (k)-(m).

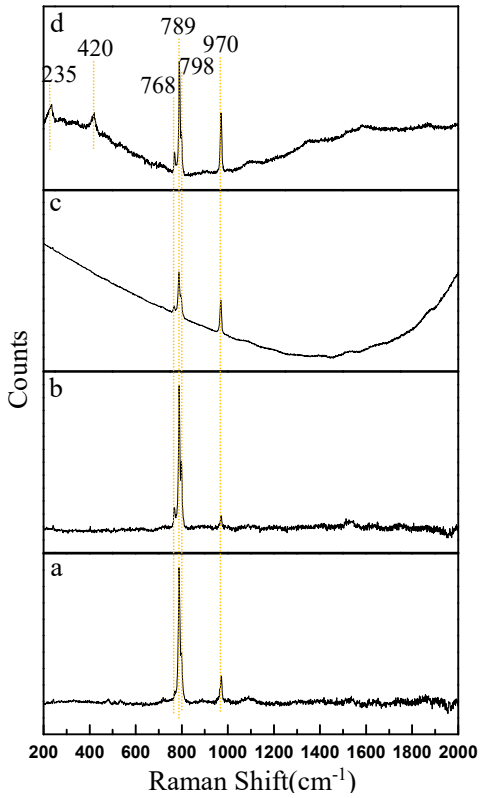

Fig. 2. Raman spectrums of the initial surfaces of samples: (a) S0, (b) S1000, (c) S1200, (d) S1500.

Fig. 2 shows the Raman spectrums of initial surfaces of SiC ceramics without and with different annealing treatments. The Raman peaks at 768 cm^{-1}, 789 cm^{-1}, 798 cm^{-1} and 970 cm^{-1} appearing in all the samples are in agreement with the Raman shift of SiC [33]. The Raman peaks at 235 cm^{-1} and 420 cm^{-1} appearing in the S1500 are in agreement with the Raman shift of α-cristobalite [34]. From Fig. 1, we have known that silicon oxide has

been formed on the surface of SiC ceramics after annealing treatments. However, no peaks of silicon oxide appear in the S1000 and S1200, suggesting that the layer of silicon oxide formed is amorphous. It is reported that quartz would be transformed into β-cristobalite when the temperature is higher than 1470 ℃, and β-cristobalite would be transformed into α-cristobalite during the subsequent cooling process [35]. Therefore, Raman peaks of α-cristobalite are observed in S1500. Combined with Fig. 1 and Fig. 2, it can be concluded that the compositions of the oxides on the surfaces of S1000, S1200 and S1500 are amorphous silicon oxide, amorphous silicon oxide and α-cristobalite, respectively.

Some representative 2D profiles of the initial surfaces of SiC ceramics without and with different annealing treatments are provided in Fig. 3. It can be seen from Fig. 3 that the roughness of initial surface increases with the increase of annealing temperature, as reflected by the observation of multiple hills and valleys (often sharp) on the individual 2D profiles. The average surface roughness of samples S0, S1000, S1200 and S1500 is 0.005 μm, 0.016 μm, 0.043 μm and 0.141 μm, respectively. During annealing treatments, the silicon oxide formed with the increase of oxidation degree of SiC as well as the phase transformation of silicon oxide destroyed the surface finish of initial polished surface, causing the increased surface roughness. Although less pores were observed on the surfaces of S1200 and S1500, the roughness of the surfaces was increased by the unevenness of the formed silicon oxide and the increased depth of pores. The influence of increased surface roughness on the friction behaviors of SiC ceramics will be discussed later.

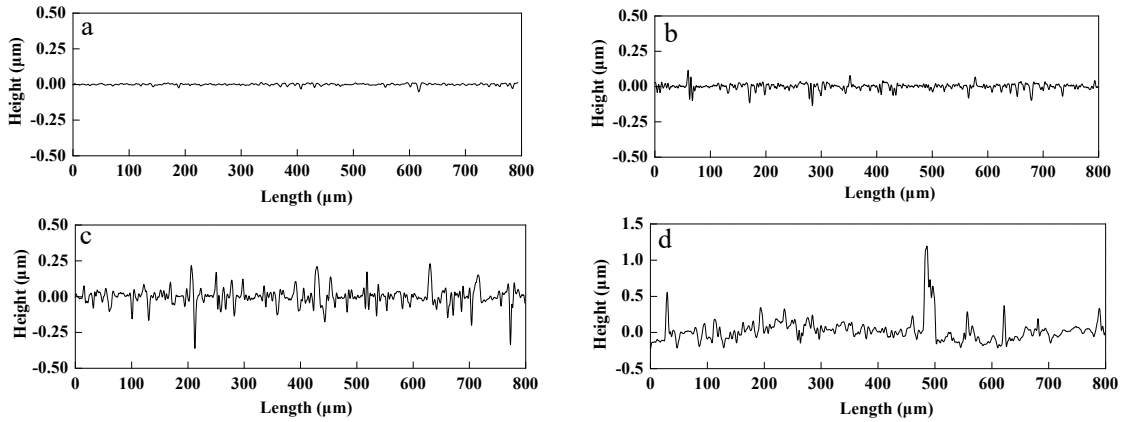

Fig. 3. 2D profiles of the initial surfaces of samples: (a) S0, (b) S1000, (c) S1200, (d) S1500.

9.3.2. Coefficient of friction (COF) and specific wear rate

Fig. 4 shows the typical coefficients of friction with sliding distance for SiC ceramics without and with different annealing treatments. It can be found that the COF of S0 in steady state is 0.70±0.01; with the rise of annealing temperature to 1000 ℃, the COF of S1000 decreases to 0.54±0.05; with further increasing annealing temperature to 1200 ℃, the COF of S1200 falls to 0.48±0.03 in steady state; at the highest annealing temperature of 1500 ℃, the COF of S1500 is further reduced to 0.40±0.03. As a whole, S1500 reveals the best lubricity over a long sliding distance. Furthermore, it is clear that the COF of SiC ceramics decreases with the increase of annealing temperature. The result in the present study is different from the previous conclusion proposed by Yamamoto and Ura [32]. Yamamoto and Ura [32] found that the COF of SiC ceramics with annealing at 1000 ℃ could only showed low friction coefficient (0.1) during the initial stage, then the coefficient of friction was increased. However, in the present study, we found that all SiC ceramics annealed at different temperatures exhibited high coefficients of friction during the initial stage, and then the coefficients of friction decreased to lower values and remained there until the end of the experiment. In other words, annealed SiC ceramics can show self lubrication over a long sliding distance.

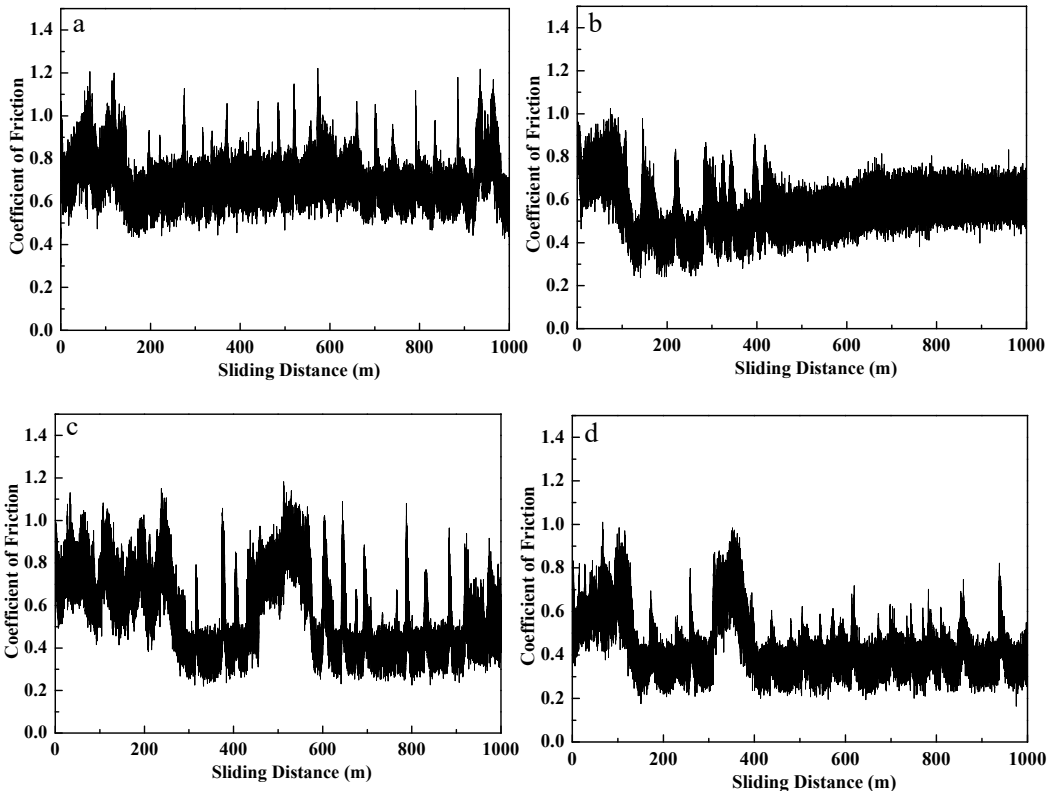

Fig. 4. The coefficients of friction with sliding distance for samples: (a) S0, (b) S1000, (c) S1200, (d) S1500.

Table 2 shows the specific wear rates of the SiC ceramics without and with different annealing treatments and of the mating SiC balls. Compared with S0, the specific wear rate of S1000 is lower. Further, the specific wear rate of the mating SiC ball of S1000 is significantly lower than that of the mating SiC ball of S0. As a result, the systematic specific wear rate of S1000/SiC pair is smaller than that of S0/SiC pair. This result in the present study is also different from the previous conclusion proposed by Yamamoto and Ura [32]. Yamamoto and Ura [32] found that the wear of SiC ceramics with annealing at 1000 ℃ in air was increased as the dry sliding test was performed in air. The reason for the increased wear is considered that oxidation of the worn surface of annealed SiC ceramics was further promoted during the sliding process in dry air, causing a thicker oxidized layer. Therefore, the wear of annealed SiC ceramics was increased. However, in the present study, we found that annealing treatment at 1000 ℃ didn't increase the wear of SiC ceramics. The annealing treatment at 1000 ℃ can even reduce the specific wear rates of the SiC ceramics and of the mating SiC balls. The reduced specific wear rate of S1000 may be attributed to the improvement of friction environment and to the formation of oxide layer with an appropriate amount. Therefore, we believe that SiC ceramics can achieve self lubrication by annealing at 1000 ℃ without increasing wear. A similar argument has also been made on the wear of annealed B_4C ceramics. Erdemir et al. [27-29] observed that annealing treatment for B_4C ceramics would not increase the wear of B_4C ceramics while reducing the COF of B_4C ceramics. In contrast, Zhang et al. [30] noted that the H_3BO_3 layer produced on the surface of B_4C ceramics after annealing increased the wear of B_4C ceramics because the H_3BO_3 layer with layered structure was easier to be removed during the sliding process. Although the specific wear rate of S1000 is lower than that of S0, when the annealing temperature is higher than 1200 ℃, the specific wear rates of S1200 and S1500 are higher than that of S0. The increased specific wear rates of S1200 and S1500 are attributed to the formation of excessive oxide layers. However, the wear rate of S1500 is lower than that of S1200, which may be related to the formation of α-cristobalite.

Table 2 Specific wear rates of samples.

NO.	Specific wear rate of disk ($\times 10^{-6}$ mm^3/N·m)	Specific wear rate of mating SiC ball ($\times 10^{-6}$ mm^3/N·m)
S0	5.12±2.86	2.38±0.07
S1000	3.89±1.06	0.77±0.03
S1200	16.0±3.08	2.36±0.13
S1500	13.2±2.28	1.65±0.08

9.3.3. Self lubrication mechanism

Fig. 5. shows the typical SEM images of worn surfaces of SiC ceramics without and with different annealing treatments, EDS analyses and elemental distributions of the corresponding surfaces. Fig. 6. shows the typical optical micrographs of wear scars on the mating SiC balls sliding against SiC ceramics without and with different annealing treatments.

As to S0, the worn surface is characterized by a little brittle fracture and grain pullout, together with some tribo-layers (Fig. 5a). According to the results of EDS analysis and elemental distributions of the worn surface of S0 (Fig. 5b-e), it can be known that oxygen content of the worn surface is significantly increased as compared to the initial surface (Fig. 1b-c). Therefore, it is logical to conclude that tribochemical reaction of SiC occurred during the sliding of S0, and discontinuous silicon oxide tribo-layers were formed. Friction and wear mechanisms of S0 are further understood by observing wear scar of the mating SiC ball (Fig. 6a). Obvious grooves are observed on the mating SiC ball, and these grooves gradually widened during the long distance sliding, so that some of them have been connected together. Therefore, it can be known that there are a large number of hard SiC wear particles from both the SiC disk (S0) and the mating SiC ball on the sliding interface. Based on the characteristics of worn surface of S0 and wear scar on the mating SiC ball, it can be inferred that both the wear particles and the rough worn surface resulted in a high COF of the S0/SiC pair. Although some of hard SiC wear particles may be crushed, oxidized, and bonded into silicon oxide tribo-layers on the worn surface of S0, these silicon oxide layers didn't effectively reduce the COF for SiC ceramics. Other scholars found that silicon oxide formed on the worn surface of SiC ceramics during sliding due to the tribochemical reaction could reduce COF of SiC ceramics [9,13], however, similar results were not observed in this study. It is possible that the formed silicon oxide didn't produce a continuous, sufficient lubricating layer to cover the entire worn surface of S0, thereby silicon oxide formed due to the tribochemical reaction failed to reduce the COF for S0. Another possible reason is that the COF of S0 was controlled by the simultaneous occurrence and competition of hard SiC wear particles and lubricating layer of silicon oxide. However, the beneficial influence from lubricating layer was less than the deteriorated influence from hard SiC wear particles.

As to S1000, the oxygen content on the worn surface (Fig. 5g) is increased as compared to the initial surface (Fig. 1e). This means that oxidation of the worn surface was further promoted, and tribochemical reaction of SiC occurred during the sliding. From Fig. 1e-h, we have known that silicon oxide formed on the surface of S1000, however, the formed silicon oxide didn't completely cover the surface of S1000 and there were still some SiC grains directly exposed to the sliding interface in the early stage of the sliding. Therefore, there were still some hard SiC wear particles formed on the sliding interface, but the number of SiC wear particles formed was less than that on the sliding interface of S0. This assumption can be confirmed by the observation of wear scar on the mating SiC ball of S1000. It can be seen from Fig. 6b that less grooves were formed on the wear scar of mating SiC ball of S1000 as compared to the mating SiC ball of S0 (Fig. 6a), which means fewer abrasive particles were present on the sliding interface of S1000/SiC pair. Although a continuous silicon oxide layer that can cover the entire worn surface of S1000 didn't form (Fig. 5h-j), the reduced SiC wear particles resulted in a reduction in the COF of S1000/SiC pair. Yamamoto and Ura [32] also stated that the oxidation of the worn surface of SiC ceramics

with annealing at 1000 ℃ was further promoted during the sliding, but the COF of annealed SiC ceramics was increased after an initial certain sliding distance, the mechanism of which was considered that the oxidized layer became thick and the worn surface was roughened. In contrast, the reduced COF was observed for the SiC ceramics with annealing at 1000 ℃ in this study, and this phenomenon was attributed to the reduced SiC wear particles on the sliding interface. In addition, more visible pores are observed on the initial surface of S1000 (Fig. 1d) owing to the annealing treatment. Borrell et al. [36] and Turatti et al. [37] stated the ceramics with more pores can cause an increased wear rate during dry sliding. However, in the present study, we didn't found the specific wear rate of S1000 with more pores on the surface was increased. The possible reason is that the negative effect of more pores formed on the surface of S1000 due to annealing is offset by the positive effect of more silicon oxide formed and less SiC on the surface of S1000 due to annealing.

As to S1200, the oxygen content on the worn surface (Fig. 5l) is decreased as compared to the initial surface (Fig. 1j), and B_4C grains that are the black areas in the figure can be seen (Fig. 5k), which means part of the silicon oxide layers formed after annealing were worn through during the sliding process. Although more SiC grains were directly exposed to the sliding interface after the silicon oxide layers were worn through and the chemical composition of the worn surface of S1200 (Fig. 5l) is similar to those of S0 (Fig. 5b) and S1000 (Fig. 5g), the COF of S1200 was lower than those of S0 and S1000. On the one hand, the worn surface of S1200 (Fig. 5k) was smoother than those of S0 (Fig. 5a) and S1000 (Fig. 5f) and less brittle fracture and grain pullout were observed on the worn surface of S1200, and on the other hand, shallower and narrower grooves were observed on the mating SiC ball of S1200 (Fig. 6c) as compared to the mating SiC balls of S0 (Fig. 6a) and S1000 (Fig. 6b). Therefore, it can be inferred that the silicon oxide wear particles generated by the wear of the silicon oxide layers formed by annealing didn't get ejected out of the sliding interface, inversely, they may be trapped on the sliding surface. These silicon oxide wear particles, which are softer than SiC wear particles appeared in the sliding interface of S0, could be used as solid lubricant, reducing the COF of S1200/SiC pair. However, because the surface roughness of S1200 was significantly increased after annealing (Fig. 3c), thus the COF of S1200 entered the steady state after a relative long run in period.

As to S1500, the oxygen content on the worn surface (Fig. 5q) is also decreased as compared to the initial surface (Fig. 1o), and it can be seen from Fig. 5r-t that some SiC grains were also directly exposed to the sliding interface after the silicon oxide layers were worn through. Firstly, the Raman results validate that α-cristobalite was formed on the surface of S1500, as shown in Fig. 2. α-cristobalite with tetragonal structure and spacegroup $P4_12_12$ is a mineral polymorph of silica. The lattice parameters of α-cristobalite are a=0.4973 nm, c=0.695 nm [35]. It has higher value of c/a. Higher value of c/a suggests weaker interplanar bonding energy and following lubricity [38]. Therefore, α-cristobalite would show some lubricity. Secondly, compared with the worn surfaces of S0, S1000 and S1200, the worn surface of S1500 is the smoothest. From Fig. 6d, it can be seen that no obvious grooves can be observed on the wear scar of the mating SiC ball of S1500. Smooth worn surface of S1500 and no obvious grooves on the wear scar of the mating SiC ball suggest that there are little SiC wear particles on the sliding interface of S1500/SiC pair. For the reasons mentioned above, S1500 exhibited the lowest COF. Although S1500 has the maximum roughness after annealing, S1500 revealed a shorter run in period than S1200 owing to the lubricity of α-cristobalite and to little SiC wear particles on the sliding interface.

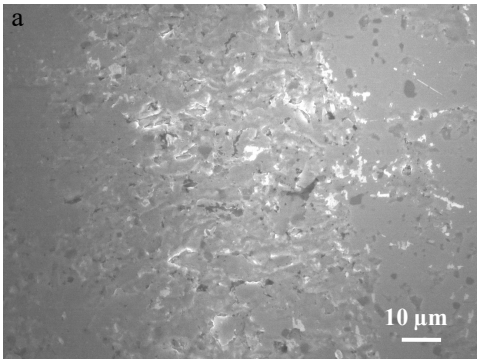

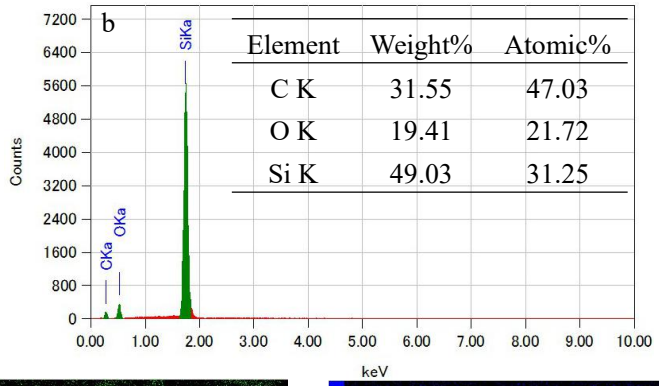

Element	Weight%	Atomic%
C K	31.55	47.03
O K	19.41	21.72
Si K	49.03	31.25

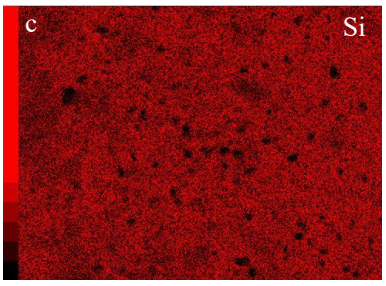

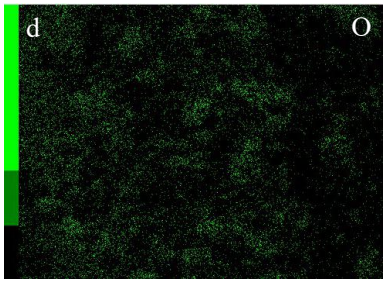

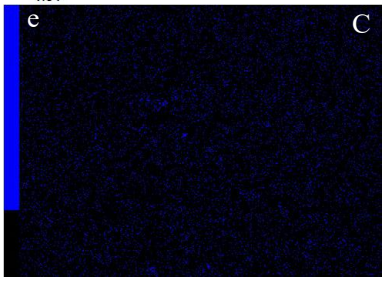

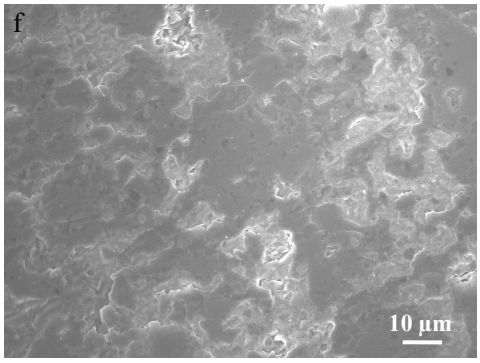

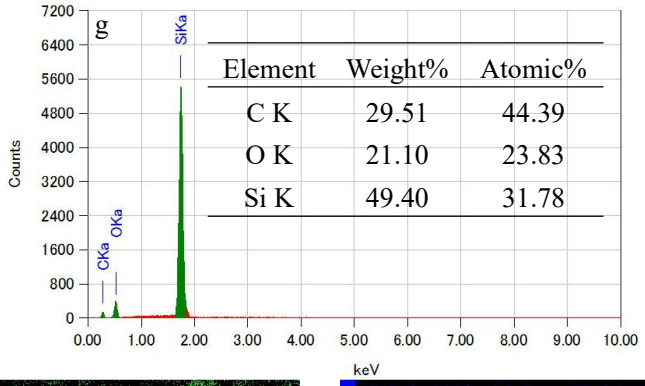

Element	Weight%	Atomic%
C K	29.51	44.39
O K	21.10	23.83
Si K	49.40	31.78

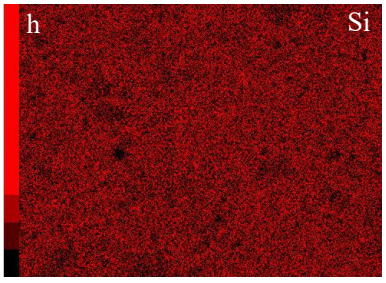

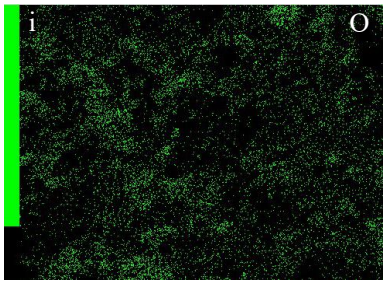

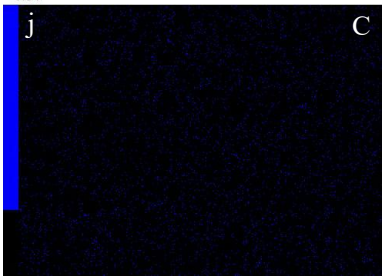

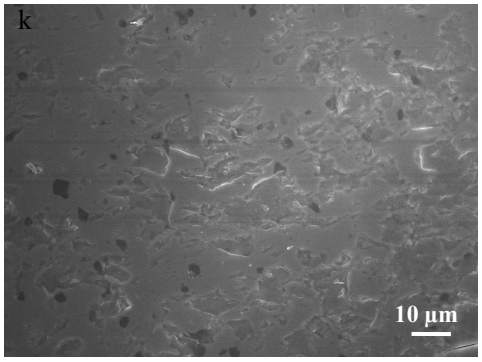

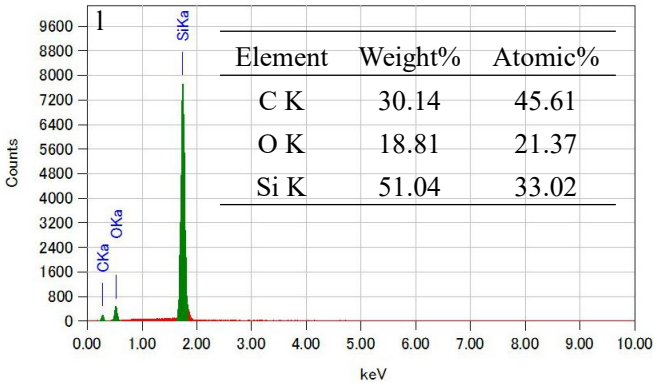

Element	Weight%	Atomic%
C K	30.14	45.61
O K	18.81	21.37
Si K	51.04	33.02

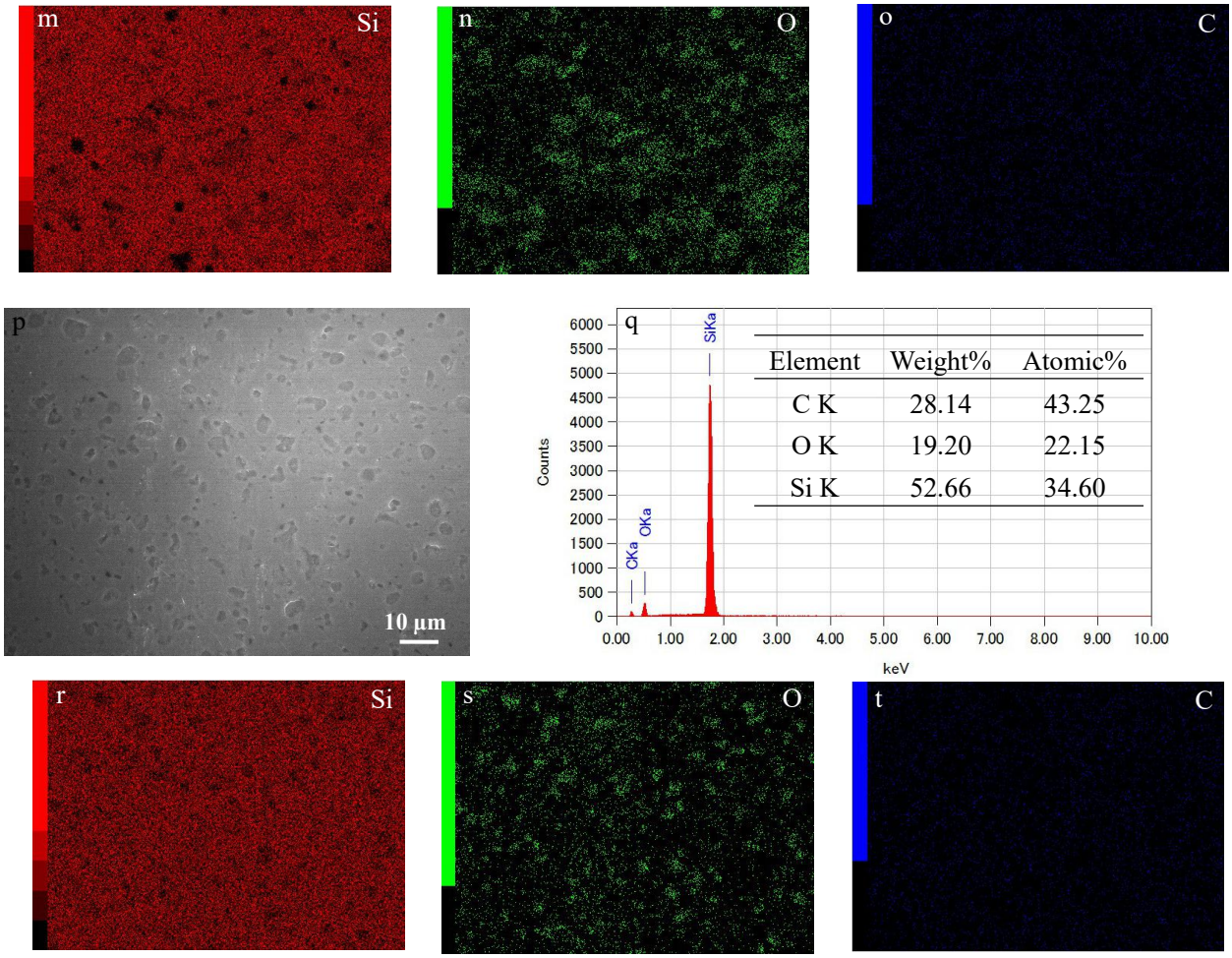

Fig. 5. SEM images of worn surfaces of samples: (a) S0, (f) S1000, (k) S1200, (p) S1500; EDS analyses of Fig. 5(a): (b), of Fig. 5(f): (g), of Fig. 5(k): (l), of Fig. 5(p): (q); Elemental distributions of Fig. 5(a): (c)-(e), of Fig. 5(f): (h)-(j), of Fig. 5(k): (m)-(o), of Fig. 5(p): (r)-(t).

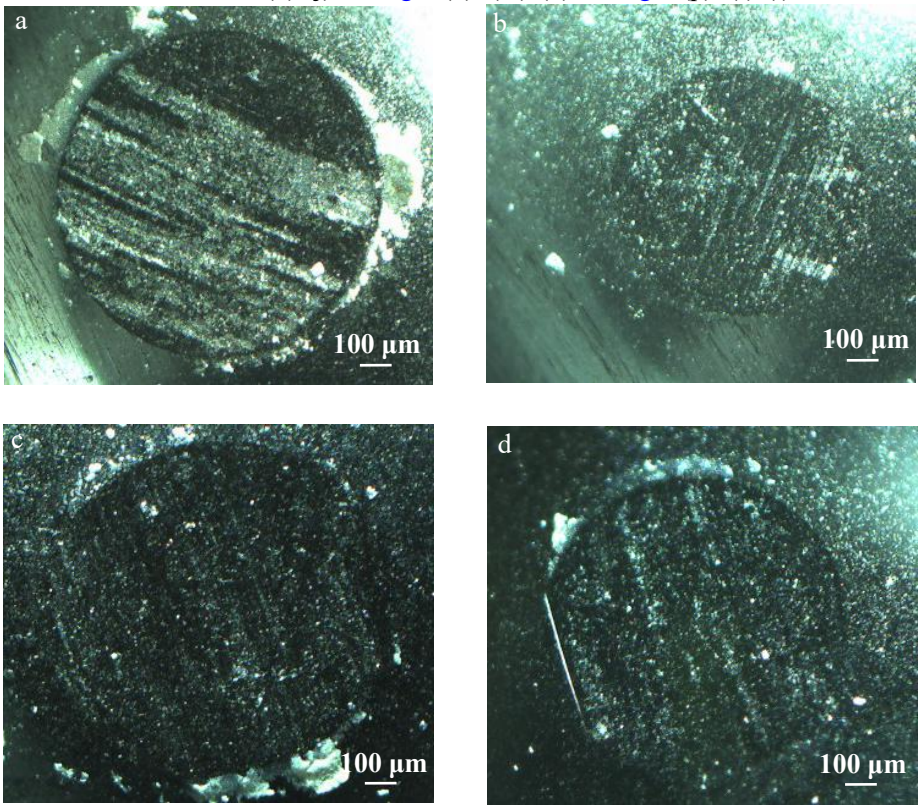

Fig. 6. Optical micrographs of wear scars on the mating SiC balls sliding against: (a) S0, (b) S1000, (c) S1200 and (d) S1500.

In summary, it is found in this study that low COF can be obtained for SiC ceramics by annealing in air, and the COF of SiC ceramics decreased with annealing temperature increasing. Further, the SiC ceramics with annealing at 1000 ℃ can show self lubrication over a long sliding distance without increasing wear. Yamamoto and Ura [32] found that the COF of SiC ceramics with annealing at 1000 ℃ could only show low friction coefficient during the initial stage, then the COF and wear of annealed SiC ceramics increased, which was attributed to the roughened worn surface as the sliding distance increased, however, different tribological results were observed in this study. Also, although the roughness of initial surface of SiC ceramics increased with the increase of annealing temperature, it is observed by SEM that the roughness of worn surface of SiC ceramics decreased with the increase of annealing temperature. It is interesting to find in this study that the formation of α-cristobalite can further lubricate SiC ceramics and shorten run in period.

9.4. Conclusions

In this study, the self lubrication of SiC ceramics prepared by pressureless sintering was investigated by annealing in air at different temperatures. The following results are obtained:

(1) Low COF can be obtained for SiC ceramics by annealing, and the COF of SiC ceramics decreases with the increase of annealing temperature. SiC ceramics with annealing at 1500 ℃ revealed the best self lubricating property, with the coefficient of friction of 0.4, while the coefficient of friction of SiC ceramics without annealing was as high as 0.7.
(2) The SiC ceramics with annealing at 1000 ℃ can show self lubrication over a long sliding distance without increasing wear.
(3) The formation of α-cristobalite on the annealed SiC ceramics can further lubricate SiC ceramics and shorten run in period.
(4) Self lubrication mechanism of SiC ceramics with annealing is considered that on the one hand, the formation of silicon oxide layers after annealing can reduce the number of SiC grains directly exposed to the sliding interface in the early stage of the sliding, decreasing the number of hard SiC wear particles formed on the sliding interface; and on the other hand, silicon oxide wear particles generated by the wear of the silicon oxide layers formed by annealing can be used as solid lubricant.

9.5. References

[1] S. Grasso, T. Saunders, H. Porwal, M. Reece. Ultra-high temperature spark plasma sintering of α-SiC. Ceramics International,2015,41(1):225-230.
[2] W. Zhang, Y. L. Han. Progress of investigation on thermal shock resistance of Al_2O_3-based ceramics. Journal of ceramics,2008,29(2):193-198.
[3] S. K. Sharma, B. V. M. Kumar, Y. W. Kim. Tribology of WC reinforced SiC ceramics: influence of counterbody. Friction,2019,7(2):129-142.
[4] U. Soy, A. Demir, F. Findik. Friction and wear behaviors of Al-SiC-B_4C composites produced by pressure infiltration method. Industrial Lubrication and Tribology,2011,63(5):387-393.
[5] W. Zhang. Progress in research on castables of monolithic refractories. Materials

Review,2012,26(8):93-97,101.
[6] T. K. Guha, B. Basu. Microfracture and limited tribochemical wear of silicon carbide during high-speed sliding in cryogenic environment. Journal of the American Ceramic Society,2010,93(6):1764-1773.
[7] A. K. Bałata, J. Mazur. Effect of carbon nanoparticle reinforcement on mechanical and thermal properties of silicon carbide ceramics. Ceramics International,2018,44(9):10273-10280.
[8] W. Zhang, S. Yamashita, H. Kita. Progress in tribological research of SiC ceramics in unlubricated sliding-A review. Materials & Design,2020,190:108528.
[9] B. V. M. Kumar, Y. W. Kim, D. S. Lim, W. S. Seo. Influence of small amount of sintering additives on unlubricated sliding wear properties of SiC ceramics. Ceramics International,2011,37(8):3599-3608.
[10] P. Andersson, A. Blomberg. Instability in the tribochemical wear of silicon carbide in unlubricated sliding contacts. Wear,1994,174(1-2):1-7.
[11] L. Micele, G. Palombarini, S. Guicciardi, L. Silvestroni. Tribological behaviour and wear resistance of a SiC-$MoSi_2$ composite dry sliding against Al_2O_3. Wear,2010,269(5):368-375.
[12] R. Boch, F. Platon, G. Kapelski. Tribological and interfacial phenomena in $A1_2O_3$/SiC and SiC/SiC couples at high temperature. Journal of the European Ceramic Society,1989,5:223-228.
[13] J. Takadoum, Z. Zsiga, M. B. Rhouma, C. R. Carmes. Correlation between friction coefficient and wear mechanism of SiC/SiC system. Journal of Materials Science Letters,1994,13(7):474-476.
[14] V. S. R. Murthy, H. Kobayashi, S. Tsurekawa, N. Tamari, T. Watanabe, K. Kato. Influence of humidity and doping elements on the friction and wear of SiC in unlubricated sliding. Tribology International,2004,37(5):353-364.
[15] K. H. Z. Gahr, R. Blattner, D. H. Hwang, K. Pöhlmann. Micro and micro-tribological properties of SiC ceramics in sliding contact.Wear,2001,250:299-310.
[16] S. Sasaki. The effects of the surrounding atmosphere on the friction and wear of alumina, zirconia, silicon carbide and silicon nitride. Wear,1989,134(1):185-200.
[17] W. Zhang, S. Yamashita, T. Kumazawa, F. Ozeki, H. Hyuga, H. Kita. Effect of nanorelief structure formed in situ on tribological properties of ceramics in dry sliding. Ceramics International,2019,45(11):13818-13824.
[18] W. Zhang, S. Yamashita, H. Kita. Tribological properties of SiC-B_4C ceramics under dry sliding condition. Journal of the European Ceramic Society,2020,40(8):2855-2861.
[19] W. Zhang, S. Yamashita, T. Kumazawa, F. Ozeki, H. Hyuga, W. Norimatsu, H. Kita. A study on formation mechanisms of relief structure formed in situ on the surface of ceramics. Ceramics International,2019,45(17):699-704.
[20] W. Zhang, S. Yamashita, H. Kita. Effects of load on tribological properties of B_4C and B_4C-SiC ceramics against SiC ball. Journal of Asian Ceramic Societies,2020,8(3):586-96.
[21] Y. Zhou, K. Hirao, Y. Yamauchi, S. Kanzaki. Tribological properties of silicon carbide and silicon carbide-graphite composite ceramics in sliding contact. Journal of the American Ceramic Society,2003,86(6):991-1002.
[22] H. L. Tang, X. R. Zeng, X. B. Xiong, L. Li, J. Z. Zou. Mechanical and tribological properties of short-fiber-reinforced SiC composites. Tribology International,2009,42(6):823-827.
[23] Z. S. Chen, H. J. Li, Q. G. Fu, X. F. Qiang. Tribological behaviors of SiC/h-BN composite coating at elevated temperatures. Tribology International,2012,56:58-65.
[24] B. Bhushan. Introduction to Tribology, second ed., John Wiley & Sons, New York,2013,276-277.
[25] X. Q. Li, Y. M. Gao, W. Pan, Z. C. Zhong, L. C. Song, W. Chen, Q. X. Yang. Effect of hBN content on the friction and wear characteristics of B_4C-hBN ceramic composites under dry sliding condition. Ceramics International,2015,41(3):3918-3926.
[26] Y. G. Gogotsi, A. M. Koval'chenko, I. A. Kossko. Tribochemical interactions of boron carbides against steel.

Wear,1992,154(1):133-140.
[27] A. Erdemir, C. Bindal, C. Zuiker, E. Savrun. Tribology of naturally occurring boric acid films on boron carbide. Surface and Coatings Technology,1996,86-87(2):507-510.
[28] A. Erdemir, C. Bindal, G. R. Fenske. Formation of ultralow friction surface films on boron carbide. Applied Physics Letters,1996,68(12):1637-1639.
[29] A. Erdemir, O.L. Eryilmaz, G.R. Fenske. Self-replenishing solid lubricant films on boron carbide. Surface Engineering,1999,15(4):291-295.
[30] W. Zhang, S. Yamashita, T. Kumazawa, F. Ozeki, H. Hyuga, H. Kita. Tribological properties of B_4C ceramics prepared by pressureless sintering and annealed at different temperatures. Tribology Transactions,2020,63(4):672-82.
[31] W. Zhang, S. Yamashita, T. Kumazawa, F. Ozeki, H. Hyuga, H. Kita. Study on friction behavior of SiC-B_4C composite ceramics after annealing. Industrial Lubrication and Tribology,2020,72(5):673-679.
[32] Y. Yamamoto, A. Ura. Influence of interposed wear particles on the wear and friction of silicon carbide in different dry atmospheres. Wear,1992,154(1):141-150.
[33] S. L. Placette, K. Delbé, J. Denape, M. Ferrato. Tribological characterization of silicon carbide and carbon materials. Journal of the European Ceramic Society,2015,35(4):1147-1159.
[34] J. B. Bates. Raman spectra of α and β cristobalite. The Journal of Chemical Physics,1972,57(9):4042-4047.
[35] J. W. Anthony, R. A. Bideaux, K. W. Bladh, M. C. Nichols. Handbook of Mineralogy: Volume II: Silica and Silicates. Tucson,1995.
[36] A. Borrell, R. Torrecillas, V. G. Rocha, A. Fernández, V. Bonache, M. D. Salvador. Effect of CNFs content on the tribological behaviour of spark plasma sintering ceramic-CNFs composites.Wear,2012,274-275:94-99.
[37] A. M. Turatti, A. S. Pereira. Wear resistant boron carbide compacts produced by pressureless sintering. Ceramics International,2017,43(11):7970-7977.
[38] F. Li, S. Y. Zhu, J. Cheng, Z. H. Qiao, J. Yang. Tribological properties of Mo and CaF_2 added SiC matrix composites at elevated temperatures. Tribology International,2017,111:46-51.

Chapter 10
A study of B_4C-SiC composite for self-lubrication

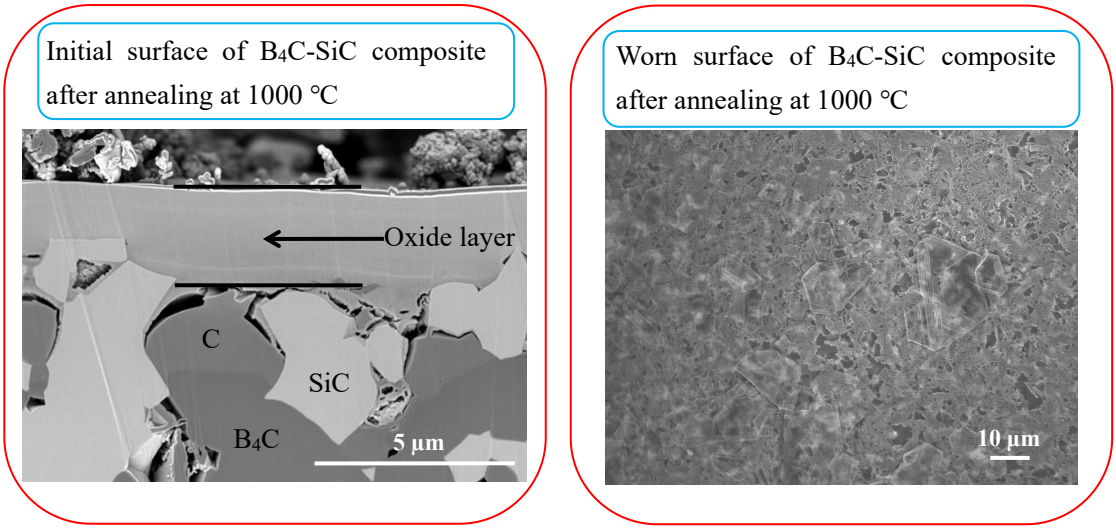

A B_4C-SiC composite without annealing and two B_4C-SiC composites followed by annealing at 1000 ℃ and 1200 ℃ for 1 h in air, respectively, were prepared. The tribological properties of the three composites were evaluated by sliding against SiC balls at room temperature under unlubricated conditions. The B_4C-SiC composite can obtain lower friction coefficient by annealing at 1000 ℃, whereas the friction coefficient of B_4C-SiC composite annealed at 1200 ℃ was significantly increased. The cause for this difference was ascribed to different surface compositions after annealing. The mechanism of self-lubrication of the B_4C-SiC composite was the formation of H_3BO_3 layer.

Contents

10.1. Introduction

Single-phase B_4C ceramics and single-phase SiC ceramics are currently used as wear-resistant components owing to their high hardness, high temperature strength, low density and good wear resistance [1-5]. Compared with single-phase B_4C ceramics and single-phase SiC ceramics, B_4C-SiC composite exhibits better oxidation resistance, higher flexural strength, fracture toughness and hardness [6-10]. Therefore, B_4C-SiC composite is expected to be a potential material for tribological application. However, the study on tribological properties for B_4C-SiC composite, to date, is quite limited [11-14]. In our previous work [15-17], we have compared the friction and wear properties of B_4C-SiC composite with those of single-phase SiC ceramics and single-phase B_4C ceramics under unlubricated sliding tests against SiC balls at the load of 5 N. As a result, B_4C-SiC composite revealed both lower friction coefficient and lower wear rate as compared to single-phase SiC ceramics and single-phase B_4C ceramics. Futhermore, B_4C-SiC composite showed shorter sliding distance up to the steady state condition as compared to those of single-phase B_4C ceramics and single-phase SiC ceramics [18].

In order to further reduce the friction coefficient of B_4C-SiC composite, in this study, we will continue to study the tribological properties of B_4C-SiC composite by investigating the effect of annealing in air on the B_4C-SiC composite. At present, the main ways of self-lubrication for nonoxide ceramics are adding secondary phase and annealing in air [19]. Although it has been proved that adding secondary phases with a lamellar crystal structure, such as graphite and MoS_2, can provide a good lubrication effect for B_4C ceramics and SiC ceramics, B_4C ceramics and SiC ceramics cannot obtain good lubrication until these secondary phases with a lamellar crystal structure are pulled out from the matrix [20,21]. This suggests that these secondary phases cannot help B_4C ceramics and SiC ceramics to achieve self-lubrication during the initial, mild wear stage, while they can only take effect during the subsequent, severe wear stage when they are pulled out and smeared on the worn surfaces. Therefore, the method of adding secondary phase is only suitable for improving the lubrication performance of B_4C ceramics and SiC ceramics in severe wear conditions. Meanwhile, these solid lubricants are sensitive to gaseous composition of environment and temperature where they work. Graphite exhibits low friction only in air, whereas its friction coefficient in nitrogen or vacuum is ten times higher than that in air; MoS_2 shows ultralow friction only in vacuum or inert gas, whereas it cannot provide low friction in O_2 or humid environments; Graphite and MoS_2 can only reveal good lubricant effect at low temperatures, but they will lose their validity at high temperatures due to oxidation. Further, ceramic triboelements sometimes are used in environments where lubricants cannot be available. For example, lubricants cannot be applied in microdevices or microelectromechanical systems because lubricants can cause contamination to other electrical or mechanical components integrated on the same chip [5,19]. Therefore, in those cases, solid lubricants, such as graphite and MoS_2, cannot be used to improve lubrication performance of B_4C-SiC composite by adding them on the surface of B_4C-SiC composite.

Annealing to nonoxide ceramics in air, which can form oxide layers on their surfaces, is another effective method to enhance tribological properties of nonoxide ceramics. Tests by Erdemir et al. [22] displayed that a H_3BO_3 layer was produced on the single-phase B_4C ceramics when the single-phase B_4C ceramics was annealed at 800 °C for one hour in air. The resulting B_4C ceramics with H_3BO_3 layer exhibited a low friction coefficient sliding against a 440C steel ball. Yamamoto and Ura [23] reported that SiO_2 layer was produced on the single-phase SiC ceramics via annealing at 1000 °C for one hour in air. The resulting SiC ceramics with SiO_2 layer also showed a reduced friction coefficient. Although many studies show that H_3BO_3 and SiO_2 can be automatically produced on the worn surfaces of B_4C ceramics and SiC ceramics, respectively, during the dry sliding because of tribochemical reactions, which can reduce friction for B_4C ceramic and SiC ceramics, these tribochemical reactions usually depend on external factors, i.e., these tribochemical reactions can only occur at high load or high

humidity in the atmosphere where there is the presence of oxygen. This means B_4C ceramics and SiC ceramics will suffer high friction when they work in low-load or low-humidity air environment and inert atmosphere. If B_4C ceramics and SiC ceramics are applied in these environments, annealing in air before application is an effective way to reduce friction for B_4C ceramic and SiC ceramics.

For single-phase B_4C ceramics and single-phase SiC ceramic, annealing treatment can achieve reduced friction by self-lubrication. However, there is no published papers about effect of annealing on tribological properties of B_4C-SiC composite. The questions that immediately come to mind are does B_4C-SiC composite can also achieve reduced friction by self-lubrication, what the surface compositions of B_4C-SiC composite are after annealing and how the annealing temperature influences friction behavior? All these questions will be answered in this paper. Therefore, the primary aim of this paper is to study tribological properties of B_4C-SiC composite after annealing and the self-lubricaion mechanism of B_4C-SiC composite after annealing.

10.2. Experiments

The test specimens were produced from 60wt%B_4C-40wt%SiC composite, whose physical properties are shown in Table 1. The annealing treatments of B_4C-SiC composite were carried out at 1000 ℃ and 1200 ℃ for 1 h in air, respectively.

Table 1 The physical properties of sintered B_4C-SiC composite.

Material	B_4C-SiC composite
Production process	Pressureless sintering
Additive	3wt% C
Impurities	O, N, Si, Fe, Al
Density (g/cm^3)	2.66
Relative density (%)	96.6
Vickers hardness (GPa)	30.39
Fracture toughness ($MPa \cdot m^{1/2}$)	3.19

The friction and wear tests of B_4C-SiC composite without annealing (hereafter referred to as BS0), B_4C-SiC composite annealed by 1000 ℃ (hereafter referred to as BS1000) and B_4C-SiC composite annealed by 1200 ℃ (hereafter referred to as BS1200) were studied by sliding against SiC balls of 4.75 mm radius using a ball-on-disk tribometer (T-18-0162, NANOVEA, US). The SiC ball was kept to a stationary holder under the applied load of 5 N to make a track radius of 10 mm, while the disk was rotated at 0.1 m/s for the sliding distance of 1000 m. Unlubricated sliding tests were performed in ambient conditions (18.5 ± 1.5 ℃ and 48 ± 3% RH). The structure and chemical nature for the surfaces of specimens were characterized by Raman spectroscopy. The depth profiling and chemical bonding of the surfaces for X-ray photoelectron spectroscopy (XPS) analysis were performed by ion-sputter etching. The wear rates of disks and balls were determined as WR=V/(Ps), where V, P and s were the wear volume of disks or balls, the applied load and the sliding distance, respectively. A profilometer and microscope were used to estimate the cross-sectional area of wear track of disks and the diameter of wear scar of balls to calculate the wear volume, respectively. The roughness profiles and morphologies of surfaces were studied using profilometer and SEM, respectively. FIB equipment was used to prepare specimens to observe cross-sectional surfaces of BS1000 and BS1200.

10.3. Results and discussion

Fig. 1 shows the friction curves and mean friction coefficient values of the specimens of BS0, BS1000 and BS1200 sliding against SiC balls. The mean friction coefficient of BS0 against SiC ball is about 0.43, whereas those of annealed specimens of BS1000 and BS1200 are 0.16 and 0.77, respectively. It can be observed that the friction coefficient of B_4C-SiC composite can be reduced by half via annealing treated by 1000 ℃, however, the friction coefficient of B_4C-SiC composite is significantly increased via annealing treated by 1200 ℃.

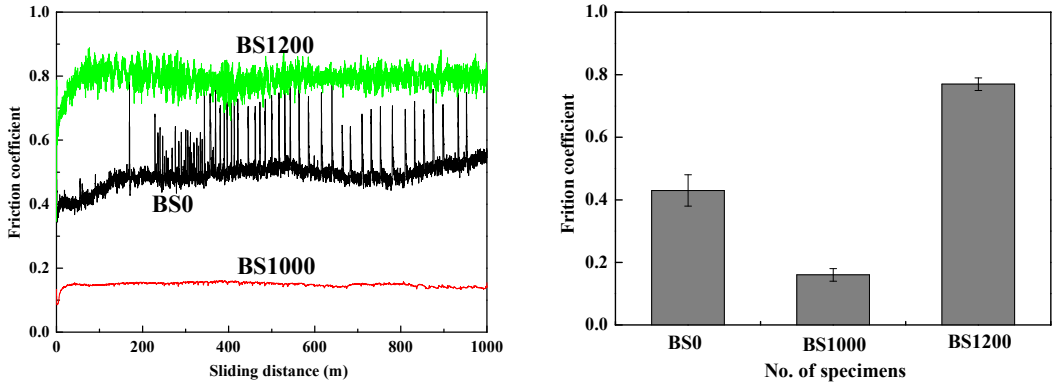

(a) (b)

Fig. 1. Friction curves (a) and mean friction coefficients of B_4C-SiC composite without and with annealing treatment sliding against SiC balls (b).

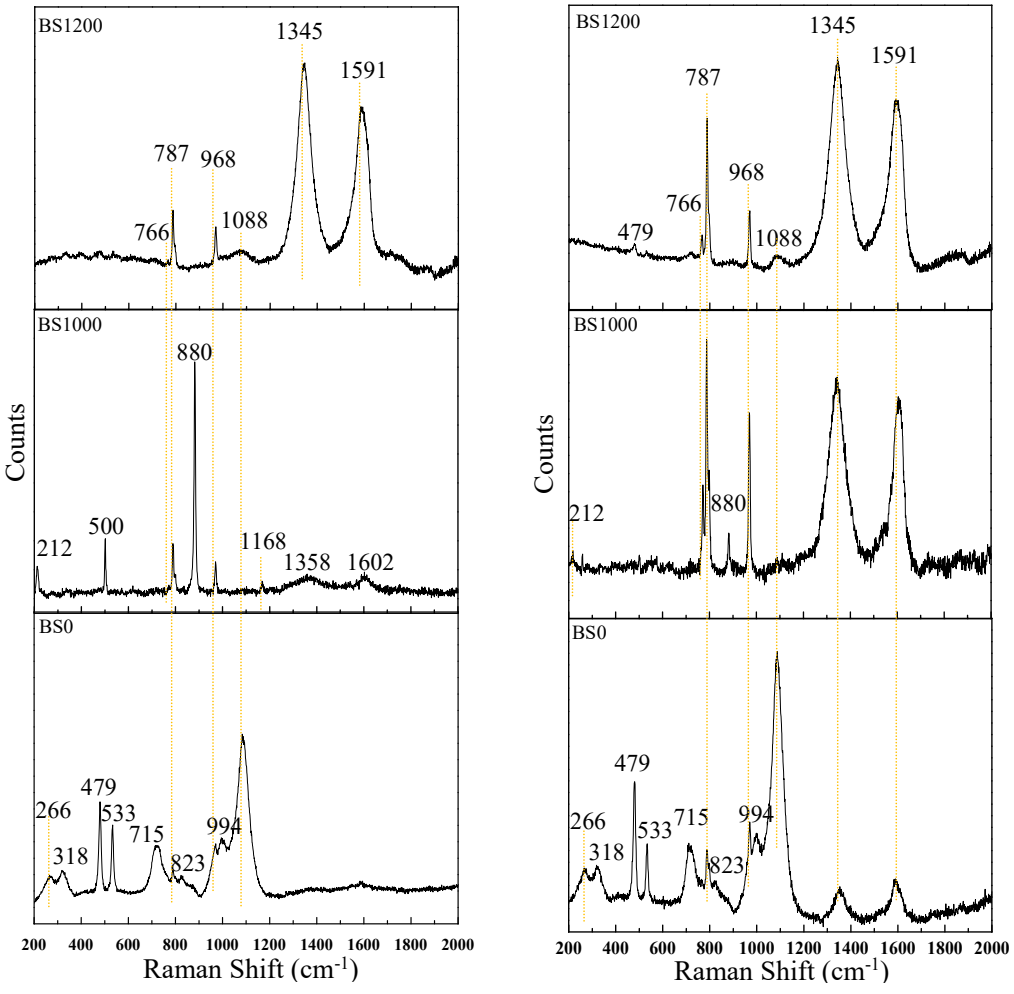

(a) (b)

Fig. 2. Raman spectroscopy of the surfaces of B_4C-SiC composite without and with annealing treatment: (a) outside the wear track of disks; (b) inside the wear track of disks.

Fig. 2 shows the Raman spectroscopy of the surfaces of BS0, BS1000 and BS1200 outside and inside the wear tracks. It can be observed that the three specimens have a very different Raman feature from each other for the initial surfaces (outside the wear tracks). The Raman peaks at 266 cm^{-1}, 318 cm^{-1}, 479 cm^{-1}, 533 cm^{-1}, 715 cm^{-1}, 823 cm^{-1}, 994 cm^{-1} and 1088 cm^{-1} appearing in the BS0 and BS 1200 outside and inside the wear tracks are in agreement with the Raman shifts of B_4C [24-28]. The Raman peaks at 212 cm^{-1}, 500 cm^{-1}, 880 cm^{-1}, 1168 cm^{-1} appearing in the BS1000 outside and inside the wear track are in agreement with the Raman shifts of H_3BO_3 [29,30]. The Raman peak at 766 cm^{-1} appearing in the BS1000 and BS1200 as well as the Raman peaks at 787 cm^{-1} and 968 cm^{-1} appearing in the BS0, BS1000 and BS1200 outside and inside the wear tracks are in agreement with the Raman shift of SiC [31]. The Raman peaks at 1345 cm^{-1} and 1591 cm^{-1} appearing in the BS1200 outside and inside the wear track and in the BS1000 and BS0 inside the wear tracks, and the Raman peaks at 1358 cm^{-1} and 1602 cm^{-1} appearing in the BS1000 outside the wear track are in agreement with the Raman shift of C [26]. The Raman peaks of C observed in the initial surfaces of BS1000 and BS1200 come from the residual carbon after the oxidation of B atoms in B_4C [32]. From Raman results, it can be found that no Raman peaks of SiO_2 appear in BS1000 and BS1200, which means SiO_2 layer was not formed or formed in amorphous nature. Further, the Raman peaks of H_3BO_3 are very sharp, which indicates that the crystallinity of H_3BO_3 is very good.

Furthermore, Fig. 3 shows depth profiles of B, C, O and Si measured by XPS on the surfaces of BS0, BS1000 and BS1200, as well as SEM images of cross-sectional surfaces of BS1000 and BS1200. The O was detected in the BS0, and the content is low and nearly a constant with increasing of sputtering depth. On the one hand, the presence of O may result from the impurity of raw materials. On the other hand, the O may be caused by contamination during the process of the XPS analysis. In comparison with BS0, the amount of oxides on the surfaces of BS1000 and BS1200 is significantly increased by the annealing treatment. Different from the variation trend of O in BS1000, the O concentration in BS1200 decreased with the increase of sputtering depth. When the annealing temperature was increased from 1000 ℃ to 1200 ℃, almost all of the B_2O_3 vaporized, resulting in the extremely low content of B on the surface of BS1200. Because the liquid B_2O_3 has low viscosity, so, the B_2O_3 layer could not effectively protect BS1000 from oxidation. Therefore, BS1000 obtained an oxide layer with higher oxide content and deeper thickness. However, liquid B_2O_3 with low viscosity vaporized and amorphous solid SiO_2 became more dense at 1200 ℃, which can prevent further oxidation of SiC in BS1200. Therefore, the O concentration in BS1200 was higher on the surface and decreased with the increase of depth. Meanwhile, it can be seen from Fig. 3 (d) and (e) that the thickness of the oxide layer on the surface of BS1000 is about 1.5~2.5 μm, while the thickness of the oxide layer on the surface of BS1200 is about 0.9~1.5 μm.

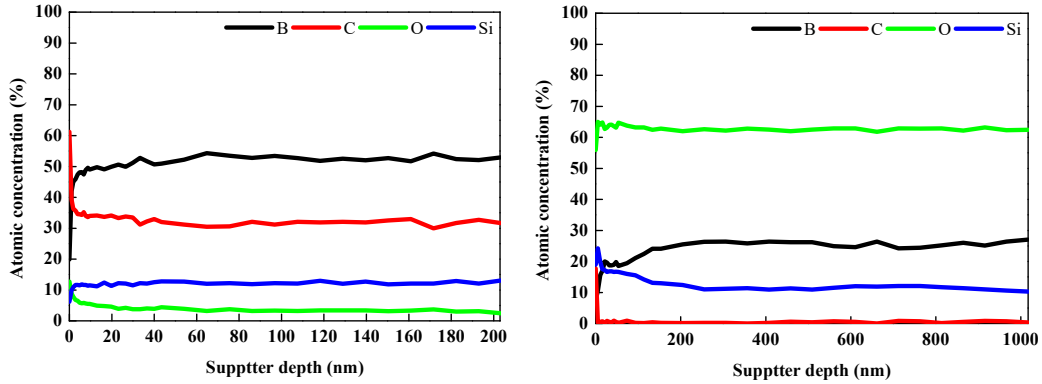

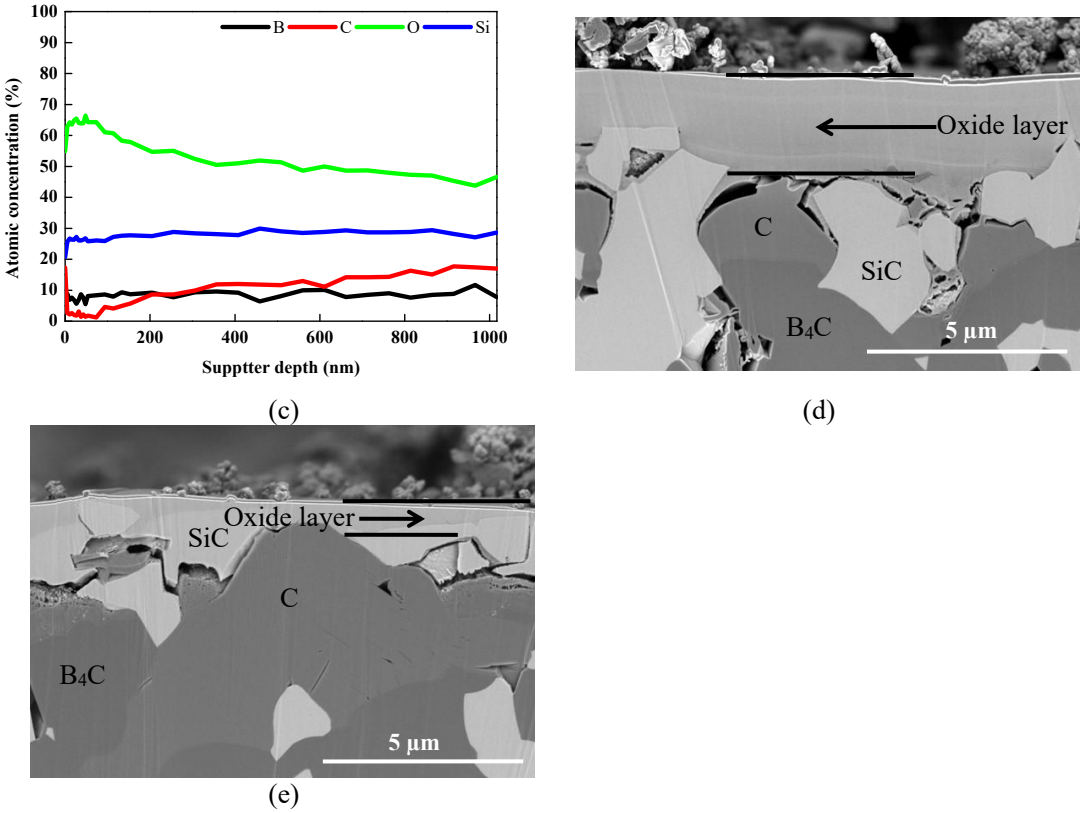

Fig. 3. XPS depth profiles for B, C, O and Si on the surfaces of: (a) BS0, (b) BS1000, (c) BS1200, as well as SEM images of cross-sectional surfaces of: (d) BS1000, (e) BS1200.

Figs. 4-6 illustrated XPS analyses of B_{1s}, Si_{2p}, and C_{1s} of the surfaces of BS0, BS100 and BS1200. The B_{1s} binding energy of 188.5 eV (Fig. 4) can be assigned to B_4C [33], and the Si_{2p} binding energy of 100.3 eV (Fig. 4) can be assigned to SiC [34]. As seen in Fig. 4, the deconvoluted C_{1s} spectra exhibited two peaks at the binding energies of 283.0 and 283.9 eV, which can be assigned to B_4C [35] and SiC [36], respectively. When the B_4C-SiC composite was annealed by 1000 ℃, the deconvoluted B_{1s} spectra of BS1000 exhibited two peaks at binding energies of 192.4 and 193.7 eV (Fig. 5). In comparison of the data of Refs. [37, 38], the peaks at binding energies of 192.4 and 193.7 eV were assigned to B_2O_3 and H_3BO_3, respectively. H_3BO_3 is the main component, and the molar ratio of H_3BO_3 to B_2O_3 is about 10:1. B_2O_3 on the surface of BS1000 cannot be detected by Raman (Fig. 2a) may be attributed to its amorphous nature or less amount. The Si_{2p} binding energy of 103.6 eV (Fig. 5) was assigned to SiO_2 [39], which cannot be detected by Raman (Fig. 2a) was attributed to its amorphous nature. No peak can be observed for C_{1s} in Fig. 5, except the most superficial foreign pollution carbon. When the B_4C-SiC composite was annealed by 1200 ℃, the deconvoluted B_{1s} spectra of BS1200 exhibited two peaks at binding energies of 192.6 and 193.9 eV (Fig. 6), which were assigned to B_2O_3 [37] and H_3BO_3 [38], respectively. Combined with Fig. 3b and Fig. 3c, the B content in BS1200 is significantly lower than that in BS1000, suggesting that the content of H_3BO_3 on the surface of BS1200 is very low, which may be the reason that no H_3BO_3 can be detected on the surface of BS1200 by Raman (Fig. 2a). The deconvoluted Si_{2p} spectra of BS1200 displayed two peaks at binding energies of 100.4 and 103.6 eV (Fig. 6), which can be assigned to SiC [34] and SiO_2 [39], respectively. The deconvoluted C_{1s} spectra of BS1200 exhibited two peaks at binding energies of 283.7 and 284.5 eV (Fig. 6), which can be assigned to SiC [36] and free carbon [40], respectively. Narushima et al. [42] also observed that C was enriched in the borosilicate layer near the oxide/B_4C-(25-60 mol%)SiC composite interface when the composite was oxidized at 800-1500 ℃ because the oxygen partial pressure at the oxide/composite interface was lower than that at the oxide/gas interface, which is consistent with the result of present study. Combined with Fig. 3c, it is very interesting to find that there is no SiC only within about 80 nm from the top

surface, and the SiC content gradually increases to a certain value with the depth increases below 80 nm from the top surface. This suggests that SiC on the surface of the B_4C-SiC composite was not completely oxidized after the composite was annealed at 1200 ℃, which is different from the result of the B_4C-SiC composite being annealed at 1000 ℃, and SiC and SiO_2 coexisted on the surface of BS1200.

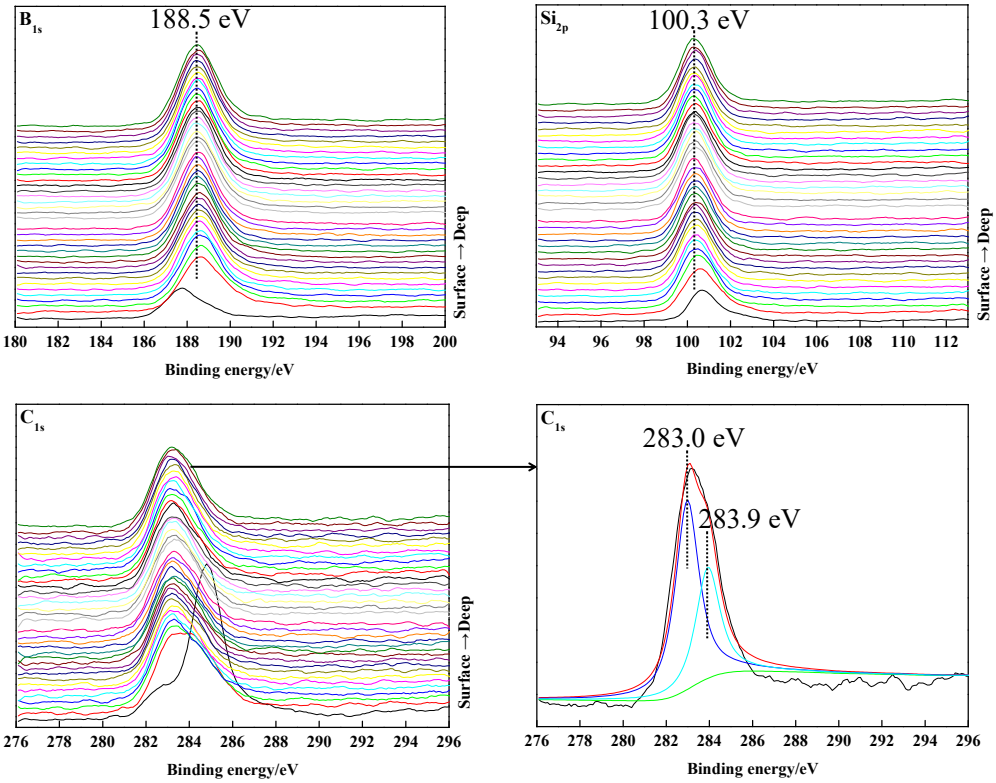

Fig. 4. XPS results of initial surface of BS0.

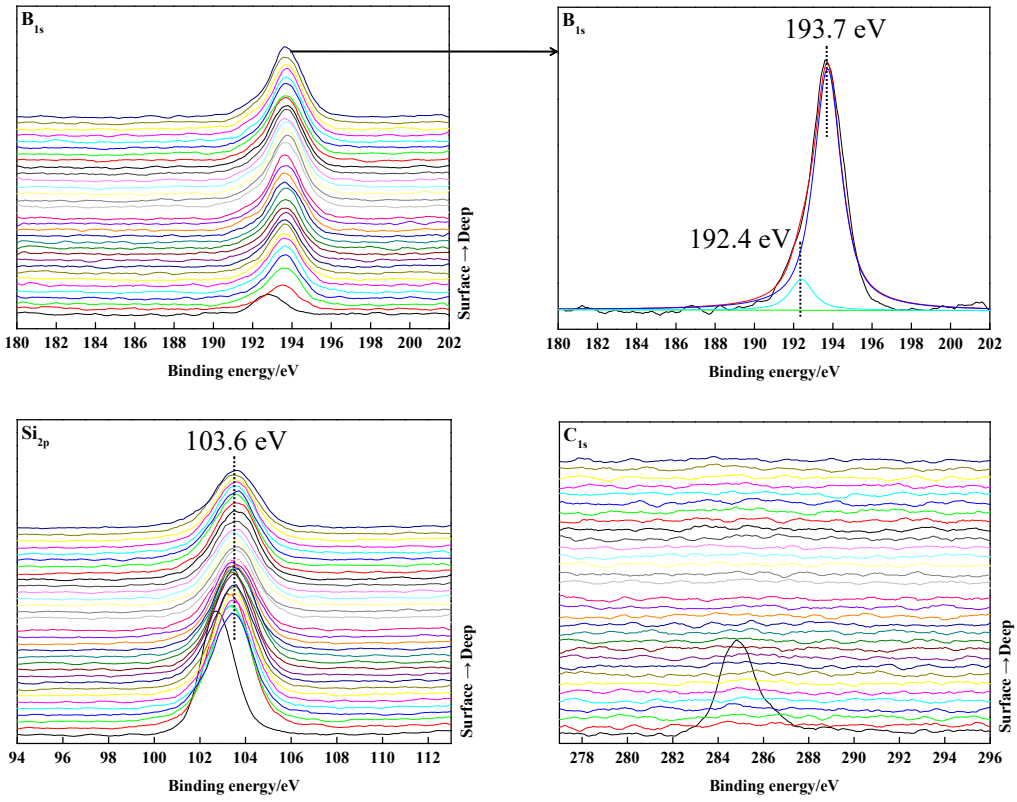

Fig. 5. XPS results of initial surface of BS1000.

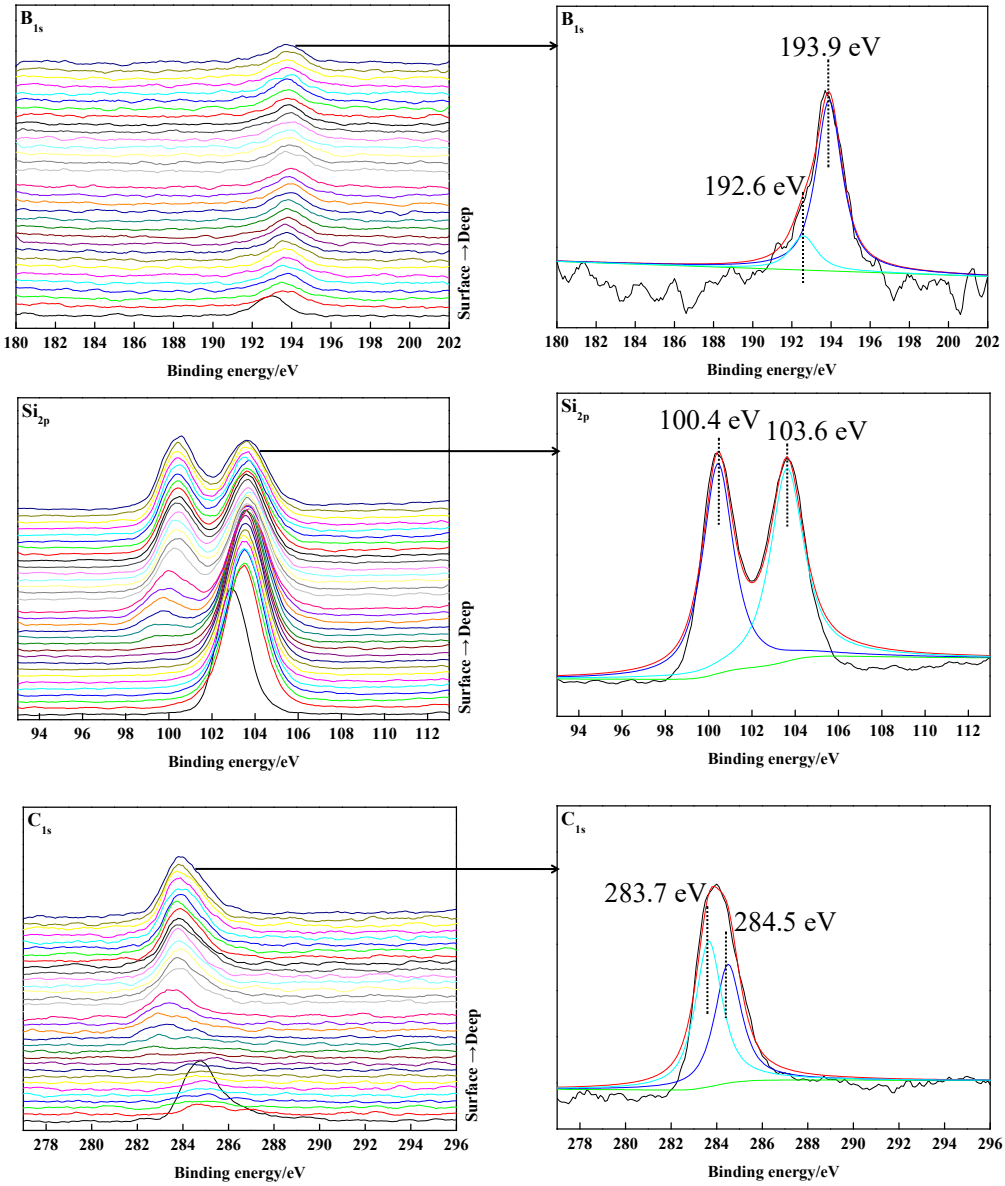

Fig. 6. XPS results of initial surface of BS1200.

Combining the results of Raman spectroscopy (Fig. 2a) and XPS (Figs. 3-6), it can be concluded that the main compositions of initial surface of BS0 are B_4C and SiC; the main compositions of initial surface of BS1000 are H_3BO_3, SiO_2 and slight B_2O_3; while the main compositions of initial surface of BS1200 are SiO_2, SiC, C, and a small amount of H_3BO_3 and B_2O_3.

Fig. 7 provides some representative 2D profiles of the initial surfaces of BS0, BS1000 and BS1200. Fig. 8 shows SEM images of initial surfaces of BS0, BS1000 and BS1200. The average surface roughnesses of BS0, BS1000 and BS1200 are 0.018 μm, 0.190 μm and 0.357 μm, respectively. It can be seen from Fig. 7 and Fig. 8 that the surface roughness of B_4C-SiC composite increased with annealing temperature increasing. On the other hand, a large number of plate-like particles can be seen on the surface of BS1000. It is known that crystalline H_3BO_3 with layered structure usually exists in the form of plate-like particles, combining the results of Raman spectroscopy (Fig. 2a) and XPS (Fig. 5), it can be concluded that these plate-like particles are H_3BO_3 particles. Also, many pores with size of more than 10 μm were formed on the surface of BS1200 due to the vaporization of B_2O_3 and the release of gas formed during the oxidation reactions of B_4C and SiC.

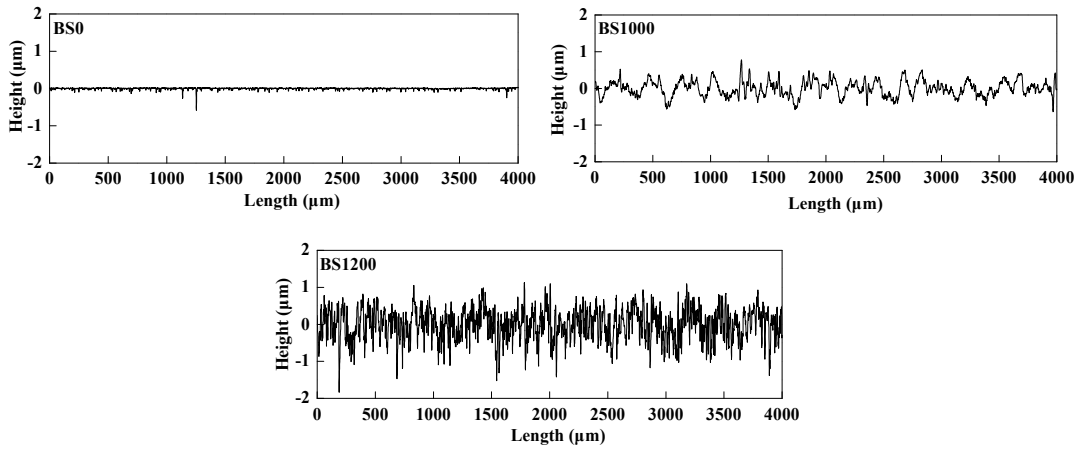

Fig. 7. 2D profiles of the initial surfaces of BS0, BS1000 and BS1200.

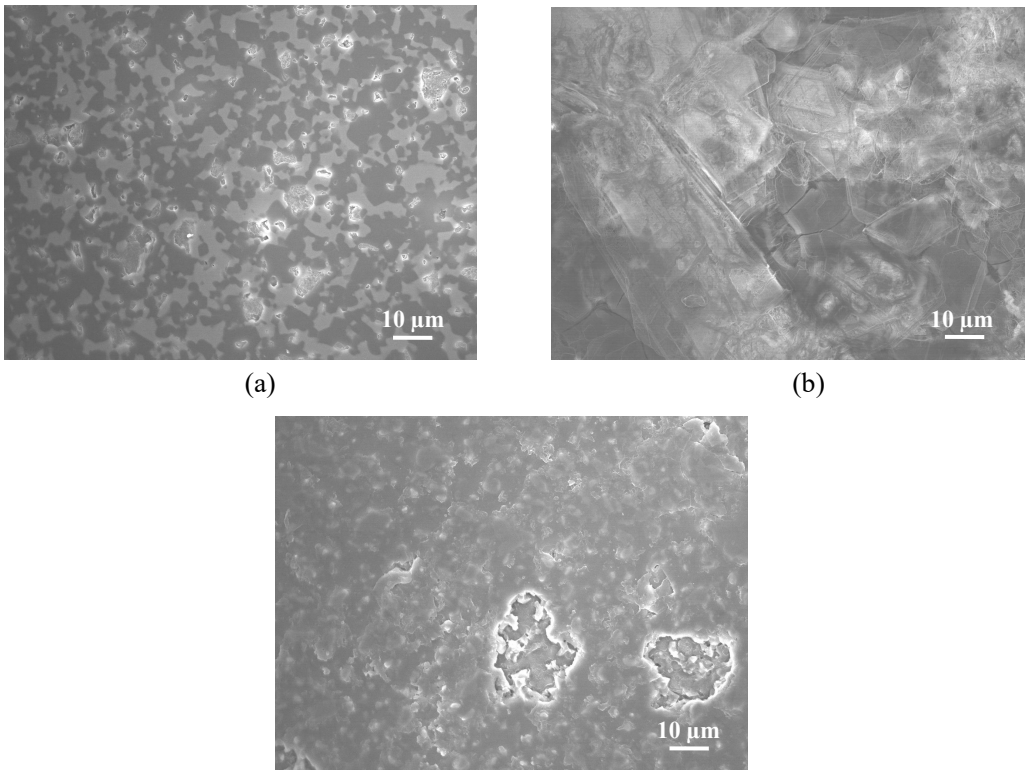

(a) (b)

(c)

Fig. 8. SEM images of initial surfaces of: (a) BS0, (b) BS1000 and (c) BS1200.

For BS0, the main compositions of initial surface are B_4C and SiC. Fig. 9a and Fig. 9b show the SEM image of worn surface of BS0 and elemental distributions of worn surface of BS0. A small amount wear track seemed to be covered with a thin debris layer, whereas the B_4C grains and SiC grains were clearly visible on the wear track where there was no covered debris layer. The elemental distributions analysis of BS0 indicates that the covered debris layer is composed of O rich phase and Si rich phase, and the uncovered wear track is composed of Si rich phase, B rich phase and C rich phase. It can be deduced that the thin debris layer mainly consists of SiO_2, which were formed by tribochemical reaction during the sliding, and the uncovered surface consists of B_4C and SiC. Further, some brittle fracture or grain pull-out was observed on uncovered wear track of BS0. It is reported that the SiO_2 film formed by tribochemical reaction is beneficial to reduce friction for sliding interface of SiC ceramics [41], however, the debris layer on the worn surface of BS0 is not a continuous, fully covered layer. Therefore, the friction coefficient of BS0 was controlled by the simultaneous occurrence and competition of debris layer and

brittle fracture. In our previous work [16,17], no debris layer and no brittle fracture were detected on the worn surface of B_4C-SiC composite sliding against SiC ball at the load of 5 N when the sliding distance was 100 m. In the present study, when the sliding distance was set to 1000 m, some brittle fracture occurred, which may be attributed to the increased time-dependent tensile stresses induced by the plasticity in polycrystalline ceramics. When the stress intensity factors acting on the flaws under the contact reach the grain boundary toughness, grain boundary fracture occurs [42].

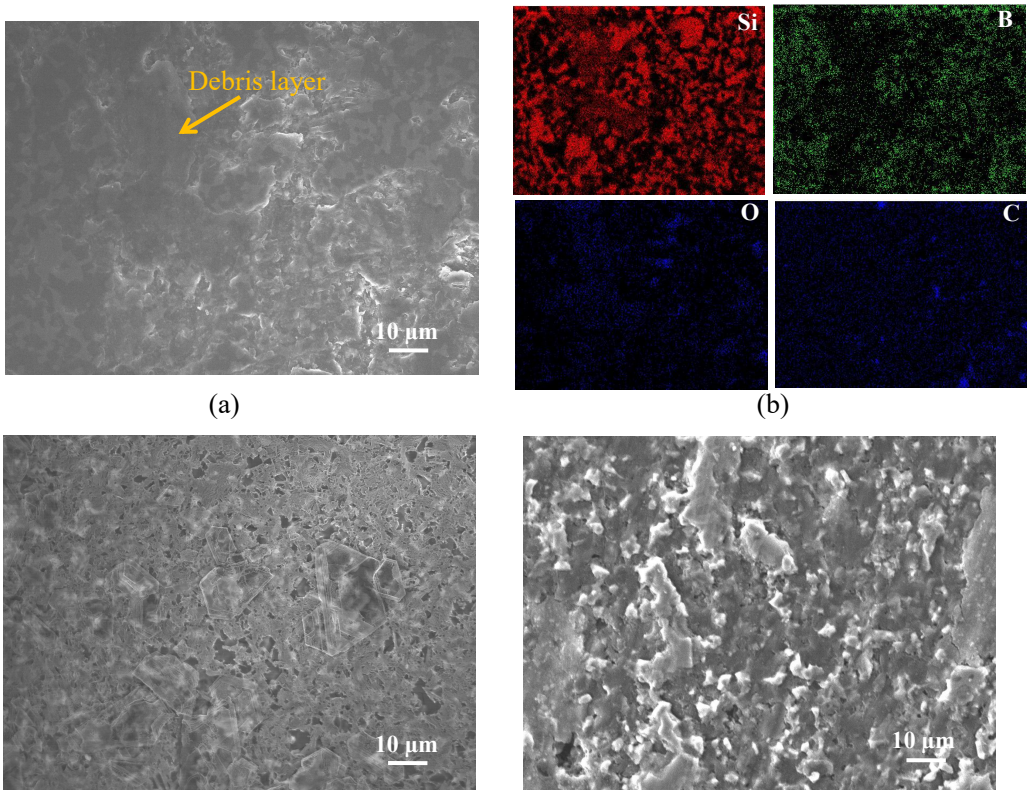

Fig. 9. SEM images of worn surfaces of: (a) BS0, (c) BS1000, (d) BS1200, and (b) elemental distributions of Fig. 9 (a).

For BS1000, the main compositions of initial surface are H_3BO_3, SiO_2 and slight B_2O_3. During annealing at 1000 °C, the exposed surface of B_4C-SiC composite underwent oxidation. B, Si and C atoms at or near the surface became thermally active and highly energetic. They can react with O_2 in surrounding air to form B_2O_3, SiO_2 and CO_2. When the specimen was cooled to room temperature, B_2O_3 can react with moisture in air spontaneously to form H_3BO_3 layer owing to a negative Gibbs free energy of reaction. This reaction can be expressed as follow:

$$B_2O_3\,(s)+3H_2O\,(g)\rightarrow 2H_3BO_3\,(s) \quad \Delta G^{\circ}=-69.9\ kJ/mol$$ [32]

Erdemir et al. [22,29,43] reported that the formation of H_3BO_3 on the B_4C ceramics was beneficial to reduce friction coefficient for B_4C ceramics sliding against ZrO_2 pin or 440C steel ball because H_3BO_3 has a layered structure that can reduce shear force for sliding interface. The layers composed of strongly bonded B, O and H atoms by covalent, ionic and hydrogen bonds, which are parallel to the basal plane, held together by weak van der Waal forces. These plate-like crystallites of H_3BO_3 can align themselves parallel to the direction of relative motion under shear force; once so aligned, these layers slide over one another with relative ease to provide low friction. Further, Mutlu et al. [44,45] pointed out the addition of H_3BO_3 into phenolic composites could supply stable friction coefficient. Meanwhile, SiO_2 formed by annealing owing to oxidation of SiC can also reduce friction for B_4C-SiC composite [23]. Therefore, the lower friction coefficient of BS1000 is ascribed to the formation of thick oxide layer. Fig. 9c shows the SEM image of worn surface of BS1000. The crystalline H_3BO_3 can still be observed on the worn surface of BS1000, which can also be demonstrated by Raman result (Fig. 2b). This means the effect

of self-lubrication can be maintained for the total sliding period. Although the surface roughness of BS1000 was increased after the annealing, the change of the surface chemical composition is the key reason for decreasing the friction coefficient of B_4C-SiC composite.

For BS1200, the main compositions of initial surface are SiO_2, SiC, C, and a small amount of H_3BO_3 and B_2O_3. On the one hand, the amount of H_3BO_3 was too little to lubricant sliding interface, and SiC existed on the surface of BS1200. Guicciardi et al. [46] stated that self-mated SiC ceramics showed a higher friction coefficient than in the case of not self-mated. Kovalčíková et al. [47] found that the friction coefficient of tribopair with chemical similarity was higher than that of the tribopair without chemical similarity. As a result, SiC existed on the surface of BS1200 may induce higher friction coefficient by chemical similarity. On the other hand, the initial surface roughness was significantly increased after annealing, which may be caused by the formation of a number of pores. Fig. 9d shows the the SEM image of worn surface of BS1200. It can be seen that the worn surface of BS1200 was rather rough. Therefore, the higher friction coefficient of BS1200 may be attributed to the low amount of H_3BO_3 formed by annealing, to the presence of SiC on the surface, which may cause chemical similarity between the disk and the mating SiC ball, and to the rough worn surface.

As a whole, B_4C-SiC composite can obtain lower friction coefficient by self-lubrication when the composite is annealed at 1000 ℃ in air because of the formation of thick oxide layer, which mainly consists of H_3BO_3 and SiO_2. However, B_4C-SiC composite exhibited significantly increased friction coefficient after annealing at 1200 ℃ because the amount of H_3BO_3 was too little to lubricant sliding interface, SiC existed on the surface of BS1200, resulting in the chemical similarity between the disk and the mating SiC ball which can increase friction, and the worn surface was rather rough. Finally, it is very interesting to find that both the single-phase B_4C ceramics [32] and the single-phase SiC ceramics [48] can obtain lower friction coefficients after annealing at 1200 ℃ in air than those of the single-phase B_4C ceramics without annealing and the single-phase SiC ceramics without annealing, respectively, however, the B_4C-SiC composite cannot obtain lower friction coefficient after annealing at 1200 ℃ in air than that of the B_4C-SiC composite without annealing.

Fig. 10 shows the specific wear rates of disks (BS0, BS1000 and BS1200), and balls mated to the corresponding disks of B_4C-SiC composite. It completes the information about the wear damage of the tribopairs. Fig. 11 reveals the optical micrographs of wear scars on the mating SiC balls. Although the specific wear rate of B_4C-SiC composite increased as the annealing temperature increased, which is attributed to the formation of oxide layers, the specific wear rate of mating ball showed the minimum value when sliding against BS1000. It can be seen from Fig. 11a and Fig. 11c that obvious grooves were formed on the wear scars of mating SiC balls of BS0 and BS1200, which means that there were hard wear particles on the sliding interfaces of BS0/SiC tribopair and BS1200/SiC tribopair. However, no grooves were observed on the wear scar of mating SiC ball of BS1000, which suggests that there were no hard wear particles on the sliding interface of BS1000/SiC tribopair. Therefore, the formation of thick oxide layer on the surface of BS1000 could prevent the formation of hard wear particles on the sliding interface and could reduce the wear rate of mating SiC ball.

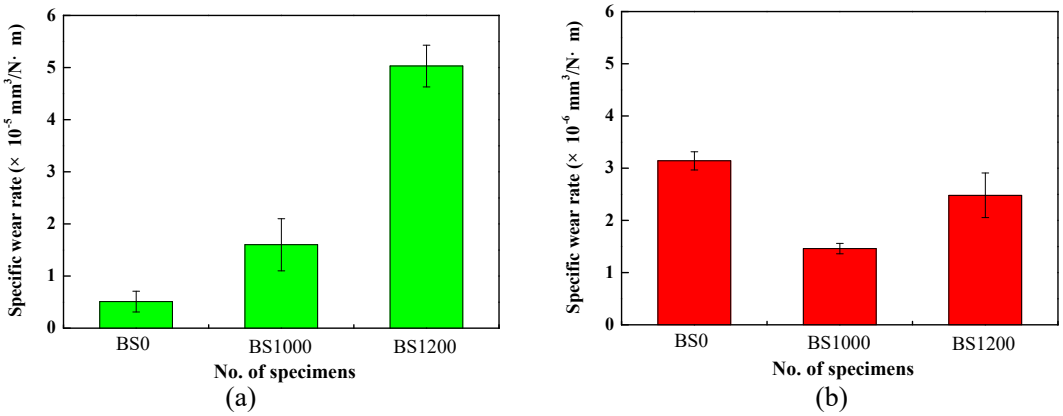

Fig. 10. Specific wear rates of disks (a), and balls mated to the corresponding disks of B_4C-SiC composite (b).

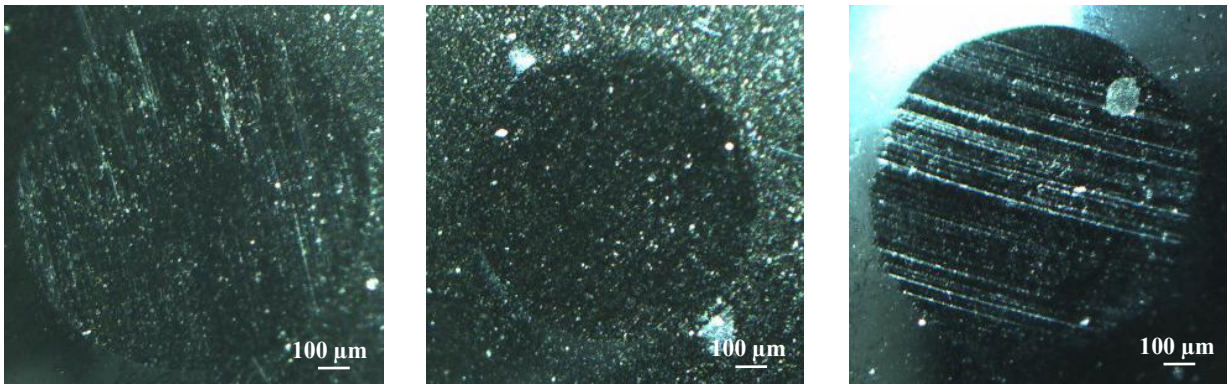

(a) (b) (c)

Fig. 11. Optical micrographs of wear scars on the mating SiC balls against: (a) BS0, (b) BS1000 and (c) BS1200.

10.4. Conclusions

A B_4C-SiC composite (BS0) and two B_4C-SiC composites followed by annealing at 1000 ℃ and 1200 ℃ for 1 h in air (BS1000 and BS1200), respectively, were prepared. The tribological properties of the three composites were evaluated by sliding against SiC balls at room temperature under unlubricated conditions. The following results were drawn:

(1) The B_4C-SiC composite can obtain lower friction coefficient by annealing at 1000 ℃, whereas the friction coefficient of B_4C-SiC composite annealed at 1200 ℃ was significantly increased. The cause for this difference was ascribed to different surface compositions after annealing.

(2) The B_4C-SiC composite annealed at 1000 ℃ had lower friction coefficient than the B_4C-SiC composite without annealing, indicating that suitable annealing temperature could cause self-lubrication for the B_4C-SiC composite. The mechanism of self-lubrication was the formation of H_3BO_3 layer.

10.5. References

[1] X. Q. Li, Y. M. Gao, S. Z. Wei, Q. X. Yang, Z. C. Zhong. Dry sliding tribological properties of self-mated couples of B_4C-hBN ceramic composites. Ceramics International,2017,43:162-166.

[2] W. Zhang, S. Yamashita, H. Kita. Progress in pressureless sintering of boron carbide ceramics- a review. Advances in Applied Ceramics,2019,118(4):222-239.

[3] F. Rubino, M. Pisaturo, A. Senatore, P. Carlone, T. S. Sudarshan. Tribological characterization of SiC and B_4C manufactured by plasma pressure compaction. Journal of Materials Engineering & Performance,2017,26(7):1-12.

[4] S. Gupta, S. K. Sharma, B. V. M. Kumar, Y. W. Kim. Tribological characteristics of SiC ceramics sintered with a small amount of yttria. Ceramics International,2015,41(10):14780-14789.

[5] W. Zhang, S. Yamashita, H. Kita. Progress in tribological research of SiC ceramics in unlubricated sliding-A review. Materials & Design,2020,190:108528.

[6] I. S. Han, K. S. Lee, D. W. Seo, S. K. Woo. Improvement of mechanical properties in RBSC by boron carbide addition. Journal of Materials Science Letters,2002,21(9):703-706.

[7] Y. G. Tkachenko, V. F. Britun, É. V. Prilutskii, D. Z. Yurchenko, G. A. Bovkun. Structure and properties of B_4C-SiC composites. Powder Metallurgy and Metal Ceramics,2005,44(3-4):196-201.

[8] H. Sano, G. B. Zheng, Y. Uchiyama. Effect of SiC particle size on anti-oxidation behavior of C/B_4C/SiC composite. Materials Science Forum,2010,658:308-311.

[9] B. M. Moshtaghioun, A. L. Ortiz, D. Gómez-García, A. Domínguez-Rodríguez. Toughening of super-hard ultra-fine grained B_4C densified by spark-plasma sintering via SiC addition. Journal of the European Ceramic Society,2013,33(8):1395-1401.

[10] Y. L. Zhang, X. G. Song, G. J. Li, Y. M. Zhang. Oxidation behavior research of the SiC/B_4C multiphase ceramics. Applied Mechanics and Materials,2015,727-728:288-291.

[11] W. Zhang, S. Yamashita, T. Kumazawa, F. Ozeki, H. Hyuga, W. Norimatsu, H. Kita. A study on formation mechanisms of relief structure formed in situ on the surface of ceramics. Ceramics International,2019,45(17), 23143-23148.

[12] F. Findik. Latest progress on tribological properties of industrial materials. Materials & Design,2014,57:218-244.

[13] U. Soy, A. Demir, F. Findik. Friction and wear behaviors of Al-SiC-B_4C composites produced by pressure infiltration method. Industrial Lubrication and Tribology,2011,63(5):387-393.

[14] N. P. Wasekar, L. Bathini, L. Ramakrishna, D. S. Rao, G. Padmanabham. Pulsed electrodeposition, mechanical properties and wear mechanism in Ni-W/SiC nanocomposite coatings used for automotive applications. Applied Surface Science,2020,527:146896.

[15] W. Zhang, S. Yamashita, T. Kumazawa, F. Ozeki, H. Hyuga, H. Kita. Effect of nanorelief structure formed in situ on tribological properties of ceramics in dry sliding. Ceramics International,2019,45(11):13818-13824.

[16] W. Zhang, S. Yamashita, H. Kita. Tribological properties of SiC-B_4C ceramics under dry sliding condition. Journal of the European Ceramic Society,2020,40(8):2855-2861.

[17] W. Zhang, S. Yamashita, H. Kita. Effects of load on tribological properties of B_4C and B_4C-SiC ceramics against SiC ball. Journal of Asian Ceramic Societies,2020,8(3):586-596.

[18] W. Zhang, S. Yamashita, T. Kumazawa, F. Ozeki, H. Hyuga, H. Kita. Influence of surface roughness parameters and surface morphology on friction performance of ceramics. Journal of the Ceramic Society of Japan,2019,127(11):837-842.

[19] W. Zhang. A review of tribological properties for boron carbide ceramics. Progress in Materials Science,2021,116,100718.

[20] R. Sedlák, A. Kovalčíková, J. Balko, P. Rutkowski, A. Dubiel, D. Zientara, V. Girman, E. Múdra, J. Dusza. Effect of graphene platelets on tribological properties of boron carbide ceramic composites. Int. Journal of Refractory Metals and Hard Materials,2017,65:57-63.

[21] Y. Zhou, K. Hirao, Y. Yamauchi, S. Kanzaki. Tribological properties of silicon carbide and silicon carbide-graphite composite ceramics in sliding contact. Journal of the American Ceramic Society, 2003,86(6):991-1002.

[22] A. Erdemir, C. Bindal, G. R. Fenske. Formation of ultralow friction surface films on boron carbide. Applied Physics Letters,1996,68(12):1637-1639.

[23] Y. Yamamoto, A. Ura. Influence of interposed wear particles on the wear and friction of silicon carbide in different dry atmospheres. Wear,1992,154(1):141-150.

[24] D. R. Tallant, T. L. Aselage, A. N. Campbell, D. Emin. Boron carbide structure by Raman spectroscopy. Physical Review B Condensed Matter,1989,40(8):5649-5656.

[25] U. Kuhlmann, H. Werheit. Improved Raman effect studies on boron carbide($B_{4.3}C$). Physica Status Solidi(B),1993,175:85-92.

[26] T. Narushima, T. Goto, M. Maruyama, H. Arashi, Y. Iguchi. Oxidation of boron carbide-silicon carbide composite at 1073 to 1773K. Materials Transactions,2003,44(3):401-406.

[27] X. Q. Yan, W. J. Li, T. Goto, M. W. Chen. Raman spectroscopy of pressure-induced amorphous boron carbide. Applied Physics Letters,2006,88:131905.

[28] C.Kunka, A. Awasthi, G. Subhash. Evaluating boron-carbide constituents with simulated Raman spectra.

Scripta Materialia,2017,138:32-34.
[29] A. Erdemir, C. Bindal, C. Zuiker, E. Savrun. Tribology of naturally occurring boric acid films on boron carbide. Surface and Coatings Technology,1996,86-87(2):507-510.
[30] W. Zhang, S. Yamashita, T. Kumazawa, F. Ozeki, H. Hyuga, H. Kita. Study on friction behavior of SiC-B_4C composite ceramics after annealing. Industrial Lubrication and Tribology,2020,72(5):673-679.
[31] S. Nakashima, H. Harima. Raman investigation of SiC polytypes. Physica Status Solidi A,1997,162(1):39-64.
[32] W. Zhang, S. Yamashita, T. Kumazawa, F. Ozeki, H. Hyuga, H. Kita. Tribological properties of B_4C ceramics prepared by pressureless sintering and annealed at different temperatures. Tribology Transactions,2020,63(4):672-82.
[33] X. Q. Cao, L. L. Shang, Y. M. Liang, G. G. Zhang, Z. B. Lu, Q. J. Xue. The tribological performances of the boron carbide films tested under wet air and wet N_2 conditions. Tribology Letters,2019,67(3):70.
[34] A. Tabata, S. Fujii, Y. Suzuoki, T. Mizutani, M. Ieda. X-ray photoelectron spectroscopy (XPS) of hydrogenated amorphous silicon carbide (a-Si_xC_{1-x}: H) prepared by the plasma CVD method. Journal of Physics D: Applied Physics,1990,23(3):316-320.
[35] P. D. Cuong, H. S. Ahn, E. S. Yoon, K. H. Shin. Effects of relative humidity on tribological properties of boron carbide coating against steel. Surface and Coatings Technology,2006,201(7):4230-4235.
[36] L. Muehrhoff, W. J. Choyke, M. J. Bozack, John T. Yates, Jr.. Comparative electron spectroscopic studies of surface segregation on SiC(0001) and SiC(0001). Journal of Applied Physics,1986,60(8):2842-2853.
[37] A. R. Burke, C. R. Brown, W. C. Bowling, J. E. Glaub, D. Kapsch, C. M. Love, R. B. Whitaker, W. E. Moddeman. Ignition mechanism of the titanium-boron pyrotechnic mixture. Surface and Interface Analysis,1988,11:353-358.
[38] B. R. Strohmeier. Surface characterization of aluminum foil annealed in the presence of ammonium fluoborate. Applied Surface Science,1989,40(3):249-263.
[39] Y. Tanizawa, T. Suzuki. Effects of silicate ions on the formation and transformation of calcium phosphates in neutral aqueous solutions. Journal of the Chemical Society, Faraday Transactions, 1995,91(19):3499-3503.
[40] W. F. A. Besling, A. Goossens, B. Meester, J. Schoonman. Laser-induced chemical vapor deposition of nanostructured silicon carbonitride thin films. Journal of Applied Physics,1998,83(1):544-553.
[41] V. S. R. Murthy, H. Kobayashi, S. Tsurekawa, N. Tamari, T. Watanabe, K. Kato. Influence of humidity and doping element on the friction and wear of SiC in unlubricated sliding. Tribology International,2004,37(5):353-364.
[42] O. B. López, A. L. Ortiz, F. Guiberteau. Sliding-wear-resistant liquid-phase-sintered SiC processed using α-SiC staring powders. Journal of the American Ceramic Society,2007,90(2):541-545.
[43] A. Erdemir, O.L. Eryilmaz, G.R. Fenske. Self-replenishing solid lubricant films on boron carbide. Surface Engineering,1999,15(4):291-295.
[44] I. Mutlu, C. Oner, F. Findik. Boric acid effect in phenolic composites on tribological properties in brake linings. Materials & Design,2007,28(2):480-487.
[45] I. Mutlu, C. Oner, I. Cevik, F. Findik. Wear performance of some phenolic composites with boric acid. Industrial Lubrication and Tribology,2007,59(1):38-45.
[46] Guicciardi S, Sciti D, Melandri C, Pezzotti G. Dry sliding wear behavior of nano-sized SiC pins against SiC and Si_3N_4 discs. Wear,2007,262(5-6):529-535.
[47] A. Kovalčíková, P. Kurek, J. Balko, J. Dusza, P. Šajgalík, M. Mihaliková. Effect of the counterpart material on wear characteristics of silicon carbide ceramics. Int. Journal of Refractory Metals and Hard Materials,2014,44:12-18.
[48] W. Zhang, S. Yamashita, H. Kita. Self lubrication of pressureless sintered SiC ceramics,2020,9(6):12880-12888.

Chapter 11
Study on friction behavior of SiC-B_4C composite ceramics after annealing

This study aims to investigate the friction behavior of SiC-B_4C composite ceramics treated by annealing in air sliding against SiC balls. The dry sliding tests were performed with a ball-on-disk tribometer in ambient air condition. Analysis of friction coefficient, phase compositions of the surfaces, morphologies of worn surfaces of disks and wear scars of balls and surface profiles of wear tracks for disks were carried out using Raman spectroscope, microscope and surface profilometer. The results show that a self-lubricating layer with the main composition of H_3BO_3 was successfully fabricated on the surface of SiC-B_4C composite ceramics by the annealing treatment in air. When the mass fraction of SiC is more than that of B_4C, SiC-B_4C composite ceramics show higher friction coefficients, the values of which are 0.38 for 80 wt%SiC-20 wt%B_4C and 0.72 for 60 wt%SiC-40 wt%B_4C, respectively. SiC-B_4C composite ceramics show lower friction coefficients when the mass fraction of B_4C is more than that of SiC. The low friction coefficients of 40 wt%SiC-60 wt%B_4C composite ceramics (0.16) and 20 wt%SiC-80 wt%B_4C composite ceramics (0.20) are attributed to the formation of a sufficient amount of H_3BO_3 layer, rather than the layer of silicon oxides. This study will help to understand the friction behavior of SiC-B_4C composite ceramics with different ratios of SiC to B_4C treated by annealing in air.

Contents

11.1. Introduction

Monolithic B_4C ceramics and monolithic SiC ceramics have drawn considerable attention in the industrial applications owing to their outstanding performance, including high melting point, high hardness, low density, high elastic modulus, and high chemical resistance [1-3]. Recently, self-healing on fractured surfaces [4] and unprecedented piezoresistance properties of SiC [5] are discovered, which is a breakthrough and milestone contribution to design and fabricate high performance devices. In addition, a novel scratching approach was developed on a developed setup at nanoscale depth of cut and m/s, which opens a new route to investigate the tribological mechanisms of abrasive machining [6]. Soy et al. [7] pointed out that the addition of B_4C, SiC and B_4C/SiC particles can improve friction and wear properties of aluminum casting alloy. Altinkok et al. [8] reported Al_2O_3/SiC particles reinforced aluminium matrix composites can obtain better tribological properties.

Because of low fracture toughness of ceramic materials, the applications of monolithic B_4C ceramics and monolithic SiC ceramics are restricted. Moshtaghioun et al. [9] reported adding 15 wt% SiC into monolithic B_4C ceramics can improve toughness from 3.5 $MPa \cdot m^{1/2}$ to 5.7 $MPa \cdot m^{1/2}$. Tkachenko et al. [10] and Han et al. [11] found SiC-B_4C composite ceramics reveals higher hardness, fracture toughness and flexural strength than monolithic B_4C ceramics and monolithic SiC ceramics. Sano et al. [12] and Zhang et al. [13] stated that SiC-B_4C composite ceramics has a better oxidation resistance. Therefore, it is considered that SiC-B_4C composite ceramics have wider potential applications than monolithic B_4C ceramics and monolithic SiC ceramics. As a result, the study of properties of SiC-B_4C composite ceramics attracted much attention in the last few years. However, to date, the studies focus on tribological properties of SiC-B_4C composite ceramics are limited [14-17].

Annealing heat treatment in air to form lubricious oxide layer on the surface is an effective way to improve friction behavior for nonoxide ceramics. Tests by Yamamoto and Ura [18] showed that SiO_2 layer was formed on the surface of monolithic SiC ceramics when the SiC ceramics was annealed at 1000 ℃ for 1 h in air. The resulting SiC ceramics had a lower friction coefficient during initial 20 min. Erdemir et al. [19] reported that H_3BO_3 layer was formed on the oxidized surface of monolithic B_4C ceramics via annealing treatment at 800 ℃ for 1 h in air. The frictional test of the resulting B_4C ceramics revealed a low friction coefficient during a long-duration sliding distance. Monolithic SiC ceramics and monolithic B_4C ceramics reveal low friction coefficients after annealing in air, however, there have been no published literatures of annealing effects on friction behavior of SiC-B_4C composite ceramics.

In this study, the aims are to investigate that (i) phase compositions of the surfaces of SiC-B_4C composite ceramics with different ratios of SiC to B_4C after annealing in air; (ii) friction behavior of SiC-B_4C composite ceramics with different ratios of SiC to B_4C treated by annealing; and (iii) self-lubricating mechanisms of annealed SiC-B_4C composite ceramics. This investigation can provide some useful information to self-lubrication of SiC-B_4C composite ceramics.

11.2. Experimental procedures

The raw materials were commercially available powders of SiC (~0.3 μm), of B_4C (~0.8 μm), and of carbon black (~24 nm). Four powder batches were prepared with different compositions. The compositions were 80 wt%SiC-20 wt%B_4C, 60 wt%SiC-40 wt%B_4C, 40 wt%SiC-60 wt%B_4C and 20 wt%SiC-80 wt%B_4C, respectively. All the four powder batches were added additional 3 wt% carbon black as sintering additivies. The powder mixtures were subjected to mix, die pressed followed by cold isostatic pressing, pressureless sintering protected by argon and cool to room temperature. Then the resulting SiC-B_4C composite ceramics with different ratios of SiC to B_4C were annealed in a box furnace at 1000 ℃ for 1 h.

Friction and wear tests were conducted in a ball-on-disk tribometer. SiC balls with diameter of 9.5 mm were used as counterparts. All tests were carried out at room temperature (about 25 ℃) in ambient air with the RH 40-50%. Normal force applied to the SiC balls was 5 N. Tests were preformed at a constant sliding velocity of 0.1 m/s with wear track diameter of 20 mm. The sliding distance was 1000 m.

The phase compositions of the surfaces of SiC-B_4C composite ceramic disks outside and inside the wear tracks were characterized by Raman spectroscope. The morphologies of worn surfaces of SiC-B_4C composite ceramic disks and wear scars of SiC balls were studied using a microscope. Surface profiles of wear tracks for disks were measured by a surface profilometer.

11.3. Results and discussion

The typical friction coefficients with sliding distance for the SiC-B_4C composite after annealing are shown in Figure 1. The friction coefficient of 80 wt%SiC-20 wt%B_4C composite ceramics is 0.38±0.02 at steady state. In the case of 60 wt%SiC-40 wt%B_4C composite, the friction coefficient is 0.72±0.03 at steady state and exhibits a larger fluctuation. The friction coefficients of both 40 wt%SiC-60 wt%B_4C composite and 20 wt%SiC-80 wt%B_4C composite exhibit smaller values than those of 80 wt%SiC-20 wt%B_4C composite and 60 wt%SiC-40 wt%B_4C composite, and the values are 0.16±0.02 and 0.20±0.01, respectively. The friction coefficient of the 40 wt%SiC-60 wt%B_4C composite after annealing is the lowest in the present investigation. As for 20 wt%SiC-80 wt%B_4C composite, the initial friction coefficient reveals large fluctuation in the run-in period, and then the friction coefficient remains relatively stable until the end of the test. In this experiment, SiC-B_4C composites show lower friction coefficients when the mass fraction of B_4C is more than that of SiC.

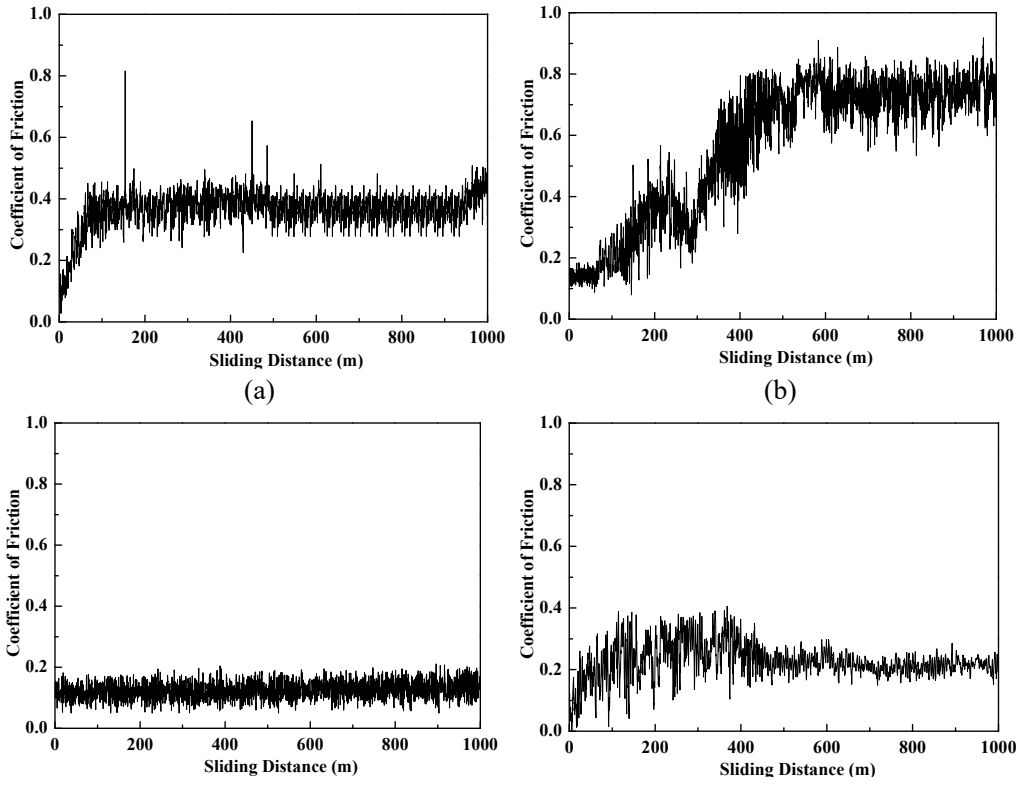

Figure 1 The typical friction coefficients with sliding distance for the SiC-B_4C composite ceramics after annealing: (a) 80 wt%SiC-20 wt%B_4C; (b) 60 wt%SiC-40 wt%B_4C; (c) 40 wt%SiC-60 wt%B_4C; (d) 20 wt%SiC-80 wt%B_4C.

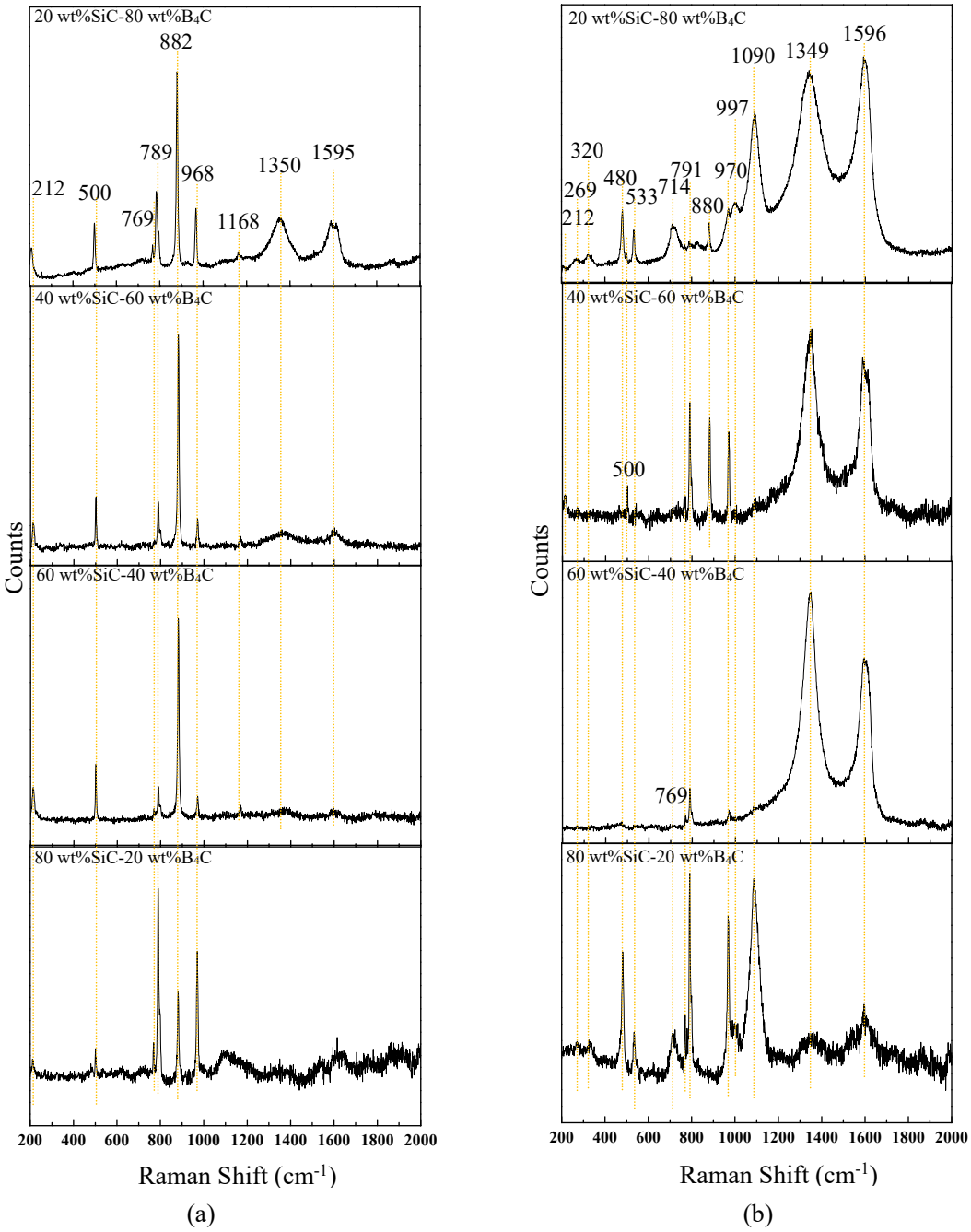

Figure 2 Raman spectrums of the surfaces of SiC-B_4C composite ceramics after annealing: (a) outside the wear tracks of disks; (b) inside the wear tracks of disks.

Figure 2 shows Raman spectrums of the phase compositions of the surfaces of different SiC-B_4C composite ceramic disks outside and inside the wear tracks. For the phase compositions of the surfaces outside the wear tracks for different SiC-B_4C composite ceramics (i.e., initial phase compositions of the surfaces after annealing in air), as shown in Figure 2(a), the Raman peaks at 212 cm^{-1}, 500 cm^{-1}, 882 cm^{-1} appearing in all the four SiC-B_4C composite ceramics as well as at 1168 cm^{-1} appearing in the composite ceramics of 60 wt%SiC-40 wt%B_4C, 40 wt%SiC-60 wt%B_4C and 20 wt%SiC-80 wt%B_4C are in agreement with the Raman shift of H_3BO_3 [19, 20]. The Raman peaks at 769 cm^{-1}, 789 cm^{-1} and 968 cm^{-1} appearing in all the four SiC-B_4C composite ceramics are in agreement with the Raman shift of SiC [21]. Further, the Raman spectra of two broad peaks centered at 1350 cm^{-1} and 1595 cm^{-1} are in agreement with the characteristic Raman bands of carbon [22]. For the phase compositions of the surfaces inside the wear tracks for different SiC-B_4C composite ceramics, as shown in Figure 2(b), the Raman

peaks at 212 cm^{-1}, 500 cm^{-1} and 880 cm^{-1} appearing in the composite ceramics of 40 wt%SiC-60 wt%B_4C and 20 wt%SiC-80 wt%B_4C are in agreement with the Raman shift of H_3BO_3 [19]. The Raman peaks at 269 cm^{-1}, 320 cm^{-1}, 480 cm^{-1}, 533 cm^{-1}, 714 cm^{-1}, 997 cm^{-1}, 1090 cm^{-1} appearing in the composite ceramics of 80 wt%SiC-20 wt%B_4C and 20 wt%SiC-80 wt%B_4C are in agreement with the Raman shift of B_4C [23, 24]. The Raman peaks at 769 cm^{-1}, 791 cm^{-1} and 970 cm^{-1} appearing in all the four SiC-B_4C composite ceramics are in agreement with the Raman shift of SiC [21]. The Raman peaks at 1349 cm^{-1} and 1596 cm^{-1} are in agreement with the characteristic Raman bands of carbon [22].

For all the four SiC-B_4C composite ceramics, H_3BO_3 and SiC are the main phase compositions after the annealing. It can be deduced that the surfaces of B_4C grains are oxidized to H_3BO_3 during the annealing. However, silicon oxides were not detected after the four SiC-B_4C composite ceramics were treated by annealing. One of the possible reasons is that SiC has better oxidation resistance than B_4C so that SiC was not oxidized during the annealing. The other possible reason is that the the oxide layer of SiC grains is too thin to be detected by Raman spectroscope. When the content of B_4C of composite ceramics is 40% or more, carbon is observed as a annealed product. C may result from the residual C after the oxidation of B atoms of B_4C. Further, the C amount in the phase compositions of the initial surfaces after annealing is gradually increased with the increase of B_4C content in the SiC-B_4C composite ceramics.

As to the 80 wt%SiC-20 wt%B_4C composite ceramics treated by annealing, the phase compositions of the worn surface after dry sliding are B_4C, SiC and C. Although H_3BO_3 layer is considered to be effective to reduce friction between sliding surfaces because of its layered structure, the amount of H_3BO_3 layer formed is expected to be not enough to maintain the low friction because the content of B_4C in the SiC-B_4C composite ceramics is only 20 wt%. Therefore, friction coefficient exhibited a low value (0.3) only within the initial sliding distance of 75 m. The friction coefficient is increased after the H_3BO_3 layer is worn out and remains relatively stable until the end of test.

As to the 60 wt%SiC-40 wt%B_4C composite ceramics treated by annealing, the phase compositions of the worn surface after dry sliding are SiC and C. Similarly, the friction coefficient is increased when the H_3BO_3 layer is worn away. However, the content of B_4C in the composite ceramics is 40 wt%, which is more than that in the 80 wt%SiC-20 wt%B_4C composite ceramics, resulting in higher amount of H_3BO_3 layer formed. Therefore, friction coefficient of the 60 wt%SiC-40 wt%B_4C composite ceramics exhibited a low value (0.3) within the initial sliding distance of 200 m, which is longer than that of the 80 wt%SiC-20 wt%B_4C composite ceramics. Compared with the friction coefficient of the 80 wt%SiC-20 wt%B_4C composite, the friction coefficient of the 60 wt%SiC-40 wt%B_4C composite in the steady state is much larger. The larger friction coefficient of 60 wt%SiC-40 wt%B_4C composite may be attributed to greater adhesion between the SiC ball and the 60 wt%SiC-40 wt%B_4C composite. The worn surface of the 80 wt%SiC-20 wt%B_4C composite is composed of B_4C and SiC in addition to C after the H_3BO_3 layer is worn out, whereas the worn surface of the 60 wt%SiC-40 wt%B_4C composite is composed of SiC in addition to C after the H_3BO_3 layer is worn out. It is well known that SiC is softer than B_4C, thus the real contact area between the counterbody of SiC ball and the 60 wt%SiC-40 wt%B_4C composite is larger than that of between the counterbody of SiC ball and the 80 wt%SiC-20 wt%B_4C composite. The larger real contact area leads to the greater adhesion, causing higher friction coefficient. Further, the chemical similarity between the worn surface of 60 wt%SiC-40 wt%B_4C composite and the counterbody of SiC ball may also be one of the reasons for higher friction coefficient.

As to the 40 wt%SiC-60 wt%B_4C composite ceramics treated by annealing and 20 wt%SiC-80 wt%B_4C composite ceramics treated by annealing, both of which have low friction coefficients, the H_3BO_3 layers still exist on the worn surfaces after dry sliding, as shown in Figure 2. The low friction coefficients of the two ceramics during the total sliding distance are attributed to the existence of H_3BO_3 layers at the sliding interfaces, which didn't disappear at the end of tests. Compared with the friction coefficient of 20 wt%SiC-80 wt%B_4C composite,

40 wt%SiC-60 wt%B_4C composite has a sightly lower value of friction coefficient. The phase compositions of the worn surfaces after dry sliding between 40 wt%SiC-60 wt%B_4C composite and 20 wt%SiC-80 wt%B_4C composite are different. B_4C phase is not detected in the phase compositions of the worn surface of 40 wt%SiC-60 wt%B_4C composite, which means H_3BO_3 layer was not worn out during the dry sliding. However, B_4C phase is detected in the phase compositions of the worn surface of 20 wt%SiC-80 wt%B_4C composite. The content of B_4C in the 20 wt%SiC-80 wt%B_4C composite is more than that in the 40 wt%SiC-60 wt%B_4C composite, resulting in higher amount of H_3BO_3 formed. It is known that the atomic layers of H_3BO_3 with layered structure are held together by the weak van der Waal forces, thus, the hardness of H_3BO_3 is very low. The hardness of SiC-B_4C composite ceramics treated by annealing decreases with the increase of amount of H_3BO_3 formed. The higher hardness of 40 wt%SiC-60 wt%B_4C composite than that of 20 wt%SiC-80 wt%B_4C composite can be demonstrated by the wear scar diameters of their mating balls. The wear scars of mating balls against 40 wt%SiC-60 wt%B_4C composite and against 20 wt%SiC-80 wt%B_4C composite are shown in Figure 3. The wear scar diameters of mating balls against 40 wt%SiC-60 wt%B_4C composite and against 20 wt%SiC-80 wt%B_4C composite are 1040 μm and 838 μm, respectively. The higher hardness of 40 wt%SiC-60 wt%B_4C composite results in a larger wear scar diameter of the mating ball. The lower hardness of 20 wt%SiC-80 wt%B_4C composite caused a greater, faster wear of H_3BO_3 layers than that of 40 wt%SiC-60 wt%B_4C composite. Although the wear track of 20 wt%SiC-80 wt%B_4C composite is narrower than that of 40 wt%SiC-60 wt%B_4C composite according to Figure 4, the depth of wear track of 20 wt%SiC-80 wt%B_4C composite is deeper than that of 40 wt%SiC-60 wt%B_4C composite, as shown in Figure 5. As a result, some B_4C grains in the 20 wt%SiC-80 wt%B_4C composite ceramics are exposed to the sliding interface after the H_3BO_3 layer is worn off. The exposed B_4C grains has been detected by the Raman spectroscope, as shown in Figure 2. Because some B_4C grains have been exposed to the sliding interface, the friction coefficient of 20 wt%SiC-80 wt%B_4C composite ceramics is slightly higher than that of 40 wt%SiC-60 wt%B_4C composite ceramics.

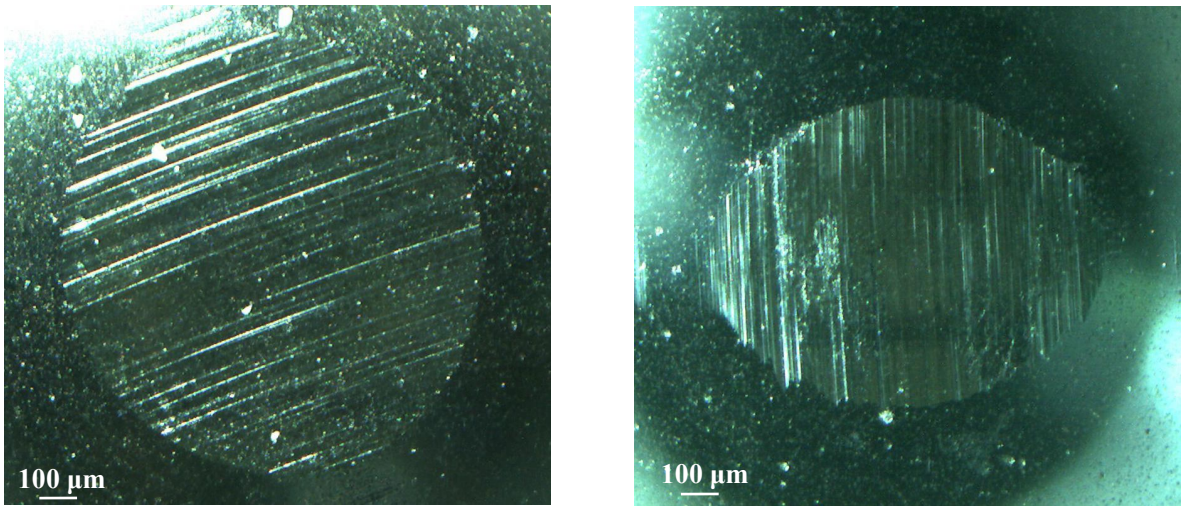

(a) (b)

Figure 3 Wear scars of mating balls: (a) against 40 wt%SiC-60 wt%B_4C composite ceramics; (b) against 20 wt%SiC-80 wt%B_4C composite ceramics.

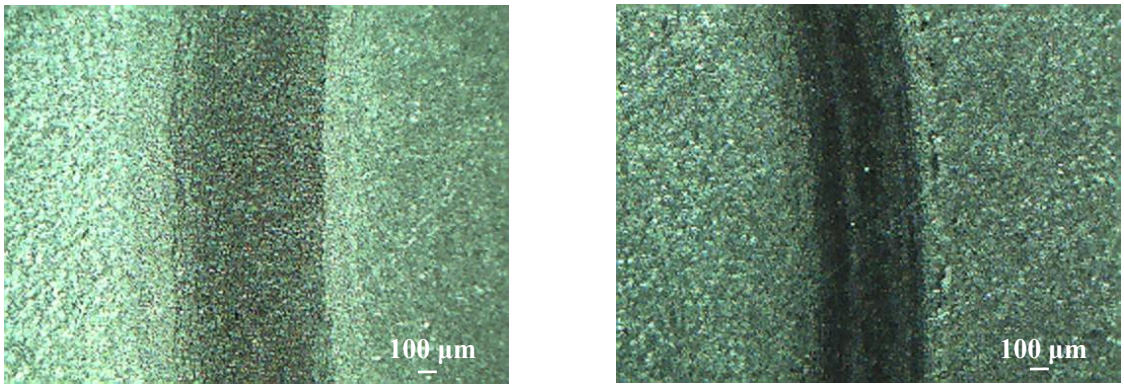

(a) (b)

Figure 4 Microscopic morphologies of wear tracks: (a) 40 wt%SiC-60 wt%B_4C composite ceramics; (b) 20 wt%SiC-80 wt%B_4C composite ceramics.

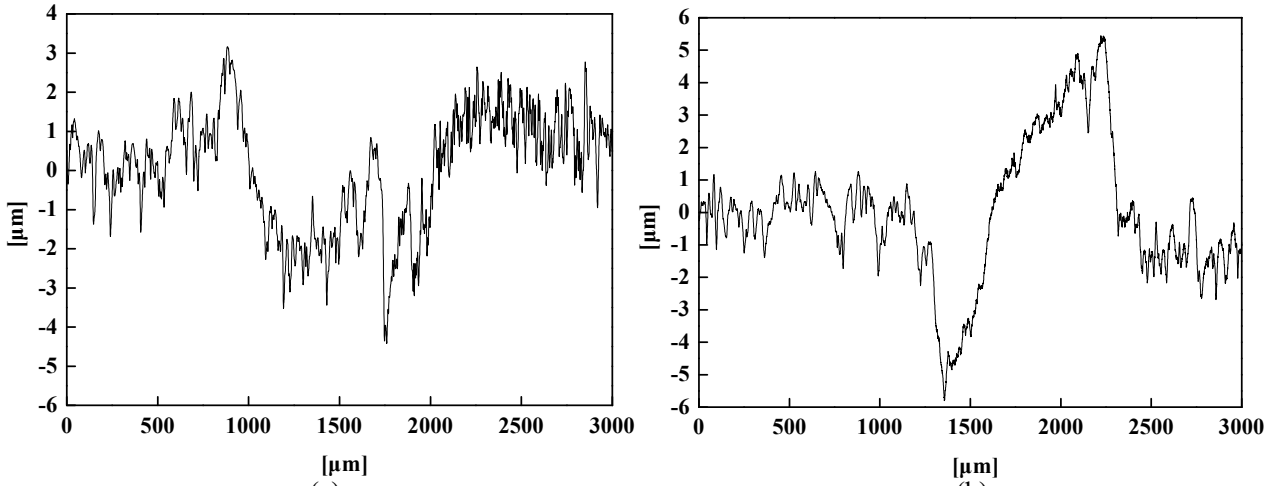

(a) (b)

Figure 5 Surface profiles of wear tracks on (a) 40 wt%SiC-60 wt%B_4C composite ceramics; (b) 20 wt%SiC-80 wt%B_4C composite ceramics.

11.4. Conclusions

A self-lubricating layer was successful fabricated on the surface of SiC-B_4C composite ceramics by the annealing treatment in air. The main composition of the self-lubricating layer is H_3BO_3, and silicon oxides layer was not detected. SiC-B_4C composite ceramics show lower friction coefficients when the mass fraction of B_4C is more than that of SiC. The low friction coefficients of 40 wt%SiC-60 wt%B_4C composite ceramics treated by annealing and 20 wt%SiC-80 wt%B_4C composite ceramics treated by annealing are attributed to the formation of a sufficient amount of H_3BO_3 layer, rather than the layer of silicon oxides. This study will help to understand the friction behavior of SiC-B_4C composite ceramics with different ratios of SiC to B_4C after annealing.

For further research, more kinds of annealing conditions, such as higher annealing temperatures and longer annealing time should be involved.

11.5. References

[1] X. G. Li, D. L. Jiang, J. X. Zhang, Q. L. Lin, Z. M. Chen, Z. R. Huang. Pressureless sintering of boron carbide with Cr_3C_2 as sintering additive. Journal of the European Ceramic Society,2014,34(5):1073-1081.

[2] Y. W. Kim, K. Y. Lim, W. S. Seo. Microstructure and thermal conductivity of silicon carbide with yttria and

scandia. Journal of the American Ceramic Society,2014,97(3):923-928.
[3] W. Zhang, S. Yamashita, H. Kita. Progress in pressureless sintering of boron carbide ceramics- a review. Advances in Applied Ceramics,2019,118(4):222-239.
[4] Z. Y. Zhang, J. F. Cui, B. Wang, H. Y. Jiang, G. X. Chen, J. H. Yu, C. T. Lin, C. Tang, A. Hartmaier, J. J. Zhang, J. Luo, A. Rosenkranz, N. Jiang, D. M. Guo. In situ TEM observation of rebonding on fractured silicon carbide. Nanoscale,2018,10(14):6261-6269.
[5] J. F. Cui, Z. Y. Zhang, D. D. Liu, D. L. Zhang, W. Hu, L. Zou, Y. Lu, C. Zhang, H. H. Lu, C. Tang, N. Jiang, I. P. Parkin, D. M. Guo. Unprecedented piezoresistance coefficient in strained silicon carbide. Nano Letters, 2019,19(9):6569-6576.
[6] B. Wang, Z. Y. Zhang, K. K. Chang, J. F. Cui, A. Rosenkranz, J. H. Yu, C. T. Lin, G. X. Chen, K. T. Zang, J. Luo, N. Jiang, D. M. Guo. New deformation-induced nanostructure in silicon. Nano Letters,2018,18(7):4611-4617.
[7] U. Soy, A. Demir, F. Findik. Friction and wear behaviors of Al-SiC-B_4C composites produced by pressure infiltration method. Industrial Lubrication and Tribology,2011,63(5):387-393.
[8] A. Altinkok, İ. Özsert, F. Findik. Dry sliding wear behavior of Al_2O_3/SiC particle reinforced aluminium based MMCs fabricated by stir casting method. Acta Physica Polonica A,2013,124(1):11-19.
[9] B. M. Moshtaghioun, A. L. Ortiz, D. Gómez-García, A. Domínguez-Rodríguez. Toughening of super-hard ultra-fine grained B_4C densified by spark-plasma sintering via SiC addition. Journal of the European Ceramic Society,2013,33(8):1395-1401.
[10] Y. G. Tkachenko, V. F. Britun, É. V. Prilutskii, D. Z. Yurchenko, G. A. Bovkun. Structure and properties of B_4C-SiC composites. Powder Metallurgy and Metal Ceramics,2005,44(3-4):196-201.
[11] I. S. Han, K. S. Lee, D. W. Seo, S. K. Woo. Improvement of mechanical properties in RBSC by boron carbide addition. Journal of Materials Science Letters,2002,21(9):703-706.
[12] H. Sano, G. B. Zheng, Y. Uchiyama. Effect of SiC particle size on anti-oxidation behavior of C/B_4C/SiC composite. Materials Science Forum,2010,658:308-311.
[13] Y. L. Zhang, X. G. Song, G. J. Li, Y. M. Zhang. Oxidation behavior research of the SiC/B_4C multiphase ceramics. Applied Mechanics and Materials,2015,727-728:288-291.
[14] F. Findik. Latest progress on tribological properties of industrial materials. Materials and Design,2014,57:218-244.
[15] P. Sahani, D. Chaira. Nonlubricated sliding wear behavior study of SiC-B_4C-Si cermet against a diamond indenter. Journal of Tribology,2017,139:051601.
[16] W. Zhang, S. Yamashita, T. Kumazawa, F. Ozeki, H. Hyuga, H. Kita. Effect of nanorelief structure formed in situ on tribological properties of ceramics in dry sliding. Ceramics International,2019,45(11):13818-13824.
[17] W. Zhang, S. Yamashita, T. Kumazawa, F. Ozeki, H. Hyuga, W. Norimatsu, H. Kita. A study on formation mechanisms of relief structure formed in situ on the surface of ceramics. Ceramics International,2019,45(17):23143-23148.
[18] Y. Yamamoto, A. Ura. Influence of interposed wear particles on the wear and friction of silicon carbide in different dry atmospheres. Wear,1992,154(1):141-150.
[19] A. Erdemir, C. Bindal, C. Zuiker, E. Savrun. Tribology of naturally occurring boric acid films on boron carbide. Surface and Coatings Technology,1996,86-87(2):507-510.
[20] Y. Liu, W. Hao, H. Lu. Boric acid crystal structure analysis and Raman spectra test. The Journal of Light Scattering,2014,26(2):144-147. (in Chinese)
[21] S. Nakashima, H. Harima. Raman investigation of SiC polytypes. Physica Status Solidi A,1997,162(1):39-64.
[22] T. Narushima, T. Goto, M. Maruyama, H. Arashi, Y. Iguchi. Oxidation of boron carbide-silicon carbide composite at 1073 to 1773K. Materials Transactions,2003,44(3):401-406.

[23] U. Kuhlmann , H. Werheit. Improved Raman Effect Studies on Boron Carbide ($B_{4.3}C$). Physica status solidi(b),1993,175(1):85-92.

[24] C. Kunka, A. Awasthi, G. Subhash. Evaluating boron-carbide constituents with simulated Raman spectra. Scripta Materialia,2017,138:32-34.

Part IV

The Influence of Counterpart Materials on Tribological Properties of B_4C-SiC Ceramics

Chapter 12
Effect of counterbody on tribological properties of B_4C-SiC composite ceramics under dry sliding

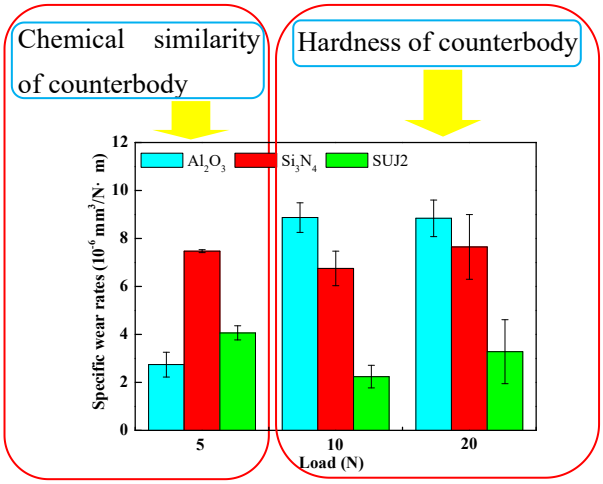

Pressureless sintered B_4C-SiC composite ceramics were subjected to dry sliding friction and wear against Al_2O_3, Si_3N_4 and SUJ2 bearing steel counterbodies at 5 N,10 N and 20 N. Friction coefficient and specific wear rate were measured, and wear mechanisms were studied. For the B_4C-SiC composite ceramics, both the friction coefficient and specific wear rate were dependent on counterbody materials. However, the influence of counterbody materials on friction coefficient and systematic specific wear rate of B_4C-SiC composite ceramics was not obvious at high load, which was attributed to the formation of a number of compaction layers on all the worn surfaces of B_4C-SiC composite ceramics against Al_2O_3, Si_3N_4 and SUJ2 counterbodies. At the same loads, the wear of B_4C-SiC composite ceramics sliding against different counterbodies at low load was mainly controlled by the chemical similarity of counterbody, whereas the wear of B_4C-SiC composite ceramics sliding against different counterbodies at intermediate and high loads was mainly controlled by the hardness of counterbody.

Contents

12.1. Introduction

B_4C ceramics and SiC ceramics have been proved to be suitable for tribological applications owing to their excellent performance like good wear resistance, high hardness, low density and high elastic modulus [1-7]. They are widely used as cutting tools, nozzles, mechanical seals, bearing, etc. [8-10]. Further, B_4C particles and SiC particles are often used as reinforcements to improve tribological properties of metal or alloy. Some researchers found that the friction coefficient and wear rate of metal or alloy were remarkably reduced after hard B_4C particles and/or SiC particles were added [11-13].

A number of scholars studied the tribological properties for B_4C ceramics and SiC ceramics under different test conditions. It is found that the tribological behaviors of B_4C ceramics and SiC ceramics are complex and dependent on external factors. Important external factors which can influence tribological behaviors of B_4C ceramics and SiC ceramics include applied load, sliding velocity, environment temperature, humidity and counterbody materials. Zhang et al. [14] found both the friction coefficient and wear rate of B_4C ceramics first decreased and then increased as the load increased. Sharma et al. [15] reported the friction coefficient of SiC ceramics increased first and then decreased and wear rate decreased with load increasing. Gogotsi et al. [16] pointed out the friction coefficient of B_4C ceramics decreased as the sliding velocity increased. Micele et al. [17] stated SiC ceramics exhibited mild wear at sliding speed of 0.5 m/s, while they revealed severe wear at sliding speed of 2 m/s. Lin et al. [18] and Li et al. [19] observed increased friction and wear for B_4C ceramics and SiC ceramics with the increase of environment temperature, respectively. Cao et al. [20] and Murthy et al. [21] studied the influence of relative humidity on tribological properties of B_4C ceramics and SiC ceramics, respectively. Both the friction coefficients and wear rates of B_4C ceramics and SiC ceramics decreased with an increase of humidity. However, only very few papers have been reported about the effect of counterbody on the tribological properties of B_4C ceramics or SiC ceramics. Guicciardi et al. [22] found friction coefficient of SiC ceramics was increased when they were self-mated. Kovalčíková et al. [23] reported that friction coefficient of SiC ceramics depended on the different counterbody (Al_2O_3, ZrO_2, Si_3N_4 and WC-Co), and wear rate of SiC ceramics increased with increasing of hardness of counterbody. Sharma et al. [24] studied frictional behaviors of SiC ceramics sliding against steel ball and WC-Co ball, and pointed out that friction coefficient of SiC ceramics depended on nature of counterbody.

Recently, Zhang et al. [25,26] reported that B_4C-SiC composite ceramics sliding against SiC balls showed lower friction coefficient and wear rate as compared with monolithic SiC ceramics and monolithic B_4C ceramics under the same test condition. The improved tribological properties were attributed to the relief structure formed on the surface of B_4C-SiC composite ceramics owing to the different hardness between B_4C and SiC grains and clean grain boundary [27]. Further, it is also reported that compared with monolithic B_4C ceramics and monolithic SiC ceramics, B_4C-SiC composite ceramics sliding against SiC balls revealed a lower coefficient of friction during run-in period and a shorter sliding distance to steady state [28]. Therefore, B_4C-SiC composite ceramics are believed to be a potential application in the filed of tribology as tribological structural components. However, the studies focused on tribological properties of B_4C-SiC composite ceramics are rather limited. To the best of our knowledge, there is no research exploring the effect of counterbody on tribological performance of B_4C-SiC composite ceramics under the same sliding condition. As mentioned above, ceramic materials showed different tribological behaviors when they slid against different counterbodies, and it is believed that different counterbodies will cause different effects on the tribological behaviors of B_4C-SiC composite ceramics. Therefore, the aim of this work is to research the tribological performance of B_4C-SiC composite ceramics and to determine the influence of counterbody on friction and wear of B_4C-SiC composite ceramics. In this work, an oxide ceramic ball (Al_2O_3 ball), a non-oxide ceramic ball (Si_3N_4 ball) and a metal ball (SUJ2 bearing steel ball) are chosen as counterbody

materials. Meanwhile, in order to explore the potential of B_4C-SiC composite ceramics for their use in automotive and aerospace industries as triboelements like bearings, seals or heat exchanger tubes, it is important to evaluate the tribological properties of B_4C-SiC composite ceramics at different loads (5 N, 10 N and 20 N).

12.2. Experimental

12.2.1. Experimental materials

B_4C powder (0.8 μm; Grade HS, H. C. Starck Gmbh & Co., Berlin, Germany) was mixed with SiC powder (0.4 μm; Grade OY-15, Yakushima Denko, Tokyo, Japan). The weight ratio of B_4C to SiC was 60:40. Additional 3 wt.% carbon black powder (20-30 nm; Mitsubishi Chemical; Japan) was added into the composite ceramics as a sintering aid. After being milled in ethanol for 24 h using SiC balls, the powder mixture was uniaxially pressed into pellets followed by cold isostatic pressing at 196 MPa. The blocks were sintered by pressureless sintering at 2300 ℃/16 h in Ar atmosphere. After sintering, the blocks were cut with nominal dimensions of 23×23×6 mm^3, ground, polished to obtain a surface roughness (Ra) of 10-30 nm, which was measured by a surface profilometer (SJ-310, Mitutoyo, Japan). The polished surfaces were then observed by SEM (JEOL, JSM-7500F, Japan). A typical micrograph of the polished surface of B_4C-SiC composite ceramics is shown in Fig. 1. According to XRD result, the phase composition of the B_4C-SiC composite ceramics is 4H-SiC, 6H-SiC, B_4C and a small amount of C [27]. The darker and lighter areas in Fig. 1 are B_4C grains and SiC grains, respectively. Also, visible pores can be seen on the polished surface.

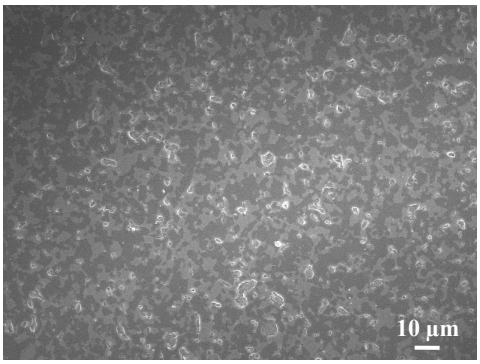

Fig. 1. A typical micrograph of the polished surface of B_4C-SiC composite ceramics.

12.2.2. Physical properties

The densities of the sintered ceramics were measured by Archimedes' principle. The relative density was calculated by dividing the density of the sintered ceramics by the theoretical density of B_4C-SiC composite ceramics which was calculated by the rule of mixtures using 2.51 g/cm^3, 3.21 g/cm^3 and 2 g/cm^3 as densities for B_4C, SiC and carbon black, respectively. The hardness and fracture toughness were investigated using a Vickers diamond pyramidal indenter (VKH-1, Japan) under a load of 1 kg with a dwell time of 10 s. The diagonals (d) and radial-crack diameters (2c) of each indent were measured. Hardness and Fracture toughness (K_{IC}) were calculated using $H=1.8544P/d^2$ and $K_{IC}=0.016(E/H)^{0.5}Pc^{-1.5}$, respectively [29]. The measurements for each sample were carried out 5 times, and the data obtained were the mean values. The physical properties of the sintered B_4C-SiC composite ceramics are shown in Table 1.

Table 1 Physical properties of the sintered B_4C-SiC composite ceramics.

Property	Value
Relative density (%)	93.9
Bulk density (g/cm^3)	2.62
Vickers hardness (GPa)	30.4
Fracture toughness (MPa·m$^{1/2}$)	3.2

12.2.3. Sliding friction and wear test

Sliding friction and wear tests were carried out in a ball-on-disc tribometer (T-18-0162, NANOVEA, US) in ambient conditions (24±0.5 ℃ and 45%±5% RH). Tribological performance of the prepared B_4C-SiC composite ceramics was studied in dry sliding where counterbodies were polished balls with 8 mm diameter made out of commercially available balls-Al_2O_3, Si_3N_4, SUJ2 bearing steel (Sato Tekkou, Japan). The hardness values of Al_2O_3, Si_3N_4, SUJ2 balls are 20.1 GPa, 18.2 GPa and 7.5 GPa, respectively, which are obtained from the supplier. Before test, both the B_4C-SiC composite ceramics and the counterbodies were ultrasonically cleaned in an acetone bath for 10 min. Sliding friction and wear tests were done at three loads: 5 N, 10 N and 20 N, and the mean Hertzian contact stress of B_4C-SiC composite ceramics sliding against different counterbodies at different loads is presented in Table 2. The sliding velocity was 0.1 m/s, the wear track radius was 10 mm, and the total sliding distance was 100 m, during which the steady-state period was reached. Three tests were carried out for each tribopair. The friction coefficients were recorded continuously and wear volume on each B_4C-SiC disc was calculated from the surface profile traces across the wear track using a surface profilometer.

Table 2 Mean Hertzian contact stress of B_4C-SiC composite ceramics sliding against different counterbodies at different loads.

Load (N)	Counterbody	Mean Hertzian contact stress (GPa)
5	Al_2O_3	0.90
	Si_3N_4	0.80
	SUJ2	0.73
10	Al_2O_3	1.14
	Si_3N_4	1.01
	SUJ2	0.92
20	Al_2O_3	1.43
	Si_3N_4	1.27
	SUJ2	1.16

The worn volume of the disc (V_d, mm^3) was calculated according to the following equation:

$$V_d = 2\pi r(\frac{S_1 + S_2 + S_3 + S_4}{4})$$

where S (mm^2) and r (mm) are the cross sectional areas of the wear track, each at 90º with respect to the previous one, and sliding radius, respectively.

The worn volume of the ball (V_b, mm^3) was calculated according to the following equations:

$$V_b = \pi h^2(R - \frac{h}{3})$$

$$h = R - \sqrt{R^2 - r_w^2}$$

where h (mm) is the height of the removed material, R (mm) is original radius of the ball, and r_w (mm) is the radius of wear scar on the ball.

The specific wear rate (WR, $mm^3/N \cdot m$) was further calculated according to the following equation:

$$WR = \frac{V}{L \cdot S}$$

where V (mm^3) is the wear volume of the disc (V_d) or ball (V_b), L (N) is the normal load, and S (m) is the total sliding distance.

The worn surfaces were studied by SEM and EDS to identify wear mechanisms. The schematic diagram of balls used to measure the friction temperature is presented in Fig. 2. The thermocouple was inserted into the hole (diameter=1 mm) of the balls.

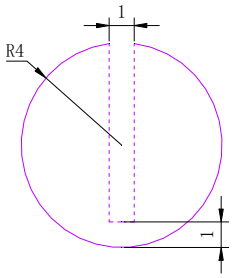

Fig. 2. The schematic diagram of balls used to measure the friction temperature.

12.3. Results and discussion

12.3.1. Friction coefficient

Typical evolution of the friction coefficients of B_4C-SiC composite ceramics sliding against Al_2O_3, Si_3N_4 and SUJ2 counterbodies at different loads are shown in Fig. 3. An initial run-in period followed by a steady-state period was observed in all the tribopairs. Average friction coefficients of B_4C-SiC composite ceramics in steady-state period sliding against Al_2O_3, Si_3N_4 and SUJ2 counterbodies at different loads are summarized in Fig. 4. The friction coefficient of B_4C-SiC composite ceramics changed in the range of 0.53-0.82 against Al_2O_3, Si_3N_4 and SUJ2 counterbodies at the load of 5 N, between 0.59 and 0.81 against Al_2O_3, Si_3N_4 and SUJ2 counterbodies at the load of 10 N, in the range of 0.55-0.63 against Al_2O_3, Si_3N_4 and SUJ2 counterbodies at the load of 20 N. When sliding against Al_2O_3 ball, friction coefficient of B_4C-SiC/Al_2O_3 tribopair increased first and then decreased as the load increased. When sliding against Si_3N_4 ball, friction coefficient of B_4C-SiC/Si_3N_4 tribopair did not change with load increasing. When sliding against SUJ2 ball, friction coefficient of B_4C-SiC/SUJ2 tribopair did not change as the load increased from 5 N to 10 N, and then decreased with load increasing from 10 N to 20 N. At low load (5 N), the B_4C-SiC/Al_2O_3 tribopair exhibited the lowest friction coefficient, while B_4C-SiC/Si_3N_4 tribopair revealed the lowest friction coefficient at intermediate load (10 N). At high load (20 N), the differences in friction coefficients of B_4C-SiC/Al_2O_3, B_4C-SiC/Si_3N_4 and B_4C-SiC/SUJ2 tribopairs were not obvious. B_4C-SiC composite ceramics showed the highest friction coefficient in steady-state period against SUJ2 counterbody at any load. Guicciardi et al. [22] stated that SiC ceramics showed a higher friction coefficient in the case of self-mated than in the case of not self-mated. Kovalčíková et al. [23] researched the effect of counterbody materials-Al_2O_3, ZrO_2, Si_3N_4 and WC-Co on the frictional property of SiC ceramics under the same experimental conditions. It is found that SiC/ZrO_2 tribopair exhibited the lowest coefficient of friction, whereas SiC/Si_3N_4 tribopair displayed the highest coefficient of friction, which was attributed to the chemical similarity between SiC and Si_3N_4. However, in present experiment, the friction coefficient of B_4C-SiC/Si_3N_4 tribopair was only higher than that of B_4C-SiC/Al_2O_3 tribopair at 5 N, and the B_4C-SiC/Si_3N_4 tribopair revealed the lowest friction coefficient at 10 N,

the reasons of which will be discussed in Section 3.4. Similar results were also observed by other researchers. Wäsche et al. [30] found the coefficient of friction of SiC/Al_2O_3 tribopair was 0.5, whereas the coefficient of friction of SiC/SiC tribopair was 0.4 under the same experimental conditions. Li et al. [31,32] showed coefficient of friction of 0.59 for self-mated B_4C and 0.63 for B_4C with AISI 321 austenitic stainless steel counterbody. These self-mated tribopairs didn't show higher friction coefficients owing to chemical similarity, which is in agreement with some results of this work.

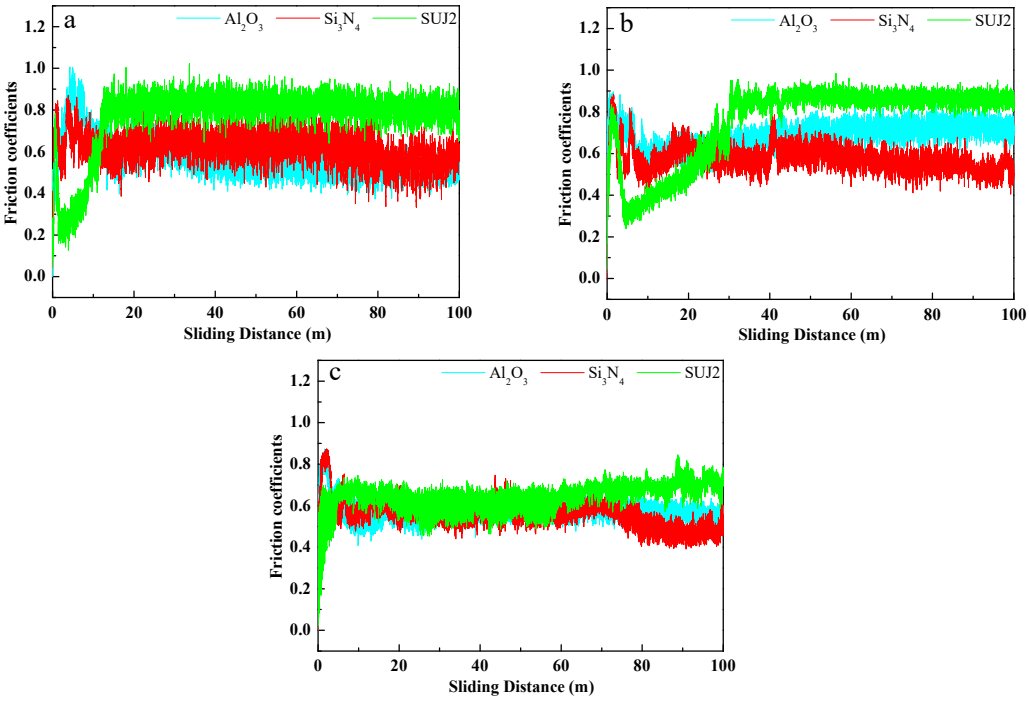

Fig. 3. Evolution of friction coefficients of B_4C-SiC composite ceramics sliding against Al_2O_3, Si_3N_4 and SUJ2 counterbodies at (a) 5 N, (b) 10 N and (c) 20 N.

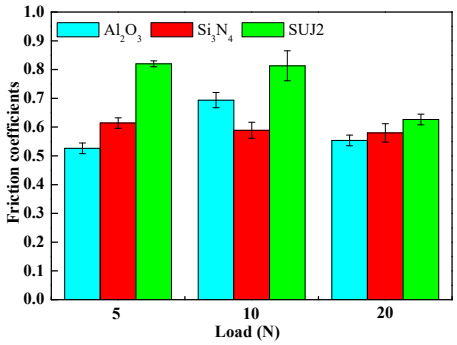

Fig. 4. Average friction coefficients of B_4C-SiC composite ceramics in steady-state period sliding against Al_2O_3, Si_3N_4 and SUJ2 counterbodies at different loads.

12.3.2. Friction temperature

Typical evolution of friction temperatures measured for B_4C-SiC composite ceramics sliding against Al_2O_3, Si_3N_4 and SUJ2 counterbodies at different loads are shown in Fig. 5. An initial temperature change was observed in all the tribopairs at any load, which corresponded to frictional run-in period of the tribopairs. When friction entered into steady-state period, friction temperature measured also became relatively stable. Generally, the friction temperatures during steady-state period were higher than those during run-in period for all the tribopairs at any load. Average measured friction temperatures of B_4C-SiC composite ceramics in steady-state period sliding against Al_2O_3, Si_3N_4 and SUJ2 counterbodies at different loads are summarized in Fig. 6. All the measured friction

temperatures of B_4C-SiC composite ceramics sliding against Al_2O_3, Si_3N_4 and SUJ2 counterbodies increased as the load increased. The measured friction temperatures of all the tribopairs had the same change tendency with friction coefficients at any load, except B_4C-SiC/SUJ2 tribopair at 20 N. For example, the B_4C-SiC/Al_2O_3 tribopair exhibited the lowest friction coefficient and B_4C-SiC/SUJ2 tribopair exhibited the highest friction coefficient at 5 N, correspondingly, B_4C-SiC/Al_2O_3 tribopair displayed the lowest friction temperature and B_4C-SiC/SUJ2 tribopair displayed the highest friction temperature at 5 N. As a special case, the B_4C-SiC/SUJ2 tribopair showed the significant increased friction temperature as compared to B_4C-SiC/Al_2O_3 tribopair and B_4C-SiC/Si_3N_4 tribopair at 20 N, however, the corresponding friction coefficient showed a similar value as compared to B_4C-SiC/Al_2O_3 tribopair and B_4C-SiC/Si_3N_4 tribopair at 20 N. Meanwhile, the B_4C-SiC/SUJ2 tribopair showed a higher friction temperature at 20 N than those measured at 5 N and 10 N, however, the friction coefficient showed a decreased value as compared to those measured at 5 N and 10 N. Although the values for friction temperatures measured in this study are not the real values occurred on the sliding interface, these values can reflect the change trend of the sliding interface temperature when the B_4C-SiC composite ceramics slide against different counterbodies. It is well known that friction heat would be produced during dry sliding process, resulting in the formation of flash temperature. This intense heat is beneficial to accelerate overall kinetics which can induce tribochemical reactions for nonoxide ceramics. Li et al. [31], Alexander et al. [33] and Sonber et al. [34] reported that B_2O_3 was first formed on the surface of B_4C ceramics owing to tribochemical reaction, and then B_2O_3 reacted with moisture in atmosphere to form H_3BO_3. This formed H_3BO_3 with layered structure can significantly reduce friction coefficient for B_4C ceramics [35,36]. Kumar et al. [37], Guha and Basu [38], Murthy et al. [21] and Gahr et al. [39] pointed out SiO_2 was first formed on the surface of SiC ceramics due to tribochemical reaction, and SiO_2 can react with moisture at high humidity to form $Si(OH)_4$, which can significantly reduce friction coefficient for SiC ceramics. It can be seen from Fig. 5 and Fig. 6 that the friction temperature of B_4C-SiC/SUJ2 tribopair at 20 N was higher than those measured at 5 N and 10 N. Therefore, the possibility of occurrence of tribochemical reaction in B_4C-SiC/SUJ2 tribopair at 20 N is quite high, resulting in the reduced friction coefficient than those of B_4C-SiC/SUJ2 tribopair at 5 N and 10 N. It is also reported that ceramics with dissimilar sliding pairs revealed different friction coefficient under dry sliding conditions because of difference in the ionic potential of oxides formed on the sliding interface. The tendency for the formation of oxide layers was larger at higher loads because of high temperature induced by friction on the sliding interface [40,41].

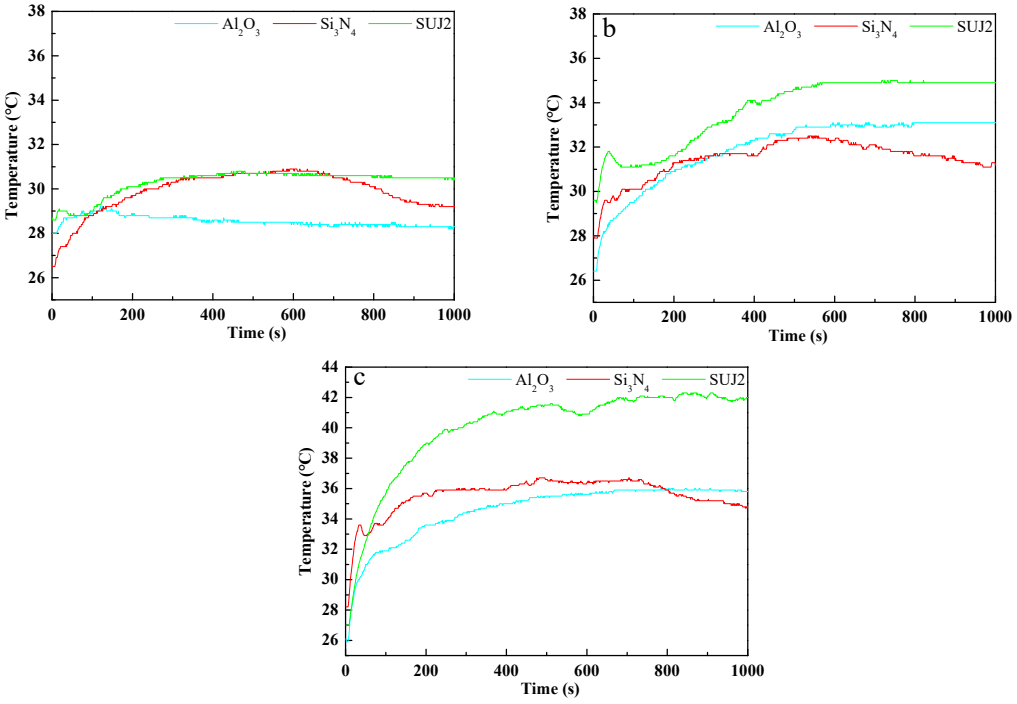

Fig. 5. Evolution of friction temperatures measured for B_4C-SiC composite ceramics sliding against Al_2O_3, Si_3N_4 and SUJ2 counterbodies at (a) 5 N, (b) 10 N and (c) 20 N.

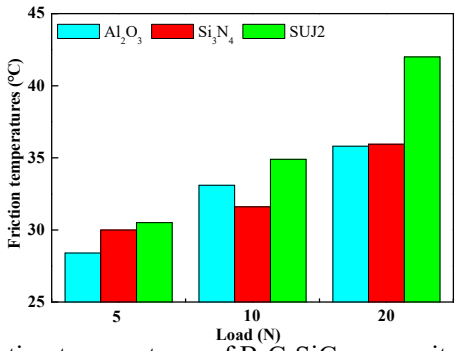

Fig. 6. Average measured friction temperatures of B_4C-SiC composite ceramics in steady-state period sliding against Al_2O_3, Si_3N_4 and SUJ2 counterbodies at different loads.

12.3.3. Specific wear rate

Average specific wear rates of B_4C-SiC composite ceramics sliding against Al_2O_3, Si_3N_4 and SUJ2 counterbodies at different loads are summarized in Fig. 7. The specific wear rate of B_4C-SiC composite ceramics changed in the range of 2.7×10^{-6}-7.5×10^{-6} $mm^3/N\cdot m$ against Al_2O_3, Si_3N_4 and SUJ2 counterbodies at the load of 5 N, between 2.2×10^{-6} $mm^3/N\cdot m$ and 8.9×10^{-6} $mm^3/N\cdot m$ against Al_2O_3, Si_3N_4 and SUJ2 counterbodies at the load of 10 N, in the range of 3.3×10^{-6}-8.8×10^{-6} $mm^3/N\cdot m$ against Al_2O_3, Si_3N_4 and SUJ2 counterbodies at the load of 20 N. When sliding against Al_2O_3 ball, the specific wear rate of B_4C-SiC composite ceramics showed the minimum value at the load of 5 N. When sliding against Si_3N_4 ball, the specific wear rate of B_4C-SiC composite ceramics changed not obviously with load increasing. When sliding against SUJ2 ball, the specific wear rate of B_4C-SiC composite ceramics decreased with load increasing from 5 N to 10 N, and then increased not obviously as the load increased from 10 N to 20 N. At low load, the B_4C-SiC composite ceramics exhibited the lowest specific wear rate as sliding against Al_2O_3 ball. However, the B_4C-SiC composite ceramics revealed the lowest specific wear rate as sliding against SUJ2 ball at intermediate and high loads. Prioli et al. [42,43] stated the wear of B_4C ceramics increased as friction coefficient increased, exhibiting a strong liner dependence. However, in this study, the specific wear rate of B_4C-SiC composite ceramics sliding against Al_2O_3, Si_3N_4 and SUJ2 counterbodies didn't show obvious dependence on their friction coefficients at the same load. Although B_4C-SiC/SUJ2 tribopair showed highest friction coefficient at any load, the specific wear rates of B_4C-SiC composite ceramics sliding against SUJ2 ball were lower at any load. Sonber et al. [34], Murthy et al. [44] and Li et al. [45] mentioned that the wear rate of B_4C ceramics increased with the increase of normal load under dry sliding condition. Sharma et al. [15] pointed out that the wear rate of SiC ceramics decreased with the increase of normal load from 5 to 20 N. Conversely, in present work, the specific wear rate of B_4C-SiC composite ceramics sliding against Al_2O_3, Si_3N_4 and SUJ2 counterbodies didn't show a liner dependence on load.

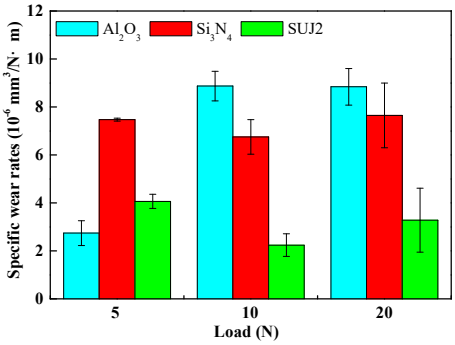

Fig. 7. Average specific wear rates of B_4C-SiC composite ceramics sliding against Al_2O_3, Si_3N_4 and SUJ2

counterbodies at different loads.

Average specific wear rates of Al_2O_3, Si_3N_4 and SUJ2 counterbodies at different loads are summarized in Fig. 8. It can be found from Fig. 8 that Al_2O_3 ball exhibited lower specific wear rate at any load compared with other counterbodies. The specific wear rate of Si_3N_4 ball was the highest at 5 N, whereas the specific wear rates of SUJ2 ball were the highest at 10 N and 20 N. From the comparison between Fig. 8 and Fig. 7, three findings can be found. First, at low load, the specific wear rates between B_4C-SiC composite ceramics and counterbodies showed the consistency, however, at intermediate and high loads, the specific wear rates of B_4C-SiC composite ceramics and counterbodies were complementary. The test carried out by Kovalčíková et al. [23] revealed that the specific wear rate of SiC ceramics increased as the hardness of the counterbodies increased at the load of 5 N under dry sliding conditions, however, this dependence of specific wear rate of B_4C-SiC composite ceramics on hardness of counterbodies was only shown at 10 N and 20 N in this study. Second, the specific wear rate of Al_2O_3 balls increased as the load increased, while the specific wear rate of B_4C-SiC composite ceramics sliding against Al_2O_3 balls increased first and then changed not obviously as the load increased. The specific wear rate of Si_3N_4 balls decreased first and then increased as the load increased, while the specific wear rate of B_4C-SiC composite ceramics sliding against Si_3N_4 balls changed not obviously as the load increased. The specific wear rate of SUJ2 balls changed not obviously as the load increased from 5 N to 10 N and then increased as the load increased from 10 N to 20 N, while the specific wear rate of B_4C-SiC composite ceramics sliding against SUJ2 balls decreased with load increasing from 5 N to 10 N, and then increased not obviously as the load increased from 10 N to 20 N. Third, the specific wear rates of B_4C-SiC composite ceramics sliding against Al_2O_3 balls were higher than those of the corresponding Al_2O_3 balls at any load. The specific wear rates of B_4C-SiC composite ceramics sliding against Si_3N_4 balls were higher than those of the corresponding Si_3N_4 balls at 10 N and 20 N, whereas the specific wear rates of B_4C-SiC composite ceramics sliding against SUJ2 balls were lower than those of the corresponding SUJ2 balls at 10 N and 20 N. The differences in specific wear rates between B_4C-SiC composite ceramics sliding against Si_3N_4 balls and SUJ2 balls and the corresponding Si_3N_4 ball and SUJ2 balls at 5 N were not obvious, respectively.

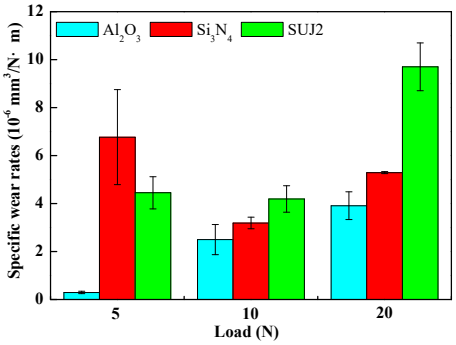

Fig. 8. Average specific wear rates of Al_2O_3, Si_3N_4 and SUJ2 counterbodies at different loads.

Fig. 9 gives the systematic specific wear rates of tribopairs of B_4C-SiC composite ceramics sliding against Al_2O_3, Si_3N_4 and SUJ2 counterbodies at different loads. The value of the systematic specific wear rate of every tribopair is the sum of B_4C-SiC disc's and corresponding ball's specific wear rate. From Fig. 9, it can be observed that the B_4C-SiC/Al_2O_3 tribopair showed the lowest systematic specific wear rate when the load was 5 N, while the B_4C-SiC/SUJ2 tribopair revealed the lowest systematic specific wear rate when the load was 10 N. At high load, similar systematic specific wear rates were observed for the three tribopairs and the influence of counterbody on systematic specific wear rate was not predominant. For B_4C-SiC/Al_2O_3 tribopair, the systematic specific wear rate increased as the load increased from 5 N to 20 N. For B_4C-SiC/Si_3N_4 tribopair and B_4C-SiC/SUJ2 tribopair, the systematic specific wear rates decreased first and then increased when the load varied from 5 N to 20 N, both of which showed minimum as the load was 10 N.

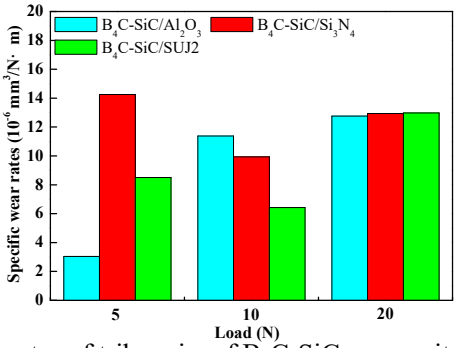

Fig. 9. The systematic specific wear rates of tribopairs of B_4C-SiC composite ceramics sliding against Al_2O_3, Si_3N_4 and SUJ2 counterbodies at different loads.

12.3.4. Friction and wear mechanism

12.3.4.1. At the load of 5 N

Fig. 10 shows typical SEM images of worn surfaces of B_4C-SiC composite ceramics sliding against Al_2O_3, Si_3N_4 and SUJ2 counterbodies at 5 N. Fig. 11 reveals optical micrographs of the wear scars on the Al_2O_3, Si_3N_4 and SUJ2 counterbodies at the load of 5 N. From Fig. 10, it can be observed that the worn surfaces of B_4C-SiC composite ceramics sliding against Al_2O_3 ball and SUJ2 ball are smooth, and no debris layers can be observed. Obvious grain pullout or grain fracture is not observed on the worn surface of B_4C-SiC composite ceramics sliding against Al_2O_3 ball. A few grain pullout or grain fracture is observed on the worn surface of B_4C-SiC composite ceramics sliding against SUJ2 ball, whose extent is slightly greater than that of B_4C-SiC composite ceramics sliding against Al_2O_3 ball. However, obvious micro-fracture can be seen on the worn surface of B_4C-SiC composite ceramics sliding against Si_3N_4 ball as compared to sliding against Al_2O_3 ball and SUJ2 ball, which may be attributed to the chemical similarity between the B_4C-SiC composite ceramics and the Si_3N_4 ball. Compared with Al_2O_3 ball and SUJ2 ball, Si_3N_4 ball is easier to cause a strong chemical bond with B_4C-SiC composite ceramics by surface chemical reaction owing to chemical affinity between Si_3N_4 and B_4C-SiC. Therefore, micro-fracture was caused on the B_4C-SiC composite ceramics as sliding against Si_3N_4 ball because of this strong chemical bond between Si_3N_4 and B_4C-SiC, resulting in the highest specific wear rates of B_4C-SiC composite ceramics sliding against Si_3N_4 ball and the mating Si_3N_4 ball. In addition, compared with Al_2O_3 ball and Si_3N_4 ball, it can be seen from Fig. 11 that obvious grooves are observed on the wear scar of SUJ2 ball, however, polished surfaces are observed on the wear scars of Al_2O_3 ball and Si_3N_4 ball. Thus, it can be inferred that there were more wear particles on the sliding interface of B_4C-SiC/SUJ2 tribopair. Compared with the hardness of Al_2O_3 ball, the hardness of SUJ2 ball is lower, causing more Fe wear particles on the sliding interface of B_4C-SiC/SUJ2 tribopair. Therefore, higher specific wear rate of B_4C-SiC composite ceramics sliding against SUJ2 ball than that of B_4C-SiC composite ceramics sliding against Al_2O_3 ball is attributed to increased abrasive wear, however, specific wear rate of B_4C-SiC composite ceramics sliding against SUJ2 ball induced by abrasive wear is still lower than that of B_4C-SiC composite ceramics sliding against Si_3N_4 ball induced by chemical similarity. Furthermore, some debris compaction layers are observed on the worn surface of B_4C-SiC composite ceramics sliding against Si_3N_4 ball, which is different from the worn surfaces of B_4C-SiC composite ceramics sliding against Al_2O_3 ball and SUJ2 ball. On the one hand, such compaction layers are beneficial to reduce friction for sliding interface of B_4C-SiC/Si_3N_4 tribopair [15,23], and on the other hand, more wear particles were on the sliding interface of B_4C-SiC/SUJ2 tribopair. Therefore, the friction coefficient of B_4C-SiC/Si_3N_4 tribopair was lower than that of B_4C-SiC/SUJ2 tribopair, although obvious micro-fracture occurred on the worn surface of B_4C-SiC composite ceramics sliding against Si_3N_4 ball. The chemical similarity between B_4C-SiC composite ceramics and Si_3N_4 ball

increased the wear rate of B_4C-SiC/Si_3N_4 tribopair, however, the friction coefficient of B_4C-SiC/Si_3N_4 tribopair was not increased owing to this chemical similarity, which can be attributed to the formation of the compaction layers. The main wear mechanisms of B_4C-SiC composite ceramics sliding against Al_2O_3 and SUJ2 counterbodies at 5 N are surface polishing and mild abrasion, whereas the main wear mechanism of B_4C-SiC composite ceramics sliding against Si_3N_4 counterbody at 5 N is micro-fracture.

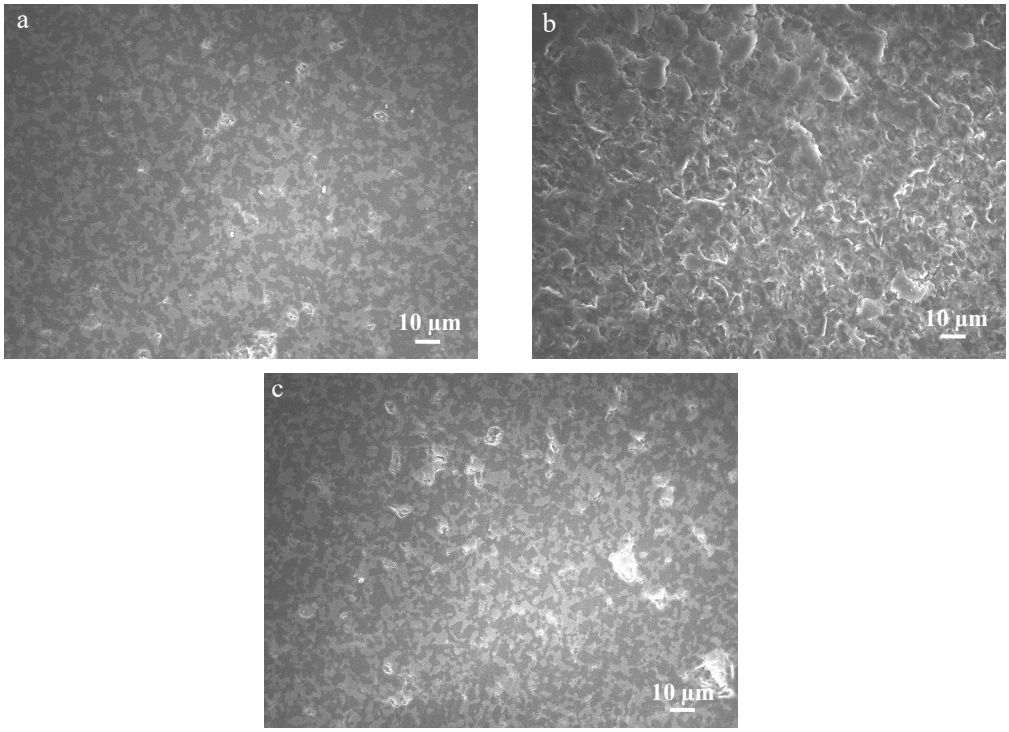

Fig. 10. SEM images of worn surfaces of B_4C-SiC composite ceramics sliding against (a) Al_2O_3 ball, (b) Si_3N_4 ball and (c) SUJ2 ball at 5 N.

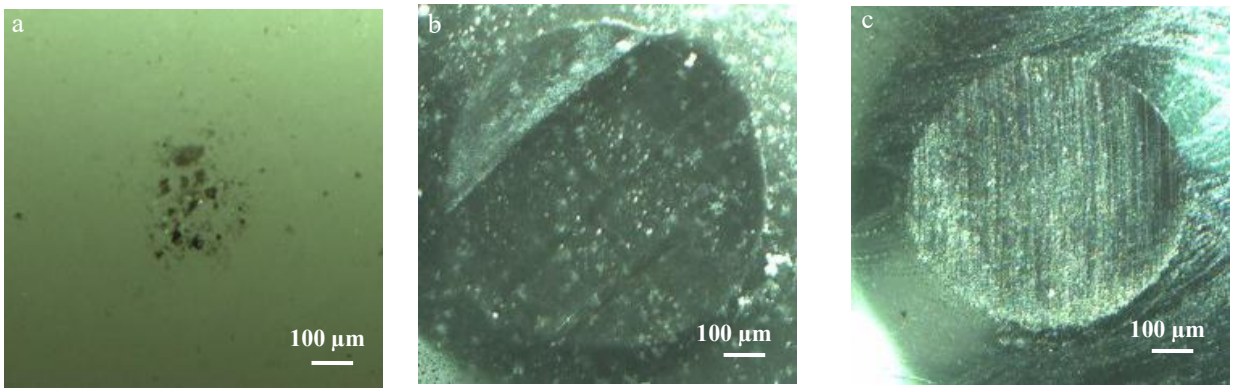

Fig. 11. Optical micrographs of the wear scars on the counterbodies: (a) Al_2O_3 ball, (b) Si_3N_4 ball and (c) SUJ2 ball at the load of 5 N.

12.3.4.2. At the load of 10 N

Fig. 12-Fig. 14 show typical SEM images of worn surfaces of B_4C-SiC composite ceramics sliding against Al_2O_3, Si_3N_4 and SUJ2 counterbodies as well as elemental distributions of the corresponding worn surfaces at 10 N, respectively. Fig. 15 reveals optical micrographs of the wear scars on the Al_2O_3, Si_3N_4 and SUJ2 counterbodies at the load of 10 N. It can be observed from Fig. 12 that the worn surface of B_4C-SiC composite ceramics sliding against Al_2O_3 ball shows the characteristic of severe brittle fracture and lateral fracture mechanism of material removal, and the worn surface is rather rough. Because of higher hardness of Al_2O_3 ball, depth of penetration of

Al_2O_3 ball to the B_4C-SiC composite ceramics increased with load increasing, causing micro-fracture of B_4C-SiC composite ceramics at 10 N. Further, small amount of debris compaction layers can be seen on the worn surface of B_4C-SiC composite ceramics sliding against Al_2O_3 ball. According to the results of elemental distributions (Fig. 12), the compaction layers are composed of O rich phase and Al rich phase. Therefore, the main composition of debris compaction layer is Al_2O_3. From Fig. 15a, it can be seen that some pits are observed on the wear scar of Al_2O_3 ball, which is attributed to the pullout of Al_2O_3 grains during the sliding process. Combined with Fig. 12, it can be known that Al_2O_3 grains pulled out from Al_2O_3 ball adhered on the worn surface of B_4C-SiC composite ceramics, and these grains were compacted during the sliding process and formed compaction layers. Such compaction layers are reported to have the ability to protect worn surfaces from further wear, causing less friction and wear [15,23,46,47], however, the compaction layer formed on the worn surface of B_4C-SiC composite ceramics sliding against Al_2O_3 ball is not a continuous, fully covered layer, and the number of this compaction layer is very small. As a result, these compaction layers can't effectively reduce friction and wear for B_4C-SiC composite ceramics sliding against Al_2O_3 ball, resulting in the increased friction coefficient and wear rate at 10 N than those at 5 N owing to severe micro-fracture. The main wear mechanisms of B_4C-SiC composite ceramics sliding against Al_2O_3 counterbody change from surface polishing and mild abrasion at 5 N to micro-fracture at 10 N.

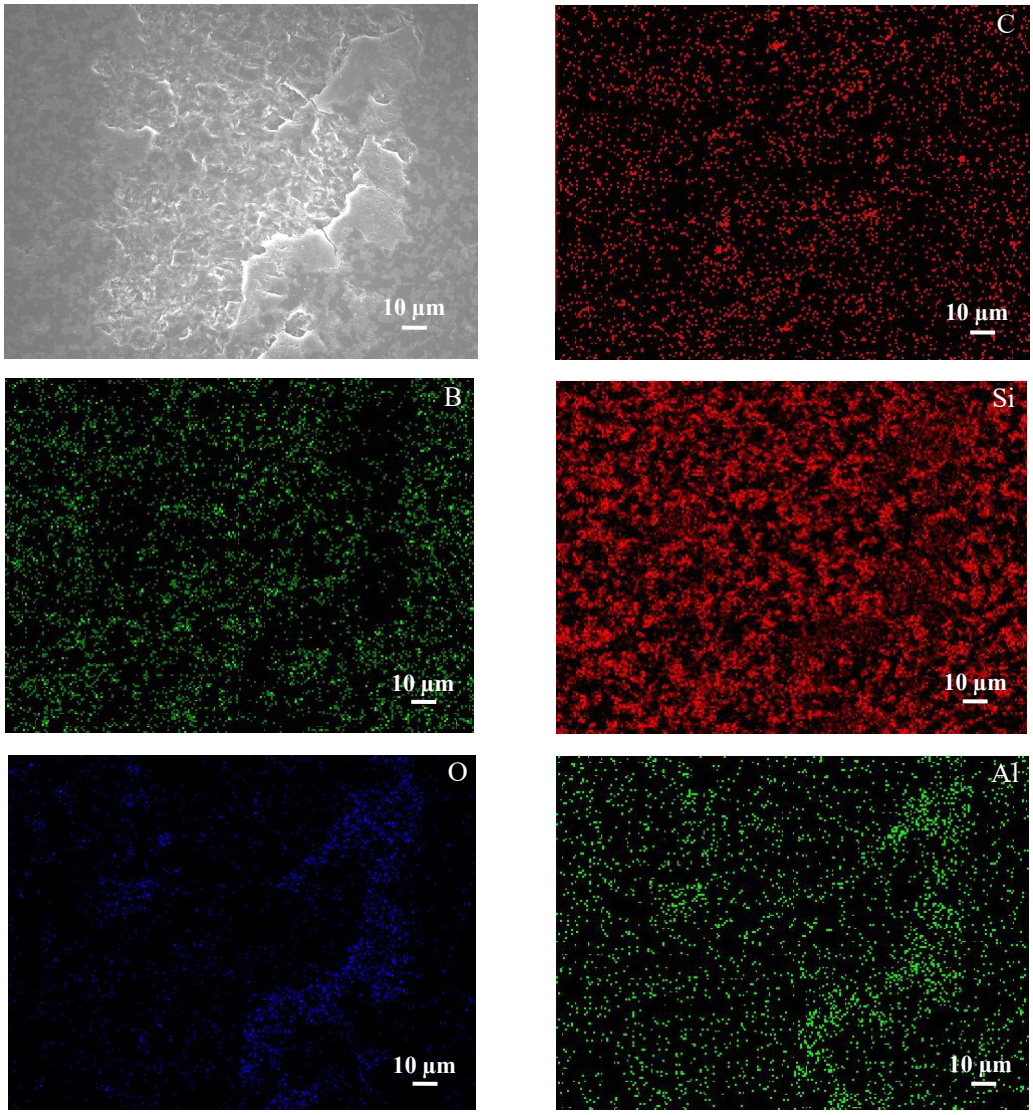

Fig. 12. SEM image of worn surface of B_4C-SiC composite ceramics sliding against Al_2O_3 ball and corresponding elemental distributions at 10 N.

In case of Si_3N_4 counterbody, the damage degree of worn surface of B_4C-SiC composite ceramics (Fig. 13) is more serious than that at the load of 5 N (Fig. 10b), and the continuous micro-fracture area was formed on the worn surface. However, the amount of compaction layers increased on the worn surface of B_4C-SiC composite ceramics as compared to that on the worn surface of B_4C-SiC composite ceramics sliding against Si_3N_4 ball at 5 N. According to the results of elemental distributions (Fig. 13), the compaction layers are composed of O rich phase and Si rich phase. Therefore, the main composition of debris compaction layer is SiO_2. Further, it can be seen from Fig. 13 that the element of N is also rich in the area of oxide compaction layers. Therefore, it can be inferred that the formation of compaction layer of SiO_2 was caused by the debris produced from the Si_3N_4 ball, rather than the oxidation of SiC grains in B_4C-SiC composite ceramics. Although the wear of Si_3N_4 ball was decreased at the load of 10 N (Fig. 15b) as compared to that at the load of 5 N (Fig. 11b), the measured friction temperature increased (Fig. 6), therefore, it is reasonable to infer that the sliding interface temperature also increased. Meanwhile, increased load made wear particles finer, and these finer wear particles were more easily oxidized due to the increased specific surface area and connected into compaction layers. Thus, increased sliding interface temperature and load promoted the formation of more compaction layers of SiO_2. Therefore, the friction and wear of B_4C-SiC composite ceramics sliding against Si_3N_4 ball were controlled by the simultaneous occurrence and competition of increased micro-fracture and more compaction layers. As a result, both the friction coefficient and the specific wear rate of B_4C-SiC composite ceramics sliding against Si_3N_4 ball changed not obviously with load increasing from 5 N to 10 N, in spite of more serious micro-fracture. The main wear mechanism of B_4C-SiC composite ceramics sliding against Si_3N_4 counterbody is still micro-fracture at 10 N.

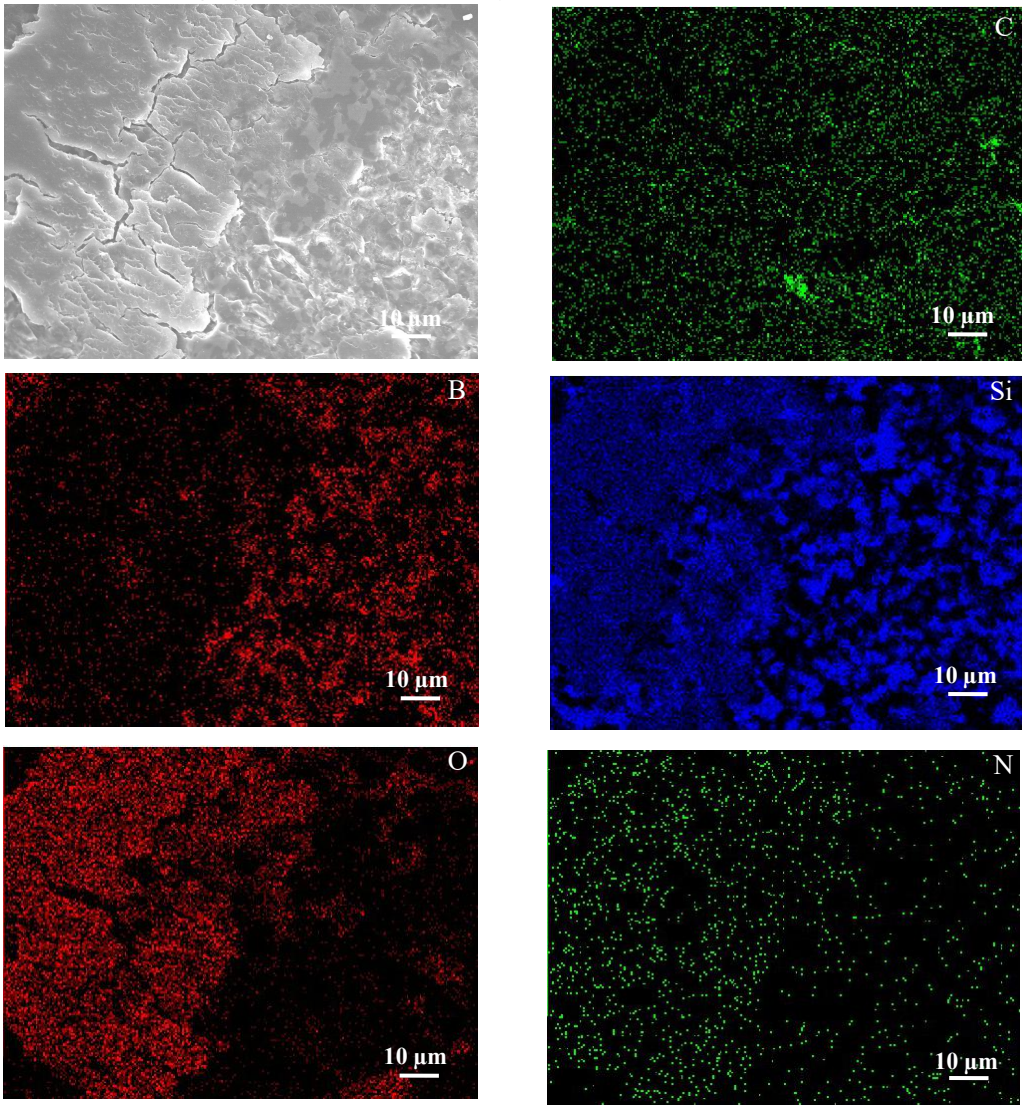

Fig. 13. SEM image of worn surface of B_4C-SiC composite ceramics sliding against Si_3N_4 ball and corresponding elemental distributions at 10 N.

It can be observed from Fig. 14 that the worn surface of B_4C-SiC composite ceramics sliding against SUJ2 ball is rather smooth, less grain pullout is observed as compared to that at the load of 5 N (Fig. 10c). The observation of the reduced damage degree of worn surface of B_4C-SiC composite ceramics sliding against SUJ2 ball at 10 N as compared with that at 5 N is consistent with the measurements of reduced specific wear rate (Fig. 7). Also, it can be seen from Fig. 15c that obvious grooves are observed on the wear scar of SUJ2 ball, which means abrasive wear was still dominant on the B_4C-SiC/SUJ2 tribopair. Furthermore, a few compaction layers are observed on the worn surface of B_4C-SiC composite ceramics sliding against SUJ2 ball. According to the results of elemental distributions (Fig. 14), the compaction layers are composed of O rich phase and Fe rich phase. Therefore, the main composition of debris compaction layer is iron oxide. The wear rate of SUJ2 ball at 10 N is similar to that at 5 N (Fig. 8, Fig. 11c and Fig. 15c), however, the measured friction temperature of B_4C-SiC/SUJ2 tribopair at 10 N is higher than that at 5 N (Fig. 6). Increased sliding interface temperature is favorable for promoting the formation of iron oxides, thus these iron oxides formed compaction layers during the dry sliding. However, the number of the compaction layers formed on the worn surface of B_4C-SiC composite ceramics sliding against SUJ2 ball is so small that these compaction layers can't effectively reduce friction coefficient for B_4C-SiC composite ceramics sliding against SUJ2 ball at 10 N. The main wear mechanisms of B_4C-SiC composite ceramics sliding against SUJ2 ball at the load of 10 N are the same as that at the load of 5 N, viz. surface polishing and mild abrasion.

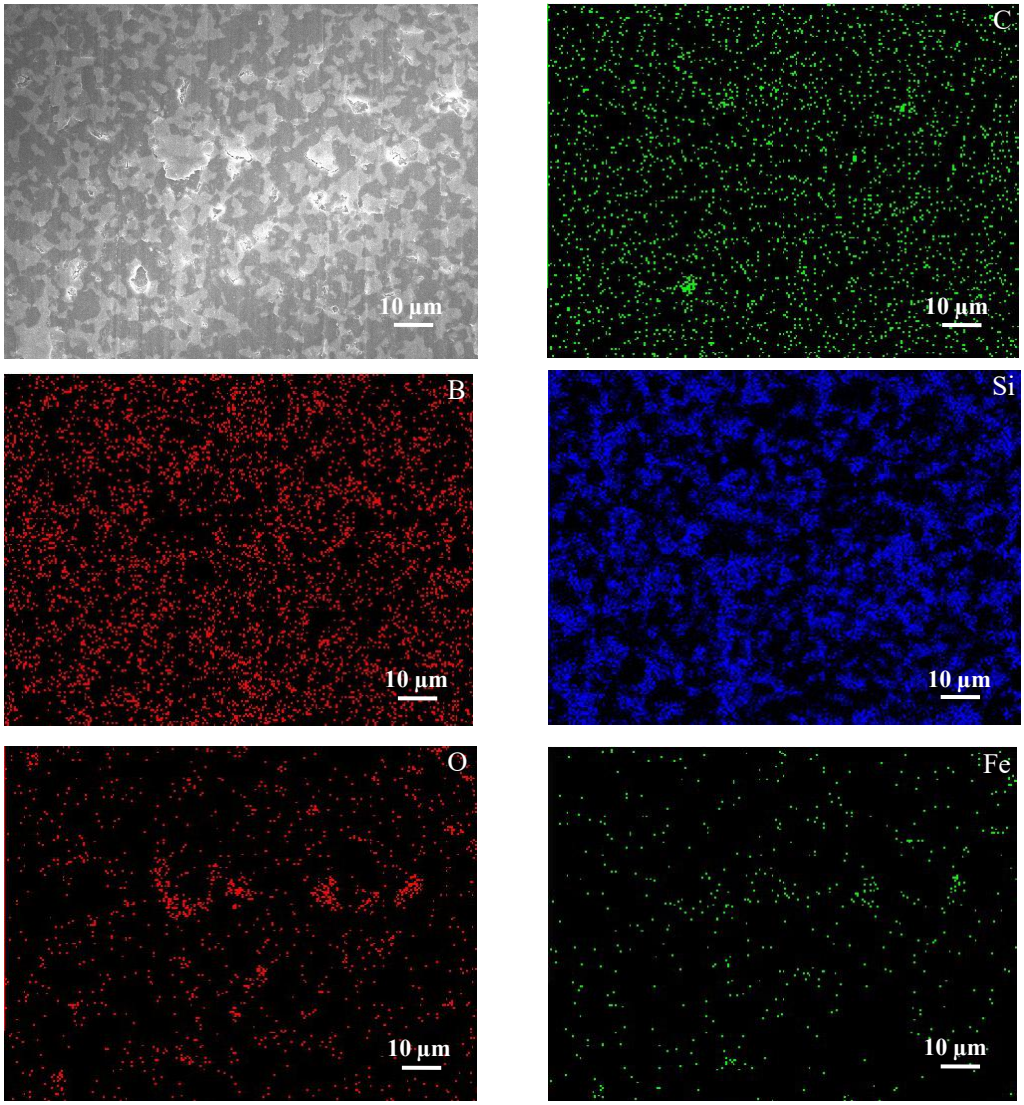

Fig. 14. SEM image of worn surface of B_4C-SiC composite ceramics sliding against SUJ2 ball and corresponding elemental distributions at 10 N.

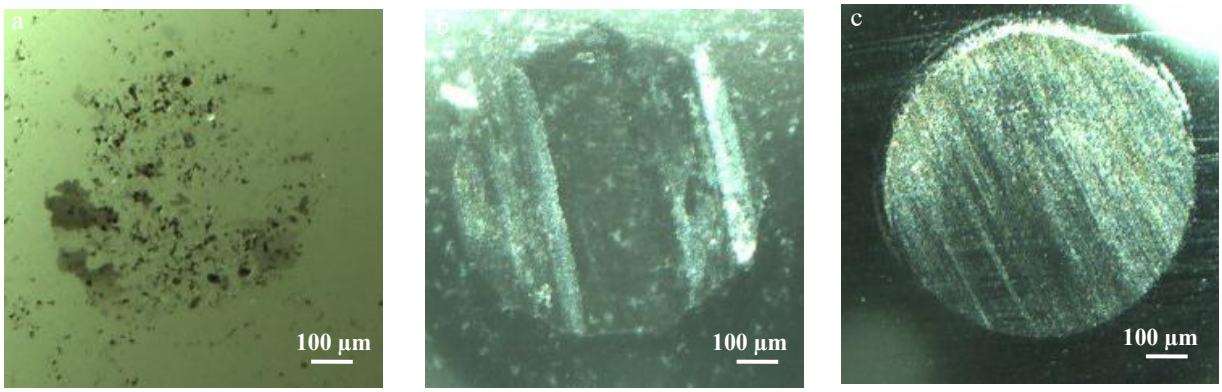

Fig. 15. Optical micrographs of the wear scars on the counterbodies: (a) Al_2O_3 ball, (b) Si_3N_4 ball and (c) SUJ2 ball at the load of 10 N.

The specific wear rate of B_4C-SiC composite ceramics is greater as sliding against Al_2O_3 ball, followed by Si_3N_4 ball, and lastly SUJ2 ball at 10 N. The hardness of counterbody is higher for Al_2O_3 ball, followed by Si_3N_4 ball, and lastly SUJ2 ball, therefore, the increased specific wear rate of B_4C-SiC composite ceramics is attributed to the increased hardness of counterbody, which is resulting from the increased depth of penetration to the B_4C-SiC composite ceramics with the increase of hardness of counterbody. On the other hand, the mean Hertzian contact stress is higher for B_4C-SiC/Al_2O_3 tribopair, followed by B_4C-SiC/Si_3N_4 tribopair, and lastly B_4C-SiC/SUJ2 tribopair, therefore, the increased specific wear rate of B_4C-SiC composite ceramics may also be attributed to the slightly increased mean Hertzian contact stress. Deng et al. [48] studied the erosion wear of B_4C ceramics by abrasive particle impact, and found that the wear rate of B_4C ceramics increased with hardness of erodent abrasive particles increasing. Kovalčíková et al. [23] reported that the specific wear rate of SiC ceramics increased as the hardness of the counterbodies increased under dry sliding condition. Similar results are also observed for the B_4C-SiC composite ceramics under dry sliding condition at 10 N in this study, i.e. specific wear rate of B_4C-SiC composite ceramics increased with the increase of hardness of counterbody, suggesting that lower hardness counterbodies were not able to easily initiate deformation in B_4C-SiC composite ceramics. Despite higher hardness of Al_2O_3 counterbody, mechanical fracture was not induced on the B_4C-SiC composite ceramics sliding against Al_2O_3 ball at 5 N. Therefore, B_4C-SiC composite ceramics showed higher specific wear rate at low load when the B_4C-SiC composite ceramics slid against the counterbody with chemical similarity, viz. Si_3N_4 ball. This means the wear of B_4C-SiC composite ceramics at low load is mainly controlled by the chemical similarity of counterbody, rather than the hardness of counterbody. However, Al_2O_3 ball with higher hardness can cause mechanical fracture on the B_4C-SiC composite ceramics as the load increased to 10 N, in this situation, the wear of B_4C-SiC composite ceramics at intermediate load is mainly controlled by the hardness of counterbody. Deeper penetration against counterbody with higher hardness caused more material removal of B_4C-SiC composite ceramics, thus the B_4C-SiC composite ceramics showed the lowest specific wear rate when they slid against the SUJ2 ball with the lowest hardness. On the other hand, the number of the compaction layers formed on the worn surface of B_4C-SiC composite ceramics is larger as sliding against Si_3N_4 ball, followed by Al_2O_3 ball, and lastly SUJ2 ball. Therefore, the friction coefficient of B_4C-SiC composite ceramics is lower as sliding against Si_3N_4 ball, followed by Al_2O_3 ball, and lastly SUJ2 ball at 10 N.

12.3.4.3. At the load of 20 N

Fig. 16-Fig. 18 show typical SEM images of worn surfaces of B_4C-SiC composite ceramics sliding against Al_2O_3, Si_3N_4 and SUJ2 counterbodies as well as elemental distributions of the corresponding worn surfaces at 20 N, respectively. Fig. 19 shows optical micrographs of the wear scars on the Al_2O_3, Si_3N_4 and SUJ2 counterbodies at 20 N. It can be seen from Fig. 16 that the severe micro-fracture is still the main feature of the worn surface of B_4C-SiC composite ceramics sliding against Al_2O_3 ball. According to the results of elemental distributions (Fig. 16), the main composition of debris compaction layer is still Al_2O_3. However, the number of compaction layers becomes more than that on the worn surface of B_4C-SiC composite ceramics sliding against Al_2O_3 ball at 10 N. From Fig. 19a and Fig. 8, it can be seen that the wear of Al_2O_3 ball induced by fatigue increased with load increasing, causing more Al_2O_3 debris on the worn surface of B_4C-SiC composite ceramics. These increased Al_2O_3 debris was compacted during the sliding process to form more compaction layers. Increased compaction layers can further smooth the worn surface of B_4C-SiC composite ceramics. Therefore, the friction coefficient of B_4C-SiC composite ceramics sliding against Al_2O_3 ball at 20 N was lower than that of B_4C-SiC composite ceramics sliding against Al_2O_3 ball at 10 N, but still higher than that of B_4C-SiC composite ceramics sliding against Al_2O_3 ball at 5 N because the worn surface was not completely covered by the compaction layers and part of the worn surface was rather rough due to severe micro-fracture at 20 N. Meanwhile, the increased compaction layers can also further protect the worn surface of B_4C-SiC composite ceramics from further wear, therefore, the specific wear rate of B_4C-SiC composite ceramics sliding against Al_2O_3 ball at 20 N was not significantly increased compared to that at 10 N.

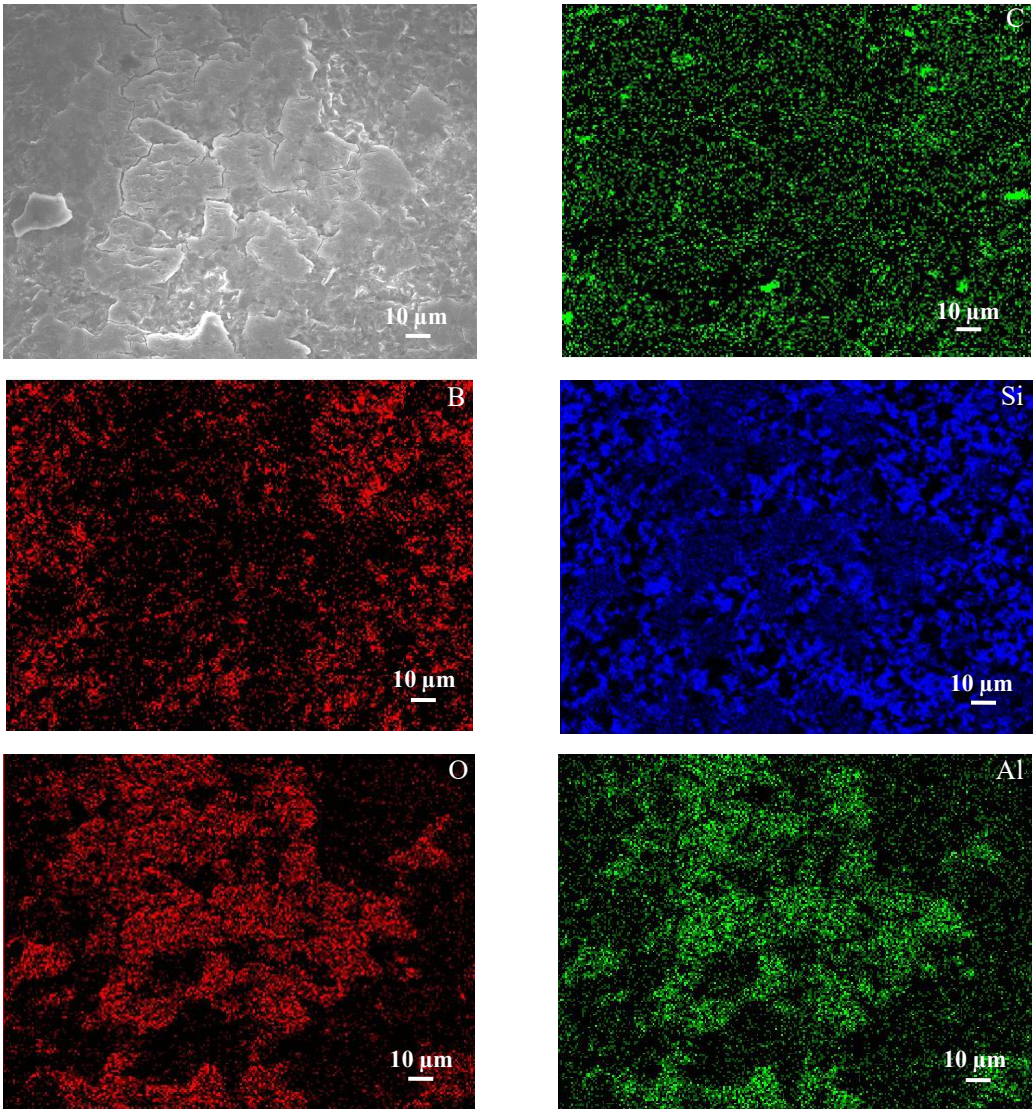

Fig. 16. SEM image of worn surface of B_4C-SiC composite ceramics sliding against Al_2O_3 ball and corresponding elemental distributions at 20 N.

In case of Si_3N_4 counterbody, the characteristic of worn surface of B_4C-SiC composite ceramics (Fig. 17) is similar to that at 10 N (Fig. 13). According to the results of elemental distributions (Fig. 17), the main composition of debris compaction layer is still SiO_2, which was still caused by the debris produced from the Si_3N_4 ball. Therefore, similar friction coefficients and specific wear rates were observed for B_4C-SiC/Si_3N_4 tribopair between the load of 10 N and the load of 20 N.

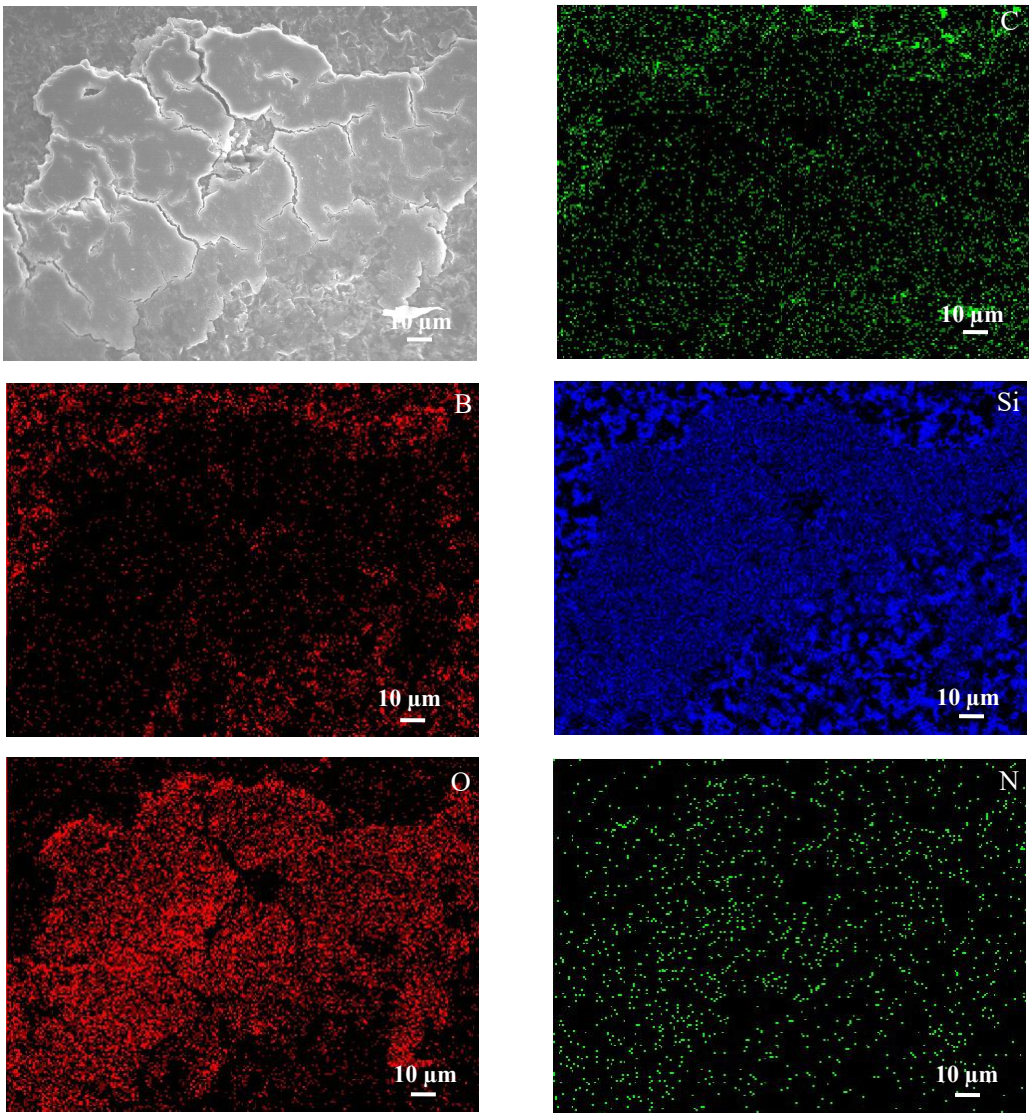

Fig. 17. SEM image of worn surface of B_4C-SiC composite ceramics sliding against Si_3N_4 ball and corresponding elemental distributions at 20 N.

It can be seen from Fig. 18 that micro-fracture and a number of compaction layers are observed on the worn surface of B_4C-SiC composite ceramics sliding against SUJ2 ball. According to the results of elemental distributions (Fig. 18), the main composition of debris compaction layers is iron oxide. From Fig. 19c and Fig. 8, it can be seen that the specific wear rate of SUJ2 ball was significantly increased at 20 N as compared to those at 5 N and 10 N. Thus, more Fe debris was produced on the sliding interface owing to the increased load. From Fig. 6, it can be seen that the measured friction temperature of B_4C-SiC/SUJ2 tribopair at the load of 20 N was significantly higher than those at 5 N and 10 N. Therefore, more compaction layers were formed on the worn surface of

B_4C-SiC composite ceramics sliding against SUJ2 ball owing to more Fe debris and higher sliding interface temperature. Although more Fe debris was produced, these debris was crushed, oxidized, connected to form protective compaction layers at high load instead of being present on the sliding interface as hard abrasive particles. Compared with Fig. 15c, it can be seen from Fig. 19c that, on the one hand, these iron oxide layers were also formed on the wear scar of SUJ2 ball, and on the other hand, the number of grooves was significant reduced, which means abrasive wear was reduced in B_4C-SiC/SUJ2 tribopair at 20 N. Because the friction of B_4C-SiC/SUJ2 tribopair at 20 N occurred between the iron oxide layer on the worn surface of B_4C-SiC composite ceramics and the iron oxide layer on the wear scar of SUJ2 ball, therefore, the friction coefficient of B_4C-SiC/SUJ2 tribopair at 20 N was lower than those at 5 N and 10 N. Although the main wear mechanisms of B_4C-SiC composite ceramics sliding against SUJ2 counterbody changed from surface polishing and mild abrasion at 10 N to micro-fracture at 20 N, the formation of a number of compaction layers protected the worn surface from further wear, thus the increase in specific wear rate of B_4C-SiC composite ceramics was not obvious compared to that at 10 N.

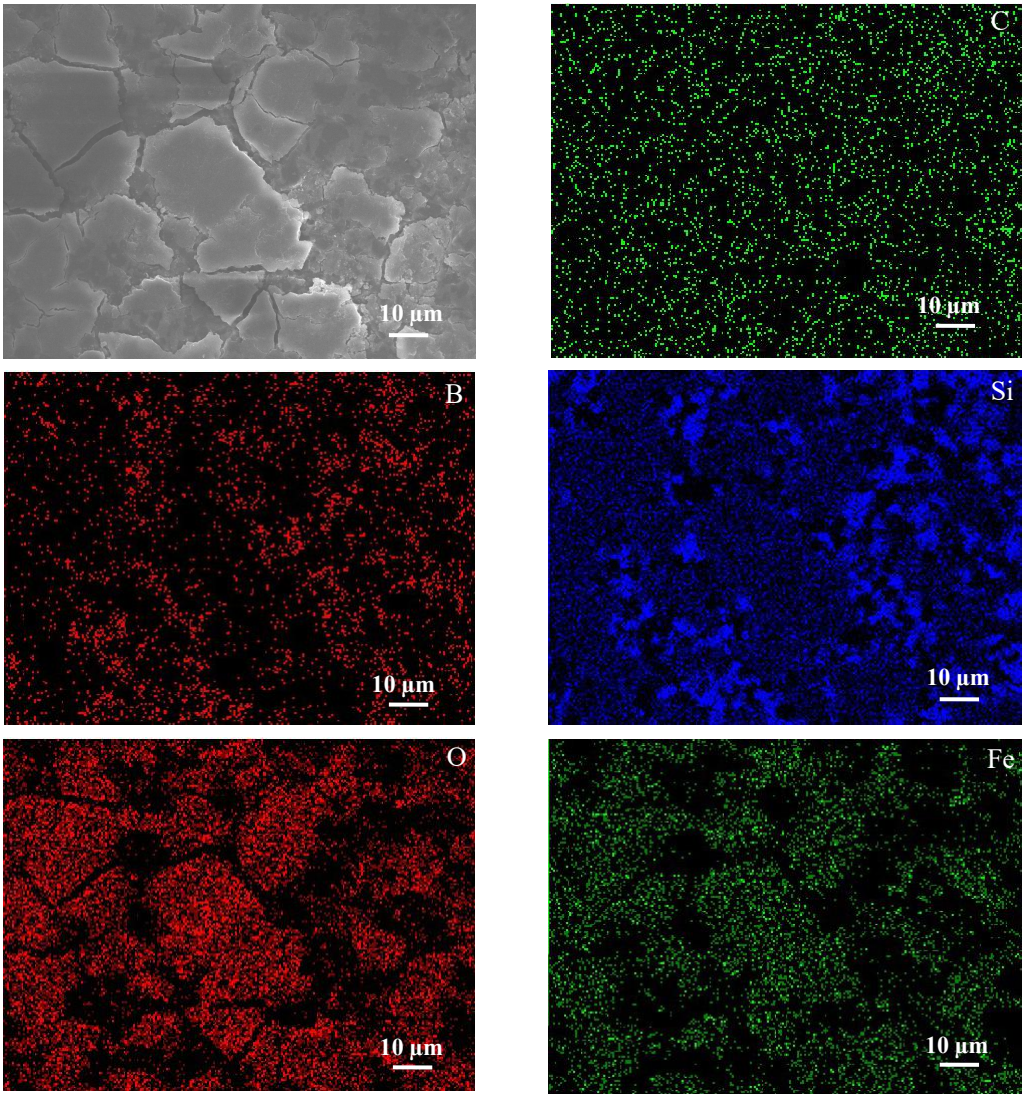

Fig. 18. SEM image of worn surface of B_4C-SiC composite ceramics sliding against SUJ2 ball and corresponding elemental distributions at 20 N.

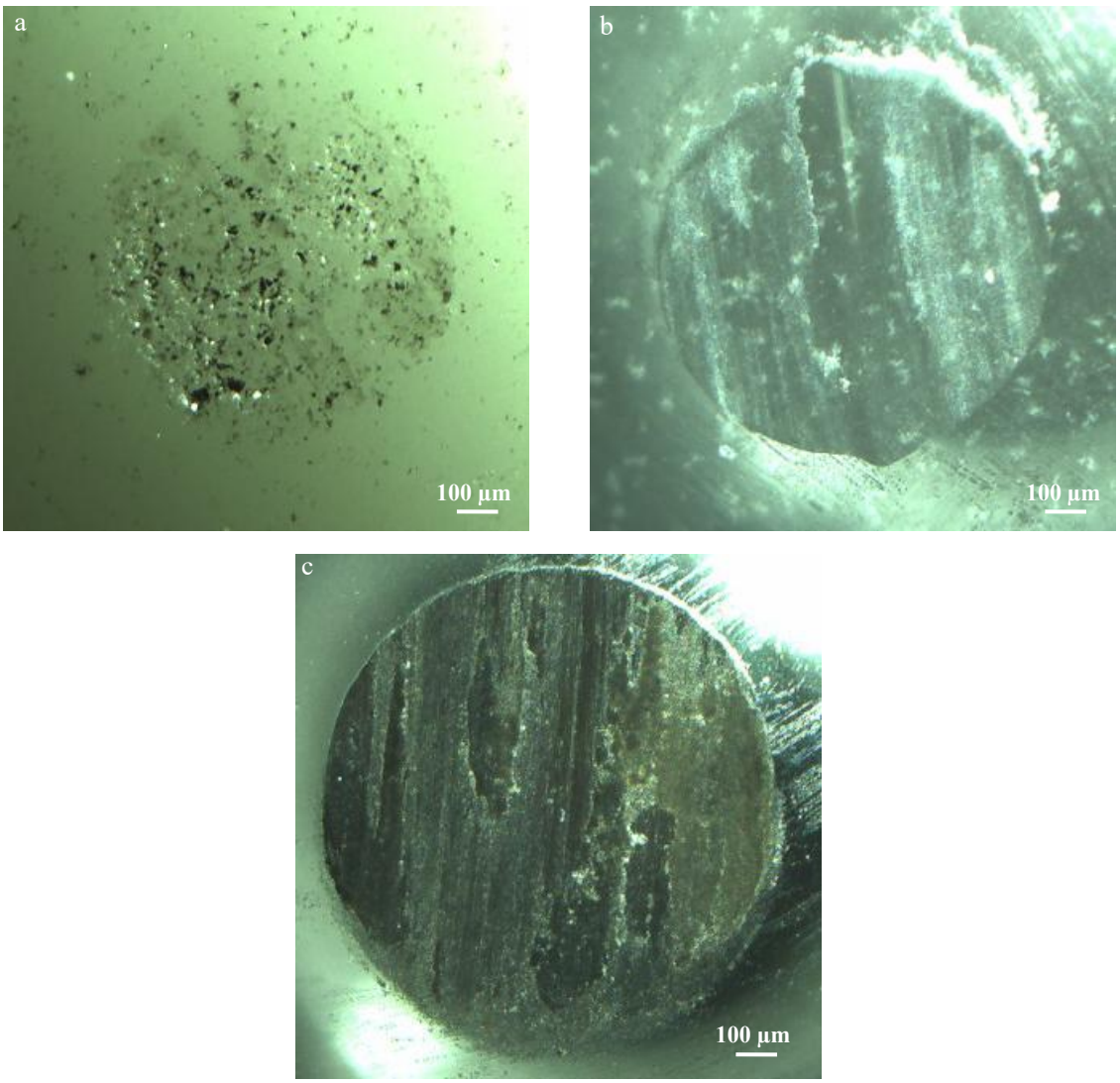

Fig. 19. Optical micrographs of the wear scars on the counterbodies: (a) Al_2O_3 ball, (b) Si_3N_4 ball and (c) SUJ2 ball at the load of 20 N.

Because of the formation of a number of compaction layers on all the worn surfaces of B_4C-SiC composite ceramics sliding against Al_2O_3, Si_3N_4 and SUJ2 counterbodies at 20 N, therefore, the differences in friction coefficients of B_4C-SiC/Al_2O_3, B_4C-SiC/Si_3N_4 and B_4C-SiC/SUJ2 tribopairs were not obvious. Meanwhile, similar to at the load of 10 N, the specific wear rate of B_4C-SiC composite ceramics increased with the increase of hardness of counterbody at 20 N. As a whole, the B_4C-SiC/Al_2O_3, B_4C-SiC/Si_3N_4 and B_4C-SiC/SUJ2 tribopairs showed similar friction coefficients and systematic specific wear rates at 20 N, although the specific wear rate of B_4C-SiC composite ceramics was affected by different counterbodies.

12.3.5. Brief summary

In summary, for B_4C-SiC composite ceramics, the friction coefficient is dependent on counterbody materials, especially at low load and intermediate load, and the specific wear rate is also dependent on counterbody materials. Further, systematic specific wear rate of B_4C-SiC composite ceramics sliding against different counterbodies is dependent on counterbody materials, however, the influence of counterbody materials on systematic specific wear rate of B_4C-SiC composite ceramics is not obvious at high load. Major wear types for the B_4C-SiC composite ceramics sliding against different counterbodies at different loads are summarized in Table 3. When sliding against

Al_2O_3 ball and SUJ2 ball, the main wear mechanisms of B_4C-SiC composite ceramics change from surface polishing and mild abrasion to micro-fracture with load increasing from 5 N to 20 N. When sliding against Si_3N_4 ball, the main wear mechanism of B_4C-SiC composite ceramics is micro-fracture at any load. At the same loads, the wear of B_4C-SiC composite ceramics at low load is mainly controlled by the chemical similarity of counterbody, whereas the wear of B_4C-SiC composite ceramics at intermediate and high loads is mainly controlled by the hardness of counterbody. Moreover, although many scholars [15, 34, 44, 45] found the load dependence of specific wear rate of ceramic materials, no load dependence was observed on B_4C-SiC composite ceramics sliding against different counterbodies in this study, which should be ascribed to the formation of compaction layers, except the increased specific wear rate of the B_4C-SiC composite ceramics sliding against Al_2O_3 ball with the load increasing from 5 N to 10 N. The formation of compaction layers on the worn surface of B_4C-SiC composite ceramics can protect the worn surface from further wear. In addition, with the increased number of compaction layers formed on the worn surface of B_4C-SiC composite ceramics at high load, the differences in friction coefficients of B_4C-SiC composite ceramics sliding against different counterbodies reduced. This study gives the base for the design of B_4C-SiC composite ceramics sliding against different counterbodies at different normal loads under dry sliding condition.

Table 3 Wear types for the B_4C-SiC composite ceramics sliding against different counterbodies at different loads.

Load	Counterbody		
(N)	Al_2O_3	Si_3N_4	SUJ2
5	Surface polishing, mild abrasion	Micro-fracture	Surface polishing, mild abrasion
10	Micro-fracture	Micro-fracture	Surface polishing, mild abrasion
20	Micro-fracture	Micro-fracture	Micro-fracture

12.4. Conclusions

Dry sliding friction and wear tests have been used to study the effect of commercially available counterbody materials (Al_2O_3, Si_3N_4 and SUJ2 bearing steel) on tribological properties of B_4C-SiC composite ceramics at 5 N, 10 N and 20 N loads. The following are major conclusions:

(1) For the B_4C-SiC composite ceramics, both the friction coefficient and specific wear rate were dependent on counterbody materials. The friction coefficient of B_4C-SiC composite ceramics sliding against Al_2O_3, Si_3N_4 and SUJ2 counterbodies changed in the range of 0.53-0.82 at the load of 5 N, between 0.59 and 0.81 at the load of 10 N, in the range of 0.55-0.63 at the load of 20 N. The specific wear rate of B_4C-SiC composite ceramics sliding against Al_2O_3, Si_3N_4 and SUJ2 counterbodies changed in the range of 2.7×10^{-6}-7.5×10^{-6} $mm^3/N\cdot m$ at the load of 5 N, between 2.2×10^{-6} $mm^3/N\cdot m$ and 8.9×10^{-6} $mm^3/N\cdot m$ at the load of 10 N, in the range of 3.3×10^{-6}-8.8×10^{-6} $mm^3/N\cdot m$ at the load of 20 N. However, the influence of counterbody materials on friction coefficient and systematic specific wear rate of B_4C-SiC composite ceramics was not obvious at high load, which was attributed to the formation of a number of compaction layers on all the worn surfaces of B_4C-SiC composite ceramics sliding against Al_2O_3, Si_3N_4 and SUJ2 counterbodies.

(2) When sliding against Al_2O_3 ball and SUJ2 ball, the main wear mechanisms of B_4C-SiC composite ceramics changed from surface polishing and mild abrasion to micro-fracture with load increasing from 5 N to 20 N. When sliding against Si_3N_4 ball, the main wear mechanism of B_4C-SiC composite ceramics was micro-fracture at any load. At the same loads, the wear of B_4C-SiC composite ceramics sliding against different counterbodies at low load was mainly controlled by the chemical similarity of counterbody, whereas the wear of B_4C-SiC composite

ceramics sliding against different counterbodies at intermediate and high loads was mainly controlled by the hardness of counterbody. Therefore, the B_4C-SiC composite ceramics sliding against Si_3N_4 ball showed highest specific wear rate at low load, whereas the B_4C-SiC composite ceramics sliding against Al_2O_3 ball showed highest specific wear rate at intermediate and high loads.

12.5. References

[1] A. Demir, N. Altinkok, F. Findik, I. Ozsert. The wear behaviour of dual ceramic particles (Al_2O_3/SiC) reinforced aluminium matrix composites. Key Engineering Materials,2004,264-268:1079-1082.

[2] C. X. Liu, J. L. Sun. Erosion behaviour of B_4C-based ceramic composites. Ceramics International,2010,36(4):1297-1302.

[3] N. Altinkok, A. Demir, I. Ozsert, F. Findik. Compressive behavior of Al_2O_3-SiC ceramic composite foams fabricated by decomposition of aluminum sulfate aqueous solution. Journal of Composite Materials,2007,41(11):1361-1373.

[4] E. Ciudad, O. Borrero-López, F. Rodríguez-Rojas, A. L. Ortiz, F. Guiberteau. Effect of intergranular phase chemistry on the sliding-wear resistance of pressureless liquid-phase-sintered α-SiC. Journal of the European Ceramic Society,2012,32(2):511-516.

[5] W. Zhang, S. Yamashita, H. Kita. Progress in tribological research of SiC ceramics in unlubricated sliding- A review. Materials & Design,2020,190:108528.

[6] F. Findik. Latest progress on tribological properties of industrial materials. Materials & Design,2014,57:218-244.

[7] S. Lafon-Placette, K. Delbé, J. Denape, M. Ferrato. Tribological characterization of silicon carbide and carbon materials. Journal of the European Ceramic Society,2015,35(4):1147-1159.

[8] J. L. Sun, C. X. Liu, J. Tian, B. F. Feng. Erosion behavior of B_4C based ceramic nozzles by abrasive air-jet. Ceramics International,2012,38(8):6599-6605.

[9] H. Y. Zhu, Y. R. Niu, C. C. Lin, L. P. Huang, H. Ji, X. B. Zheng. Microstructures and tribological properties of vacuum plasma sprayed B_4C-Ni composite coatings. Ceramics International,2013,39(1):101-110.

[10] W. Zhang, S. Yamashita, H. Kita. Progress in pressureless sintering of boron carbide ceramics-A review. Advances in Applied Ceramics: Structural, Functional and Bioceramics,2019,118(4):222-239.

[11] U. Soy, A. Demir, F. Findik. Friction and wear behaviors of Al-SiC-B_4C composites produced by pressure infiltration method. Industrial Lubrication and Tribology,2011,63(5):387-393.

[12] M. Aydin, F.Findik. Wear properties of magnesium matrix composites reinforced with SiO_2 particles. Industrial Lubrication & Tribology,2010,62(4):232-237.

[13] N. Altinkok, İ. Özsert, F. Findik. Dry sliding wear behavior of Al_2O_3/SiC particle reinforced aluminium based mmcs fabricated by stir casting method. Acta Physica Polonica A,2013,124(1):11-19.

[14] W. Zhang, S. Yamashita, H. Kita. Effects of load on tribological properties of B_4C and B_4C-SiC ceramics against SiC ball. Journal of Asian Ceramic Societies,2020,8(3):586-596.

[15] S. K. Sharma, B. V. M. Kumar, Y. W. Kim. Effect of WC addition on sliding wear behavior of SiC ceramics. Ceramics International,2015,41(3):3427-3437.

[16] Y. G. Gogotsi, A. M. Koval'chenko, I. A. Kossko. Tribochemical interactions of boron carbides against steel. Wear,1992,154:133-140.

[17] L. Micele, G. Palombarini, S. Guicciardi, L. Silvestroni. Tribological behaviour and wear resistance of a SiC-$MoSi_2$ composite dry sliding against Al_2O_3. Wear,2010,269(5):368-375.

[18] W. S. Lin, N. X. Fang, L. He. Wear properties of reaction sintered B_4C composites. Advanced Materials Research,2011,152-153:883-886.

[19] F. Li, S. Y. Zhu, J. Cheng, Z. H. Qiao, J. Yang. Tribological properties of Mo and CaF_2 added SiC matrix composites at elevated temperatures. Tribology International,2017,111:46-51.

[20] X. Q. Cao, L. L. Shang, Y. M. Liang, G. G. Zhang, Z. B. Lu, Q. J. Xue. The tribological performances of the boron carbide films tested under wet air and wet N_2 conditions. Tribology Letters,2019,67(3):70.

[21] V. S. R. Murthy, H. Kobayashi, S. Tsurekawa, N. Tamari, T. Watanabe, K. Kato. Influence of humidity and doping elements on the friction and wear of SiC in unlubricated sliding. Tribology International,2004,37(5):353-364.

[22] S. Guicciardi, D. Sciti, C. Melandri, G. Pezzotti. Dry sliding wear behavior of nano-sized SiC pins against SiC and Si_3N_4 discs. Wear,2007,262(5-6):529-535.

[23] A. Kovalčíková, P. Kurek, J. Balko, J. Dusza, P. Šajgalík, M. Mihaliková. Effect of the counterpart material on wear characteristics of silicon carbide ceramics. Int. Journal of Refractory Metals and Hard Materials:2014,44: 12-18.

[24] S. K. Sharma, B. V. M. Kumar, Y. W. Kim. Tribology of WC reinforced SiC ceramics: Influence of counterbody. Friction,2019,7(2):129-142.

[25] W. Zhang, S. Yamashita, T. Kumazawa, F. Ozeki, H. Hyuga, H. Kita. Effect of nanorelief structure formed in situ on tribological properties of ceramics in dry sliding. Ceramics International,2019,45(11):13818-13824.

[26] W. Zhang, S. Yamashita, H. Kita. Tribological properties of SiC-B_4C ceramics under dry sliding condition. Journal of the European Ceramic Society,2020,40(8):2855-2861.

[27] W. Zhang, S. Yamashita, T. Kumazawa, F. Ozeki, H. Hyuga, W. Norimatsu, H. Kita. A study on formation mechanisms of relief structure formed in situ on the surface of ceramics. Ceramics International,2019,45(17):23143-23148.

[28] W. Zhang, S. Yamashita, T. Kumazawa, F. Ozeki, H. Hyuga, H. Kita. Influence of surface roughness parameters and surface morphology on friction performance of ceramics. Journal of the Ceramic Society of Japan,2019,127(11):837-842.

[29] B. R. Lawn. In fracture of brittle solids. 2nd ed. Cambridge University Press, Cambridge, UK, 1993.

[30] R. Wäsche, D. Klaffke, T. Troczynski. Tribological performance of SiC and TiB_2 against SiC and Al_2O_3 at low sliding speeds. Wear,2004,256(7-8):695-704.

[31] X. Q. Li, Y. M. Gao, W. Pan, Z. C. Zhong, L. C. Song, W. Chen, Q. X. Yang. Effect of hBN content on the friction and wear characteristics of B_4C-hBN ceramic composites under dry sliding condition. Ceramics International,2015,41(3):3918-3926.

[32] X. Q. Li, Y. M. Gao, W. Pan, X. Wang, L. C. Song, Z. C. Zhong, S. S. Wu. Fabrication and characterization of B_4C-based ceramic composites with different mass fractions of hexagonal boron nitride. Ceramics International,2015,41(1):27-36.

[33] R. Alexander, K.V. Ravikanth, R. D. Bedse, T. S. R. Ch. Murthy, K. Dasgupta. Effect of carbon fiber on the tribo-mechanical properties of boron carbide: Comparison with carbon nanotube reinforcement. International Journal of Refractory Metals & Hard Materials,2019,85:105055.

[34] J. K. Sonber, P. K. Limaye, T. S. R. Ch. Murthy, K. Sairam, A. Nagaraj, N. L. Soni, R. J. Patel, J. K. Chakravartty. Tribological properties of boron carbide in sliding against WC ball. International Journal of Refractory Metals and Hard Materials,2015,51:110-117.

[35] W. Zhang, S. Yamashita, T. Kumazawa, F. Ozeki, H. Hyuga, H. Kita. Tribological properties of B_4C ceramics prepared by pressureless sintering and annealed at different temperatures. Tribology Transactions,2020,63(4):672-682.

[36] W. Zhang, S. Yamashita, T. Kumazawa, F. Ozeki, H. Hyuga, H. Kita. Study on friction behavior of SiC-B_4C composite ceramics after annealing. Industrial Lubrication and Tribology,2020,72(5):673-679.

[37] B. V. M. Kumar, Y. W. Kim, D. S. Lim, W. S. Seo. Influence of small amount of sintering additives on

unlubricated sliding wear properties of SiC ceramics. Ceramics International,2011,37(8):3599-3608.
[38] T. K. Guha, B. Basu. Microfracture and limited tribochemical wear of silicon carbide during high-speed sliding in cryogenic environment. Journal of the American Ceramic Society,2010,93(6):1764-1773.
[39] K. H. Z. Gahr, R. Blattner, D. H. Hwang, K. Pöhlmann. Micro and micro-tribological properties of SiC ceramics in sliding contact.Wear,2001,250:299-310.
[40] B. V. M. Kumar, B. Basu, M. Kalin, J. Vizintin. Load-dependent transition in sliding wear properties of TiCN-WC-Ni cermets. Journal of the American Ceramic Society,2007,90(5):1534-1540.
[41] B. V. M. Kumar, B. Basu, J. Vizintin, M. Kalin. Tribochemistry in sliding wear of TiCN-Ni-based cermets. Journal of Materials Research,2008,23(5):1214-1227.
[42] R. Prioli, D. C. Reigada, F. L. Freire, Jr.. Nanoscale friction and wear mechanisms at the interface between a boron carbide film and an atomic force microscope tip. Journal of Applied Physics,2000,87(3):1118-1122.
[43] R. Prioli, D.C. Reigada, F. L. Freire Jr.. The role of capillary condensation of water in the nanoscale friction and wear properties of boron carbide films. Journal of Applied Physics,2000,88(2):679-682.
[44] T. S. R. C. Murthy, S. Ankata, J. K. Sonber, K. Sairam, K. Singh, A. Nagaraj, P. Sengupta, R. D. Bedse, S. Majumdar, V. Kain. Microstructure, thermo-physical, mechanical and wear properties of in-situ formed boron carbide-zirconium diboride composite. Ceramics-Silikáty,2018,62(1):15-30.
[45] X. Q. Li, S. Z. Wei, Q. X. Yang, Y. M. Gao, Z. C. Zhong. Tribological performance of self-matching pairs of B_4C/hBN composite ceramics under different frictional loads. Ceramics International,2020,46(1):996-1001.
[46] J. Llorente, B. Román-Manso, P. Miranzo, M. Belmonte. Tribological performance under dry sliding conditions of graphene/silicon carbide composites. Journal of the European Ceramic Society,2016,36(3):429-435.
[47] K. H. Z. Gahr, W. Bundschuh, B. Zimmerlin. Effect of grain size on friction and sliding wear of oxide ceramics. Wear,1993,162-164:269-279.
[48] J. X. Deng. Erosion wear of boron carbide ceramic nozzles by abrasive air-jets. Materials Science and Engineering A,2005,408(1-2):227-233.

Chapter 13
Tribology of B_4C-SiC composite ceramics under water lubrication: Influence of counterpart

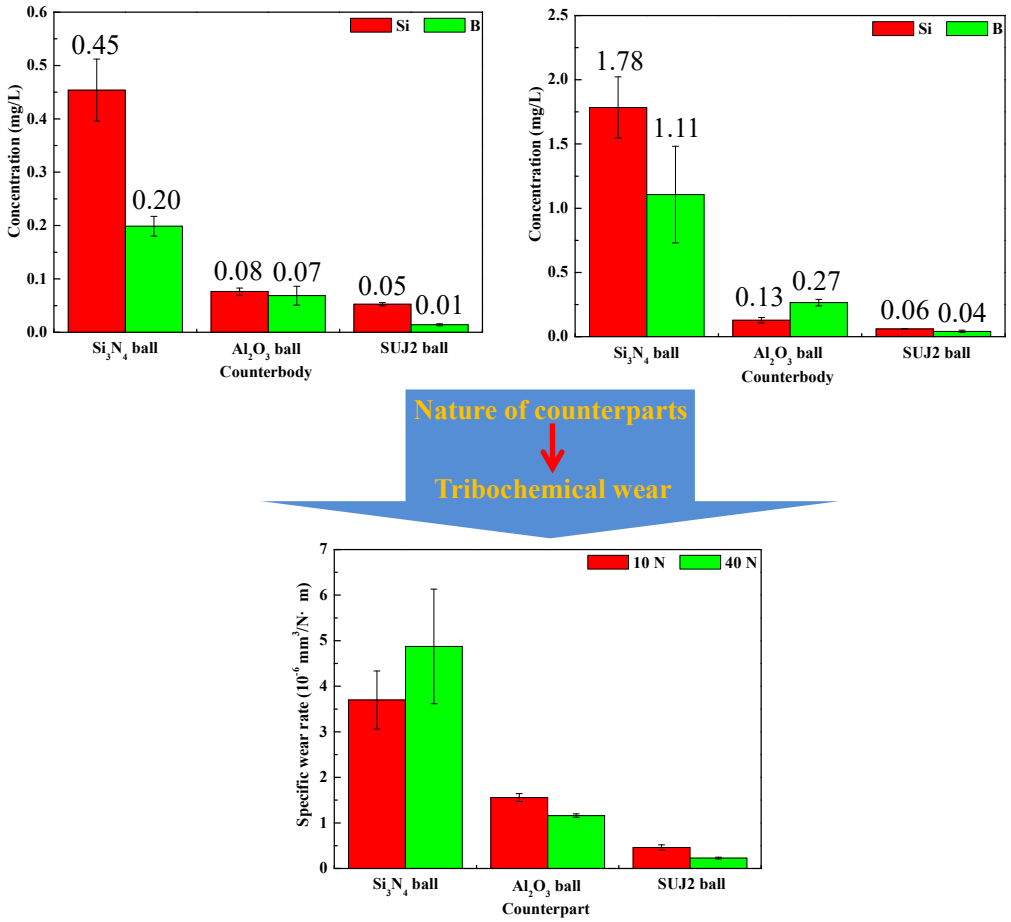

The tribological tests under water lubrication have been made on B_4C-SiC composite ceramics in contact with different counterparts (Si_3N_4, Al_2O_3 and SUJ2) at 10 and 40 N loads. Coefficient of friction (COF) and wear rate were measured, and friction and wear mechanisms were identified. When the B_4C-SiC discs slide against different counterparts in water, the similar COF is obtained, except against SUJ2 counterpart at 40 N. The increased COF of B_4C-SiC/SUJ2 tribo-couple at 40 N is attributed to the formation of more wear debris with larger size and to the rougher wear scar of SUJ2 counterpart. The B_4C-SiC disc show the highest wear rate when sliding against Si_3N_4 counterpart, followed by Al_2O_3 counterpart, and lastly SUJ2 counterpart at any load. The wear of B_4C-SiC disc when sliding in water mainly depends on nature of counterparts, followed by hardness of counterparts. Different counterparts have different wear mechanisms when sliding against B_4C-SiC composite ceramics in water. As a whole, B_4C-SiC/Al_2O_3 tribo-couple shows better tribological properties when sliding in water as compared to B_4C-SiC/Si_3N_4 tribo-couple and B_4C-SiC/SUJ2 tribo-couple.

Contents

13.1. Introduction

B_4C and B_4C based ceramics have superior properties like low density, high elastic modulus and hardness, and good wear resistance [1-6]. They are attractive for various tribological applications, such as cutting tools, blast nozzles, wheel dressing tools, mechanical seals, and bearings [7].

Many tribologists have explored the potential of B_4C and B_4C based ceramics in different tribological conditions. It is reported that the tribological properties of B_4C and B_4C based ceramics depend not only on their own properties, such as grain size, grain boundary, pore, fracture toughness, hardness, and surface characteristics, but also on external factors, such as humidity, sliding speed, load, etc. [8-10]. Tkachenko et al. [11] stated that the hot-pressed B_4C ceramics with lower porosity showed lower wear and friction as sliding against B_4C ball under dry sliding. Zhang et al. [12] found that the wear of spark plasma sintered B_4C ceramics decreased with increase in their hardness as sliding against WC ball under dry sliding. These investigations suggest a strong influence of microstructure and mechanical properties on the tribological properties of B_4C ceramics. Moreover, Zhang et al. [13] stated that the wear mechanism of pressureless sintered B_4C ceramics changed from adhesive wear to delamination and spalling of tribofilm with increase in load as sliding against SiC ball under dry sliding. Umeda et al. [14] mentioned that the COF of B_4C ceramics was 0.22~0.33 as sliding against B_4C ball in water at low sliding velocities, however, the COF of B_4C ceramics decreased to as low as 0.03 with sliding velocity increasing. Larsson et al. [15] noted that the friction and wear of B_4C ceramics reduced with humidity increasing as sliding against B_4C ball under unlubricated sliding. These research results indicate that the tribological performance of B_4C ceramics strongly depend on external factors. Among external factors, counterpart material is also an important factor. Appropriate use of counterpart can enhance tribological properties for ceramics [16]. However, the report on the effect of counterpart on the friction and wear of B_4C and B_4C based ceramics is quite limited.

For B_4C based ceramics, Li et al. [17] studied the friction and wear of B_4C-hBN ceramics as sliding against B_4C pin under dry sliding. The addition of hBN to B_4C ceramics could decrease friction for B_4C ceramics, however, the wear of B_4C-hBN ceramics increased with the increasing of hBN content. Alexander et al. [18] researched the tribological performance of B_4C ceramics with addition of carbon nanotube or carbon fiber as sliding against WC-Co ball under dry sliding. Both the COF and wear rate of B_4C ceramics with addition of carbon nanotube or carbon fiber were lower than those of monolithic B_4C ceramics. Murthy et al. [19] investigated the friction and wear of B_4C-ZrB_2 ceramics as sliding against WC-Co cemented ball under dry sliding. Both the mechanical properties and tribological performance of B_4C ceramics were enhanced after the addition of ZrB_2. SiC ceramics, as another material with high hardness, have been developed for tribological applications [20-22]. In our previous work [23, 24], it is found that adding SiC in B_4C ceramics to form B_4C-SiC composite ceramics, the B_4C-SiC composite ceramics showed lower COF, lower wear rate, and shorter sliding distance to steady-state than those of B_4C ceramics as sliding against SiC ball under dry sliding. To the best of our knowledge, the friction and wear behaviors of B_4C-SiC composite ceramics under water lubrication have not been reported hitherto. As mentioned above, the tribological performance of B_4C ceramics are strongly dependent on external factors. In addition to enhancing the properties of the B_4C ceramic itself, the use of suitable counterpart materials is also an efficient way to enhance the tribological properties of tribo-couples. To explore the potential of B_4C-SiC composite ceramics for applications as tribological structural component under water lubrication, such as mechanical seals and bearings, it is important to find the optimal tribo-couple combination for B_4C-SiC composite ceramics under water lubrication. Therefore, the aim of this investigation is to determine the influence of counterpart on the tribological properties of B_4C-SiC composite ceramics under water lubrication, and to elucidate the friction and wear mechanism of B_4C-SiC composite ceramics sliding against different counterparts under water lubrication.

13.2. Experimental procedures

Powder mixtures containing B_4C (60 wt%), SiC (40 wt %) and 3 wt% carbon black additive were pressureless sintered at 2300 ℃ for 16 h in an Ar atmosphere to obtain sintered specimens with a dimension of 23 mm × 23 mm × 6 mm. Vickers hardness measured at 1 kg load for the B_4C-SiC composite ceramics was 30.4 GPa, and indentation fracture toughness was 3.2 MPa. The final surface roughness (Ra) of B_4C-SiC discs was 15-30 nm. More details about preparation and performance testing methods can be found in our previous work [23]. The morphology of the initial surface of B_4C-SiC disc is presented in Fig. 1.

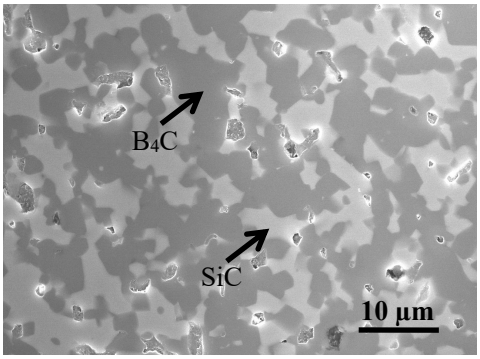

Fig. 1. The morphology of the initial surface of B_4C-SiC disc.

The tribological properties test of B_4C-SiC discs sliding against different counterparts under water lubrication were studied using a ball-on-disk tester (T-18-0162, NANOVEA, US). The schematic diagram of ball-on-disc sliding friction and wear tests in deionized water is presented in Fig. 2. Commercially available counterparts with different chemical nature and different hardness, viz., non-oxide ceramic balls (Si_3N_4), oxide ceramic balls (Al_2O_3), and metal balls (SUJ2 bearing steel), were used to slide against B_4C-SiC composite ceramics, whose physical properties provided by supplier are shown in Table 1. The diameter of counterparts is 8 mm. Before friction and wear testing, the B_4C-SiC composite ceramics and counterparts were cleaned using ethanol in an ultrasonic bath for 10 min, followed by drying in a hot air stream. Sliding tests were performed at room temperature (22-25 ℃) at two loads: 10 and 40 N. The ball was kept stationary under the load to make a track radius of 7 mm, while the B_4C-SiC disc was rotated at 0.1 m/s for 1000 m. Three repeated tests were performed for each tribo-couple. COF was recorded continuously. Wear volumes on B_4C-SiC discs and different counterparts were calculated from the surface profile traces across the wear track using a surface profilometer and from the wear scar using a microscope, respectively. The wear rates were calculated by the wear volume divided by the normal load and sliding distance.

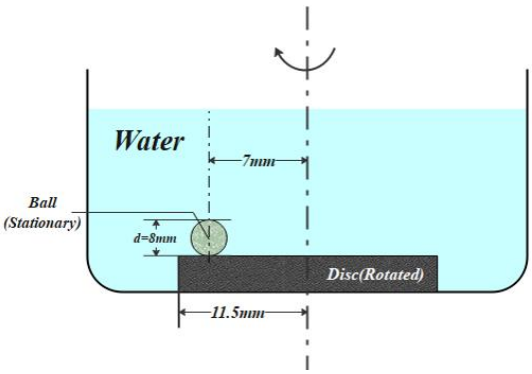

Fig. 2. Schematic diagram of ball-on-disc sliding friction and wear tests in water.

Table 1 Physical properties of commercially available counterparts provided by supplier.

Property	Si_3N_4 ball	Al_2O_3 ball	SUJ2 ball
Density (g/cm^3)	3.29	3.75	7.8
Thermal expansion coefficient (×10^{-6}/℃)	3.4	7.5	12.5
Thermal conductivity (W/(m·℃))	23	21	46
Elastic modulus (GPa)	250	340	207
Flexural strength (MPa)	735	560	-
Compressive strength (MPa)	2940	2450	-
Vickers hardness (GPa)	18.2	20.1	7.5

Wear surfaces of B_4C-SiC composite ceramics were observed by SEM equipped with EDS (JSM-7500F, JEOL, Japan). Surface compositions were investigated by XPS (ESCALAB250Xi, THERMO SCIENTIFIC, US). Water samples with filtration after sliding tests were analyzed using ICP-AES (SPS7800, HITACHI, Japan) to understand the influence of counterpart materials on tribochemical reaction of B_4C-SiC composite ceramics.

13.3. Results and discussion

13.3.1. Friction results

The COF curves of the B_4C-SiC discs sliding against different counterparts as a function of sliding distance in water at 10 and 40 N are presented in Fig. 3(a) and (b), respectively, and average COF of tribo-couples of B_4C-SiC discs sliding against different counterparts are shown in Fig. 3(c). At 10 N, the B_4C-SiC disc showed lower initial COF as sliding against Al_2O_3 counterpart and SUJ2 counterpart; After run-in period, the B_4C-SiC disc exhibited similar COF when sliding against the three different counterparts. At 40 N, although the B_4C-SiC disc showed lower initial COF as sliding against SUJ2 counterpart, the B_4C-SiC disc exhibited higher COF as sliding against SUJ2 counterpart after run-in period. In summary, the B_4C-SiC composite ceramics showed similar average COF as sliding against different counterparts in water at 10 N; the B_4C-SiC composite ceramics showed higher average COF as sliding against SUJ2 counterpart in water at 40 N, while the B_4C-SiC composite ceramics showed similar average COF as sliding against Si_3N_4 and Al_2O_3 counterparts in water at 40 N. When sliding against SUJ2 counterpart, the COF of B_4C-SiC composite ceramics increased with increase in load. However, when sliding against Si_3N_4 and Al_2O_3 counterparts, the COF of B_4C-SiC composite ceramics didn't increase with increase in load.

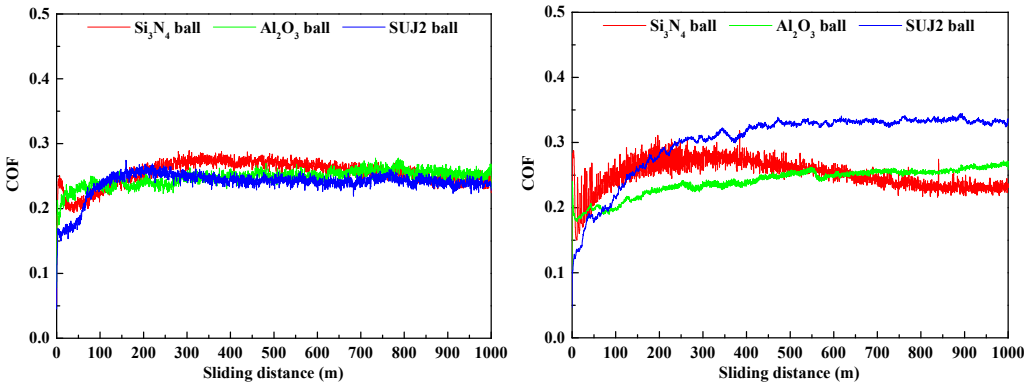

(a) (b)

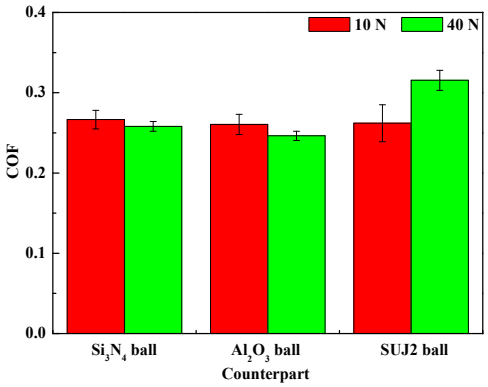

(c)

Fig. 3. COF curves of the B_4C-SiC discs sliding against different counterparts as a function of sliding distance in water at different loads: (a) 10 N, (b) 40 N, and (c) average COF of tribo-couples of B_4C-SiC discs sliding against different counterparts.

13.3.2. Wear results

The wear rates of B_4C-SiC discs, wear rates of different counterparts, and systematic wear rates of tribo-couples of B_4C-SiC discs sliding against different counterparts in water are presented Fig. 4. For the wear rates of B_4C-SiC discs (Fig. 4(a)), the B_4C-SiC discs showed the highest wear rate when sliding against Si_3N_4 counterpart, followed by Al_2O_3 counterpart, and lastly SUJ2 counterpart at any load. For the wear rates of different counterparts (Fig. 4(b)), Si_3N_4 counterpart showed the highest wear rate when sliding against B_4C-SiC discs, followed by SUJ2 counterpart, and lastly Al_2O_3 counterpart at any load. For the systematic wear rates (Fig. 4(c)), the B_4C-SiC/Si_3N_4 tribo-couple showed the highest systematic wear rate, followed by B_4C-SiC/SUJ2 tribo-couple, and lastly B_4C-SiC/Al_2O_3 tribo-couple at any load, however, the difference in systematic wear rate between B_4C-SiC/SUJ2 tribo-couple and B_4C-SiC/Al_2O_3 tribo-couple at 40 N is not obvious. For B_4C-SiC/Si_3N_4 tribo-couple, the wear rate of B_4C-SiC disc increased with increase in load, whereas the wear rate of Si_3N_4 counterpart decreased with increase in load. For B_4C-SiC/Al_2O_3 tribo-couple, the wear rate of B_4C-SiC disc decreased with increase in load , whereas the wear rate of Al_2O_3 counterpart increased with increase in load. For B_4C-SiC/SUJ2 tribo-couple, the wear rates of both B_4C-SiC disc and SUJ2 counterpart decreased with increase in load.

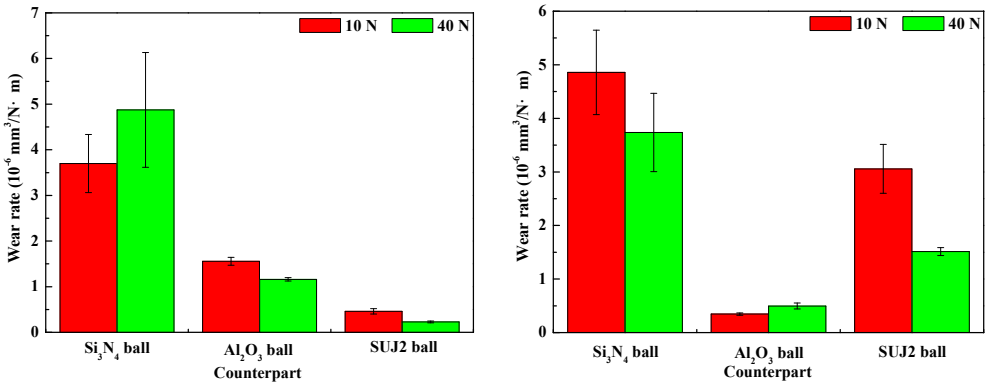

(a) (b)

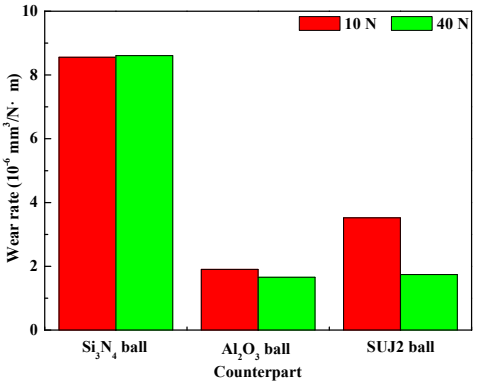

(c)

Fig. 4. (a) Wear rates of B_4C-SiC discs, (b) wear rates of different counterparts, and (c) systematic wear rates of tribo-couples of B_4C-SiC discs sliding against different counterparts in water.

13.3.3. Friction and wear mechanism

Fig. 5-Fig. 7. show the wear surfaces of the B_4C-SiC discs sliding against different counterparts in water at different loads. The wear surfaces of the B_4C-SiC disc sliding against Si_3N_4 counterpart are relatively smooth, and no scratches are observed (Fig. 5). Furthermore, C phase is found on the wear surfaces. The occurrence of C phase on the wear surfaces is believed to come from the tribochemical reaction of B_4C in the B_4C-SiC composite ceramics, which can be expressed as follow:

$$B_4C + 12H_2O = 4H_3BO_3 + C + 6H_2 \quad (1)$$

or:

$$B_4C + 6H_2O = 2B_2O_3 + C + 6H_2 \quad (2)$$

$$B_2O_3 + 3H_2O = 2H_3BO_3 \quad (3)$$

Also, it seems that the content of residual C phase on the wear surface increased with increase in load. This means that the tribochemical reaction of B_4C-SiC discs is promoted with increase in load. Some scratches are observed on the wear surfaces of B_4C-SiC disc sliding against Al_2O_3 counterpart, and the wear surfaces are relatively smooth (Fig. 6). Residual C phase is also observed on the wear surfaces, and the content of residual C phase also increased with increase in load. Moreover, some Al_2O_3 debris is found to be trapped in the pores on the wear surfaces of B_4C-SiC discs. Different from the wear surface characteristics of B_4C-SiC discs sliding against Si_3N_4 and Al_2O_3 counterparts, there are a lot of iron oxide on the wear surfaces of B_4C-SiC discs sliding against SUJ2 counterpart (Fig. 7). Further, the residual C phase on the wear surfaces of B_4C-SiC discs formed because of the tribochemical reaction of B_4C is little.

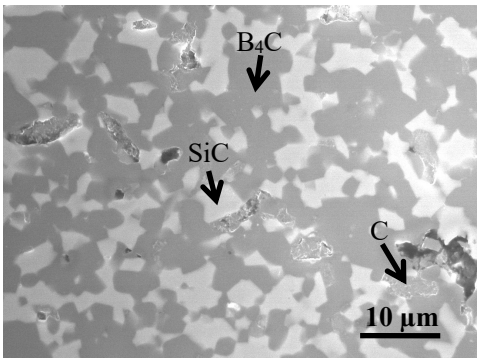

(a)

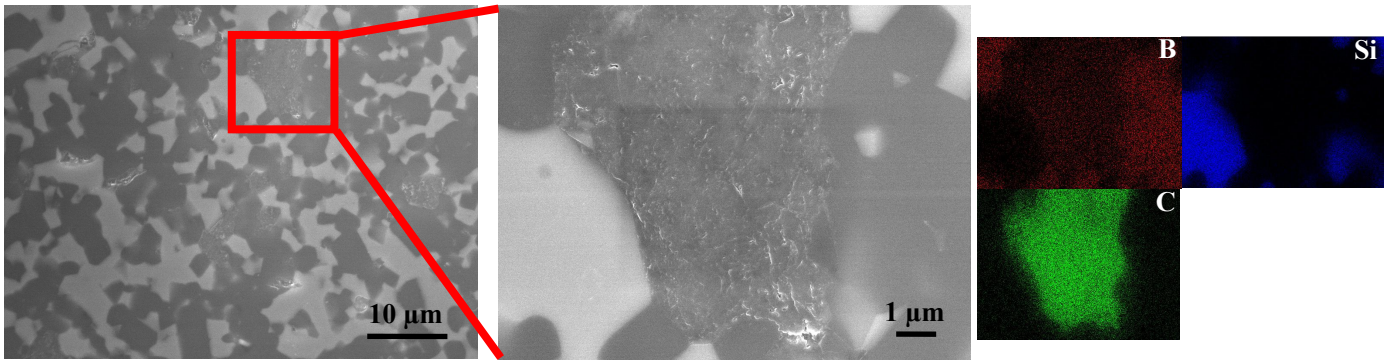

(b) (c) (d)

Fig. 5. Wear surfaces of the B_4C-SiC discs sliding against Si_3N_4 counterpart in water at: (a) 10 N, and (b-c) 40 N and (d) elemental distribution of (c).

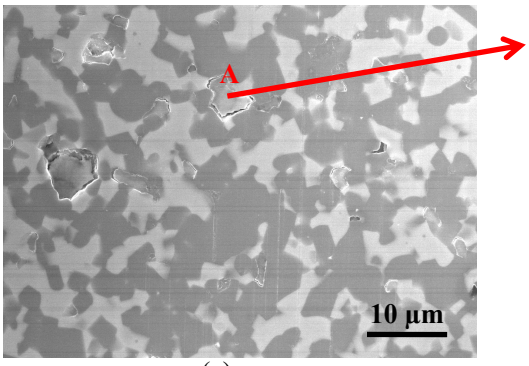

(a)

Element	Weight%	Atomic%
C	6.62	10.02
O	59.19	67.29
Al	20.59	13.88
Si	13.61	8.81

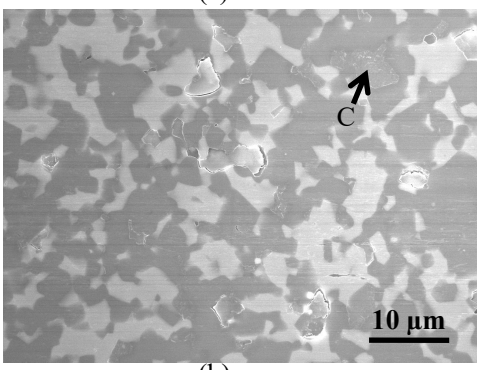

(b)

Fig. 6. Wear surfaces of the B_4C-SiC discs sliding against Al_2O_3 counterpart in water at: (a) 10 N and EDS analysis of point A, and (b) 40 N.

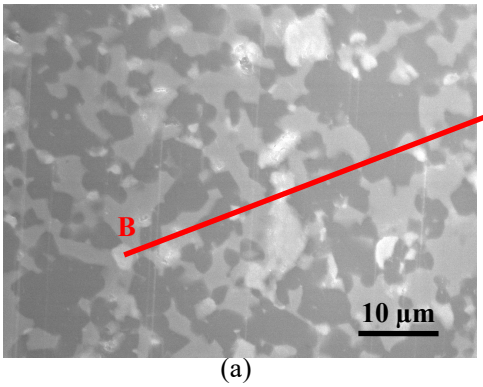

(a)

Element	Weight%	Atomic%
C	6.12	13.78
O	33.33	56.37
Si	0.99	0.95
Cr	1.00	0.52
Fe	58.56	28.37

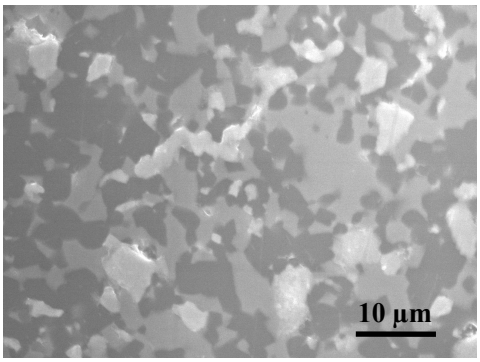

(b)

Fig. 7. Wear surfaces of the B_4C-SiC discs sliding against SUJ2 counterpart in water at: (a) 10 N and EDS analysis of point B, and (b) 40 N .

The wear surface characteristics of B_4C-SiC discs sliding against different counterparts are further shown by BSE images, as shown in Fig. 8. Almost no wear debris exists on the wear surfaces of B_4C-SiC discs when sliding against Si_3N_4 and Al_2O_3 counterparts, however, there is a number of wear debris composed of iron oxide on the wear surfaces of B_4C-SiC discs when sliding against SUJ2 counterpart. Meanwhile, the wear debris of iron oxide agglomerates with increase in the number of debris at 40 N, forming a lot of larger-sized debris. The optical micrographs of the wear scars of different counterparts sliding against B_4C-SiC composite ceramics in water are shown in Fig. 9. The wear scars of Si_3N_4 and Al_2O_3 counterparts are relatively smooth. Slight grain pull-out is found on the wear scar of Al_2O_3 counterpart, and its extent increased with increase in load. However, grooves can be found on the wear scar of SUJ2 counterpart, and the wear scar of SUJ2 counterpart became very rough at 40 N. Based on the relatively smooth wear surface characteristics of B_4C-SiC discs sliding against Si_3N_4 counterpart and Al_2O_3 counterpart and on the wear scar characteristics of Si_3N_4 counterpart and Al_2O_3 counterpart, the B_4C-SiC/Si_3N_4 tribo-couple and the B_4C-SiC/Al_2O_3 tribo-couple showed similar COF at 10 N and 40 N. For the B_4C-SiC/SUJ2 tribo-couple, although there is a number of wear debris on the wear surface of B_4C-SiC disc at 10 N, the iron oxide is soft and the size of most of wear debris is small. Therefore, the B_4C-SiC/SUJ2 tribo-couple showed similar COF with those of B_4C-SiC/Si_3N_4 tribo-couple and B_4C-SiC/Al_2O_3 tribo-couple at 10 N. The higher COF of B_4C-SiC/SUJ2 tribo-couple at 40 N is attributed to the formation of more wear debris with larger size and to the rougher wear scar of SUJ2 counterpart. The COF range of B_4C-SiC discs sliding against different counterparts in water between 10 N and 40 N is 0.25-0.32, therefore, these tribo-couples are sliding under boundary lubrication condition. In summary, the COF of B_4C-SiC composite ceramics is not dependent on kind of counterpart at 10 N. At 40 N, the COF of B_4C-SiC/SUJ2 tribo-couple is higher than those of B_4C-SiC/Si_3N_4 tribo-couple and B_4C-SiC/Al_2O_3 tribo-couple, and the COF between B_4C-SiC/Si_3N_4 tribo-couple and B_4C-SiC/Al_2O_3 tribo-couple is similar.

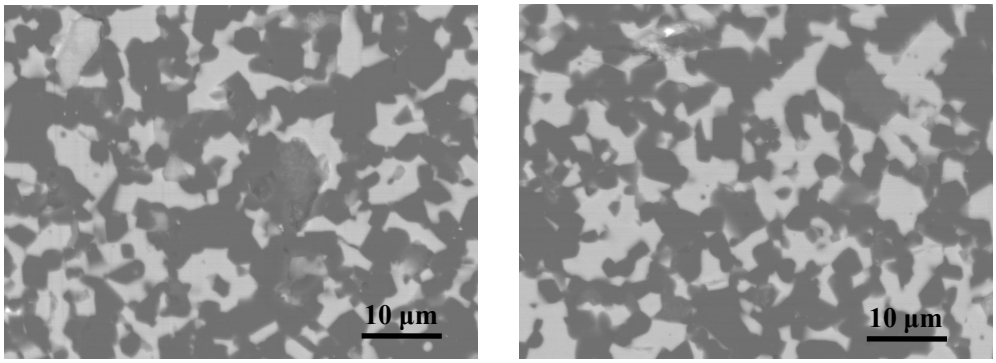

(a) (b)

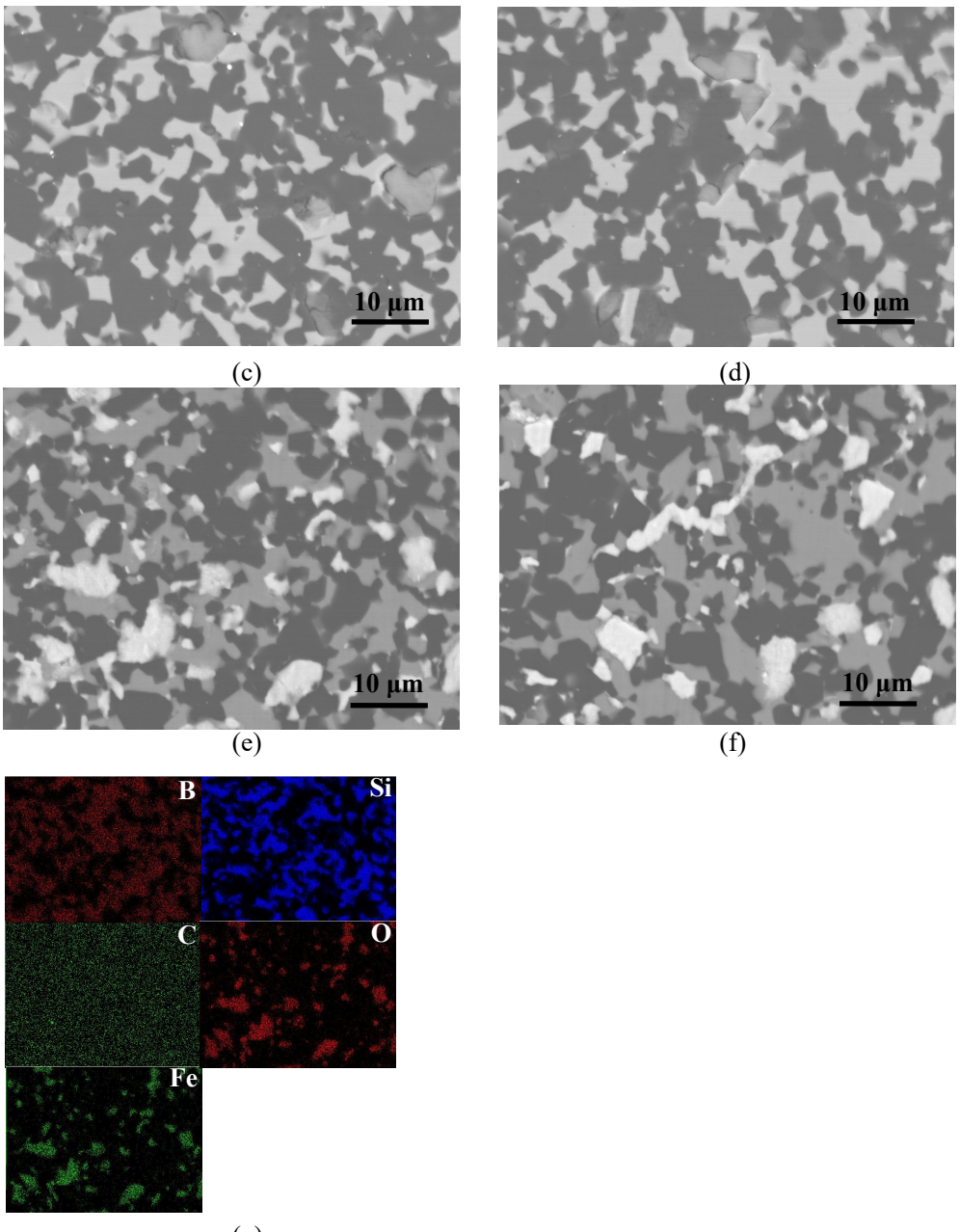

Fig. 8. BSE images of wear surfaces of the B_4C-SiC discs sliding against different counterparts in water: (a) Si_3N_4 ball at 10 N, (b) Si_3N_4 ball at 40 N, (c) Al_2O_3 ball at 10 N, (d) Al_2O_3 ball at 40 N, (e) SUJ2 ball at 10 N, (f) SUJ2 ball at 40 N, and (g) elemental distribution of (e).

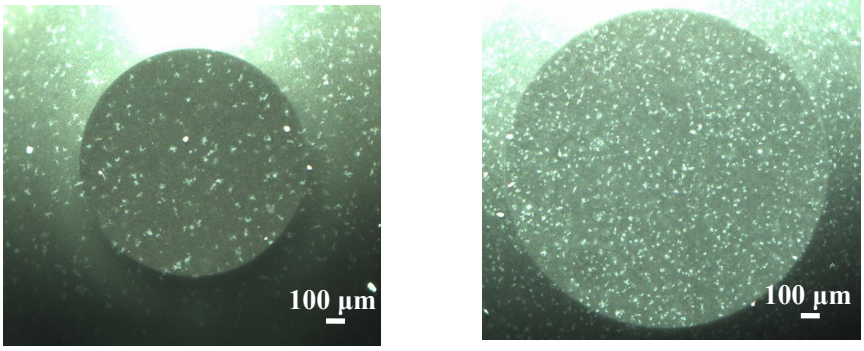

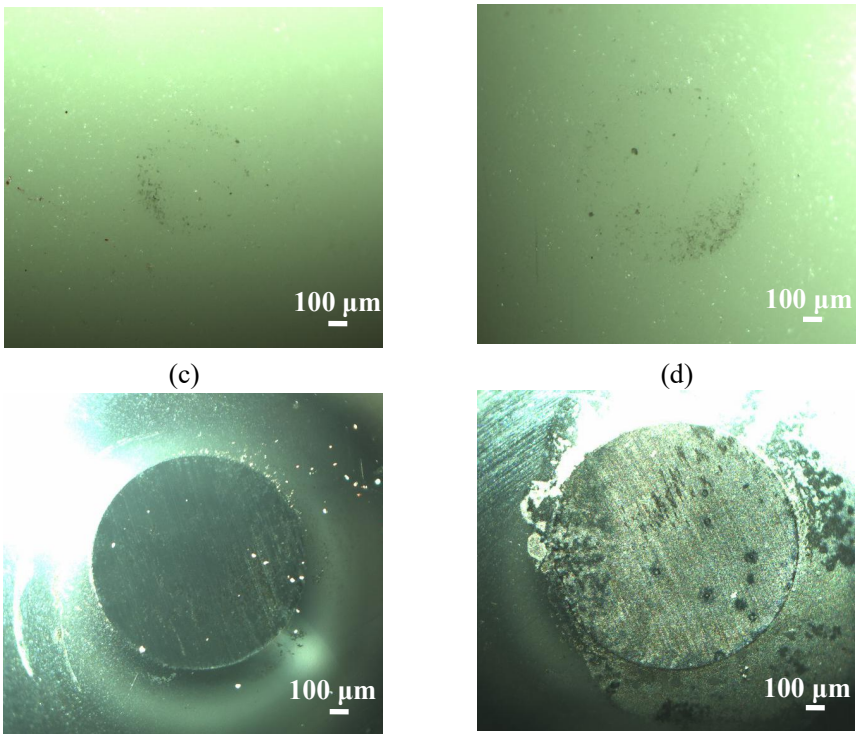

Fig. 9. Optical micrographs of the wear scars of different counterparts sliding against B_4C-SiC composite ceramics in water: (a) Si_3N_4 ball at 10 N, (b) Si_3N_4 ball at 40 N, (c) Al_2O_3 ball at 10 N, (d) Al_2O_3 ball at 40 N, (e) SUJ2 ball at 10 N, (f) SUJ2 ball at 40 N.

Fig. 10-Fig. 12. show the XPS results of the wear surfaces of B_4C-SiC discs sliding against different counterparts in water at different loads. The symmetrical B_{1s} peaks in the range of 187.6-187.7 eV belong to B_4C [25, 26]. The Si_{2p} spectrum can be fitted with two peaks by Gaussian function: the main peak with a binding energy of 100.3-100.7 eV corresponds to SiC and the binding energy of 102.2-102.8 eV is attributed to SiO_2 [27]. As mentioned above, B_4C in the B_4C-SiC composite ceramics occurred tribochemical reaction when sliding against different counterparts, in spite of different extent. The final tribochemical reaction product of B_4C, viz., H_3BO_3, would be completely dissolved in water. Neither boron oxide nor hydroxide exists on the wear surfaces of B_4C-SiC discs after sliding against different counterparts in water. SiO_2 exists on all the wear surfaces of B_4C-SiC discs after sliding against different counterparts in water. However, it is difficult to judge by the XPS results that whether the SiO_2 came from the tribochemical reaction of SiC in the B_4C-SiC composite ceramics, because SiO_2 also exists on the surface outside the wear track of B_4C-SiC discs after sliding in water (Fig. 13).

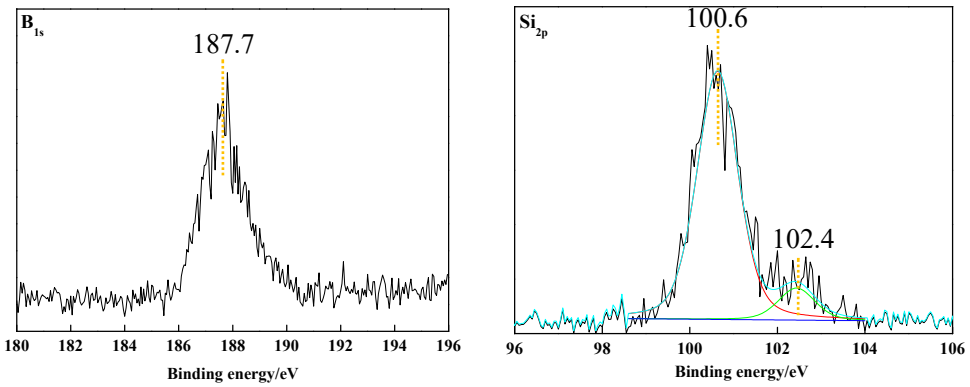

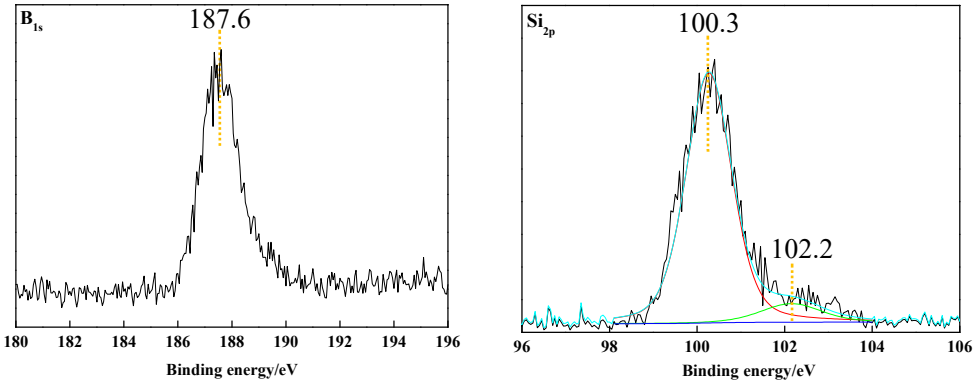

(c) (d)

Fig. 10. XPS results of wear surfaces of the B_4C-SiC discs sliding against Si_3N_4 counterpart in water at: (a-b) 10 N, (c-d) 40 N.

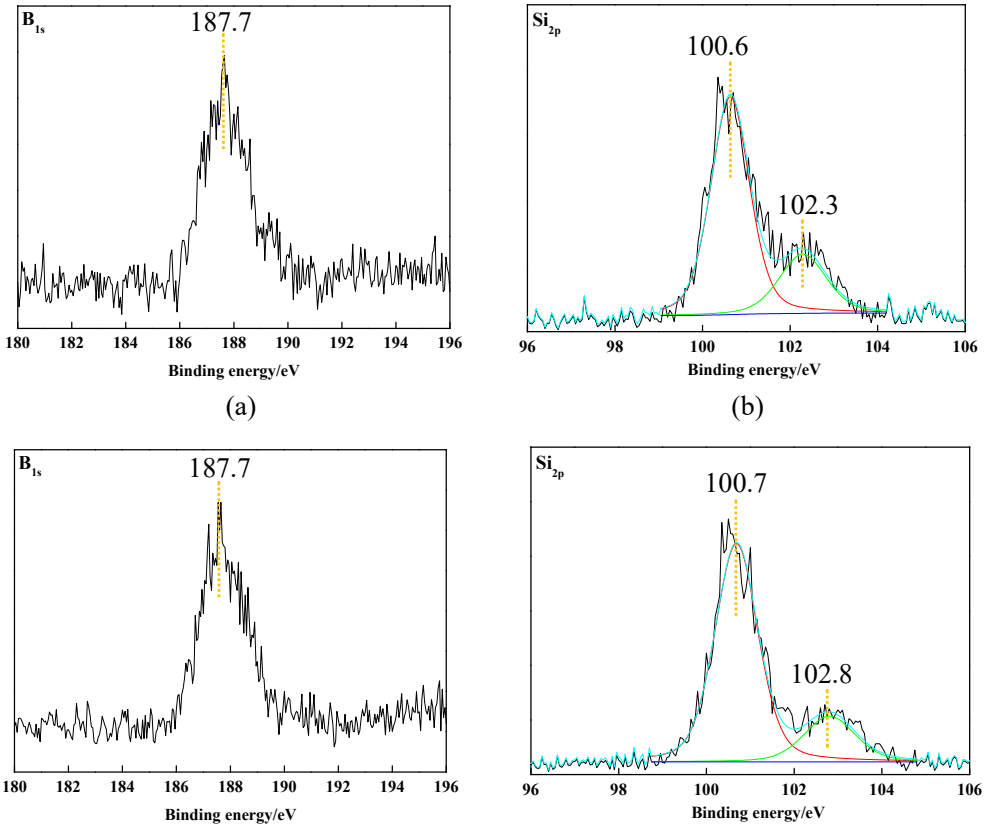

(a) (b)

(c) (d)

Fig. 11. XPS results of wear surfaces of the B_4C-SiC discs sliding against Al_2O_3 counterpart in water at: (a-b) 10 N, (c-d) 40 N.

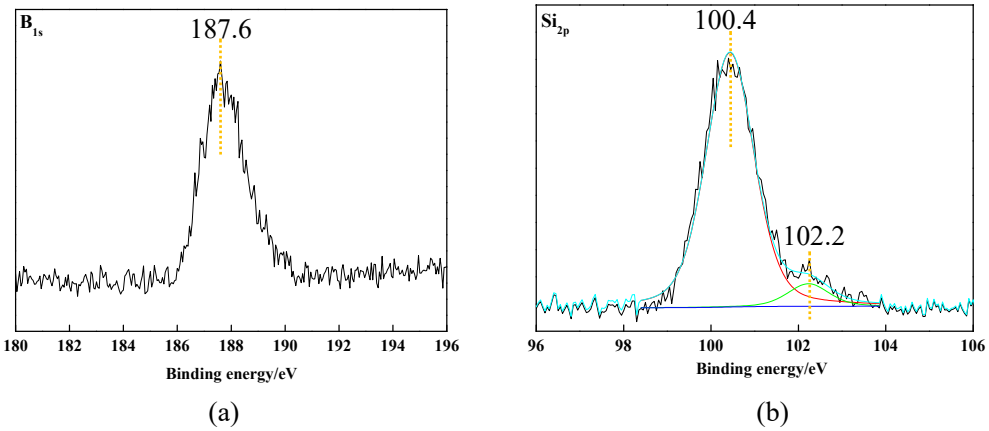

(a) (b)

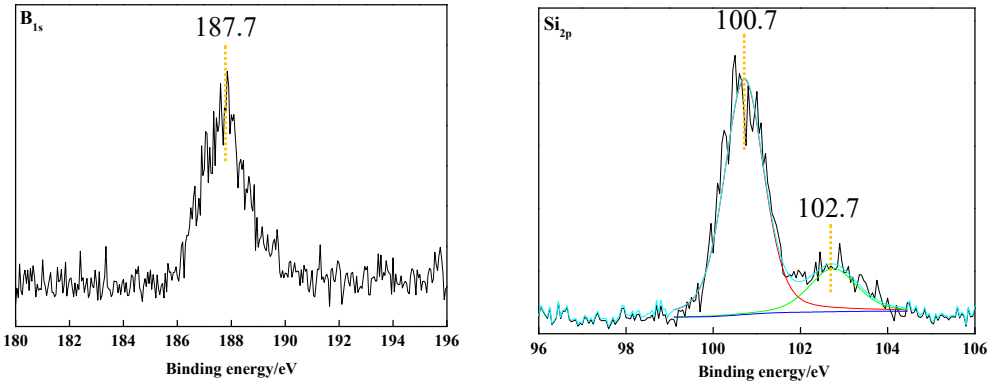

(c) (d)

Fig. 12. XPS results of wear surfaces of the B_4C-SiC discs sliding against SUJ2 counterpart in water at: (a-b) 10 N, (c-d) 40 N.

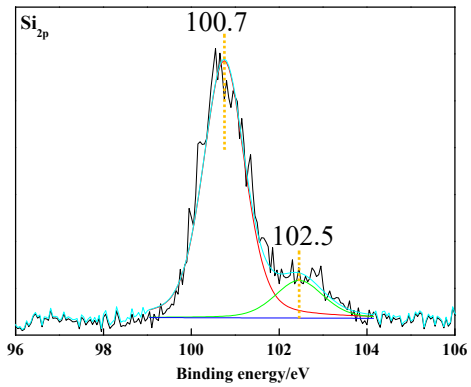

Fig. 13. Si_{2p} spectrum on the surface outside the wear track of B_4C-SiC discs after sliding in water.

To check the tribochemical reactions of B_4C-SiC discs when sliding against different counterparts in water, ICP-AES was employed to analyze the water samples collected after the sliding. The concentration of Si and B elements in the water after B_4C-SiC discs sliding against different counterparts at different loads is shown in Fig. 14. First, the concentration of both Si and B elements in water is the highest when the B_4C-SiC discs sliding against Si_3N_4 counterpart, followed by Al_2O_3 counterpart, and lastly SUJ2 counterpart at any load. In B_4C-SiC composite ceramics, besides the tribochemical reaction of B_4C, SiC also underwent the tribochemical reaction. It is reported that self-mated monolithic SiC ceramics will take place tribochemical reactions when sliding in water, which can be expressed as follows [28, 29]:

$$SiC + 2H_2O = SiO_2 + CH_4 \quad (4)$$

$$SiO_2(s) + 2H_2O(l) = H_4SiO_4\ (aq) \quad (5)$$

Therefore, based on the ICP results, it can be known that both B_4C and SiC in the B_4C-SiC composite ceramics took place tribochemical reactions when sliding against different counterparts. Also, the ICP results further prove that the extent of tribochemical reaction of B_4C-SiC discs changes with the change of counterparts, which is consistent with the observation on the wear surfaces of B_4C-SiC discs sliding against different counterparts (Fig. 5- Fig. 7). Second, the concentration of both Si and B elements increases significantly with increase in load when the B_4C-SiC discs sliding against Si_3N_4 counterpart. However, when the B_4C-SiC discs sliding against Al_2O_3 and SUJ2 counterparts, compared with the increment of Si concentration, the increase of B concentration is more obvious. Although the concentration of Si includes the concentration from the tribochemical reaction of counterpart of Si_3N_4 ball ($Si_3N_4 + 6H_2O = 3SiO_2 + 4NH_3$ [30]) when the B_4C-SiC discs sliding against Si_3N_4 counterpart, the concentration of B is higher than those when the B_4C-SiC discs sliding against Al_2O_3 counterpart and SUJ2 counterpart. Thereby, the B_4C-SiC discs showed the strongest tribochemical reaction when sliding

against Si_3N_4 counterpart, followed by Al_2O_3 counterpart, and lastly SUJ2 counterpart at any load. Combined with the observations of the wear surfaces of B_4C-SiC discs sliding against different counterparts (Fig. 5-Fig. 7), the residual C phase formed because of the tribochemical reaction of B_4C is found on the wear surfaces of B_4C-SiC discs sliding against different counterparts. However, the content of residual C phase on the wear surfaces of B_4C-SiC discs sliding against Si_3N_4 counterpart is more than that on the wear surfaces of B_4C-SiC dicss sliding against Al_2O_3 counterpart, which is more than that on the wear surfaces of B_4C-SiC discs sliding against SUJ2 counterpart. Therefore, it can be concluded that the tribochemical reaction of B_4C-SiC composite ceramics is dependent on kind of counterparts. B_4C-SiC composite ceramics are non-oxide ceramics, and the composite ceramics are mainly covalent bonds. The covalent bond ratio of B_4C is 93.9%, and the covalent bond ratio of SiC is 88% [1]. For different counterparts, Si_3N_4 ball is a non-oxide ceramic, whose covalent bond ratio is 70% and ionic bond ratio is 30%; Al_2O_3 ball is a oxide ceramic, whose covalent bond ratio is 33% [1]; SUJ2 ball is a kind of metal, and it is bonded by metallic bond. When B_4C-SiC disc sliding against Si_3N_4 counterpart, on the one hand, there is a chemical similarity between B_4C-SiC and Si_3N_4, both of which are non-oxide ceramics; and on the other hand, both B_4C-SiC and Si_3N_4 are mainly bonded by covalent bond. Therefore, a strong chemical bond between B_4C-SiC disc and Si_3N_4 counterpart is caused easily by surface chemical reaction because of chemical affinity. The strong chemical bond is easier to induce higher friction heat at the sliding interface of B_4C-SiC/Si_3N_4 tribo-couple, resulting in the promoted tribochemical reactions of B_4C-SiC disc when sliding against Si_3N_4 counterpart in water. Compared with SUJ2 counterpart, oxide Al_2O_3 counterpart still has a certain proportion of covalent bond, thus the B_4C-SiC composite ceramics is more prone to tribochemical reaction when sliding against Al_2O_3 counterpart, resulting in higher concentration of Si and B when sliding against Al_2O_3 counterpart as compared to against SUJ2 counterpart.

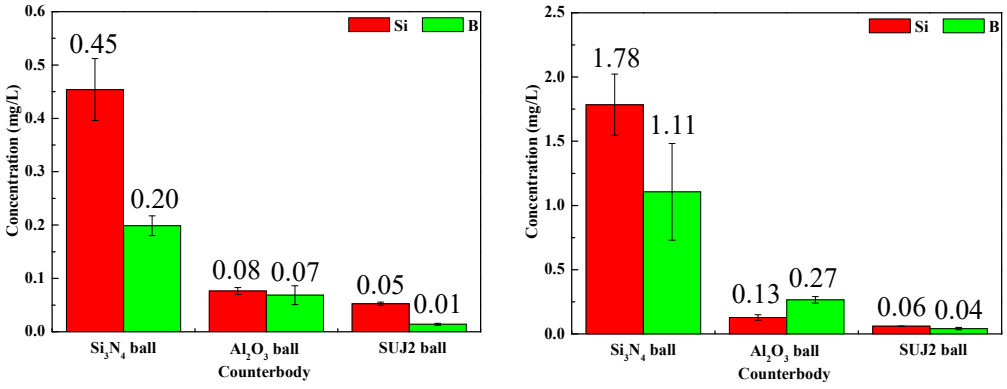

Fig. 14. Concentration of Si and B elements in the water tested by ICP-AES after B_4C-SiC discs sliding against different counterparts at: (a) 10 N, and (b) 40 N.

For the wear rate of B_4C-SiC discs when sliding against different counterparts, it is proportional to the degree of tribochemical reaction. This suggests that the wear of B_4C-SiC discs depends primarily on tribochemical wear. Meanwhile, obvious fracture is not found on the wear surfaces of B_4C-SiC discs when sliding against different counterparts, and just some scratches are found on the wear surfaces. The concentration of Si and B elements in water after the B_4C-SiC disc sliding against Al_2O_3 counterpart is slightly higher than that after the B_4C-SiC disc sliding against SUJ2 counterpart, however, the wear rate of B_4C-SiC disc sliding against Al_2O_3 counterpart is about 3 to 5 times higher than that against SUJ2 counterpart. This means that in addition to tribochemical wear, mechanical wear induced by the hardness of counterparts is also one of the wear mechanisms of B_4C-SiC disc. Although the hardness of Al_2O_3 counterpart is higher than that of Si_3N_4 counterpart, the tribochemical wear induced by the chemical similarity between Si_3N_4 and B_4C-SiC plays a dominant role in the wear of B_4C-SiC disc.

Therefore, the wear of B_4C-SiC discs when sliding against different counterparts in water is mainly controlled by tribochemical wear, followed by mechanical wear. This conclusion is different from the wear mechanism when the B_4C-SiC discs sliding against these three different counterparts under dry sliding. The wear of B_4C-SiC disc is mainly controlled by the hardness of counterparts when the load is more than 10 N under dry sliding condition [31]. Furthermore, under dry sliding, Kovalčíková et al. [32] noted that the wear of monolithic SiC ceramics increased with increase in hardness of the counterparts. However, in this study, some different findings are found when the B_4C-SiC discs sliding against different counterparts in water, i.e., the wear of B_4C-SiC disc when sliding in water mainly depends on nature of counterparts, followed by hardness of counterparts.

Different counterparts have different wear mechanisms when sliding against B_4C-SiC composite ceramics in water. For Si_3N_4 counterpart, the wear scar is smooth, and no fracture and no grooves are observed. Also, the concentration of Si is significantly higher than that of B in the water samples of B_4C-SiC/Si_3N_4 tribo-couple. Thus, it is reasonable to believe that part of the Si concentration comes from the tribochemical reaction of Si_3N_4 counterpart. Therefore, the main wear mechanism of Si_3N_4 counterpar is tribochemical wear. For Al_2O_3 counterpart, grain pull-out is observed on the wear scar. Also, the concentration of Al element in water is lower than 0.02 mg/L (Fig. 15), which means that the tribochemical reaction of Al_2O_3 hardly occurred. Therefore, the main wear mechanism of Al_2O_3 counterpart is grain pull-out. For SUJ2 counterpart, obvious grooves are found on the wear scar. Further, a number of wear debris of iron oxide, which is formed by tribochemical reaction of Fe, is found on the wear surface of B_4C-SiC discs, and the iron oxide is difficult to dissolve in water, resulting in a lower concentration of Fe element in water (Fig. 15). Therefore, the main wear mechanisms of SUJ2 counterpart are abrasive wear, plastic deformation, and tribochemical wear. The highest wear rate of Si_3N_4 counterpart is attributed to the strongest tribochemical wear induced by the chemical similarity between Si_3N_4 and B_4C-SiC; the higher wear rate of SUJ2 counterpart than that of Al_2O_3 counterpart is ascribed to lower hardness of SUJ2 counterpart.

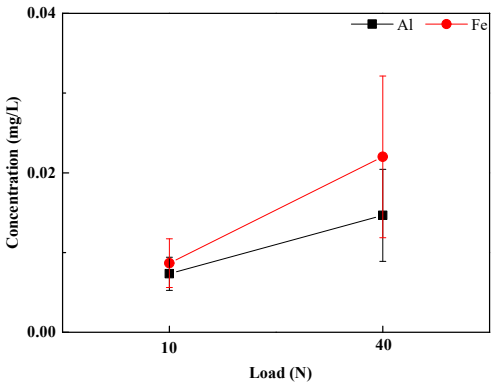

Fig. 15. Concentration of Al element and Fe element in water tested by ICP-AES after B_4C-SiC discs sliding against Al_2O_3 counterpart and SUJ2 counterpart, respectively, at different loads.

For the systematic wear rate of B_4C-SiC discs when sliding against different counterparts, the B_4C-SiC/Si_3N_4 tribo-couple showed the highest systematic wear rate, followed by B_4C-SiC/SUJ2 tribo-couple, and lastly B_4C-SiC/Al_2O_3 tribo-couple. Although the difference in systematic wear rate between B_4C-SiC/SUJ2 tribo-couple and B_4C-SiC/Al_2O_3 tribo-couple at 40 N is not obvious, the B_4C-SiC/SUJ2 tribo-couple showed higher COF at 40 N. As a whole, B_4C-SiC/Al_2O_3 tribo-couple showed better tribological properties when sliding in water as compared to B_4C-SiC/Si_3N_4 tribo-couple and B_4C-SiC/SUJ2 tribo-couple. These findings can provide some design bases for the application of B_4C-SiC composite ceramics. Meanwhile, the friction and wear mechanisms of B_4C-SiC composite ceramics when sliding against different counterparts are revealed in this paper.

13.4. Conclusions

The tribological tests were used for the investigation of influence of counterparts (Si_3N_4, Al_2O_3 and SUJ2) on COF, wear rate, and friction and wear mechanisms of B_4C-SiC composite ceramics under water lubrication. The following results are obtained:

(1) When the B_4C-SiC discs slide against different counterparts in water, the similar COF is obtained, except against SUJ2 counterpart at 40 N. The increased COF of B_4C-SiC/SUJ2 tribo-couple at 40 N is attributed to the formation of more wear debris with larger size and to the rougher wear scar of SUJ2 counterpart.
(2) The B_4C-SiC disc show the highest wear rate when sliding against Si_3N_4 counterpart, followed by Al_2O_3 counterpart, and lastly SUJ2 counterpart at any load. The wear of B_4C-SiC disc when sliding in water mainly depends on nature of counterparts, followed by hardness of counterparts. The highest wear rate of B_4C-SiC/Si_3N_4 tribo-couple is attributed to the greatest extent of tribochemical wear.
(3) Different counterparts have different wear mechanisms when sliding against B_4C-SiC composite ceramics in water. The main wear mechanism of Si_3N_4 counterpart is tribochemical wear. The main wear mechanism of Al_2O_3 counterpart is grain pull-out. The main wear mechanisms of SUJ2 counterpart are abrasive wear, plastic deformation, and tribochemical wear.
(4) As a whole, B_4C-SiC/Al_2O_3 tribo-couple shows better tribological properties when sliding in water as compared to B_4C-SiC/Si_3N_4 tribo-couple and B_4C-SiC/SUJ2 tribo-couple.

13.5. References

[1] W. Zhang, S. Yamashita, H. Kita. Progress in pressureless sintering of boron carbide ceramics-A review. Advances in Applied Ceramics: Structural, Functional and Bioceramics,2019,118(4):222-239.

[2] F. Thévenot. Boron carbide- a comprehensive review. Journal of the European Ceramic Society,1990,6(4):205-225.

[3] W. Zhang, S. Yamashita, T. Kumazawa, F. Ozeki, H. Hyuga, H. Kita. Tribological properties of B_4C ceramics prepared by pressureless sintering and annealed at different temperatures. Tribology Transactions,2020,63(4):672-682.

[4] F. Findik. Latest progress on tribological properties of industrial materials. Materials & Design,2014,57:218-244.

[5] W. Zhang, S. Yamashita, H. Kita. A study of B_4C-SiC composite for self-lubrication. Journal of the American Ceramic Society, DOI: 10.1111/jace.17584.

[6] W. Zhang, S. Yamashita, T. Kumazawa, F. Ozeki, H. Hyuga, H. Kita. Study on friction behavior of SiC-B_4C composite ceramics after annealing. Industrial Lubrication and Tribology,2020,72(5):673-679.

[7] W. Zhang. A review of tribological properties for boron carbide ceramics. Progress in Materials Science,2021,116,100718.

[8] J. K. Sonber, P. K. Limaye, T. S. R. Ch. Murthy, K. Sairam, A. Nagaraj, N. L. Soni, R. J. Patel, J. K. Chakravartty. Tribological properties of boron carbide in sliding against WC ball. International Journal of Refractory Metals & Hard Materials,2015,51:110-117.

[9] Y. G. Gogotsi, A. M. Koval'chenko, I. A. Kossko. Tribochemical interactions of boron carbides against steel. Wear,1992,154(1):133-140.

[10] P. D. Cuong, H. S. Ahn, E. S. Yoon, K. H. Shin. Effects of relative humidity on tribological properties of boron carbide coating against steel. Surface and Coatings Technology,2006,201(7):4230-4235.

[11] Y. G. Tkachenko, B. L. Grabchuk, N. I. Bodnaruk, V. V. Sychev. Friction and wear of boron carbide at temperatures in the range 20-1500 °C. Soviet Powder Metallurgy & Metal Ceramics,1977,16(7):541-543.

[12] M. Zhang, T. C. Yuan, R. D. Li. Effect of spark plasma sintering on microstructure and friction characteristics of boron carbide. Journal of Micromechanics and Molecular Physics,2018,3(1-2):1750014.

[13] W. Zhang, S. Yamashita, H. Kita. Effects of load on tribological properties of B_4C and B_4C-SiC ceramics sliding against SiC balls. Journal of Asian Ceramic Societies,2020,8(3):586-596.

[14] K. Umeda, Y. Enomoto, A. Mitsui, K. Mannami. Friction and wear of boride ceramics in air and water. Wear,1993,169(1):63-68.

[15] P. Larsson, N. Axén, S. Hogmark. Tribofilm formation on boron carbide in sliding wear. Wear,1999,236(1-2):73-80.

[16] W. Zhang, S. Yamashita, H. Kita. Progress in tribological research of SiC ceramics in unlubricated sliding-A review. Materials & Design,2020,190:108528.

[17] X. Q. Li, Y. M. Gao, W. Pan, Z. C. Zhong, L. C. Song, W. Chen, Q. X. Yang. Effect of hBN content on the friction and wear characteristics of B_4C-hBN ceramic composites under dry sliding condition. Ceramics International,2015,41(3):3918-3926.

[18] R. Alexander, K.V. Ravikanth, R. D. Bedse, T. S. R. Ch. Murthy, K. Dasgupta. Effect of carbon fiber on the tribo-mechanical properties of boron carbide: Comparison with carbon nanotube reinforcement. International Journal of Refractory Metals & Hard Materials,2019,85:105055.

[19] T. S. R. Ch. Murthy, S. Ankata, J. K. Sonber, K. Sairam, K. Singh, A. Nagaraj, P. Sengupta, R. D. Bedse, S. Majumdar, V. Kain. Microstructure, thermo-physical, mechanical and wear properties of in-situ formed boron carbide-zirconium diboride composite. Ceramics-Silikáty,2018,62(1):15-30.

[20] W. Zhang, S. Yamashita, H. Kita. Self lubrication of pressureless sintered SiC ceramics. Journal of Materials Research and Technology,2020,9(6):12880-12888.

[21] W. Zhang, S. Yamashita, T. Kumazawa, F. Ozeki, H. Hyuga, H. Kita. Effect of nanorelief structure formed in situ on tribological properties of ceramics in dry sliding. Ceramics International,2019,45(11):13818-13824.

[22] N. P. Wasekar, L. Bathini, L. Ramakrishna, D. S. Rao, G. Padmanabham. Pulsed electrodeposition, mechanical properties and wear mechanism in Ni-W/SiC nanocomposite coatings used for automotive applications. Applied Surface Science,2020,527:146896.

[23] W. Zhang, S. Yamashita, H. Kita. Tribological properties of SiC-B_4C ceramics under dry sliding condition. Journal of the European Ceramic Society,2020,40(8):2855-2861.

[24] W. Zhang, S. Yamashita, T. Kumazawa, F. Ozeki, H. Hyuga, H. Kita. Influence of surface roughness parameters and surface morphology on friction performance of ceramics. Journal of the Ceramic Society of Japan,2019,127(11):837-842.

[25] X. Q. Li, Y. M. Gao, W. Pan, Z. C. Zhong, L. C. Song, W. Chen, Q. X. Yang. Effect of hBN content on the friction and wear characteristics of B_4C-hBN ceramic composites under dry sliding condition. Ceramics International,2015,41(3):3918-3926.

[26] P. D. Cuong, H. S. Ahn, E. S. Yoon, K. H. Shin. Effects of relative humidity on tribological properties of boron carbide coating against steel. Surface and Coatings Technology,2006,201(7):4230-4235.

[27] W. F. A. Besling, A. Goossens, B. Meester, J. Schoonman. Laser-induced chemical vapor deposition of nanostructured silicon carbonitride thin films. Journal of Applied Physics,1998,83(1):544-553.

[28] M. Chen, K. Kato, K. Adachi. The difference in running-in period and friction coefficient between self-mated Si_3N_4 and SiC under water lubrication. Tribology letters,2001,11(1):23-28.

[29] J. D. Rimstidt, H. L. Barnes. The kinetics of silica-water reactions. Geochimica et Cosmochimica Acta,1980, 44(11):1683-1699.

[30] J. G. Xu, K. Kato. Formation of tribochemical layer of ceramics sliding in water and its role for low friction.

Wear,2000,245(1-2):61-75.

[31] W. Zhang, S. Yamashita, H. Kita. Effect of counterbody on tribological properties of B_4C-SiC composite ceramics. Wear,2020,458-459:203418.

[32] A. Kovalčíková, P. Kurek, J. Balko, J. Dusza, P. Šajgalík, M. Mihaliková. Effect of the counterpart material on wear characteristics of silicon carbide ceramics. Int. Journal of Refractory Metals and Hard Materials:2014,44: 12-18.

Summary of this thesis

In this thesis, the author evaluated the tribological properties of B_4C based ceramics under both dry sliding and water-lubricated sliding conditions, aimed to find the optimized condition and composition of B_4C based ceramics for mechanical seals and to analyze the friction and wear mechanisms for B_4C based ceramics.

Part I deals with the effect of relief structure on B_4C-SiC composite ceramics with different ratio. B_4C-SiC ceramics with ratio of 60wt% to 40wt% can show lower friction and wear as compared to those of SiC ceramics and B_4C ceramics under both dry sliding condition and water-lubricated sliding condition. The relief structure formed in situ on the surface of B_4C-SiC ceramics is the main mechanism for their good tribological properties under both dry sliding and water-lubricated sliding. Under dry sliding, the relief structure can result in decreased adhesion effect and reduced abrasive wear. The increased friction coefficient of B_4C-SiC ceramics at high load under dry sliding is attributed to the damaged relief structure. Under water-lubricated sliding, nano-relief formed by in situ can show beneficial influence similar to micron-relief produced by laser for frictional property of materials under water lubrication. On the one hand, the water stored in the valleys of nano-relief can provide continuous lubrication to the B_4C-SiC ceramic friction surfaces; on the other hand, load carrying capacity of B_4C-SiC ceramics is expected to be improved by this nano-relief, making B_4C-SiC ceramics exhibit lower COF under higher loads (20 N) than those of monolithic SiC ceramics and monolithic B_4C ceramics.

Part II is focused on the tribological properties of B_4C-SiC ceramics in water. B_4C/SiC tribopair showed lower friction coefficients than those of SiC/SiC tribopair and B_4C-SiC/SiC tribopair in boundary lubrication and mixed lubrication. The low friction of carbide ceramics is achieved by the combination of hydrodynamic lubrication and tribochemical reactions. The products of tribochemical reactions of carbide ceramics improve the viscosity of water at or near the worn surfaces of carbide ceramics, promoting the hydrodynamic lubrication for carbide ceramics. B_4C-SiC ceramics can obtain lower friction and wear when sliding in water at the water temperatures between 40 and 60 ℃, which is attributed to the promoted tribochemical reaction of SiC in the B_4C-SiC ceramics, rather than the tribochemical reaction of B_4C in the B_4C-SiC ceramics. More SiO_2 film was gradually formed on the wear surfaces as the sliding distance increases, which could cover or protect more B_4C grains. The formation of more SiO_2 film results in the reduced friction coefficient, tribochemical wear and mechanical wear for B_4C-SiC ceramics.

Part III compares the influence of annealing on tribological properties of B_4C, SiC, B_4C-SiC ceramics. B_4C ceramics obtained a favorable self-lubricating property after annealing at 1000 or 1200 ℃ because of the formation of an H_3BO_3 layer during the annealing treatment. B_4C ceramics heat treated at 1200 ℃ exhibited the best self-lubricating property, with the lowest coefficient of friction of approximately 0.08. The SiC ceramics with annealing at 1500 ℃ revealed the best self lubricating property, with the coefficient of friction of 0.4. The B_4C-SiC composite can obtain lower friction coefficient by annealing at 1000 ℃, whereas the friction coefficient of B_4C-SiC composite annealed at 1200 ℃ was significantly increased. The mechanism of self-lubrication of the B_4C-SiC composite was the formation of H_3BO_3 layer. Annealing can reduce the friction coefficient for B_4C, SiC, and B_4C-SiC ceramics, however, the wear rates of B_4C and B_4C-SiC ceramics will be increased. Only SiC ceramics can obtain reduced wear rate after annealing at 1000 ℃. The wear mechanisms of B_4C ceramics with an H_3BO_3 layer included dual effects of mechanical wear and tribochemical wear.

Part IV investigates the influence of counterpart materials on tribological properties of B_4C-SiC composite ceramics. Under dry sliding, B_4C-SiC/Al_2O_3 tribopair can show better tribological properties at low load. For the B_4C-SiC composite ceramics, both the friction coefficient and specific wear rate were dependent on counterbody materials. The influence of counterbody materials on tribological properties of B_4C-SiC ceramics is not obvious at high load, which was attributed to the formation of a number of compaction layers on all the worn surfaces of

B_4C-SiC composite ceramics sliding against Al_2O_3, Si_3N_4 and SUJ2 counterbodies. When sliding against Al_2O_3 ball and SUJ2 ball, the main wear mechanisms of B_4C-SiC composite ceramics changed from surface polishing and mild abrasion to micro-fracture with load increasing from 5 N to 20 N. When sliding against Si_3N_4 ball, the main wear mechanism of B_4C-SiC composite ceramics was micro-fracture at any load. At the same loads, the wear of B_4C-SiC composite ceramics sliding against different counterbodies at low load was mainly controlled by the chemical similarity of counterbody, whereas the wear of B_4C-SiC composite ceramics sliding against different counterbodies at intermediate and high loads was mainly controlled by the hardness of counterbody. Under water-lubricated sliding, B_4C-SiC/Al_2O_3 tribo-couple shows better tribological properties when sliding in water as compared to B_4C-SiC/Si_3N_4 tribo-couple and B_4C-SiC/SUJ2 tribo-couple in a wide load range. The wear of B_4C-SiC ceramics when sliding in water mainly depends on nature of counterbody materials, followed by hardness of counterbody materials.

Future works

The future works on tribological properties of B_4C-SiC ceramics are mainly focus on:

(1) The formation mechanism of nano-relief structure should be researched in detail.

(2) Now, the depth of relief structure formed in situ during the sliding can't be controlled. Next work, how to control the depth of relief structure formed in situ should be investigated.

(3) The cost of preparation of B_4C-SiC ceramics should be down.

(4) The fracture toughness of B_4C-SiC ceramics should be increased, so that the nano-relief structure of B_4C-SiC ceramics could be maintained at high load.

Achievements

List of publications

<Original papers>

Chapter 1

(1) **Wei Zhang**, Seiji Yamashita, Takeshi Kumazawa, Fumihito Ozeki, Hideki Hyuga, Hideki Kita. Effect of nanorelief structure formed in situ on tribological properties of ceramics in dry sliding. Ceramics International,2019,45(11):13818-13824.

(2) **Wei Zhang**, Seiji Yamashita, Hideki Kita. Tribological properties of SiC-B_4C ceramics under dry sliding condition. Journal of the European Ceramic Society,2020,40(8):2855-2861.

Chapter 2

(3) **Wei Zhang**, Seiji Yamashita, Takeshi Kumazawa, Fumihito Ozeki, Hideki Hyuga, Wataru Norimatsu, Hideki Kita. A study on formation mechanisms of relief structure formed in situ on the surface of ceramics. Ceramics International,2019,45(17):23143-23148.

Chapter 3

(4) **Wei Zhang**, Seiji Yamashita, Takeshi Kumazawa, Fumihito Ozeki, Hideki Hyuga, Hideki Kita. Influence of surface roughness parameters and surface morphology on friction performance of ceramics. Journal of the Ceramic Society of Japan,2019,127(11):837-842.

Chapter 4

(5) **Wei Zhang**, Seiji Yamashita, Hideki Kita. Effects of load on tribological properties of B_4C and B_4C-SiC ceramics sliding against SiC balls. Journal of Asian Ceramic Societies,2020,8(3):586-596.

Chapter 5

(6) **Wei Zhang**, Xiaoyu Chen, Seiji Yamashita, Mitsuhiro Kubota, Hideki Kita. A ceramic with low friction and low wear under water lubrication: B_4C-SiC. (Under review)

Chapter 6

(7) **Wei Zhang**, Xiaoyu Chen, Seiji Yamashita, Mitsuhiro Kubota, Hideki Kita. Frictional characteristics of carbide ceramics in water. (Under review)

Chapter 7

(8) **Wei Zhang**, Xiaoyu Chen, Seiji Yamashita, Mitsuhiro Kubota, Hideki Kita. Effect of water temperature on tribological performance of B_4C-SiC ceramics under water lubrication. (Under review)

Chapter 8

(9) **Wei Zhang**, Seiji Yamashita, Takeshi Kumazawa, Fumihito Ozeki, Hideki Hyuga, Hideki Kita. Tribological properties of B_4C ceramics prepared by pressureless sintering and annealed at different temperatures. Tribology Transactions,2020,63(4):672-682.

Chapter 9

(10) **Wei Zhang**, Seiji Yamashita, Hideki Kita. Self lubrication of pressureless sintered SiC ceramics. Journal of Materials Research and Technology,2020,9(6):12880-12888.

Chapter 10

(11) **Wei Zhang**, Seiji Yamashita, Hideki Kita. A study of B_4C-SiC composite for self-lubrication. Journal of the American Ceramic Society. 2021,DOI: 10.1111/jace.17584.

Chapter 11

(12) **Wei Zhang**, Seiji Yamashita, Takeshi Kumazawa, Fumihito Ozeki, Hideki Hyuga, Hideki Kita. Study on friction behavior of SiC-B_4C composite ceramics after annealing. Industrial Lubrication and Tribology,2020,72(5):673-679.

Chapter 12

(13) **Wei Zhang**, Seiji Yamashita, Hideki Kita. Effect of counterbodyon tribological properties of B_4C-SiC composite ceramics. Wear,2020,458-459:203418.

Chapter 13

(14) **Wei Zhang**, Xiaoyu Chen, Seiji Yamashita, Mitsuhiro Kubota, Hideki Kita. Tribology of B_4C-SiC composite ceramics under water lubrication: Influence of counterpart. (Under review)

<Other Publications>

General Introduction

(1) **Wei Zhang**. A review of tribological properties for boron carbide ceramics. Progress in Materials Science,2021,116:100718.

(2) **Wei Zhang**, Seiji Yamashita, Hideki Kita. Progress in tribological research of SiC ceramics in unlubricated sliding-A review. Materials & Design,2020,190:108528.

(3) **Wei Zhang**, Seiji Yamashita, Hideki Kita. Progress in pressureless sintering of boron carbide ceramics-a review. Advances in Applied Ceramics: Structural, Functional and Bioceramics,2019,118(4):222-239.

(4) **Wei Zhang**. Tribology of SiC ceramics under lubrication: Features, developments and perspectives. (Under review)

(5) **Wei Zhang**. Recent progress in processing and properties of boron carbide-silicon carbide composite ceramics. (Under review)

Related papers, not used in this thesis

(1) **张巍**,张金,段春雷,耿浩,韩阳. Al_2O_3 抗热震陶瓷的研究进展.沈阳工业大学学报,2020,42(6):624-647.

List of presentation in international conference

(1) **Wei Zhang**, Seiji Yamashita, Hideki Kita. Effect of nanorelief structure formed in situ on tribological properties of B_4C based composite ceramics. The 8th Global Conference on Materials Science and Engineering (CMSE2019), November 12-15,2019, Sanya, China.

Acknowledgement

The studies in this thesis were carried out under the guidance of Professor Kita, Assistant Professor Yamashita, and Assistant Professor Kubota at Graduate School of Engineering, Nagoya University during the period from April 2018 to February 2021.

The author would like to express his sincere gratitude to Professor Kita, Assistant Professor Yamashita, and Assistant Professor Kubota for their guidance, instructive discussion, and valuable comments throughout this study.

The author make acknowledgements to Professor Umehara, Professor Takami and Associate Professor Norimatsu for reviewing his doctoral thesis.

The author wishes to express his appreciation to Project to Support Manufacturing SME collaboration. Part of the studies in this thesis was supported by this project. The author also would like to acknowledge the scholarship support from Daiko Foundation, Japan.

The author makes grateful acknowledgements to Mino Ceramics Co. Ltd. for preparing ceramics. The author would like to thank Associate Professor Norimatsu for TEM pictures measurements. The author also would like to thank Chen Xiaoyu, who is also an international student from China, for ICP measurements.

Finally, the author would like to express his gratitude to his wife, Xia Jing, for her loving considerations and great confidence in him all though these years. To support his career, she takes care of their child alone.